UNIVERSITÉ DE LORRAINE

École doctorale IAEM Lorraine

Modélisation mathématique pour l'étude des oscillations neuronales dans des réseaux de mémoire hippocampiques pendant l'éveil et sous anesthésie générale

Mathematical Modelling of Neural Oscillations in Hippocampal Memory Networks during Waking and under General Anaesthesia

THÈSE

présentée et soutenue publiquement le 19 Septembre 2017

pour l'obtention du

Doctorat de l'Université de Lorraine

(mention informatique)

par

Francesco GIOVANNINI

Composition du jury

Directeur :	HUTT Axel, Directeur de Recherche à l'INRIA Nancy Grand-Est
Co-Directeur :	BUHRY Laure, Maître de Conférences à l'Université de Lorraine
Rapporteurs :	DESTEXHE Alain, Directeur de Recherche au CNRS ROUGIER Nicolas, Chargé de Recherche à l'INRIA Bordeaux Sud-Ouest
Examinateurs :	LOUIS-DORR Valérie, Professeur à l'Université de Lorraine BORAUD Thomas, Directeur de Recherche au CNRS

Laboratoire Lorrain de Recherche en Informatique et ses Applications – UMR 7503

Abstract

Memory is commonly defined as the ability to encode, store, and recall information we perceived. As we experience the world, we sense stimuli, we witness events, we ascertain facts, we study concepts, and we acquire skills. Although memory is an innate and familiar human behaviour, the interior workings of the brain which provide us with such faculties are far from being fully unravelled. Experimental studies have shown that during memory tasks, certain brain structures exhibit synchronous activity in the theta and gamma bands, which is thought to be correlated with the short-term memory maintenance of salient stimuli. The objective of this thesis is to use biologically-inspired mathematical modelling and simulations of neural activity to shed some light on the mechanisms enabling the emergence of these memory-related synchronous oscillations. We focus in particular on hippocampal mnemonic activity during wake, and the amnesia and paradoxical memory consolidation occurring under propofol-induced general anaesthesia.

We begin our work by introducing a detailed model of a type of persistent-firing pyramidal neuron commonly found in the CA3 and CA1 areas of the hippocampus. Persistent firing is thought to be one of the mechanisms underlying active maintenance of stimuli in short-term and working memory. Our model neuron and its parameters are derived from experimental in-vitro recordings of persistent firing hippocampal neurons carried out by our collaborators Beate Knauer and Motoharu Yoshida at the Ruhr University in Bochum, Germany. The model captures all the specific characteristics of in-vitro intrinsic persistent firing. Stimulated with a brief transient current pulse, these neurons continue discharging action potentials after the stimulus ceases. This persistent activity is mediated by cholinergic calcium-activated non-specific (CAN) receptors and can last for long delay periods, in the order of several tens of seconds. Moreover, persistent firing is maintained solely by intrinsic cellular mechanisms, and does not require synaptic activity nor external stimulation.

Subsequently, we turn our attention to the dynamics of a population comprising such interconnected pyramidal-CAN neurons. We hypothesise that networks of persistent firing neurons could provide the neural mechanism for the maintenance of memory-related hippocampal oscillations. The firing patterns elicited by this network are in accord with both experimental recordings and modelling studies. In addition, the network displays self-sustained oscillatory activity in the theta frequency. When connecting the pyramidal-CAN network to fast-spiking inhibitory interneurons, the dynamics of the model reveal that feedback inhibition improves the robustness of fast theta oscillations, by tightening the synchronisation of the pyramidal CAN neurons. We demonstrate that, in the model, the frequency and spectral power of the oscillations are modulated solely by the cholinergic mechanisms mediating the intrinsic persistent firing, allowing for a wide range of oscillation rates within the theta band. This is a biologically plausible mechanism for the maintenance of synchronous theta oscillations in the hippocampus which aims at extending the traditional models of septum-driven hippocampal rhythmic activity.

In addition, we study the disruptive effects of general anaesthesia on hippocampal gamma-frequency oscillations to gain some insights on the mechanisms causing amnesia and sometimes memory formation in anaesthetised patients. Gamma oscillatory frequency range is often recorded in functionally-coupled brain regions for cooperation during memory tasks, and this rhythmic behaviour is thought to result from synaptic GABAergic interactions between interneurons. Interestingly, GABAergic synaptic and extrasynaptic receptors have been shown to be the preferred target of the most commonly used anaesthetic agents. We present an in-depth study of the action of anaesthesia on neural oscillations by introducing a new computational model which takes into account the four main effects of the anaesthetic agent propofol on GABAergic hippocampal interneurons. Our results indicate that propofol-mediated tonic inhibition contributes to an unexpected enhancement of synchronisation in the activity of a network of hippocampal interneurons. This enhanced synchronisation could provide a possible mechanism supporting the occurrence of intraoperative awareness, explicit memory formation, and even paradoxical excitation under general anaesthesia, by facilitating the communication between brain structures which should supposedly be not allowed to do so when

anaesthetised.

To complete this work, we developed a python library of ionic transmembranal currents to be assembled together to create template neurons and a library which acts as a wrapper for the simulation parameters. The purpose of these is to speed up simulation set-up time and reduce code duplication across simulation scripts. Both libraries are aimed at extending the functionality provided by the Brian simulator.

In conclusion, the findings described within this thesis provide new insights into the mechanisms underlying mnemonic neural activity, both during wake and anaesthesia, opening compelling avenues for future work. Understanding the neural processes behind memory formation is a paramount task for clinical applications tackling neurodegenerative memory diseases, and anaesthesia monitoring.

Keywords: memory, hippocampus, oscillations, general anaesthesia

Résumé

La mémoire est communément définie comme la capacité de coder, stocker et rappeler les informations que nous percevons. À mesure que nous éprouvons le monde, nous ressentons des stimuli, nous assistons à des événements, nous constatons des faits, nous étudions des concepts et nous acquérons des compétences. Bien que la mémoire soit un comportement humain inné et familier, les mécanismes cérébraux qui nous fournissent de telles facultés sont loin d'être entièrement démêlés. De nombreuses études expérimentales ont montré que, lors des tâches de mémoire, certaines structures cérébrales produisent une activité synchrone dans les bandes thêta et gamma, qui est censée être corrélée avec la maintenance à court terme de la mémoire des stimuli saillants. L'objectif de cette thèse est d'utiliser la modélisation mathématique biologiquement inspirée et la simulation d'activité neuronale pour éclairer les mécanismes permettant l'émergence de ces oscillations liées à la mémoire. Nous nous concentrons en particulier sur l'activité mnémonique de l'hippocampe pendant l'état éveillé, et l'amnésie et la consolidation de la mémoire paradoxale se produisant sous anesthésie générale induite par le propofol.

Nous commençons notre travail en introduisant un modèle détaillé d'un type de neurone pyramidal à tir persistant couramment trouvé dans les zones CA3 et CA1 de l'hippocampe. On pense que l'activité persistante puisse être l'un des mécanismes qui sous-tendent la maintenance active des stimuli dans la mémoire à court terme et la mémoire travail. Notre neurone modèle et ses paramètres sont dérivés d'enregistrements in vitro expérimentaux de neurones à tir persistants dans l'hippocampe, réalisés par nos collaborateurs Beate Knauer et Motoharu Yoshida à l'Université de la Ruhr à Bochum, en Allemagne. Le modèle capture toutes les caractéristiques spécifiques du tir persistant intrinsèque observé in vitro. Stimulés par une courte impulsion de courant transitoire, ces neurones continuent à décharger des potentiels d'action après l'arrêt de la stimulation. Cette activité persistante est médiée par des récepteurs non spécifiques cholinergiques activés par le calcium (CAN) et peuvent durer pour des longues périodes dans l'ordre de plusieurs dizaines de secondes. En outre, le tir persistant est maintenu uniquement par des mécanismes cellulaires intrinsèques, et ne nécessite pas d'activité synaptique ni stimulation externe.

Par la suite, nous attirons notre attention sur la dynamique d'une population de ces neurones pyramidaux-CAN interconnectés. Nous supposons que les réseaux de neurones à tir persistant pourraient fournir le mécanisme neuronal pour la maintenance des oscillations hippocampiques liées à la mémoire. Les patterns d'activité générés par ce réseau sont en accord avec les enregistrements expérimentaux et les études de modélisation. De plus, le réseau exposent une activité oscillante auto-soutenue dans la fréquence thêta. Lors de la connexion du réseau pyramidal-CAN à des interneurones inhibiteurs rapides, la dynamique du modèle révèle que l'inhibition rétroactive améliore la robustesse des oscillations thêta rapides, en resserrant la synchronisation des neurones pyramidaux-CAN. Nous démontrons que, dans le modèle, la fréquence et la puissance spectrale des oscillations sont modulées uniquement par les mécanismes cholinergiques médiant le tir persistant intrinsèque, permettant une large gamme de fréquences d'oscillation dans la bande thêta. Il s'agit d'un mécanisme biologiquement plausible pour la maintenance des oscillations thêta synchrones dans l'hippocampe qui vise à étendre les modèles traditionnels d'activité rythmique hippocampique entraînée par le septum.

En outre, nous étudions les effets perturbateurs de l'anesthésie générale sur les oscillations gamma dans l'hippocampe pour obtenir des aperçus sur les mécanismes provoquant l'amnésie et parfois la formation de la mémoire chez les patients anesthésiés. La gamme de fréquences oscillantes gamma est souvent enregistrée dans les régions cérébrales couplées fonctionnellement pour la coopération pendant les tâches de mémoire, et ce comportement rythmique résulte d'interactions synaptiques GABAergiques entre les interneurones. Fait intéressant, les récepteurs synaptiques et extrasynaptiques GABAergiques se sont avérés être la cible préférée des agents anesthésiques les plus couramment utilisés, et notamment du propofol. Nous présentons une étude approfondie de l'action de l'anesthésie sur les oscillations neuronales en introduisant un nouveau modèle computationnel

qui prend en compte les quatre principaux effets de l'agent anesthésique propofol sur les récepteurs $GABA_A$. Nos résultats indiquent que l'inhibition tonique médiée par le propofol contribue à une amélioration inattendue de la synchronisation de l'activité d'un réseau d'interneurones hippocampiques. Cette augmentation de synchronisation pourrait fournir un mécanisme possible pour l'apparition de la conscience intra-opératoire, de la formation explicite de la mémoire, et même d'une excitation paradoxale sous anesthésie générale, en facilitant la communication entre des structures cérébrales qui me devraient pas être autorisées à le faire lorsqu'elles sont anesthésiées.

Pour compléter ce travail, nous avons développé une bibliothèque de courants transmembraniques ioniques à assembler pour créer des neurones modèles ainsi qu'une bibliothèque qui gère les paramètres des simulations. Le but est d'accélérer le temps de configuration des simulations et de réduire la duplication de code sur les scripts de simulation. Les deux bibliothèques visent à étendre les fonctionnalités fournie par le simulateur Brian.

En conclusion, les résultats présentés dans cette thèse fournissent de nouvelles idées sur les mécanismes sous-jacents de l'activité neuronale mnémonique, à la fois au cours de l'éveil et sous anesthésie générale, en ouvrant des voies convaincantes pour des travaux futurs. Comprendre les processus neuronaux sous-jacents la formation de la mémoire est une tâche primordiale pour les applications cliniques qui s'attaquent aux maladies de la mémoire neurodégénératives et à la surveillance de l'anesthésie.

Mots-clés: mémoire, hippocampe, oscillations, anesthésie générale

Acknowledgements

I would like to thank my PhD advisors, Laure Buhry and Axel Hutt, for their help and supervision.

I would express sincere gratitude to my thesis committee – Thomas Boraud, Alain Destexhe, Valérie Louis-Dorr, and Nicolas Rougier – for taking their time to examine my manuscript and to attend my defence. Your questions and comments were as copious as they were invaluable.
I would like to thank Motoharu Yoshida for the fruitful discussions on the modelling aspects of hippocampal persistent firing, and for inviting me to his laboratory.
I am grateful to Laurent Bougrain and Dave Ritchie for always having some spare time for a chat during the last three years.

I would like to thank the entirety of Team Neurosys for having accompanied me so far.
I would like to thank my colleagues Maxime Clément, Mariia Fedotenkova, Iñaki Fernandez, Meysam Hashemi, Cecilia Lindig-León, Guillaume Serrière, Nicole Voges, and Nadjib Med Zennir for providing me with the chance to argue with every single one of you. I really needed that.
I would like to thank Laurence Benini, Isabelle Herlich, and Hélène Cavallini for their invaluable human and administrative support.
I would like to thank Tamara Tošić for teaching me that people take from you exactly what you choose to give them.
I would like to thank Rahaf Al-Chwa for teaching me to appreciate the simplicity in life.
I would like to thank Sébastien Rimbert for teaching me that, ultimately, we are all in the same boat.
I would like to thank Beate Knauer for motivating me to work when times were dire, as well as for sharing her expertise and, lastly, the electrophysiological data.

I would like to thank Guido Gigante for teaching me how to carry out research, although I should really blame him for dragging me into this evil world.
I would like to thank John Stonham for teaching me to never stop asking "Why?".

Finally, I thank my loving family and my friends for being present exactly the right amount.
I would like to thank Dionysios Kalantzis for teaching me to care.
I would like to thank Argyris Papadakis for teaching me to take life one step at a time.
I would like to thank Mohammad Rashid for teaching me to never stop pursuing dreams.
I would like to thank Simone Carnì for teaching me the true meaning of perseverance.
I would like to thank Carlo Pandini for teaching me what responsibility really is.
I would like to thank Filomena Cuseo for teaching me that love knows no borders.

Ringrazio mia nonna Maria per avermi insegnato a vivere la vita con freschezza e allegria.
Ringrazio mio nonno Paolo per avermi insegnato a puntare in alto.
Ringrazio mia nonna Gina per avermi insegnato la forza del sorriso di chi non molla mai di fronte alle difficoltà.
Ringrazio mio nonno Filippo per avermi insegnato che se uno fa qualcosa deve farla bene, altrimenti tanto varrebbe non fare niente.
Ringrazio mia madre Franca per avermi insegnato cosa sia l'amore incondizionato.
Ringrazio mio padre Marco per avermi insegnato, da buon rugbysta, l'impegno, la dedizione e il sacrificio.
Ringrazio mio fratello Filippo per avermi insegnato a prendere sempre la vita a mozzichi.
Ringrazio mio fratello Paolo per avermi insegnato ad essere paziente.

CONTENTS

LIST OF FIGURES

LIST OF TABLES

GLOSSARY

ACh: Acetylcholine
AHP: After Hyperpolarising Potential
AMPA: α-amino-3-hydroxy-5-methyl-4-isoxazolepropionic Acid

CA: Cornus Ammonis
CAN: Calcium-Activated Nonspecific
CAN-In: CAN-Inhibitory
Cch: Carbachol

DAP: Depolarising After Potential
DG: Dentate Gyrus

EC: Entorhinal Cortex
ECoG: Electrocorticography
EEG: Electroencephalography

fMRI: Functional Magnetic Resonance Imaging

GABA: γ-Aminobutyric Acid

LFP: Local Field Potential
LIF: Leaky Integrate-and-Fire

MEA: Multielectrode Array
MEG: Magnetoencephalography

NMDA: N-Methyl-D-aspartate

O-LM: Oriens Lacunosum-Moleculare

PCAN: Pyramidal CAN
PET: Positron Emission Tomography

SEEG: Stereoelectroencephalography

TRPC: Transient Receptor Potential Channel

RÉSUMÉ ETENDU

Introduction

Qui a été le premier homme à poser le pied sur la Lune, et quand est-ce arrivé? Que dit le théorème de Pythagore? Quand ai-je marqué mon premier essai de rugby? Comment contre-braque-t-on une moto? Répondre à chacune de ces questions nécessite de fonctions mnémoniques distinctes et de capacités qui reposent toutes sur une unité de traitement extrêmement complexe: le cerveau. Bien que la neuroanatomie du cerveau et la neurophysiologie des neurones composants les différentes structures du système nerveux central puissent être bien décrites, l'émergence de la cognition à partir de l'activité neurale reste à ce jour en grande partie un mystère.

La mémoire est communément définie comme la capacité de coder, stocker et rappeler les informations que nous percevons. À mesure que nous éprouvons le monde, nous ressentons des stimuli, nous assistons à des événements, nous constatons des faits, nous étudions des concepts et nous acquérons des compétences. Bien que la mémoire soit un comportement humain inné et familier, les mécanismes cérébraux qui nous fournissent de telles facultés sont loin d'être entièrement démêlés. De nombreuses études expérimentales ont montré que, lors des tâches de mémoire, certaines structures cérébrales produisent une activité synchrone dans les bandes thêta et gamma, qui est censée être corrélée avec la maintenance à court terme de la mémoire des stimuli saillants. L'objectif de cette thèse est d'utiliser la modélisation mathématique biologiquement inspirée et la simulation d'activité neuronale pour éclairer les mécanismes permettant l'émergence de ces oscillations liées à la mémoire. Nous nous concentrons en particulier sur l'activité mnémonique de l'hippocampe pendant l'état éveillé, et l'amnésie et la consolidation de la mémoire paradoxale se produisant sous anesthésie générale induite par le propofol.

Mémoire à long terme

Plusieurs systèmes de mémoire existent dans le cerveau [Eichenbaum and Cohen, 2004]. Ceux-ci peuvent être regroupés en deux macro-classes - court terme et long terme - en fonction de la durée et de la capacité de stockage des mémoires [Cowan, 2008]. La figure 1.1 illustre la subdivision des types de mémoire existants.

La mémoire à long terme peut durer des minutes jusqu'à une durée de vie, et peut être classifiée selon la façon dont elle est stockée et rappelée [Kandel et al., 2000b]. La mémoire implicite (non déclarative) est rappelée inconsciemment tandis que la mémoire explicite (déclarative) nécessite un effort délibéré et conscient pour être rappelée. Nous utilisons la mémoire implicite pour les tâches habituelles, par exemple attacher nos lacets, conduire une voiture ou même sourire. De telles actions procédurales ont été une fois apprises et sont depuis lors devenues coutumières au point qu'elles sont effectuées de façon quelque peu automatique. Inversement, la mémoire explicite stocke des faits, des concepts, des événements et des expériences, et est caractérisée par une connotation spatiotemporelle précise de l'information stockée. La mémoire déclarative peut être subdivisée en mémoire épisodique, qui sert à stocker les expériences personnelles passées [Baddeley, 2002, Tulving, 1985], et la mémoire sémantique, qui joue un rôle crucial dans l'apprentissage et le traitement de l'information [Martin and Chao, 2001].

Mémoire à court terme

La mémoire à court terme fait généralement référence à une mémoire à accès rapide et facilement disponible avec une capacité et une durée de stockage limitée. Bien qu'il y ait encore des controverses quant à sa durée exacte, la mémoire à court terme est généralement considérée comme ne durant que quelques dizaines de secondes [Revlin, 2012], prolongée à quelques minutes en s'appuyant sur des processus de contrôle attentifs tels que la répétition [Jonides et al., 2008]. Selon une théorie célèbre [Berman et al., 2009] la durée de la mémoire à court terme est sujette à une détérioration spontanée avec le temps. En effet, des études expérimentales ont montré qu'il existe une corrélation entre la durée du délai entre la présentation du stimulus et le rappel, et la dégradation des performances mnémoniques. Un autre point de vue répandu soutient que l'oubli est dû à des nouveaux stimuli – à stocker – en concurrence, c'est-à-dire interférant avec l'information déjà mémorisée [Lewandowsky et al., 2004, Nairne, 2002], et que les phénomènes de détérioration temporelle peuvent être réinterprétés en termes de ces interférences. [Lewandowsky et al., 2009].

En termes de capacité, l'opinion commune est que les systèmes de mémoire à court terme peuvent stocker un maximum de sept éléments plus ou moins deux [Miller, 1994], bien que cela semble être vrai principalement pour les nombres. En effet, les résultats des expériences de mémoire à court terme semblent indiquer que la capacité de ces systèmes de mémoire est affectée par la longueur des mots [Baddeley et al., 1975], la similitude phonologique [Baddeley et al., 1975], la fréquence d'apparition des mots dans un langage donné [Baddeley et al., 1975], et le groupement sémantique [Poirier and Saint-Aubin, 1995]. Enfin, la capacité et la persistance sont influencées par l'âge, la culture, la formation et le mode de vie des sujets testés.

Mémoire de travail

La mémoire à court terme fait partie intégrante de la mémoire de travail [Baddeley and Hitch, 1974, Baddeley, 2000]. Celle-ci est un système cognitif complexe combinant à la fois des capacités de stockage temporaire et de traitement de l'information. La mémoire de travail nous permet de conserver des informations pertinentes pour l'exécution d'actions futures dépendantes de ces informations [Fuster, 2008]. Bien que provenant d'un stimulus transitoire, l'information codée est considérée comme pertinente pour la tâche en cours et doit donc être maintenue en mémoire longtemps après la disparition du stimulus original.

On pense que la mémoire de travail joue un rôle de premier plan dans l'exécution des tâches hiérarchiquement structurées [Fuster, 2008] en fournissant les fonctionnalités nécessaires pour représenter et traiter les comportements orientés vers un but, sous forme de séquences ordonnées de sous-objectifs. Le comportement humain est intrinsèquement hiérarchique et, plus important encore, orienté vers un but. En effet, nos actions sont très rarement finies en elles-mêmes mais font toujours

partie d'un plan visant à atteindre un objectif spécifique. Cela est vrai pour toutes les tâches, que celles-ci soient simples, comme manger et boire ou des efforts plus complexes tels que la poursuite de notre bonheur. Un tel comportement intentionnel conduit finalement nos vies et les rend uniques.

Consolidation de la mémoire

La consolidation de la mémoire est le processus par lequel les traces de mémoire à court terme sont converties en souvenirs plus durables. On pense que trois formes distinctes mais complémentaires de processus de consolidation coexistent [Dudai, 2004] – à savoir, la consolidation synaptique, la consolidation des systèmes et la reconsolidation–chacun agissant à différentes échelles de temps et avec son propre but. Les processus de consolidation synaptique [Bramham and Messaoudi, 2005] comprennent le renforcement séquentiel des connexions entre les neurones, c'est-à-dire les synapses, contribuant à la représentation d'une information commune [Hebb, 1949]. Initialement, la libération de neurotransmetteurs du neurone présynaptique dans la fente synaptique et la sensibilité des récepteurs postsynaptiques à ces neurotransmetteurs augmente [Malenka and Bear, 2004, Sweatt, 1999]. Par la suite, l'expression génique et la synthèse des protéines [Dudai, 2002, Gold, 2008, Kandel, 2001] permettent la croissance de nouveaux terminaux synaptiques, qui produisent des réponses améliorées dans le neurone postsynaptique à mesure que l'absorption des neurotransmetteurs augmente. La potentialisation à long terme [Bliss and Lomo, 1973], dans ses formes précoces et tardives, est un excellent exemple d'un tel processus de consolidation synaptique.

Les processus de consolidation de systèmes [Roediger et al., 2007, Squire and Alvarez, 1995] impliquent le déplacement des traces de mémoire, initialement stockées dans des tampons temporaires, dans des zones spécifiques du cerveau pour un stockage à long terme. Selon le modèle standard, les traces de mémoire à consolider sont initialement codées et stockées dans le lobe temporal médian et dans l'hippocampe [McClelland et al., 1995, Roediger et al., 2007, Squire, 1987, Squire, 1992]. De là, les souvenirs sont déplacés dans le néocortex [Buzsáki, 1989, Hasselmo et al., 1996, Qin et al., 1997, Shen and McNaughton, 1994] sur de longues périodes de l'ordre de mois ou même d'années. Il existe des preuves convaincantes indiquant que cette forme de consolidation se produit pendant le sommeil [Maingret et al., 2016, Moroni et al., 2007, Reasor and Poe, 2008, Siegel, 2001, Stickgold, 2005, Walker et al., 2005], bien que les mécanismes derrière la consolidation de l'hippocampe-corticale soient loin d'être entièrement compris.

Enfin, la reconsolidation [Dudai, 2004, Tronson and Taylor, 2007] est considérée comme l'un des processus par lesquels les mémoires stockées sont maintenues et renforcées dans le temps, en particulier après le rappel. Des études expérimentales ont montré que la récupération des mémoires consolidées à long terme ouvre une fenêtre d'opportunité au cours de laquelle celles-ci pourraient être oubliées [Misanin et al., 1968, Nader et al., 2000, Rudy et al., 2006, Sara, 2000] pour faire place à de nouveaux souvenirs. Cela indique qu'une consolidation continue puisse être nécessaire pour les mémoires qui doivent être stockées plus longtemps.

Anesthésie générale

L'anesthésie générale est l'autre phénomène macroscopique que nous étudions dans le cadre du travail actuel, à côté de la mémoire. L'anesthésie générale est un coma réversible induit par un médicament, qui est couramment administré aux patients subissant une chirurgie en raison de ses propriétés souhaitables: perte de conscience, analgésie, immobilité et amnésie, toutes obtenues en préservant la stabilité physiologique [Brown et al., 2010]. En effet, après l'induction de l'anesthésie générale, les patients entrent dans un état de sédation durant lequel ils ne sont pas conscients de la chirurgie, ils ne perçoivent ni ne réagissent aux stimuli nocifs qui en dérivent et ne se souviennent pas de l'avoir subie. Bien qu'étant devenu un mode opératoire standard pendant la chirurgie –

aux Etats-Unis seulement, environ 60000 patients subissent une anesthésie générale tous les jours [Brown et al., 2010] – les mécanismes chimiques et neuronaux par lesquels ces effets sont obtenus ne sont pas encore complètement élucidés. Aujourd'hui, la recherche en anesthésiologie cherche encore à trouver des explications à plusieurs phénomènes survenant lors d'anesthésie générale, dont la plupart impliquent des effets indésirables. Ceux-ci incluent, et ne sont pas limités à, la conscience peropératoire [Ghoneim et al., 2009, Moerman et al., 1993, Ranta et al., 1998, Sandin et al., 2000, Schwender et al., 1998], la formation de mémoires implicites sous anesthésie générale [Andrade and Deeprose, 2007, Bonett et al., 2014, Cork et al., 1996, Ghoneim and Block, 1997, Jones, 1994, Kihlstrom et al., 1990], et l'excitation paradoxale [Bevan et al., 1997, Clark and Rosner, 1973, Gibbs et al., 1936, Kiersey et al., 1951, McCarthy et al., 2008, Rampil, 1998]. En fin de compte, l'objectif de la recherche en anesthésie est d'améliorer les soins aux patients. De plus, une littérature vaste et toujours plus importante (voir [Brown et al., 2010, Franks, 2008, Mueller et al., 2011] pour des revues approfondies) a récemment commencé à étudier la perte de conscience causée par l'anesthésie comme moyen indirect d'étudier et d'améliorer notre compréhension de la conscience [Alkire et al., 2008].

Oscillations neurales

Les oscillations neurales sont le produit de l'activité des cellules nerveuses rythmiques. Le rôle de ces oscillations a été abondamment décrit dans la littérature, donnant naissance à un certain nombre de théories stimulantes. Les oscillations neuronales peuvent représenter l'état stable et non perturbé du cerveau pendant le sommeil et peuvent également être utilisées comme indicateurs de certains stades du sommeil [Llinas and Ribary, 1993]. En outre, des études expérimentales ont lié l'activité synchrone avec la perception [Engel et al., 2001]; le codage et la représentation des stimuli [Gray et al., 1989]; et l'intégration de l'information et la mémoire [Axmacher et al., 2006, Engel et al., 2001, Kahana et al., 2001, Lisman, 2010, Lisman and Jensen, 2013, Varela et al., 2001]. Le dénominateur commun de toutes ces théories est l'hypothèse de la communication par la cohérence [Fries, 2005], selon laquelle une activité synchrone permet la communication et la coopération entre les ensembles neuronaux. En effet, il a été démontré que les régions cérébrales fonctionnellement liées synchronisent leur fréquence de fonctionnement lorsqu'elles collaborent sur des taches communes. Quelques exemples pourraient inclure, entre autres, les régions pariétales et occipitales pendant les tâches d'attention visuelle [Fries et al., 2001]; l'hippocampe et le cortex (pré) frontal pendant les tâches de mémoire [Fell et al., 2001] et la consolidation pendant le sommeil [Maingret et al., 2016]; le cortex moteur et les motoneurones spinaux pendant les tâches de mouvement [Conway et al., 1995].

Dans cette thèse, nous nous concentrons principalement sur le rôle des oscillations neuronales de l'hippocampe pour le maintien et la consolidation de la mémoire. Des travaux de recherche antérieurs ont établi que les oscillations de l'hippocampe sont impliquées dans l'exécution des tâches de mémoire [Colgin and Moser, 2010, Colgin, 2016, Howard et al., 2003, Lisman and Jensen, 2013, Nyhus and Curran, 2010, Osipova et al., 2006, Sederberg et al., 2007, van Vugt et al., 2010]. Ces études suggèrent que cette activité synchrone est impliquée dans le groupement et la liaison des composantes des stimuli multimodaux lors de l'encodage et de la récupération des mémoires [Colgin and Moser, 2010], ainsi que dans la communication rapide et la coordination entre ensembles neuraux [Fries, 2005]. De plus, on pense que les oscillations de l'hippocampe interviennent dans les processus de consolidation de la mémoire pendant le sommeil [Axmacher et al., 2006, Lega et al., 2012, Maingret et al., 2016, Power, 2004, Reasor and Poe, 2008, Walker, 2009]. Phénoménologiquement, les oscillations se produisent à différentes échelles et sont généralement regroupées dans des bandes de fréquence distinctes.

Les oscillations sont un phénomène multi-échelles

Les oscillations peuvent se produire à différentes échelles et sont pilotées par des mécanismes différents (pour une revue, voir [Wang, 2010]). Au niveau microscopique, il a été démontré que les neurones individuels présentaient des variations oscillatoires de leur potentiel membranaire. Celles-ci comprennent des oscillations sous-seuils et des motifs résonnants qui résultent souvent des interactions entre les courants transmembranaires [Alonso and Llinás, 1989, Llinas et al., 1991, Wang, 1993]. De plus, certains neurones produisent des oscillations [Llinas, 1988] sous la forme de séquences rythmiques de potentiels d'action, et sous forme de courtes rafales, définies comme de brefs clusters de potentiels d'action qui peuvent entraîner une activité oscillatoire dans leurs cibles postsynaptiques. Au niveau mésoscopique, les populations locales de neurones peuvent présenter des motifs de tir synchronisés [Hansel et al., 1995, Van Vreeswijk et al., 1994, Wang and Rinzel, 1993] par des décharges simultanées de potentiels d'action. Cette synchronisation dépend des interactions synaptiques et de la topologie du réseau, ainsi que des propriétés cellulaires intrinsèques. Enfin, au niveau macroscopique, il a été montré que plusieurs structures cérébrales synchronisent leur activité lorsqu'elles coopèrent sur une tâche commune [Conway et al., 1995, Fell et al., 2005, Fries, 2005], comme observé dans les électroencéphalogrammes. Ces observations indiquent que divers phénomènes oscillatoires existent dans le système nerveux central. Dans le cadre du travail actuel, nous employons le terme "oscillations neurales" pour désigner les phénomènes mésoscopiques et macroscopiques émergeant de l'activité neurale à l'échelle microscopique.

Bandes de fréquence d'oscillation

L'activité cérébrale oscillatoire a été observée à diverses fréquences, qui sont généralement classées dans des bandes distinctes observées principalement dans les enregistrements électroencéphalographiques. Les oscillations de fréquence Delta ($0.5 - 4\ Hz$) sont les oscillations identifiables les plus lentes. Elles sont caractérisées par des amplitudes élevées et sont considérées comme l'un des indicateurs du mouvement oculaire non-rapide (non-REM) lié au stade 3 du sommeil lent [Amzica and Steriade, 1998, Kalia, 2010]. Les oscillations thêta ($4 - 7\ Hz$ chez les humains, $4 - 11\ Hz$ chez les rongeurs) [Colgin, 2013, Vinogradova, 1995] sont remarquablement observées dans l'hippocampe [Colgin, 2016], une structure allocorticale située dans le lobe temporal médian. Chez l'homme, les rythmes thêta ont été corrélés avec la navigation [Ekstrom et al., 2005, Fenton et al., 2010, O'Keefe et al., 1998] et la mémoire [Hartley et al., 2007, Lega et al., 2012, Squire, 1992, Tesche and Karhu, 2000]. De même, chez les rats, ces oscillations jouent cependant un rôle important dans l'exploration et la navigation [Buzsáki and Moser, 2013], la localisation [O'Keefe and Recce, 1993, O'Keefe et al., 1998] et l'apprentissage [Colgin, 2013, Kahana et al., 2001]. Les oscillations alpha ($7,5 - 12,5\ Hz$) sont couramment observées dans les enregistrements d'électroencéphalographie (EEG) humaine lorsque les sujets sont éveillés, au repos et avec les yeux fermés [Adrian and Matthews, 1934], et ont été associés au ralenti et à l'inhibition descendante des zones corticales en l'absence de stimulation [Klimesch et al., 2007, Niedermeyer, 1997, Palva and Palva, 2007]. Les oscillations bêta ($12,5 - 30\ Hz$) sont couramment observées dans les enregistrements d'électroencéphalographie humaine lorsque les sujets sont éveillés les yeux ouverts, et sont associés à la phase de préparation précédant l'initiation des mouvements volontaires [Jasper and Penfield, 1949, Wang, 2010] et la réponse motrice suscitée [Lalo et al., 2007]. Enfin, les oscillations gamma ($30 - 100\ Hz$) ont été liées à l'attention [Hughes, 2008], à la mémoire [Lisman, 2010, Lisman and Jensen, 2013, Montgomery and Buzsáki, 2007, Sederberg et al., 2007], et même à la conscience [Gold, 1999, Vanderwolf, 2000].

Neurones biologiques

Les signaux électriques enregistrés à partir du cerveau proviennent de l'activité des neurones. Les cellules nerveuses (neurones) sont les principales unités de signalisation du système nerveux. Les neurones sont des cellules électriquement excitables capables de générer des signaux électriques et chimiques. Cette activité neurale électrochimique est le substrat sous-jacent de schémas d'activité plus complexes, tels que les oscillations, et finalement de comportements cognitifs, de perception et de mouvement. L'activité électrique des cellules nerveuses dépend de leur anatomie et des mécanismes physiologiques générant du courant.

Anatomie d'une cellule nerveuse

Un neurone typique peut être divisé en quatre régions morphologiquement distinctes: les dendrites, le corps cellulaire, l'axone et les terminaisons présynaptiques (Figure 1.2). Les dendrites sont effectivement les bornes d'entrée du neurone. Le corps cellulaire, ou soma, a une membrane perméable qui permet un flux d'ions bidirectionnel dans et hors de la cellule. Ce flux d'ions provoque une variation du potentiel membranaire, le rendant plus négatif ou plus positif en fonction de sa direction. Ces phénomènes sont connus sous le nom de repolarisation et dépolarisation (Figure 1.3), respectivement. Si un neurone est dépolarisé au-delà d'un certain seuil, il émet un signal électrique qui se propage le long de son axone vers ses terminaisons synaptiques. Le temps nécessaire au signal pour traverser le neurone et atteindre ses terminaisons synaptiques est appelé retard axonal. L'axone est recouvert d'une gaine de myéline qui agit comme un isolant augmentant la vitesse à laquelle le signal se déplace. Ce potentiel d'action, ou spike (Figure 1.3), est le moyen par lequel le cerveau reçoit, traite et transmet l'information [Kandel et al., 2000a].

Après qu'un neurone ait émis un spike, son potentiel membranaire chute en dessous du potentiel de repos (Figure 1.3). Ce phénomène est connu comme hyperpolarisation. Le temps d'hyperpolarisation détermine la période réfractaire absolue du neurone. Celle-ci est un intervalle de temps pendant lequel le neurone ne tirera pas, quelque soit l'ampleur de la stimulation. La période réfractaire absolue est suivie de la période réfractaire relative pendant laquelle le neurone ne peut tirer que s'il est excité par des stimuli plus forts que ceux normalement requis au potentiel de repos [Kandel et al., 2000c].

Synapses

Les cellules nerveuses communiquent en établissant des connexions connues sous le nom de synapses. Celles-ci se produisent à la jonction entre les branches axonales du neurone présynaptique et les dendrites du neurone postsynaptique (Figure 1.4). Cependant, les neurones présynaptiques et postsynaptiques ne se touchent pas physiquement mais sont séparés par un espace connu sous le nom de fente synaptique. Lorsqu'un potentiel d'action atteint le terminal axonal, il provoque la libération de neurotransmetteurs du neurone présynaptique dans la fente synaptique. Les neurotransmetteurs sont des produits chimiques qui se lient à leurs récepteurs respectifs dans les dendrites post-synaptiques provoquant l'activation de la synapse. Les récepteurs médient l'ouverture et la fermeture des canaux perméables transmembranaires, contrôlant ainsi efficacement le flux d'ions dans et hors de la membrane [Kandel and Siegelbaum, 2000].

Neurotransmetteurs

Les neurones peuvent être classés en deux types principaux – excitateurs et inhibiteurs – en fonction de l'effet qu'ils ont sur les neurones vers lesquels ils projettent. Un neurone présynaptique excitateur

renforcera l'activité de ses neurones postsynaptiques. D'un autre côté, un neurone inhibiteur fera diminuer l'activité de ses neurones postsynaptiques. Ce comportement est dû à l'effet des différents neurotransmetteurs libérés par ces types de neurones.

Les neurotransmetteurs excitateurs et leurs récepteurs

Le principal neurotransmetteur excitateur est l'acide L-glutamate, communément connu sous le nom de glutamate [Kandel and Siegelbaum, 2000]. Le glutamate se lie à des récepteurs postsynaptiques spécifiques. Ceux-ci peuvent être de trois sortes: AMPA, kaïnate ou NMDA (Figure 1.5). Lorsque le glutamate se lie à un récepteur AMPA ou kaïnate, il provoque l'ouverture partielle du canal. Cela permet un écoulement vers l'extérieur des ions potassium intracellulaires (K^+) et un flux vers l'intérieur des ions sodium extracellulaires (Na^+). Une liaison supplémentaire de molécules de glutamate induit une ouverture supplémentaire du canal récepteur.

Le glutamate se lie également aux récepteurs NMDA qui contrôlent le flux des ions K^+ vers l'extérieur et du calcium (Ca^{2+}) ainsi que du Na^+ vers l'intérieur de la membrane cellulaire. Cette interaction neurotransmetteur-récepteur ressemble celle des récepteurs AMPA et kaïnate. Une fois complètement ouvert, cependant, les ions ne peuvent pas traverser le canal NMDA. Ceci est dû à un bloc de magnésium (Mg^{2+}), dépendant de la tension de membrane, qui se trouve à l'intérieur du canal. Le bloc est levé une fois que la membrane postsynaptique se dépolarise suffisamment pour réduire l'affinité entre le Mg^{2+} et son site de liaison à l'intérieur du canal [Kandel and Siegelbaum, 2000].

L'acétylcholine (ACh) est un neurotransmetteur agissant à la fois sur le système nerveux périphérique et central, dont le rôle principal est de médier l'excitation des neurones postsynaptiques. Cette neurotransmission cholinergique a comme effet d'améliorer la transmission glutamatergique augmentant ainsi l'excitabilité neuronale dans diverses zones du cerveau [Gil et al., 1997, Giocomo and Hasselmo, 2005, Radcliffe et al., 1999, Gioanni et al., 1999]. L'acétylcholine se lie à des récepteurs ligand-dépendants gouvernant le flux de cations transmembranaires et à des récepteurs métabotropiques médiant divers événements intracellulaires à l'aide de seconds messagers.

Les neurotransmetteurs inhibiteurs et leurs récepteurs

Les synapses inhibitrices sont activées par la libération de l'acide γ-Aminobutyrique (GABA) dans la fente synaptique qui se lie à ses récepteurs dédiés. Il existe deux classes connues de récepteurs GABA, à savoir $GABA_A$ [Henschel et al., 2008, Johnston, 1996] et $GABA_B$ [Chen et al., 2005, Hill and Bowery, 1981]. Les récepteurs $GABA_A$ sont des récepteurs ionotropes ligand-dépendants qui contrôlent le flux de Cl^- dans la membrane cellulaire. Les récepteurs de $GABA_B$ sont des récepteurs métabotropiques qui sont couplés à des canaux potassiques via des protéines G qui contrôlent l'écoulement de K^+ hors de la membrane cellulaire.

Potentiels postsynaptiques

Le flux d'ions bidirectionnel à travers la membrane neuronale postsynaptique génère un courant postsynaptique qui peut être soit excitateur (EPSC) ou inhibiteur (IPSC) en fonction du type de synapse. Une synapse excitatrice activée provoque l'écoulement des ions chargés positivement (Na^+ et/ou Ca^{2+}) dans la membrane postsynaptique induisant ainsi un courant positif. Inversement, une synapse inhibitrice provoque un flux vers l'extérieur d'ions chargés positifs (K^+) et un flux vers l'intérieur d'ions chargés négativement (Cl^-), qui à son tour induit un courant transmebranaire négatif. Les dépolarisations provoquées par ces courants sont appelées potentiel postsynaptique excitateur (EPSP) et inhibiteur (IPSP) respectivement (Figure 1.7A et Figure 1.7B).

La genèse des potentiels d'action et la propagation des signaux électriques neuronaux peuvent être modélisées avec précision à l'aide d'équations mathématiques. Plusieurs modèles ont été proposés depuis la première moitié du 20ème siècle. En général, les modèles fournissent des cadres détaillés pour étudier la dynamique des systèmes biologiques.

Modélisation mathématique de l'activité neuronale

La modélisation mathématique [Abbott, 2008, Churchland et al., 1990, Gerstner et al., 2012] des neurones est un outil puissant pour les neuroscientifiques, qui peut être utilisé pour simuler l'activité neuronale et les processus cognitifs à différents niveaux de réalisme biologique. Les modèles sont particulièrement utiles lorsque les expériences *in vivo* et *in vitro* sont impraticables, que ce soit pour des raisons technologiques ou pour des raisons éthiques. L'un des principaux objectifs de la recherche en neuroscience est d'expliquer les mécanismes neuronaux sous-jacents aux comportements cognitifs. En d'autres termes, nous cherchons à comprendre comment les signaux électrochimiques générés par les cellules nerveuses interconnectées, regroupées anatomiquement dans les régions du cerveau, contribuent à l'activation de la cognition, de la perception et du mouvement. Intuitivement, cela implique de corréler les phénomènes observés à différentes échelles – des synapses et des neurones individuels aux régions cérébrales –, ce qui en soi est une tâche complexe. Ces échelles comprennent, de l'échelle microscopique à l'échelle macroscopique, les processus moléculaires se produisant au niveau synaptique, l'électrophysiologie des neurones individuels, le potentiel électrique cumulatif généré par les assemblages cellulaires et les structures cérébrales, et le comportement de haut niveau qui en résulte.

Heureusement, les techniques expérimentales modernes nous permettent d'enregistrer des signaux électrophysiologiques à ces différentes échelles neuronales [Buzsáki, 2004, Engel et al., 2005, Huster et al., 2012], bien que à ce jour les enregistrements à plusieurs échelles contemporainement restent un défi. Au niveau microscopique, les enregistrements intracellulaires par "voltage-clamp", "current-clamp" et "patch-clamp" [Sakmann and Neher, 1984, Hamill et al., 1981] et les électrodes "sharp" sont couramment utilisés pour étudier la dynamique moléculaire au niveau cellulaire, y compris le fonctionnement des récepteurs et des canaux ioniques, ainsi comme l'activité de spiking des neurones. De plus, les micropipettes et les microélectrodes insérées dans le tissu cérébral peuvent être suffisamment fines pour détecter simultanément l'activité extracellulaire d'un seul neurone [Boulton et al., 1990] et de plusieurs unités, en fonction de la taille de l'électrode et du nombre d'électrodes insérées. Cependant, dans cette configuration, localiser précisément la source de l'activité électrique devient un défi dont le succès dépend fortement de la mise en place des électrodes. C'est-à-dire que les méthodes de clamp sont à ce jour les méthodes les plus spatialement précises pour enregistrer l'activité des neurones individuels puisque l'on peut contrôler la position exacte de la cellule dans laquelle l'électrode a été insérée.

Au niveau mésoscopique, les enregistrements extracellulaires multi-unités collectent l'activité de plusieurs cellules proches et sont principalement réalisées en utilisant des réseaux multi-électrodes (MEA) contenant plus de 100 électrodes pour des applications in-vivo et plus de 10000 pour des applications in-vitro (voir [Spira and Hai, 2013] pour une revue des techniques d'enregistrement les plus récentes). La possibilité d'enregistrer à partir de plusieurs sources vient à la compromission de la résolution spatiale réduite et le bruit accru dans le signal, puisque les contributions individuelles de chaque cellule et de la matière extracellulaire environnante sont fusionnées en une seule trace. Une technique plus précise implique des enregistrements de patch-clamp multi-unités qui, bien que possibles [Vardi et al., 2016], nécessitent des montages coûteux et, souvent, des systèmes de positionnement d'électrodes assistés par ordinateur. Néanmoins, les avancées technologiques récentes ont permis le développement de systèmes d'enregistrement combinant l'avantage des MEA extracellulaires et des microélectrodes intracellulaires [Spira and Hai, 2013].

Le niveau macroscopique comprend des enregistrements électrocorticographiques (ECoG) invasifs [Palmini, 2006] qui utilisent une grille d'électrodes sphériques placée sur le cortex juste au-dessous de la dure-mère, et l'électroencéphalographie non invasive [Niedermeyer and Lopes da Silva, 2005] qui utilise des électrodes placées sur le cuir chevelu. Aucune de ces techniques n'utilise des électrodes de type aiguille, c'est-à-dire qu'aucun perçage de la matière cérébrale n'est requis. Clairement, être plus éloigné de la source du signal enregistré signifie que ces techniques ont une résolution spatiale limitée [Asano et al., 2005, Kondylis et al., 2014] par rapport aux techniques d'enregistrement mésoscopique et microscopique, l'ECoG étant légèrement meilleur que l'EEG. Néanmoins, leur invasivité limitée ainsi que leur résolution temporelle (de l'ordre de la milliseconde) les rendent extrêmement utiles dans les applications cliniques et la recherche sur l'homme. L'EEG peut également être enregistrée par voie intracrânienne en utilisant des électrodes profondes implantées dans le tissu cérébral. Cette technique s'appelle la stéréoélectroencéphalographie (SEEG) [Talairach et al., 1974] et est couramment utilisée cliniquement pour identifier l'emplacement présumé du foyer de l'activité épileptiforme [Cossu et al., 2005]. De plus, l'imagerie par résonance magnétique fonctionnelle (IRMf) [Huettel et al., 2009, Logothetis et al., 2001] et la tomographie par émission de positrons (PET) [Bailey et al., 2004] peuvent être utilisées pour enregistrer l'activité cérébrale lors des expériences comportementales, en repérant l'augmentation du flux sanguin vers les structures cérébrales, et la distribution de produits chimiques étiquetés radioactivement dans les aires impliquées dans les taches cognitives. La magnétoencéphalographie (MEG) [Hämäläinen et al., 1993] est une autre technique d'imagerie fonctionnelle qui enregistre le champ magnétique résultant des courants ioniques générés par l'activité cérébrale électrique sous-jacente [Buzsáki, 2006]. Puisque EEG et MEG enregistrent les sources complémentaires de signaux similaires, l'enregistrement simultané des enregistrements EEG et MEG s'est révélé être une technique prometteuse dans la recherche neuroscientifique [Sharon et al., 2007].

Combler le fossé entre les échelles neurales micro, méso et macroscopiques est l'un des rôles fondamentaux de la modélisation mathématique. Au niveau microscopique, les modèles computationnels peuvent reproduire des interactions moléculaires et synaptiques, ainsi que des potentiels d'action [Izhikevich, 2004]. De plus, grâce à des simulations sur ordinateur, les chercheurs peuvent assembler artificiellement des populations neuronales [Wilson and Cowan, 1972], et même des structures cérébrales, pour étudier leur activité déclenchée aux échelles mésoscopique et macroscopique. Cela permet de générer des ensembles de données synthétiques qui peuvent compléter les enregistrements expérimentaux, qui sont souvent rares ou difficiles à obtenir. De plus, les modèles computationnels permettent aux neuroscientifiques de tester artificiellement des hypothèses avant de les tester expérimentalement. Enfin, la modélisation est un moyen d'étudier les phénomènes neurophysiologiques qui sont capturés par des techniques d'enregistrement.

Modèles mathématiques des neurones biologiques

Plusieurs modèles mathématiques de neurones existent et ont été largement décrits et utilisés dans la littérature (voir [Izhikevich, 2007] pour une revues approfondie). Ceux-ci présentent différents degrés de réalisme biologique, souvent obtenus par une modélisation détaillée des courants ioniques transmembranaires individuels. Le degré de réalisme biologique vient souvent au prix d'une augmentation de la complexité de calcul du modèle, qui à son tour affecte les ressources de calcul nécessaires pour simuler son activité. De plus, des modèles très complexes comportant de nombreuses équations différentielles deviennent lourds à analyser d'un point de vue dynamique [Izhikevich, 2007]. Malheureusement, le modèle optimal à choisir n'existe pas. Au contraire, un choix dépendant de la tâche doit être fait en gardant à l'esprit le compromis entre le réalisme biologique requis et l'efficacité computationnelle.

En général, un neurone biologique peut être modélisé avec un ensemble d'équations différentielles ordinaires qui décrivent l'évolution du potentiel membranaire du neurone au cours du temps [Dayan

and Abbott, 2001], comme produit du courant transmembranaire et de la résistance membranaire (selon la loi d'Ohm):

$$\frac{\mathrm{d}V_m}{\mathrm{d}t} = I_m \cdot R_m = \frac{I_m}{C_m} \tag{1}$$

où V_m est le potentiel membranaire, I_m est le courant ionique net circulant à travers la membrane, R_m est la résistance membranaire, et C_m est sa réciproque, c'est-à-dire la conductance membranaire. Par conséquent, les cellules nerveuses sont représentées comme un circuit résistance-condensateur, capable d'accumuler et de décharger des charges électriques. Les neurones individuels peuvent ensuite être connectés, en modélisant des interactions synaptiques, afin de simuler et d'étudier le comportement des populations neuronales.

Leaky Integrate-and-Fire

Le modèle "Leaky Integrate-and-Fire" (LIF) [Lapique, 1907, Stein, 1967, Tuckwell, 1988] se situe à l'extrémité inférieure du spectre du réalisme biologique et a de faibles coûts de calcul en raison de sa simplicité. Il comprend une seule équation différentielle sous la forme:

$$C_m \cdot \frac{\mathrm{d}V_m}{\mathrm{d}t} = I_{stim} - \frac{V_m}{R_m} \tag{2}$$

où I_{stim} est le courant de stimulation appliqué. Le potentiel membranaire se dépolarise au cours du temps tant que $I_{stim} > V_m/R_m$. Lorsque V_m dépasse un seuil V_θ défini par l'utilisateur, un spike est enregistré et le potentiel de la membrane est réinitialisé à sa valeur de repos (généralement $0\,mV$). Inversement, si $I_{stim} < V_m/R_m$, le potentiel membranaire décroît lentement. Les potentiels d'action générés par le modèle LIF sont instantanés et n'ont ni largeur ni morphologie.

Hodgkin-Huxley

D'autre part, le modèle de Hodgkin-Huxley [Hodgkin and Huxley, 1939, Hodgkin and Huxley, 1952] fournit le degré le plus élevé de réalisme biologique, bien que cela ait un coût de calcul élevé. Ce modèle représente le taux de variation du potentiel membranaire V_m en fonction du courant dendritique d'entrée total et des courants ioniques:

$$C_m \cdot \frac{\mathrm{d}V_m}{\mathrm{d}t} = -I_i + I_{stim} \tag{3}$$

où I_{stim} est le courant de stimulation appliqué, et I_i est le courant ionique transmembranaire total qui peut être encore divisé dans la fuite, et les composants sodium et potassium:

$$I_i = I_l + I_{Na} + I_K \tag{4}$$

Chaque courant ionique peut être exprimé en termes de sa conductance ionique en utilisant des équations de la forme:

$$I_l = \overline{g}_l \cdot (V_m - E_l) \tag{5}$$
$$I_{Na} = \overline{g}_{Na} \cdot m^3 \cdot h \cdot (V_m - E_{Na}) \tag{6}$$
$$I_K = \overline{g}_K \cdot n^4 \cdot (V_m - E_K) \tag{7}$$

où V_m est le potentiel de la membrane, $\overline{g}_K$, $\overline{g}_{Na}$, et $\overline{g}_l$ sont la conductance ionique maximale, et E_K, E_{Na}, et E_l représentent respectivement le potentiel de repos des canaux de potassium, de sodium et de fuite. m et n sont des variables décrivant l'activation des canaux potassiques et sodiques, et h est une variable décrivant l'inactivation du canal sodique. Ceux-ci sont régis par un ensemble d'équations différentielles ordinaires sous la forme:

$$\frac{\mathrm{d}x}{\mathrm{d}t} = \alpha_x \cdot (1 - x) - (\beta_x \cdot x) \tag{8}$$

pour $x \in \{ h, n, m \}$, où α_x et β_x sont des fonctions décrivant la dynamique stationnaire et temporelle des variables d'activation et d'inactivation. Par conséquent, le modèle standard de Hodgkin-Huxley comprend quatre équations différentielles ordinaires: $\mathrm{d}V_m/\mathrm{d}t$, $\mathrm{d}m/\mathrm{d}t$, $\mathrm{d}h/\mathrm{d}t$ et $\mathrm{d}n/dt$.

En outre, le modèle de neurones de Hodgkin-Huxley peut être étendu en ajoutant d'autres types de canaux ioniques, et les courants qu'ils imprègnent. Cela permet aux neuroscientifiques computationnels de disposer d'un outil puissant leur permettant de modéliser virtuellement tous les neurones biologiques existants et leur comportement. Puisqu'une partie du travail présenté ici impliquait la modélisation précise de l'électrophysiologie d'un type particulier de neurone hippocampique, nous nous sommes appuyés sur le modèle de Hodgkin-Huxley pour obtenir le plus haut degré de réalisme et un contrôle précis de l'influence des courants ioniques transmembranaires individuels sur le potentiel de la membrane cellulaire.

Modèles à deux variables simplifiés

Un effort considérable a été consacré à la simplification du modèle de Hodgkin-Huxley, en réduisant sa dimensionnalité, tout en essayant de maintenir le plus haut degré possible de réalisme biologique. Des exemples de modèles simplifiés incluent, sans s'y limiter, le modèle FitzHugh-Nagumo [FitzHugh, 1961, Nagumo et al., 1962], le modèle Morris-Lecar [Morris and Lecar, 1981], le modèle adaptatif et intégratif exponentiel [Brette and Gerstner, 2005], et le modèle Izhikevich [Izhikevich, 2003]. Tous ces modèles sont bidimensionnels et donc beaucoup plus simples que le Hodgkin-Huxley d'un point de vue informatique.

Simulateurs de réseau de neurones à impulsions

Comme nous l'avons vu, les modèles de neurones à impulsions sont généralement représentés par un système d'équations différentielles ordinaires. Résoudre analytiquement ces équations n'est souvent pas une tâche viable, et parfois même une entreprise impossible. Cependant, les solutions aux équations différentielles peuvent être approchées par le biais de l'intégration numérique, en utilisant des méthodes bien connues telles que la méthode Euler [Euler, 1768] ou Runge-Kutta [DeVries, 1994], entre autres.

Il existe plusieurs simulateurs de réseau de neurones spiking [1], qui s'appuient sur ces techniques d'intégration numérique pour simuler l'activité neurale. En outre, ces simulateurs sont pré-emballés avec un ensemble de fonctions permettant au neuroscientifiques computationnels de définir précisément les paramètres du modèle de neurone individuel, de spécifier les interactions synaptiques et la topologie du réseau, et de modifier les paramètres de simulation généraux. Pour les besoins de cette thèse, nous avons utilisé le simulateur Brian [2] en raison de sa facilité d'utilisation intuitive.

[1] La liste de tous les simulateurs existants serait hors de portée de ce travail. Cependant, le lecteur intéressé peut trouver une liste à jour à l'adresse suivante: https://grey.colorado.edu/emergent/index.php/Comparison_of_Neural_Network_Simulators

[2] Le simulateur Brian peut être trouvé à l'adresse suivante: http://briansimulator.org/

Les objectifs de cette thèse

Dans le tout premier paragraphe de ce manuscrit, nous avons posé quatre questions. Qui a été le premier homme à poser le pied sur la Lune, et quand est-ce arrivé? Que dit le théorème de Pythagore? Quand ai-je marqué mon premier essai de rugby? Comment contrecarre-t-on une moto? Répondre à chacune de ces questions nécessite des processus et des capacités mnémoniques distincts. En particulier, le premier homme à avoir posé le pied sur la Lune fut le cosmonaute américain Neil Armstrong le 21 juillet 1969 – mémoire sémantique explicite d'un fait. Le théorème de Pythagore dit que, étant donné un triangle rectangle avec les côtés a b et c, le carré de l'hypoténuse (c) est égal à la somme des carrés des deux autres côtés (a et b): $c^2 = a^2 + b^2$ – mémoire sémantique explicite d'un concept. J'ai marqué mon premier essai de rugby à un moment lors de ma saison des moins de 15 ans dans mon équipe locale de rugby à Milan – mémoire épisodique explicite d'une expérience. Le contre-braquage est réalisé en dirigeant la moto à l'opposé de la direction dans laquelle on veut tourner, de façon à l'amener à se pencher vers la direction du virage – mémoire procédurale implicite d'une compétence. Ces capacités mnémoniques distinctes reposent toutes sur une unité de traitement extrêmement complexe: le cerveau. Bien que la neuroanatomie du cerveau et la neurophysiologie des neurones composant les différentes structures du système nerveux central puissent être largement décrites, l'émergence de la cognition à partir de l'activité neuronale demeure largement inconnue.

Dans cette thèse, nous nous posons une question de recherche fondamentale: quels sont les mécanismes neuronaux sous-jacents à la mémoire? En particulier, nous nous concentrons sur l'activité mnémonique de l'hippocampe au réveil et sur l'amnésie et la consolidation paradoxale de la mémoire sous anesthésie générale induite par le propofol. Nous émettons l'hypothèse que des réseaux de neurones à décharge persistante pourraient fournir le mécanisme neuronal pour le maintien des oscillations de l'hippocampe liées à la mémoire. En effet, le tir persistant est considéré comme l'un des substrats neuraux pour le maintien de la mémoire, et ces neurones se trouvent généralement dans l'hippocampe, une structure cérébrale qui a été impliquée dans la mémoire.

En outre, nous étudions l'effet amnésique de l'anesthésie, ce qui nous permet d'aborder la question fondamentale mentionnée ci-dessus d'un point de vue différent. Nous faisons l'hypothèse que la compréhension de la façon dont les anesthésiques inhibent la consolidation de la mémoire pourrait nous permettre de faire la lumière sur ces processus de consolidation. En effet, il a été montré que les agents anesthésiques perturbent la synchronisation neuronale, et ceci est supposé être l'un des mécanismes par lesquels l'amnésie est atteinte. Cependant, en raison de l'apparition de la conscience peropératoire, de l'excitation paradoxale et parfois de la formation implicite de la mémoire sous anesthésie générale, nous émettons l'hypothèse qu'à certaines doses anesthésiques, la synchronisation neurale pourrait ne pas être affectée, voire même améliorée. Nous concevons de nouveaux modèles mathématiques de neurones biologiques et d'activité neuronale pour tester nos hypothèses.

Pour compléter ce travail, nous avons développé une bibliothèque de courants transmembranaires ioniques en Python à assembler pour créer des neurones modèles et une bibliothèque qui sert de wrapper pour les paramètres de simulation. L'objectif est d'accélérer le temps de mise en place des simulations et de réduire la duplication du code dans les scripts de simulation. Les deux bibliothèques visent à étendre la fonctionnalité fournie par le simulateur Brian, et sont disponibles gratuitement en ligne[3].

Notre travail a été réalisé à Inria[4] et au Loria[5] dans l'équipe de recherche Neurosys[6], un groupe multidisciplinaire travaillant sur les neurosciences des systèmes à différentes échelles neuronales.

[3] Les bibliothèques se trouvent aux adresses suivantes: https://github.com/JoErNanO/brianmodel and https://github.com/JoErNanO/briansims

[4] http://www.inria.fr

[5] http://www.loria.fr

[6] http://neurosys.loria.fr/

Nous avons collaboré avec Beate Knauer et Motoharu Yoshida à l'Université de la Ruhr à Bochum, en Allemagne, qui ont réalisé les enregistrements expérimentaux in vitro des neurones à décharge persistante utilisés pour dériver les paramètres de notre modèle. Les découvertes décrites dans cette thèse fournissent de nouvelles perspectives sur les mécanismes sous-jacents à l'activité neuronale mnémonique, à la fois pendant le réveil et l'anesthésie, ouvrant des voies intéressantes pour le travail futur. Comprendre les processus neuronaux derrière la formation de la mémoire est une tâche primordiale pour les applications cliniques traitant des maladies de la mémoire neurodégénératives, et la surveillance de l'anesthésie.

Structure du manuscrit

Ce manuscrit comprend six chapitres. Le premier chapitre est l'actuel qui définit la portée générale de notre travail. Le chapitre 2 présente un aperçu de notre compréhension actuelle des phénomènes neuroscientifiques que nous étudions. En outre, nous passons en revue les théories existantes et les modèles mathématiques de l'activité neurale liée à la mémoire. Au chapitre 3, nous décrivons en détail notre modèle mathématique et les outils de calcul que nous avons utilisés pour mesurer la synchronisation du réseau, pour identifier la fréquence et la puissance des oscillations et pour analyser les données.

Le chapitre 4 présente notre étude computationnelle des oscillations thêta auto-entretenues dans l'hippocampe. Nous introduisons d'abord un nouveau modèle neuronal inspiré par la biologie qui capture les caractéristiques des neurones à décharge persistante communément trouvés dans l'hippocampe. Nous émettons l'hypothèse que ces neurones pourraient jouer un rôle important dans la génération et le maintien des oscillations de l'hippocampe liées à la mémoire, en raison de leurs propriétés électrophysiologiques et de leurs comportements de spiking. De plus, nous étudions la dynamique d'un réseau de ces neurones hippocampiques à tir persistant et illustrons comment les courants intrinsèques permettent au réseau de s'autosynchroniser dans la bande thêta. Nous démontrons que, dans le modèle, la fréquence et la puissance spectrale des oscillations sont modulées uniquement par les mécanismes cholinergiques qui induisent une activation persistante, permettant une large gamme de fréquences d'oscillation dans la bande thêta. Ceci est un mécanisme biologiquement plausible pour le maintien des oscillations thêta synchrones dans l'hippocampe, qui vise à étendre les modèles traditionnels de l'activité rythmique hippocampique guidée par le septum.

Dans le chapitre 5, nous discutons de nos résultats concernant les effets perturbateurs de l'anesthésie générale sur les oscillations gamma dans l'hippocampe, pour avoir un aperçu des mécanismes causant l'amnésie, et parfois la formation de la mémoire chez les patients anesthésiés. La gamme de fréquences oscillatoires gamma est souvent enregistrée dans des régions cérébrales couplées fonctionnellement pour une coopération pendant les tâches de mémoire. Nous présentons une étude approfondie de l'action de l'anesthésie sur les oscillations neuronales en introduisant un nouveau modèle de calcul qui prend en compte les quatre principaux effets de l'agent anesthésique propofol sur les interneurones de l'hippocampe. Nos résultats indiquent que l'inhibition tonique induite par le propofol contribue à une amélioration inattendue de la synchronisation de l'activité d'un réseau d'interneurones de l'hippocampe. Cette synchronisation améliorée pourrait fournir un mécanisme possible supportant l'apparition de la conscience peropératoire, la formation explicite de la mémoire et même l'excitation paradoxale sous anesthésie générale, en facilitant la communication entre les structures cérébrales qui ne devraient pas être autorisées à le faire lorsqu'elles sont anesthésiées.

Enfin, au chapitre 6, nous résumons nos constatations et soulignons nos contributions. Nous identifions et suggérons également des pistes potentielles pour les travaux futurs.

CHAPTER

1

INTRODUCTION

Contents

1.1 Memory

Who was the first man to set foot on the Moon, and when did it happen? What does the Pythagorean theorem state? When did I score my first rugby try? How does one countersteer a motorcycle? Answering each one of these questions requires distinct mnemonic functions and capabilities which

all rely on one extremely complex processing unit: the brain. Although the neuroanatomy of the brain and the neurophysiology of the neurons composing the different structures of the central nervous system might be well described, to date, the emergence of cognition from neural activity remains largely a mystery.

Memory is commonly defined as the ability to encode, store, and recall information we perceived. As we experience the world, we sense stimuli, we witness events, we ascertain facts, we study concepts, and we acquire skills. Although memory is an innate and familiar human behaviour, the interior workings of the brain which provide us with such faculties are far from being fully unravelled. Experimental studies have shown that during memory tasks, certain brain structures exhibit synchronous activity in the theta and gamma bands, which is thought to be correlated with the short-term memory maintenance of salient stimuli. The objective of this thesis is to use biologically-inspired mathematical modelling and simulations of neural activity to shed some light on the mechanisms enabling the emergence of these memory-related synchronous oscillations. We focus in particular on hippocampal mnemonic activity during wake, and the amnesia and paradoxical memory consolidation occurring under propofol-induced general anaesthesia.

1.1.1 Long-Term Memory

Several different memory systems exist within the brain [Eichenbaum and Cohen, 2004]. These can be grouped into two macro classes – short-term and long-term – depending on the duration and the capacity of the memory storage [Cowan, 2008]. Figure 1.1 illustrates the subdivision of existing memory types.

Long-term memory can last for minutes up to a lifetime, and can be further classified according to how it is stored and recalled [Kandel et al., 2000b]. Implicit (non-declarative) memory is recalled unconsciously whereas explicit (declarative) memory needs a deliberate, conscious effort to be recalled. We use implicit memory for habitual tasks, for example tying our shoelaces up, driving a car or even smiling. Such procedural actions were once learned and have since then become customary to the point that they are carried out somewhat automatically. Conversely, explicit memory stores facts, concepts, events, and experiences, and is characterised by a precise spatiotemporal connotation of the stored information. Declarative memory can be further subdivided into episodic memory, which is used to store past personal experiences [Baddeley, 2002, Tulving, 1985], and semantic memory, which plays a crucial role in learning and information processing [Martin and Chao, 2001].

1.1.2 Short-Term Memory

Short-term memory generally refers to rapid-access readily-available memory with limited storage capacity and duration. Although there are still controversies regarding its exact duration, short-term memory is commonly believed to last for no more than a few tens of seconds [Revlin, 2012], extended to a few minutes by relying on attentive control processes such as rehearsal [Jonides et al., 2008]. According to a prominent theory [Berman et al., 2009] short-term memory duration is subject to spontaneous decay over time. Indeed, experimental studies have shown that there is a correlation between the duration of the timespan between stimulus presentation and recall, and the degradation in mnemonic performance. Another popular view argues that forgetting is due to new – to be stored – stimuli competing i.e. interfering with the already stored information [Lewandowsky et al., 2004, Nairne, 2002], and that temporal decay phenomena can be reinterpreted in terms of such an interference [Lewandowsky et al., 2009].

In terms of capacity, the common view is that short-term memory systems can store a maximum of seven element plus or minus two [Miller, 1994], although this seems to hold true mainly for numbers. Indeed, results from word-based short-term memory experiments seem to indicate that the capacity

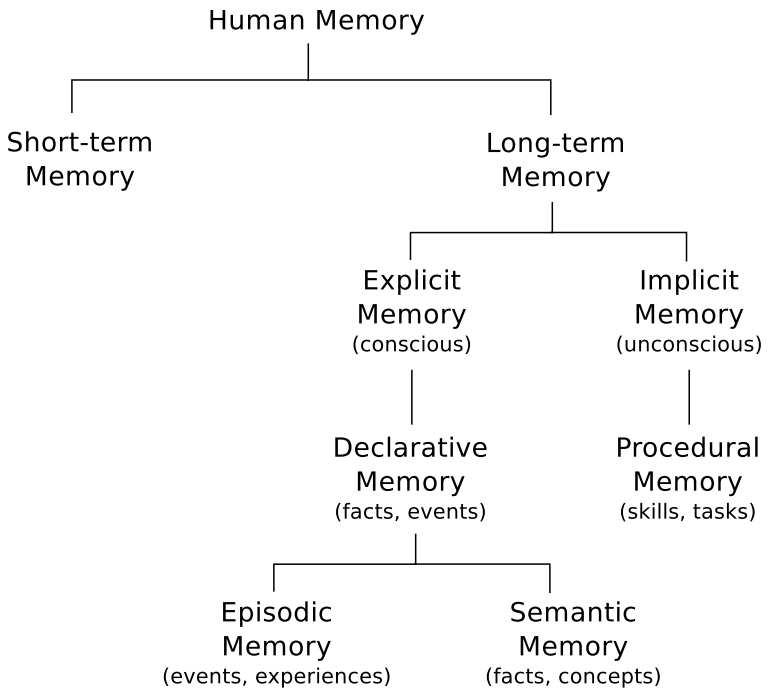

Figure 1.1: Human memory types organised by persistence and function. (Adapted from [Mastin, 2010].)

of these memory systems is affected by word length [Baddeley et al., 1975], phonological similarity [Baddeley et al., 1975], frequency of word occurrence in a given language [Baddeley et al., 1975], and semantic grouping [Poirier and Saint-Aubin, 1995]. Finally, both capacity and persistence are affected by the age, the culture, the training, and the lifestyle of the tested subjects.

1.1.3 Working Memory

Short-term memory is an integral component of working memory [Baddeley and Hitch, 1974, Baddeley, 2000], which is a complex cognitive system combining both temporary storing and information processing capabilities. Working memory endows us with the ability to retain relevant information for the execution of prospective actions depending on that information [Fuster, 2008]. Although originating from a transient stimulus, the encoded information is thought to be relevant for the task at hand and must therefore be maintained in memory long after the original stimulus has disappeared.

Working memory is thought to play a lead role in the execution of hierarchically structured tasks [Fuster, 2008] by providing the necessary functionalities to represent and work through sequences of subgoals. Human behaviour is intrinsically hierarchical and, more importantly, goal-directed. Our actions are, in fact, very rarely end in themselves but are always part of a plan aimed at completing a specific objective. This is true for all tasks, may these be simple such as eating and drinking or more complex endeavours such as the pursuit of our happiness. Such purposive behaviour ultimately steers our lives and renders them unique.

1.1.4 Memory Consolidation

Memory consolidation is the process by which short-term memory traces are converted into longer-lasting memories. It is believed that three separate but complementary forms of consolidations processes coexist [Dudai, 2004] – namely, synaptic consolidation, systems consolidation, and recon-

solidation – each acting at different time scales and with its own purpose. Synaptic consolidation processes [Bramham and Messaoudi, 2005] comprise the sequential strengthening of the connections between neurons, i.e. the synapses, contributing to the representation of a common piece of information [Hebb, 1949]. Initially, the release of neurotransmitters from the presynaptic neuron into the synaptic cleft and the sensitivity of postsynaptic receptors to these neurotransmitters augments [Malenka and Bear, 2004, Sweatt, 1999]. Subsequently, gene expression and protein synthesis [Dudai, 2002, Gold, 2008, Kandel, 2001] allow for the growth of new synaptic terminals, which produce enhanced responses in the postsynaptic neuron as neurotransmitter uptake increases. Long-term potentiation [Bliss and Lomo, 1973], in both its early and late forms, is a prime example of such a synaptic consolidation process.

Systems consolidation processes [Roediger et al., 2007, Squire and Alvarez, 1995] involve relocating memory traces, which were initially stored in temporary buffers, into specific brain areas for long-term storage. According to the standard model, the memory traces to be consolidated are initially encoded and stored in the medial temporal lobe and in the hippocampus [McClelland et al., 1995, Roediger et al., 2007, Squire, 1987, Squire, 1992]. From here, memories are moved into the neocortex [Buzsáki, 1989, Hasselmo et al., 1996, Qin et al., 1997, Shen and McNaughton, 1994] over long periods of time in the order of months or even years. There is compelling evidence indicating that this form of consolidation occurs during sleep [Maingret et al., 2016, Moroni et al., 2007, Reasor and Poe, 2008, Siegel, 2001, Stickgold, 2005, Walker et al., 2005], although the mechanisms behind hippocampal-cortical consolidation are far from being fully understood.

Finally, reconsolidation [Dudai, 2004, Tronson and Taylor, 2007] is thought to be one of the processes by which stored memories are maintained and strengthened over time, in particular following retrieval. Experimental studies have shown that the retrieval of consolidated long-term memories opens up a window of opportunity during which these could be forgotten [Misanin et al., 1968, Nader et al., 2000, Rudy et al., 2006, Sara, 2000] to make space for new memories, indicating that there is a need for continuous consolidation for memories which are to be stored for longer.

1.2 General Anaesthesia

General anaesthesia is the other macroscopical phenomenon we investigate in the scope of the current work, alongside memory. General anaesthesia is a reversible drug-induced coma which is commonly administered to patients undergoing surgery due to its desirable properties, which are: loss of consciousness, analgesia, immobility, and amnesia, all obtained whilst preserving physiological stability [Brown et al., 2010]. Indeed, after the induction of general anaesthesia, patients enter a state of sedation during which they are not aware of the surgery, they do not perceive nor react to the noxious stimuli deriving from it, and they do not remember undergoing it. Although having become a standard operating procedure during surgery – in the United States alone, approximately 60000 patients undergo general anaesthesia every day [Brown et al., 2010] – the chemical and neuronal mechanisms by which these effects are obtained are yet to be fully unravelled. Today, research in anaesthesiology is still trying to find explanations behind several phenomena occurring during general anaesthesia, most of which involve undesirable effects. These include, and are not limited to, intraoperative awareness [Ghoneim et al., 2009, Moerman et al., 1993, Ranta et al., 1998, Sandin et al., 2000, Schwender et al., 1998], the formation of implicit memories under general anaesthesia [Andrade and Deeprose, 2007, Bonett et al., 2014, Cork et al., 1996, Ghoneim and Block, 1997, Jones, 1994, Kihlstrom et al., 1990], and paradoxical excitation [Bevan et al., 1997, Clark and Rosner, 1973, Gibbs et al., 1936, Kiersey et al., 1951, McCarthy et al., 2008, Rampil, 1998]. Ultimately, the goal of anaesthesia research is to improve patient care. In addition, a vast and growing body of literature (see [Brown et al., 2010, Franks, 2008, Mueller et al., 2011] for in-depth reviews) has recently begun studying the loss of consciousness caused by anaesthesia as a way to indirectly investigate and improve our understanding of consciousness [Alkire et al., 2008].

1.3 Neural Oscillations

Neural oscillations are the product of rhythmic nerve cell activity. The role of neural oscillations has been extensively described in the literature, giving rise to a number of stimulating theories. Neural oscillations may represent the stable, unperturbed state of the brain [Buzsáki and Draguhn, 2004] during sleep, and can also be used as indicators of certain sleep stages [Llinas and Ribary, 1993]. In addition, experimental studies have linked synchronous activity with perception [Engel et al., 2001], stimulus encoding and representation [Gray et al., 1989], and information integration and memory [Axmacher et al., 2006, Engel et al., 2001, Kahana et al., 2001, Lisman, 2010, Lisman and Jensen, 2013, Varela et al., 2001]. The common denominator of all of these theories is the hypothesis of communication through coherence [Fries, 2005], according to which synchronous activity enables communication and cooperation between neural ensembles. Indeed, functionally-linked brain regions have been shown to synchronise their operational frequency when collaborating on a common task. These include, and are not limited to, parietal and occipital regions during visual attention tasks [Fries et al., 2001]; hippocampus and (pre) frontal cortex during memory tasks [Fell et al., 2001] and consolidation during sleep [Maingret et al., 2016]; motor cortex and spinal motor neurons during movement tasks [Conway et al., 1995].

In this thesis we focus mainly on the role of hippocampal neural oscillations for memory maintenance and consolidation. Previous research has established that hippocampal oscillations are implicated in the execution of memory tasks [Colgin and Moser, 2010, Colgin, 2016, Howard et al., 2003, Lisman and Jensen, 2013, Nyhus and Curran, 2010, Osipova et al., 2006, Sederberg et al., 2007, van Vugt et al., 2010]. These studies suggest that this synchronous activity is involved in grouping and binding of multimodal stimuli components when encoding and retrieving memories [Colgin and Moser, 2010], as well as fast communication and coordination between neural ensembles [Fries, 2005]. In addition, hippocampal oscillations are thought to mediate memory consolidation processes during sleep [Axmacher et al., 2006, Lega et al., 2012, Maingret et al., 2016, Power, 2004, Reasor and Poe, 2008, Walker, 2009]. Phenomenologically, oscillations occur at various scales and are commonly grouped in distinct frequency bands.

1.3.1 Oscillations Are a Multi-Scale Phenomenon

Oscillations can occur at different scales and are driven by different mechanisms (for a review see [Wang, 2010]). At the microscopic level, individual neurons have been shown to display oscillatory variations in their membrane potential. These include sub-threshold oscillations and resonating patterns which often result from transmembranal current interactions [Alonso and Llinás, 1989, Llinas et al., 1991, Wang, 1993]. In addition, some neurons produce oscillations [Llinas, 1988] in the form of rhythmic sequences of action potentials, and in the form of short bursts, defined as brief clusters of action potentials, both of which can entrain oscillatory activity in their postsynaptic targets. At the mesoscopic level, local populations of neurons can exhibit synchronised firing patterns [Hansel et al., 1995, Van Vreeswijk et al., 1994, Wang and Rinzel, 1993] by concurrent discharges of action potentials, and this synchronisation is dependent on synaptic interactions and network topology, and also on intrinsic cellular properties. Finally, at the macroscopic level, several brain structures have been shown to synchronise their firing activity when cooperating on a common task [Conway et al., 1995, Fell et al., 2005, Fries, 2005], as observed in electroencephalograms. These observations indicate that various oscillatory phenomena exist within the central nervous system. For the purpose of the current work, we employ the term "neural oscillations" to designate the mesoscopic and macroscopic phenomena emerging from neural activity at the microscopic scale.

1.3.2 Oscillation Frequency Bands

Oscillatory brain activity has been observed at various frequencies, which are commonly classified in distinct bands seen mainly in electroencephalographic recordings. Delta frequency oscillations ($0.5-4\,Hz$) are the slowest identifiable oscillations. They are characterised by high amplitudes and are considered to be one of the indicators of non-rapid eye movement (non-REM) stage 3 slow-wave sleep [Amzica and Steriade, 1998, Kalia, 2010]. Theta oscillations ($4-7\,Hz$ in humans, $4-11\,Hz$ in rodents) [Colgin, 2013, Vinogradova, 1995] are prominently observed within the hippocampus [Colgin, 2016], an allocortical structure located in the medial temporal lobe. In humans, theta rhythms have been correlated with navigation [Ekstrom et al., 2005, Fenton et al., 2010, O'Keefe et al., 1998] and memory [Hartley et al., 2007, Lega et al., 2012, Squire, 1992, Tesche and Karhu, 2000]. Similarly, in rats, these oscillations are though to play an important role in exploration and navigation [Buzsáki and Moser, 2013], localisation [O'Keefe and Recce, 1993, O'Keefe et al., 1998] and learning [Colgin, 2013, Kahana et al., 2001]. Alpha oscillations ($7.5-12.5\,Hz$) are commonly observed in human electroencephalography (EEG) recordings when subjects are awake, at rest, and with their eyes closed [Adrian and Matthews, 1934], and have been associated with idling and top-down inhibition of cortical areas in the absence of stimulation [Klimesch et al., 2007, Niedermeyer, 1997, Palva and Palva, 2007]. Beta oscillations ($12.5-30\,Hz$) are commonly observed in human electroencephalography recordings when subjects are awake with their eyes opened, and are thought to be associated with the readiness phase preceding the initiation of voluntary movements [Jasper and Penfield, 1949, Wang, 2010] and the elicited motor response [Lalo et al., 2007]. Finally, gamma oscillations ($30-100\,Hz$) have been linked with attention [Hughes, 2008], memory [Lisman, 2010, Lisman and Jensen, 2013, Montgomery and Buzsáki, 2007, Sederberg et al., 2007], and even consciousness [Gold, 1999, Vanderwolf, 2000].

1.4 Biological Neurons

The electrical signals recorded from the brain arise from the activity of neurons. Nerve cells (neurons) are the main signalling units of the nervous system. Neurons are electrically excitable cells capable of generating electrical and chemical signals. This electrochemical neural activity is the underlying substrate for more complex activity patterns, such as oscillations, and ultimately of cognitive behaviours, perception, and movement. The electrical activity of nerve cells depends on their anatomy, and physiological current-generating mechanisms.

1.4.1 Anatomy of a Nerve Cell

A typical neuron can be divided into four morphologically distinct regions: the dendrites, the cell body, the axon, and the presynaptic terminals (Figure 1.2). The dendrites are effectively the input terminals to the neuron. The cell body, or soma, has a permeable membrane which allows a bidirectional ion flow in and out of the cell. This ion flow causes the membrane potential to shift making it either more negative or more positive. These phenomena are known as repolarisation and depolarisation (Figure 1.3), respectively. If a neuron is depolarised beyond a certain threshold it emits an electric signal which propagates along its axon towards its synaptic terminals. The time it takes for the signal to traverse the neuron and reach its synaptic terminals is referred to as the axonal delay. The axon is coated with a myelin sheath which acts as an insulator increasing the speed at which the signal travels. This action potential, or spike (Figure 1.3), is the means by which the brain receives, processes and conveys information [Kandel et al., 2000a].

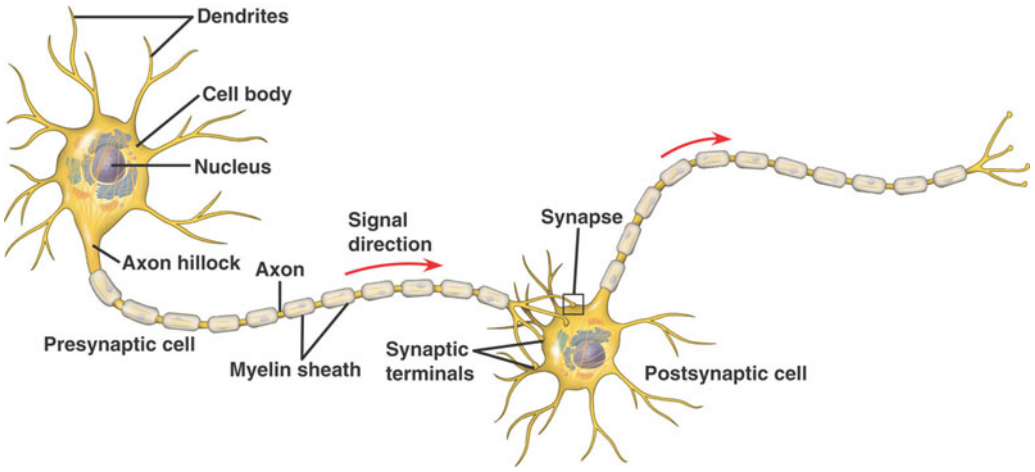

Figure 1.2: The anatomy of a nerve cell and its regions. (Adapted from [Cheung, 2008]).

After a neuron emits a spike, its membrane potential drops below resting potential (Figure 1.3). This phenomenon is known as hyperpolarisation. The hyperpolarisation time determines the absolute refractory period of the neuron. This is a time interval during which the neuron will not fire however strongly it is stimulated. The absolute refractory period is followed by the relative refractory period during which the neuron can fire only if excited by stronger stimuli than those normally required when at resting potential [Kandel et al., 2000c].

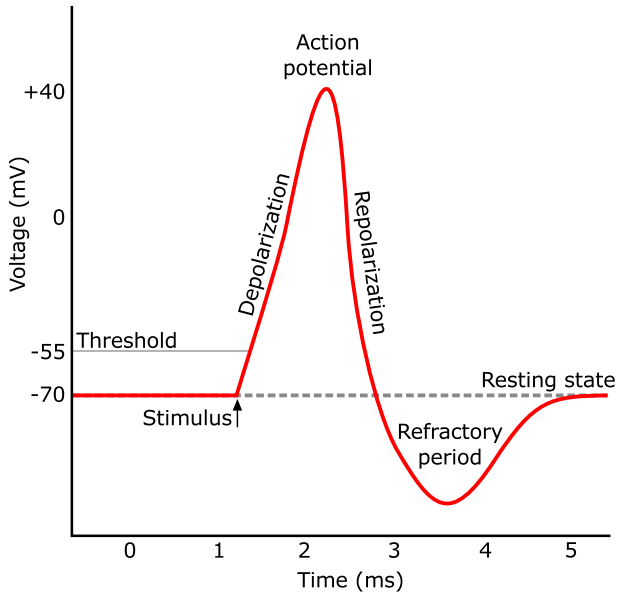

Figure 1.3: A typical voltage trace of an action potential showing the polarisation phases. Depolarisation is the positive variation in membrane potential occurring due to the stimulation. Repolarisation is the negative variation in membrane potential following the emission of the action potential. Hyperpolarisation time determines the refractory period. (Adapted from [Commons, 2016] (CC BY-SA 3.0).)

1.4.2 Synapses

Nerve cells communicate by establishing connections known as synapses. These occur at the junction between the axonal branches of the presynaptic neuron and the dendrites of the postsynaptic neuron (Figure 1.4). However, presynaptic and postsynaptic neurons do not physically touch but are instead separated by a gap known as the synaptic cleft. When an action potential reaches the axon

terminal it causes the release of neurotransmitters from the presynaptic neuron into the synaptic cleft. Neurotransmitters are chemicals which bind to their respective receptors in the postsynaptic dendrites causing the activation of the synapse. Receptors mediate the opening and closing of transmembrane permeable channels thus effectively controlling the ion flow into and out of the membrane [Kandel and Siegelbaum, 2000].

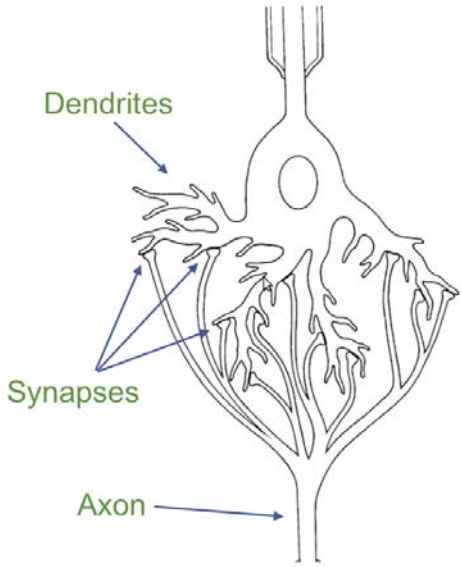

Figure 1.4: Synapses are formed at the junction between presynaptic axon terminals and postsynaptic dendrites. (Adapted from [Shanahan, 2011].)

1.4.3 Neurotransmitters

Neurons can be classed into two main types – excitatory and inhibitory – depending on the effect they have on the neurons they project on. An excitatory presynaptic neuron will enhance the activity of its postsynaptic neurons. On the other hand, an inhibitory neuron will cause the activity of its postsynaptic neurons to diminish. This behaviour is due to the effect of the different neurotransmitters released by these types of neuron.

Excitatory Neurotransmitters and their Receptors

The main excitatory neurotransmitter is L-glutamate acid, commonly known simply as glutamate [Kandel and Siegelbaum, 2000]. Glutamate binds to specific postsynaptic receptors. These can be of three kinds: AMPA, kainate or NMDA (Figure 1.5). When glutamate binds to an AMPA or kainate receptor, it causes the partial opening of the channel. This allows an outward flow of intracellular potassium ions (K^+) and an inwards flow of extracellular sodium ions (Na^+). Additional binding of glutamate molecules induces further opening of the receptor channel.

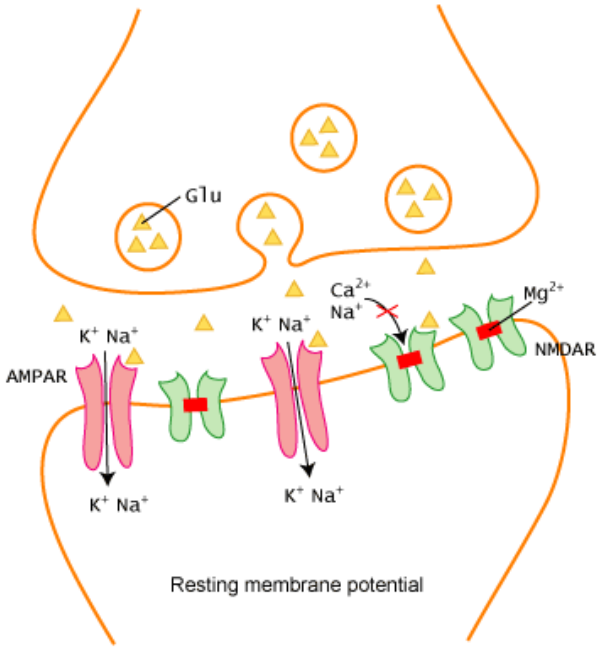

Figure 1.5: Simplified drawing of a model excitatory synapse showing open AMPA receptors and closed NMDA receptors. Following the emission of a presynaptic spike, glutamate is released into the synaptic cleft. Glutamate then binds on AMPARs and NMDARs governing their dynamics. (Adapted from [Iberri, 2004] (CC BY-SA 3.0).)

Glutamate also binds to NMDA receptors which control the gating of outwards K^+ and inwards calcium (Ca^{2+}) ions as well as Na^+. This neurotransmitter-receptor interaction is similar to the AMPAR and kainate receptors. Once fully opened, though, ions cannot flow through the NMDAR channel. This is due to a voltage-dependent magnesium (Mg^{2+}) block which sits inside the channel. The block is lifted once the postsynaptic membrane depolarises sufficiently to reduce the affinity between the Mg^{2+} and its binding site inside the channel [Kandel and Siegelbaum, 2000].

Acetylcholine (ACh) is a neurotransmitter acting on both the peripheral and central nervous system, whose main role is to mediate excitation in the target neurons. This cholinergic neurotransmission has been in fact found to enhance glutamatergic transmission thus increasing neuron excitability in various areas of the brain [Gil et al., 1997, Giocomo and Hasselmo, 2005, Radcliffe et al., 1999, Gioanni et al., 1999]. Acetylcholine binds on ligand-gated receptors gating transmembranal cations, and on metabotropic receptors mediating various intracellular events with the aid of second messengers.

Inhibitory Neurotransmitters and their Receptors

Inhibitory synapses are activated by the release of γ-Aminobutyric acid (GABA) in the synaptic cleft which binds to its dedicated receptors. There are two known classes of GABA receptors, namely $GABA_A$ [Henschel et al., 2008, Johnston, 1996] and $GABA_B$ [Chen et al., 2005, Hill and Bowery, 1981]. $GABA_A$ receptors are ligand-gated ionotropic receptors which control the gating of Cl^- into the cell membrane. $GABA_B$ receptors are metabotropic receptors which are coupled to potassium channels via G-proteins gating K^+ out of the cell membrane.

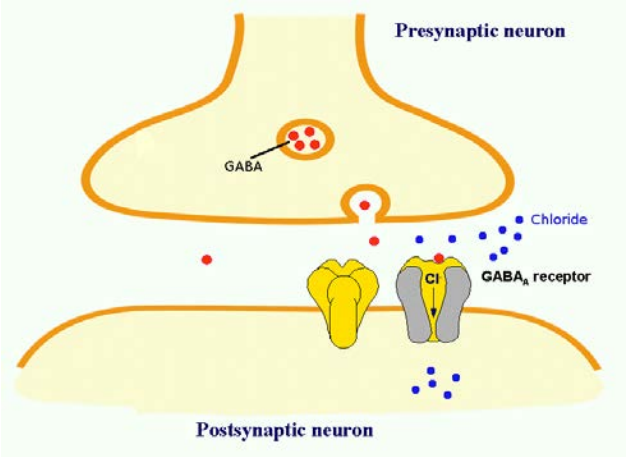

Figure 1.6: Simplified drawing of a model inhibitory synapse showing an open $GABA_A$ receptor channel. (Adapted from [Cody, 2011].)

1.4.4 Postsynaptic Potentials

The bidirectional ion flow across the postsynaptic neuron membrane generates a postsynaptic current which can be either excitatory (EPSC) or inhibitory (IPSC) depending on the type of synapse. An activated excitatory synapse causes the flow of positively charged ions (Na^+ and/or Ca^{2+}) into the postsynaptic membrane thus inducing a positive current. Conversely, an inhibitory synapse causes an outwards flow of positive charged ions (K^+) and an inwards flow of negatively charged ions (Cl^-), which in turn induce a negative current. The depolarisation caused by these currents are called excitatory (EPSP) and inhibitory postsynaptic potential (IPSP) respectively (Figure 1.7A and Figure 1.7B).

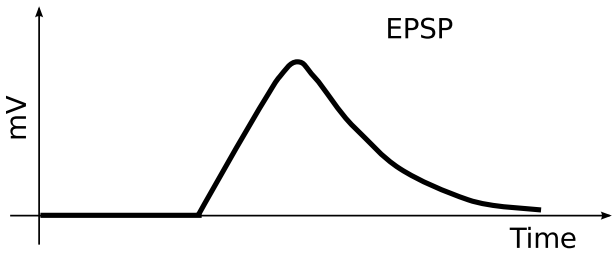

(A) Excitatory postsynaptic potential

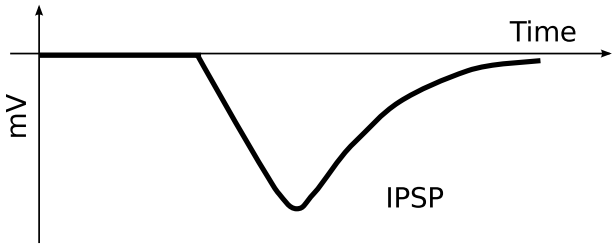

(B) Inhibitory postsynaptic potential

Figure 1.7: Postsynaptic potentials result from neurotransmitter activity mediating the opening of postsynaptic ion channels. (A) Excitatory postsynaptic potentials produce a positive variation in membrane potential. (B) Inhibitory postsynaptic potentials produce a negative variation in membrane potential.

The genesis of action potentials and the propagation of neural electrical signals can be precisely modelled with mathematical equations. Several models have been proposed since the first half of

the 20$^{\text{th}}$ century. In general, models provide detailed frameworks to investigate the dynamics of biological systems.

1.5 Mathematical Modelling of Neural Activity

Mathematical modelling [Abbott, 2008, Churchland et al., 1990, Gerstner et al., 2012] of neurons is a powerful tool for neuroscientists, which can be leveraged to simulate neural activity and cognitive processes at varying levels of biological realism. Models are particularly useful when *in-vivo* and *in-vitro* experiments are impracticable, be it for technological reasons or for ethical reasons. One of the main goals of research in neuroscience is to explain the neural mechanisms underlying cognitive behaviours. In other words, we aim at understanding how the electrochemical signals generated by interconnected nerve cells, anatomically grouped in brain regions, contribute to enabling cognition, perception and movement. Intuitively, this involves correlating phenomena observed at different scales – from synapse and individual neurons to brain areas –, which in itself is a cumbersome task. These scales include, from the microscopic to the macroscopic scale, the molecular processes occurring at the synaptic level, the electrophysiology of single neurons, the cumulative electric potential generated by cell assemblies and brain structures, and the resulting high-level behaviour.

Fortunately, modern experimental techniques allow us to record electrophysiological signals at these different neuronal scales [Buzsáki, 2004, Engel et al., 2005, Huster et al., 2012], although recordings at multiple scales concurrently to date remain a challenge. At the microscopic level, intracellular recordings via voltage clamp, current clamp, patch clamp [Sakmann and Neher, 1984, Hamill et al., 1981], and sharp electrodes are commonly used to study molecular dynamics at the cellular level, including the workings of receptors and ion channels, as well as the spiking activity of neurons. Moreover, micropipette and microelectrodes inserted within brain tissue can be fine enough to detect the extracellular activity of a single neuron [Boulton et al., 1990] and of multiple units concurrently, depending on the electrode size and the number of inserted electrodes. However, in this configuration, precisely locating the source of the electrical activity becomes a challenge whose success is highly dependent on the placement of the electrodes. That is to say that clamp methods are to date the most spatially precise methods for recording spiking activity from single neurons since one can control the exact position of the cell in which the electrode was inserted.

At the mesoscopic level, multi-unit extracellular recordings collect the activity of several closely-located cells and are carried out mainly by using multielectrode arrays (MEAs) containing over 100 electrodes for in-vivo applications and over 10000 for in-vitro applications (see [Spira and Hai, 2013] for a review of the state of the art recording techniques). The ability to record from multiple sources comes at the compromise of reduced spatial resolution and increased noisiness in the signal, since the individual contributions of each cell and of the surrounding extracellular matter are merged together in one trace. A more precise technique involves multi-unit patch clamp recordings which, although possible [Vardi et al., 2016], require costly set-ups and, often, computer-aided electrode positioning systems. Nevertheless, recent technological advancements have enabled the development of recording systems combining the advantage of extracellular MEAs and intracellular microelectrodes [Spira and Hai, 2013].

The macroscopic level comprises invasive electrocorticography (ECoG) [Palmini, 2006] recordings which use a grid of ball electrodes placed on the cortex just below the dura mater, and non-invasive electroencephalography [Niedermeyer and Lopes da Silva, 2005] which uses electrodes placed on the scalp. None of these techniques use needle-type electrodes i.e. no piercing of the brain matter is required. Clearly, being further away from the source of the recorded signal means that these techniques have limited spatial resolution [Asano et al., 2005, Kondylis et al., 2014] compared to mesoscopic and microscopic recording techniques, with ECoG being slightly better than EEG. Nevertheless, their limited invasiveness as well as their temporal resolution (in the order of milliseconds)

render them extremely useful in clinical applications and research on humans. EEG can also be recorded intracranially using deep electrodes implanted in the brain tissue. This technique is called stereoelectroencephalography (SEEG) [Talairach et al., 1974] and is commonly used clinically to identify the presumed location of the focus of epileptiform activity [Cossu et al., 2005]. In addition, functional magnetic resonance imaging (fMRI) [Huettel et al., 2009, Logothetis et al., 2001] and positron emission tomography (PET) [Bailey et al., 2004] can be used to record brain activity during behavioural experiments by tracking the increased blood flow to structures, and the distribution of radioactively labelled chemicals in areas involved in cognitive tasks. Magnetoencephalography [Hämäläinen et al., 1993] is another functional imaging techniques which records the magnetic field resulting from the ionic currents generated underlying electrical brain activity [Buzsáki, 2006]. Since EEG and MEG record the complementary sources of similar signals, simultaneously record EEG and MEG recordings has proven to be a promising technique in neuroscientific research [Sharon et al., 2007].

Bridging the gap between the micro, meso, and macroscopic neural scales is one of the fundamental roles of mathematical modelling. At the microscopic level, computational models can reproduce molecular and synaptic interactions, as well as action potentials [Izhikevich, 2004]. In addition, via computer simulations researchers can artificially assemble neural populations [Wilson and Cowan, 1972], and even brain structures, to study their elicited activity at the mesocopic and macroscopic scales. This allows for the generation of synthetic datasets which can complement experimental recordings, which are often scarce or difficult to obtain. Moreover, computational models enable neuroscientists to test hypotheses artificially before testing them experimentally. Finally, modelling is a way to investigate the neurophysiological phenomena which are captured via recording techniques. In this thesis we focus on modelling the molecular and ionic properties of individual neurons, and synaptic interactions in interconnected populations of such neurons.

1.5.1 Mathematical Models of Biological Neurons

Several different mathematical neuron models exist, and have been extensively described and used in the literature (for a reviews see [Izhikevich, 2007]). These display different degrees of biological realism which is often achieved by detailed modelling of individual transmembranal ionic currents. The degree of biological realism often comes at the cost of an increase in the computational complexity of the model, which in turn affects the computational resources needed to simulate its activity. Moreover, highly complex models comprising numerous differential equations become cumbersome to analyse from a dynamical perspective [Izhikevich, 2007]. Unfortunately, the optimal model to choose does not exist. Rather, a task-dependent choice must be made bearing in mind the compromise between the required biological realism and computational efficiency.

In general, a biological neuron can be modelled with a set of ordinary differential equations which describe the evolution of the membrane potential of the neuron over time [Dayan and Abbott, 2001], as the product of transmembranal current and membrane resistance (as stated by Ohm's law):

$$\frac{\mathrm{d}V_m}{\mathrm{d}t} = I_m \cdot R_m = \frac{I_m}{C_m} \tag{1.1}$$

where V_m is the membrane potential, I_m is the net ionic current flowing through the membrane, R_m is the membrane resistance, and C_m is its reciprocal i.e. the membrane conductance. Therefore, nerve cells are represented as a resistor-capacitor circuit, capable of accumulating and discharging electric charges. Individual neurons can then be connected, by modelling synaptic interactions, in order to simulate and study the behaviour of neuronal populations.

Leaky Integrate-and-Fire

The leaky integrate-and-fire (LIF) model [Lapique, 1907, Stein, 1967, Tuckwell, 1988] sits at the lower end of the biological realism spectrum, and has low computational costs due to its simplicity. It comprises a single differential equation in the form:

$$C_m \cdot \frac{\mathrm{d}V_m}{\mathrm{d}t} = I_{stim} - \frac{V_m}{R_m} \tag{1.2}$$

where I_{stim} is the applied stimulation current. The membrane potential depolarises over time as long as $I_{stim} > V_m/R_m$. When V_m exceeds a user-defined threshold V_θ, a spike is recorded and the membrane potential is reset to its resting value (usually $0\,mV$). Conversely, if $I_{stim} < V_m/R_m$, the membrane potential slowly leaks to zero. The action potentials generated by the LIF model are instantaneous and have no width nor shape.

Hodgkin-Huxley

On the other of the scale is the Hodgkin-Huxley model [Hodgkin and Huxley, 1939, Hodgkin and Huxley, 1952] which provides the highest degree of biological realism, although this comes at a high computational cost. This model represents the rate of change of the membrane potential V_m as a function of the total input dendritic current and the ionic currents:

$$C_m \cdot \frac{\mathrm{d}V_m}{\mathrm{d}t} = -I_i + I_{stim} \tag{1.3}$$

where I_{stim} is the applied stimulation current, and I_i is the total transmembranal ionic current which can be further split in its leak, sodium and potassium components:

$$I_i = I_l + I_{Na} + I_K \tag{1.4}$$

Each ionic current can be expressed in terms of its ionic conductance by using equations of the form:

$$I_L = \overline{g}_l \cdot (V_m - E_l) \tag{1.5}$$
$$I_{Na} = \overline{g}_{Na} \cdot m^3 \cdot h \cdot (V_m - E_{Na}) \tag{1.6}$$
$$I_K = \overline{g}_K \cdot n^4 \cdot (V_m - E_K) \tag{1.7}$$

where V_m is the membrane potential, $\overline{g}_K$, $\overline{g}_{Na}$, and $\overline{g}_l$ are the maximum ionic conductance, and E_K, E_{Na}, and E_l are the resting potential of the potassium, sodium, and leak channels respectively. m and n are variables describing the activation of the potassium and sodium channels, and h is a variable describing the inactivation of the sodium channel. These are governed by a set of ordinary differential equations in the form:

$$\frac{\mathrm{d}x}{\mathrm{d}t} = \alpha_x \cdot (1 - x) - (\beta_x \cdot x) \tag{1.8}$$

for $x \in \{\, h, n, m \,\}$, where α_x and β_x are functions describing the steady-state and temporal dynamics of the activation and inactivation variables. Therefore, the standard Hodgkin-Huxley model comprises four ordinary differential equations: $\mathrm{d}V_m/\mathrm{d}t$, $\mathrm{d}m/\mathrm{d}t$, $\mathrm{d}h/\mathrm{d}t$, and $\mathrm{d}n/\mathrm{d}t$.

In addition, the Hodgkin-Huxley neuron model can be extended by adding other types of ion channels, and the currents they permeate. This equips computational neuroscientists with a powerful tool enabling them to model virtually all existing biological neurons and their spiking behaviour. Since part of the work presented here involved accurately modelling the electrophysiology of a specific type of hippocampal neuron, we relied upon the Hodgkin-Huxley model to provide us with the highest degree of realism and a precise control over the influence of the individual transmembranal ionic currents on the cell membrane potential.

Simplified Two-Variable Models

A considerable effort has been devoted to simplifying the Hodgkin-Huxley model, by reducing its dimensionality, whilst attempting to maintain the highest possible degree of biological realism. Examples of simplified models include, but are not limited to, the FitzHugh-Nagumo model [FitzHugh, 1961, Nagumo et al., 1962], the Morris-Lecar model [Morris and Lecar, 1981], the Adaptive exponential integrate-and-fire model [Brette and Gerstner, 2005], and the Izhikevich model [Izhikevich, 2003]. All of these models are two-dimensional and therefore much simpler than the Hodgkin-Huxley from a computational standpoint.

1.5.2 Spiking Neural Network Simulators

As we have seen, spiking neuron models are generally represented by a system of ordinary differential equations. Solving these equations analytically is often not a viable task, and sometimes even an impossible endeavour. However, the solutions to differential equations can be approximated by the means of numerical integration, using well-known methods such as the Euler [Euler, 1768] or Runge-Kutta [DeVries, 1994] method, amongst others.

Several spiking neural network simulators exist[1], which rely on these numerical integration techniques to simulate the activity of neural populations. In addition, these simulators are pre-packaged with a set of functions allowing the computational neuroscientist to precisely define individual neuron model parameters, to specify the synaptic interactions and the network topology, and to tweak general simulation parameters. For the purpose of this thesis, we used the Brian[2] simulator due to its intuitive usability.

1.6 The Objectives of this Thesis

In the very first paragraph of this manuscript we asked four questions. Who was the first man to set foot on the Moon, and when did it happen? What does the Pythagorean theorem state? When did I score my first rugby try? How does one countersteer a motorcycle? Answering each one of these questions requires distinct mnemonic processes and capabilities. In particular, the first man to set foot on the Moon was the American cosmonaut Neil Armstrong on the 21st of July, 1969 – explicit semantic memory of a fact. The Pythagorean theorem states that, given a right-angled triangle with sides a b and c, the square of the hypotenuse (c) is equal to the sum of the squares of the other two sides (a and b): $c^2 = a^2 + b^2$ – explicit semantic memory of a concept. I scored my first rugby try at some point during my Under 15 season in my local rugby team in Milan – explicit episodic memory of an experience. Countersteering is achieved by steering the motorbike opposite to the direction in which one wishes to turn, so as to cause it to lean in the direction of

[1] Listing all the existing simulators would be out of the scope of this work. However, the interested reader can find an up to date list at the following address: https://grey.colorado.edu/emergent/index.php/Comparison_of_Neural_Network_Simulators

[2] The Brian simulator can be found at the following address: http://briansimulator.org/

the turn – implicit procedural memory of a skill. These distinct mnemonic capabilities all rely on one extremely complex processing unit: the brain. Although the neuroanatomy of the brain and the neurophysiology of the neurons composing the different structures of the central nervous system might be extensively described, to date,the emergence of cognition from neural activity remains largely a mystery.

In this thesis we ask ourselves one fundamental question: what are the neural mechanisms underlying memory? In particular, we narrow our focus to hippocampal mnemonic activity during waking, and the amnesia and paradoxical memory consolidation occurring under propofol-induced general anaesthesia. We hypothesise that networks of persistent firing neurons could provide the neural mechanism for the maintenance of memory-related hippocampal oscillations. Indeed, persistent firing is thought to be one of the neural substrates for memory maintenance, and these neurons are commonly found within the hippocampus, a brain structure which has been shown to be implicated in memory.

Moreover, we investigate the amnesic effect of anaesthesia which allows us to approach the aforementioned fundamental question from a different perspective. We make the assumption that understanding how anaesthetics inhibit memory consolidation could enable us to shed some light on memory consolidation processes. Indeed, anaesthetic agents have been shown to disrupt neural synchronisation, and this is presumed to be one of the mechanisms by which amnesia is achieved. However, due to the occurrence of intraoperative awareness, paradoxical excitation, and sometimes implicit memory formation under general anaesthesia, we hypothesise that, at certain anaesthetic dosages, neural synchronisation might be unaffected, if not even enhanced. We devise novel mathematical models of biological neurons and neural activity to test our hypotheses.

To complete this work, we developed a Python library of ionic transmembranal currents to be assembled together to create template neurons and a library which acts as a wrapper for the simulation parameters. The purpose of these is to accelerate simulation set-up time and reduce code duplication across simulation scripts. Both libraries are aimed at extending the functionality provided by the Brian simulator, and are freely available online[3].

Our work was carried out at Inria[4] and Loria[5] within the Neurosys[6] research team, a multidisciplinary group working on systems neuroscience at different neural scales. We collaborated with Beate Knauer and Motoharu Yoshida at the Ruhr University in Bochum, Germany who carried out the experimental in-vitro recordings of persistent firing hippocampal neurons used to derive the parameters from our model. The findings described within this thesis provide new insights into the mechanisms underlying mnemonic neural activity, both during wake and anaesthesia, opening compelling avenues for future work. Understanding the neural processes behind memory formation is a paramount task for clinical applications tackling neurodegenerative memory diseases, and anaesthesia monitoring.

1.7 Manuscript Structure

This manuscript comprises six chapters. The first chapter is the current one which sets the general scope of our work. Chapter 2 presents a survey of our current understanding of the neuroscientific phenomena we are investigating. In addition, we review existing theories and mathematical models of memory-related neural activity. In Chapter 3 we describe our mathematical model in detail,

[3] The libraries can be found here: https://github.com/JoErNanO/brianmodel and https://github.com/JoErNanO/briansims

[4] http://www.inria.fr

[5] http://www.loria.fr

[6] http://neurosys.loria.fr/

and the computational tools we used when measuring network synchronisation, when identifying oscillations frequency and power, and when analysing the data.

Chapter 4 presents our computational study of self-sustained theta oscillations in the hippocampus. We first introduce a new biologically-inspired neuron model capturing the features of persistent-firing neurons commonly found in the hippocampus. We hypothesise that these neurons could play an important role in generating and maintaining memory-related hippocampal oscillations, due to their electrophysiological properties and elicited spiking behaviours. Moreover, we study the dynamics of a network of these persistent-firing hippocampal neurons, and illustrate how intrinsic currents allow the network to self-synchronise its activity in the theta band. We demonstrate that, in the model, the frequency and spectral power of the oscillations are modulated solely by the cholinergic mechanisms mediating persistent firing, allowing for a wide range of oscillation rates within the theta band. This is a biologically plausible mechanism for the maintenance of synchronous theta oscillations in the hippocampus which aims at extending the traditional models of septum-driven hippocampal rhythmic activity.

In Chapter 5 we discuss our findings regarding the disruptive effects of general anaesthesia on hippocampal gamma-frequency oscillations, to gain some insights on the mechanisms causing amnesia, and sometimes memory formation, in anaesthetised patients. Gamma oscillatory frequency range is often recorded in functionally-coupled brain regions for cooperation during memory tasks. We present an in-depth study of the action of anaesthesia on neural oscillations by introducing a new computational model which takes into account the four main effects of the anaesthetic agent propofol on hippocampal interneurons. Our results indicate that propofol-mediated tonic inhibition contributes to an unexpected enhancement of synchronisation in the activity of a network of hippocampal interneurons. This enhanced synchronisation could provide a possible mechanism supporting the occurrence of intraoperative awareness, explicit memory formation, and even paradoxical excitation under general anaesthesia, by facilitating the communication between brain structures which should supposedly be not allowed to do so when anaesthetised.

Finally, in Chapter 6 we summarise our findings and highlight our contributions. We also identify and suggest potential avenues for future work.

CHAPTER

2

LITERATURE REVIEW

Contents

Overview

In this chapter we present a survey of our current understanding of various neuroscienfic topics, and of the research we conducted in support of this thesis. We review our current understanding of the hippocampus and the roles it is thought to play in memory encoding, storage, and consolidation. We then present a theory of memory consolidation driven by the cholinergic system and link it to recent experimental findings. We also survey the computational models of short-term and working memory based on persistent firing. Finally, we define general anaesthesia, summarise its molecular and macroscopical effects on the central nervous system, and review existing computational models.

2.1 The Hippocampus

The hippocampal formation (Figure 2.1) is a complex allocortical structure which is part of the limbic system of most mammals (Figure 2.2). In humans, the hippocampus sits bilaterally in the temporal horn of the lateral ventricles. The limbic system comprises the limbic lobe and other deep-lying structures including the amygdala, the cingulate gyrus, the corpus callosum, the thalamus, the hypothalamic nuclei and the hippocampus. The limbic system is thought to be the substrate for various functions including olfaction, motivation, behaviour, adrenaline flow, emotion and memory [Andersen et al., 2007, Kandel et al., 2000b]. Nowadays, the mnemonic functions of the limbic system, both long- [Squire, 1992] and short-term [Hannula et al., 2006, Hartley et al., 2007], are thought to be carried out mainly by the hippocampus [Squire et al., 2004].

2.1.1 Neuroanatomy of the Hippocampus

The hippocampus comprises the dentate gyrus (DG) which is a tight assembly of granule cells. The DG is the main gateway for inbound excitatory signals from the entorhinal cortex (EC) into the hippocampus via the perforant path which is the primary hippocampal input pathway [Andersen et al., 2007]. The signals are then relayed, via axonal connections dubbed mossy fibres, into the cornus ammonis (CA) area 3. The principals cells in CA3 give rise to axons projecting onto CA2 and CA1 via a pathway known as the Schaffer collateral. Finally, CA1 neurons relay signals back into the EC either directly or via the subiculum, followed by the presubiculum and parasubiculum which are intermediate continuous transition areas connecting back into the entorhinal cortex [Andersen et al., 2007, Kandel et al., 2000b] This hippocampal neural pathway is non-reciprocated and unidirectional, and vaguely resembles a loop [Amaral, 1993], beginning in the superficial layers of the entorhinal cortex, traversing the DG, the CA3-CA1 areas, the subiculum, and ending in deeper layers of the entorhinal cortex as show in Figure 2.3A, Figure 2.3B, and Figure 2.3C.

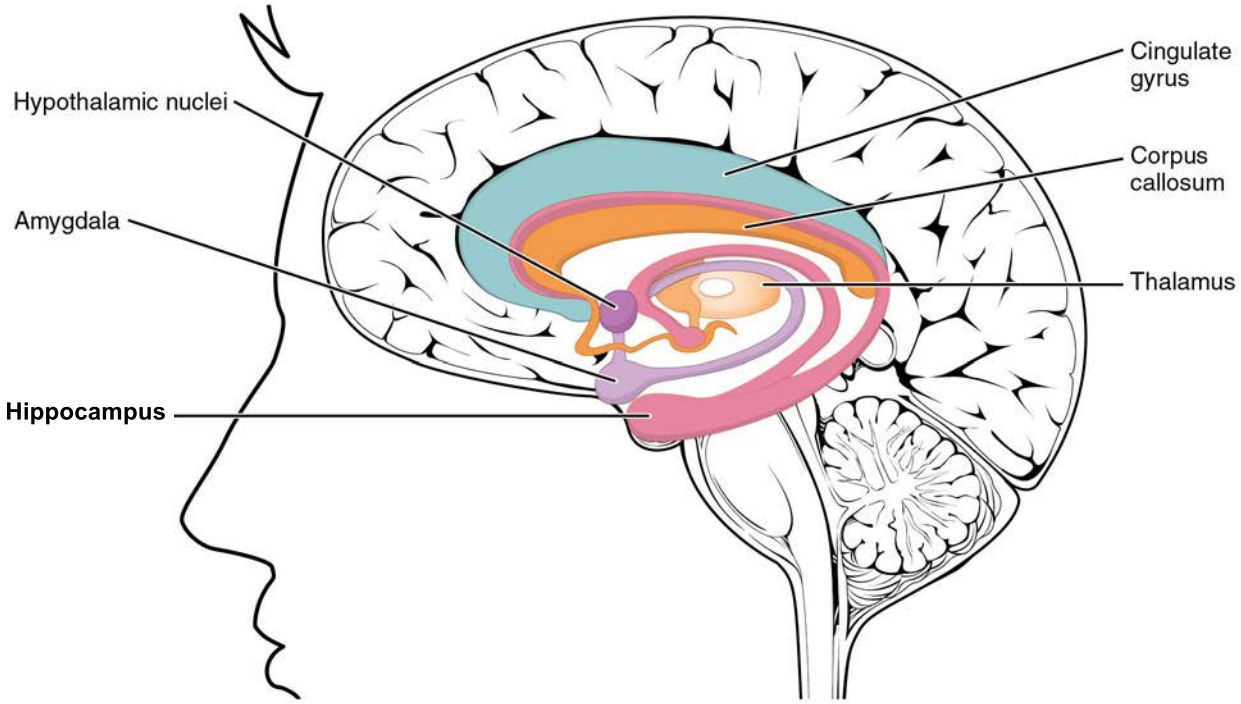

Figure 2.1: The hippocampal formation is a allocortical structure part of the limbic system. The limbic system comprises the hippocampus, along with the amygdala, the cingulate gyrus, the corpus callosum, the thalamus, and the hypothalamic nuclei. (Adapted from [College, 2013].)

The dentate gyrus comprises mainly various types of neurons, the most widespread being granule cells and basket interneurons [Andersen et al., 2007]. The dentate granule cell is the primary cell of the dentate gyrus. It is an excitatory cell and is the only DG neuron which gives rise to axons innervating another hippocampal area (i.e. CA3). Similarly, the basket cell is the main hippocampal inhibitory GABAergic interneuron found in the DG.

CA3 and CA1 comprise similar types of neurons, including pyramidal excitatory cells, and various types of inhibitory interneurons such as basket cells and oriens lacunosum-moleculare (O-LM) cells [Banks et al., 1998]. However, the two areas have been found to display substantially different connectivity. Indeed, the pyramidal neurons in CA3 have been shown to produce denser local recurrent networks than in CA1. Histological and electrophysiological studies of these two areas seem to suggest that, on average, CA3 [Miles and Wong, 1986] contains twice as many recurrent pyramidal connections as CA1 [Deuchars and Thomson, 1996]. This topological difference could account for different functional roles of CA3 and CA1, in particular with regards to supporting mnemonic neural activity as described in the following sections.

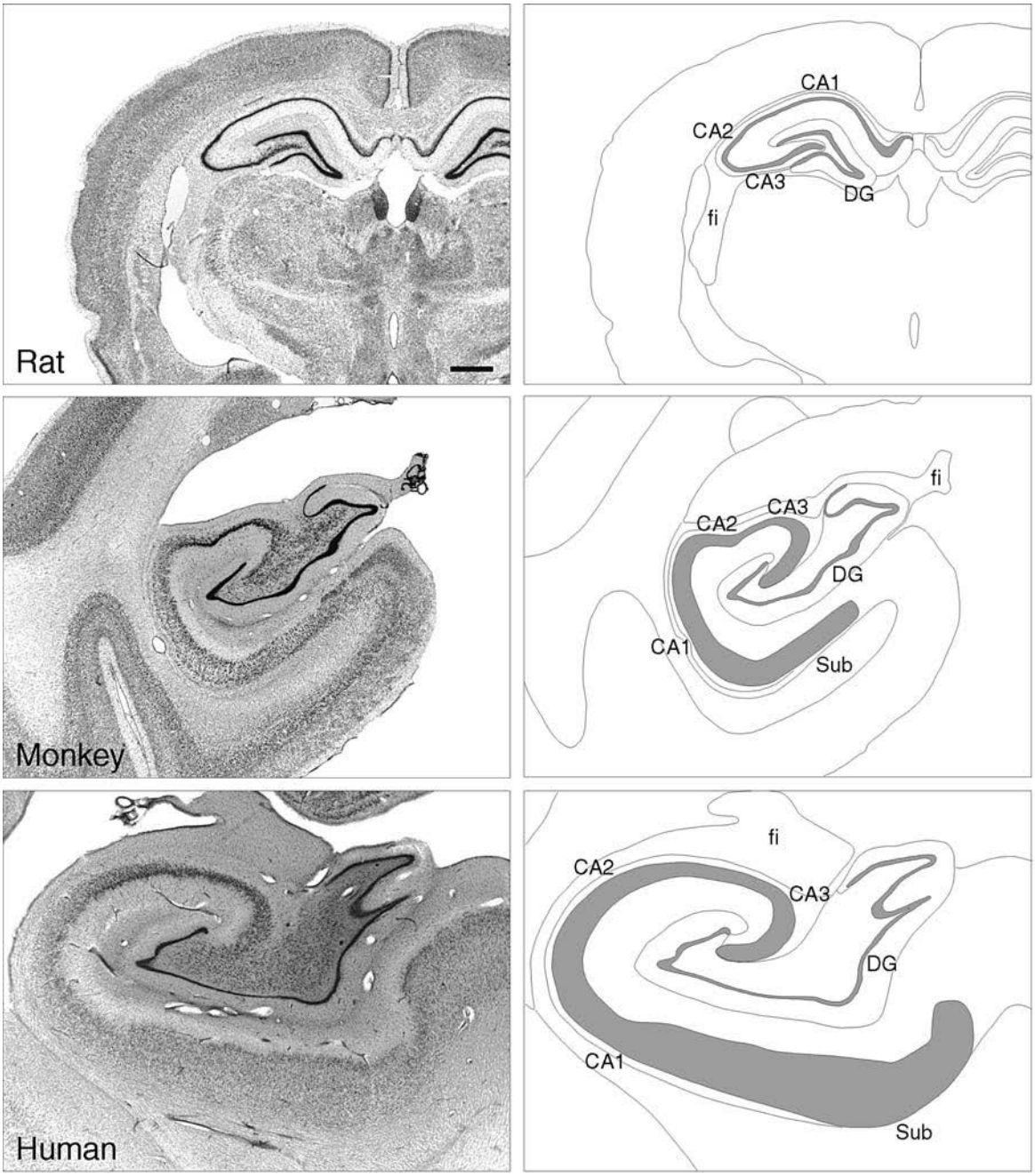

Figure 2.2: Nissl-stained sections and line drawings of the hippocampus in the rat, monkey, and human. The hippocampal formation is commonly found in most mammal brains. Its subdivision into dentate gyrus (DG), cornus ammonis (CA3-1), and subiculum (Sub), and the neuronal pathways are preserved and identifiable amongst several species. The horizontal bar in the top left panel measures $1\,mm$ and applies to all panels. (Adapted from [Andersen et al., 2007].)

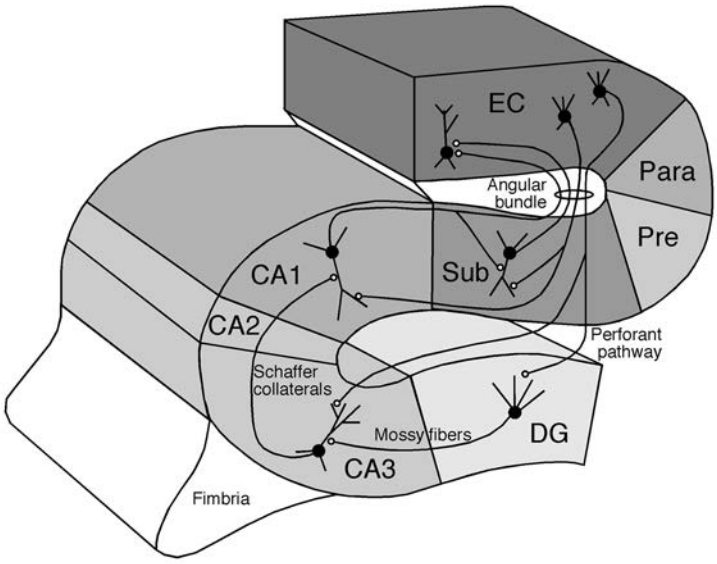

(A) Schematic of the neuronal pathways in the rat hippocampal formation. (Adapted from [Andersen et al., 2007].)

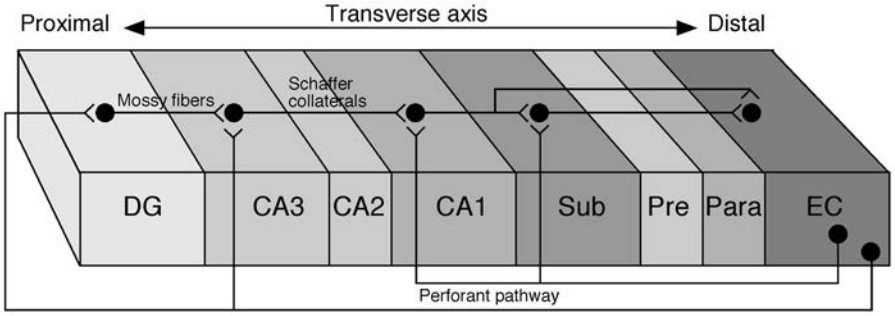

(B) Schematic of the neuronal pathways in the rat hippocampal formation along its transverse axis. (Adapted from [Andersen et al., 2007].)

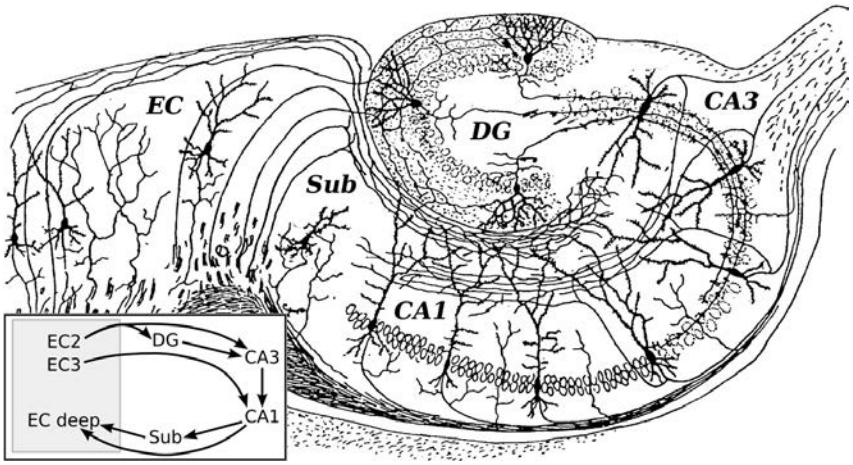

(C) A cross-section of the rodent hippocampus as drawn by Ramón y Cajal [Ramón y Cajal, 1909]. (Adapted from [Ramón y Cajal, 1909], public domain.)

Figure 2.3: The rat hippocampal formation and its neuronal pathways. Schematic of the neuronal pathways of the rat hippocampal formation viewed both as a cross-section (A), along its transverse axis (B), and a drawn by Ramón y Cajal [Ramón y Cajal, 1909]. Neurons in the superficial layers of the entorhinal cortex (EC) project into the dentate gyrus (DG) via the perforant pathway. The signal is then relayed via mossy fibres into CA3, which projects its Schaffer collaterals into CA1. CA1 then project back into the EC either directly or via the subiculum (Sub). This EC $\rightarrow$ DG $\rightarrow$ CA3 $\rightarrow$ CA1 $\rightarrow$ Sub $\rightarrow$ EC synaptic relay forms a unidirectional loop.

2.1.2 Long-Term Memory – The Role of the Hippocampus

The hippocampus has long been thought to be responsible for the formation of long-term memory [Squire, 1992] via long-term potentiation. This view is backed up by a series of studies which have shown that patients with hippocampal lesions display severely impaired mnemonic functions [Andersen et al., 2007, Corkin, 1984, Corkin, 2002, Kandel et al., 2000b, Scoville and Milner, 1957]. The severity of such dysfunctions is obviously dependant depth and importance of the lesion, however damage to any of the major components of the hippocampus has been shown to cause a significant drop in memory performance [Zola-morgan et al., 1989].

The memory storage mechanism is believed to lie in the cyclical entorhinal cortex-hippocampus loop [Andersen et al., 2007, Kandel et al., 2000b]. Sensory information – auditory, visual or somatic – is initially acquired and encoded cortically, in its relevant polymodal association areas. This information is then transferred to the entorhinal cortex via a dedicated pathway, further conveyed through the hippocampus, and relayed back into the entorhinal cortex. From here it returns to the polymodal association cortices.

The hippocampus is merely a temporary, albeit necessary, lay over for long-term memory. This claim is supported by the findings described in lesion studies according to which patients are capable of remembering factual knowledge which occurred before their hippocampus was damaged [Andersen et al., 2007, Corkin, 1984, Corkin, 2002, Kandel et al., 2000b, Scoville and Milner, 1957]. Long-term explicit memory is in fact stored in the association areas of the neocortex. The hippocampal formation might therefore play a crucial role for the long-term consolidation of such memories, by slowly transferring information to the neocortex for storage [Andersen et al., 2007, Kandel et al., 2000b].

2.1.3 Hippocampal Short Term and Working Memory

Working memory is commonly referred to as the ability to retain relevant information for the execution of prospective actions depending on that information [Fuster, 2008]. Although originating from a transient stimulus, the encoded information is thought to be relevant for the task at hand and must therefore be maintained in memory long after the original stimulus has disappeared. To achieve this, working memory relies on a short-term memory storage component.

The commonly accepted view resulting from lesion studies, is that damage to the hippocampus causes long-term memory impairment, without directly affecting short-term memory performance [Jonides et al., 2008, Squire, 1992]. However, recent studies have highlighted that the hippocampus could play an important role during working memory tasks [Hannula and Ranganath, 2008, Hartley et al., 2007, Howard et al., 2003, Kesner et al., 2005, Lisman and Jensen, 2013, Nyhus and Curran, 2010, Osipova et al., 2006, Raghavachari et al., 2001, Sederberg et al., 2007, Tesche and Karhu, 2000, van Vugt et al., 2010]. These findings suggest that the hippocampus might either mediate certain specific types of working memory – for example spatial memory [Hartley et al., 2007, O'Keefe and Recce, 1993, O'Keefe et al., 1998, Owen et al., 1995, Tesche and Karhu, 2000]. In particular, several studies [O'Keefe and Dostrovsky, 1971, O'Keefe and Recce, 1993, O'Keefe et al., 1998] have highlighted the presence of neurons, dubbed place cells, involved specifically in spatial memory encoding in the hippocampus. These place cells are thought to be responsible for precisely mapping the spatial environment in which animals behave, and the position of the animal in this environment. Finally, the hippocampus might be involved in certain phases of the working memory task – for example feature binding [Hannula and Ranganath, 2008, Kesner et al., 2005].

2.1.4 Hippocampal Oscillations Underlying Mnemonic Processes

Neurophysiological recordings during working memory tasks show increased activation in various brain regions including the hippocampus in the form of synchronous activity at theta-band $(4 - 12\,Hz)$ [Buzsáki, 2002, Raghavachari et al., 2001, Tesche and Karhu, 2000] and gamma-band $(\geq 30\,Hz)$ [Colgin and Moser, 2010, Howard et al., 2003, Lisman and Jensen, 2013, Nyhus and Curran, 2010, Osipova et al., 2006, Sederberg et al., 2007, van Vugt et al., 2010] frequencies. At the neuronal level, this increased activation happens simultaneously with rapid persistent firing, a cellular behaviour commonly associated with working memory [Fuster and Alexander, 1971], suggesting that this might be a possible mechanism underlying synchronous oscillations in theta and gamma frequencies [Lisman, 2010].

Gamma Oscillations

Previous research has established that hippocampal gamma oscillations are implicated in the execution of memory tasks [Colgin and Moser, 2010, Colgin, 2016, Howard et al., 2003, Lisman and Jensen, 2013, Nyhus and Curran, 2010, Osipova et al., 2006, Sederberg et al., 2007, van Vugt et al., 2010]. These studies suggest that these oscillations are involved in grouping and binding of multimodal stimuli components when encoding and retrieving memories [Colgin and Moser, 2010], as well as fast communication and coordination between neural ensembles [Fries, 2005].

Several gamma frequency generators have been identified in the hippocampus (for comprehensive reviews see [Bartos et al., 2007] and [Colgin and Moser, 2010]), and these often require local networks of interneurons for precise spike-timing modulation of postsynaptic pyramidal neurons [Cobb et al., 1995, Jonas et al., 2004]. Evidence from in-vitro and in-vivo experiments (reviewed in [Gloveli et al., 2010]), and computational studies (reviewed in [Kopell et al., 2010]) suggests that gamma oscillations arise because inhibitory neurons provide their postsynaptic targets with precise windows of reduced excitability, and consequently of increased excitability once the inhibition fades away. Therefore, these neurons effectively act as a pacemaker, controlling the onset and offset of the network activity. The hippocampus is thought to contain two main gamma frequency generators [Csicsvari et al., 2003]: one within the dentate gyrus and another in CA3. In experimental studies (reviewed in [Csicsvari et al., 2003]), the gamma frequency generator within the dentate gyrus was shown to depend on inputs from the entorhinal cortex, whereas the CA3 generator seemed to be intrinsic whilst propagating its activity into CA1. In general, these two gamma frequency sources are independent, but are nevertheless able to phase-couple. In addition, the gamma oscillations elicited by the dentate gyrus were shown to be faster than those elicited within CA3 [Colgin et al., 2009].

Theta Oscillations

Recordings from the hippocampus have also highlighted the existence of hippocampal theta rhythms. Theta oscillations (see [Colgin, 2013] for a review) are thought to be generated extrinsically in the medial septum, and the diagonal band of Broca and entorhinal cortex, which then impose the rhythm on the hippocampal formation via GABAergic and cholinergic projections [Vinogradova, 1995, Tóth et al., 1997, Kocsis et al., 1999, Fischer et al., 1999, Stewart and Fox, 1990]. However, recent experimental studies [Goutagny et al., 2009, Jackson et al., 2011] have shown that theta oscillations can be generated and maintained intrinsically within the hippocampus, without the need for septal afferents. These findings are supported by existing theoretical models [Traub et al., 1989, White et al., 2000] which indicate that the hippocampus could locally incorporate the necessary cells and circuitry to allow for spontaneous emergence of theta oscillations. These intrinsic mechanisms

within the hippocampus might be required to support theta oscillations triggered by projections from the medial septum.

Theoretical studies have hypothesised that, given their slow synaptic kinetics, hippocampal GABAergic oriens lacunosum-moleculare (O-LM) interneurons [Banks et al., 1998] could account for theta frequency modulation in pyramidal neurons [White et al., 2000] by forming a tightly coupled oscillator [Cobb et al., 1995]. The O-LM neurons provide the pyramidal neurons with precise windows of enhanced excitability, synchronising their activity at theta-band frequencies. This circuitry seems to play an important role in the maintenance of theta oscillations in the isolated hippocampus [Goutagny et al., 2009, Jackson et al., 2011], although the provenance of the inhibitory afferents involved in the circuit remains unclear. In addition, intrinsically bursting pyramidal neurons in CA3 [Traub et al., 1989] might also act as theta frequency pacemakers by controlling the rhythm of their postsynaptic targets. However, the hippocampal circuitry involved in both these models requires external stimulation to maintain the oscillations, and the origin of this stimulation is not specified.

Nested Gamma in Theta Oscillations

Theta and gamma oscillations have been shown to coexist within the hippocampus [Lisman and Jensen, 2013, Lenck-Santini et al., 2008, Pastalkova et al., 2008, Pastoll et al., 2013, Penttonen et al., 1998] in the form of gamma oscillations nested within a theta wave (Figure 2.4A). Experimental evidence suggests that the hippocampus might use nested gamma in theta oscillations when encoding information. In this framework, the data trace is divided into theta-frequency packets of gamma-frequency items (Figure 2.4B). Using this theta-gamma neural code allows one network to store multiple memories encoded as the collaborative firing of a subset of the neurons within the network. Different subsets can encode different items giving rise to a multi-component storage mechanism.

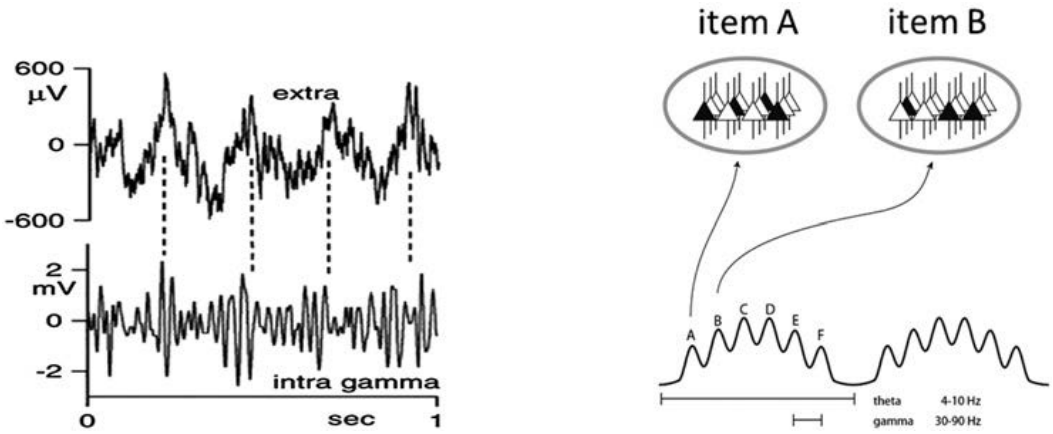

(A) LFP recordings of nested gamma in theta oscillations.

(B) Illustrating the theta-gamma neural code.

Figure 2.4: The theta-gamma neural code allows information to be encoded as theta-frequency packets of gamma-frequency items. (A) Hippocampal LFP recordings of rats showing nested gamma in theta oscillations in the form of theta-frequency clocked packets of high-amplitude fast gamma activity. (B) The theta-gamma neural code illustrated. Several items of information are encoded by different neurons within the same population, during each theta cycle. (Adapted from [Lisman and Jensen, 2013] with permission from the publisher.)

2.1.5 Neural Mechanisms Underlying Hippocampal Mnemonic Activity

The findings summarised here suggest that the hippocampus must incorporate the necessary neural mechanisms allowing it to represent and store transient salient stimuli enabling the correct execution of working memory functions. These mechanisms, cellular, synaptic, or otherwise, have been the focus of neuroscientific research on memory for decades, and to date are far from being fully unravelled. Moreover, there is compelling evidence supporting the hypothesis that oscillatory activity in the gamma and theta bands reflects these working memory functions. In this thesis, we hypothesise that networks of persistent-firing hippocampal neurons could provide a possible neural substrate supporting theta oscillations. This persistent firing relies on intrinsic cellular properties and is driven by the cholinergic system. In addition, persistent firing is a self-sustaining phenomenon which requires solely a short transient stimulus to be triggered.

2.2 The Cholinergic System

The cholinergic system comprises neurons which employ the release and uptake of acetylcholine (ACh) to mediate their electrical activity. Acetylcholine is a neurotransmitter acting on both the peripheral and central nervous system, whose main role is to mediate excitation in the target neurons. This cholinergic neurotransmission has been in fact found to enhance glutamatergic transmission thus increasing neuron excitability in thalamocortical slices of somatosensory cortex [Gil et al., 1997], in the thalamic afference into the prefrontal cortex [Gioanni et al., 1999], and in the entorhinal cortex [Giocomo and Hasselmo, 2005] and dentate gyrus [Radcliffe et al., 1999] projections onto the CA3 area of the hippocampus. Recent studies have highlighted the role that acetylcholine might play in learning and memory (for a complete review see [Hasselmo, 2006]).

2.2.1 Acetylcholine and Memory

Experimental studies have demonstrated that purposively inhibiting the cholinergic system during memory tasks blocks the formation of new memories [Atri et al., 2004, Hasselmo and McGaughy, 2004] and impairs working memory performance [Green et al., 2005]. Furthermore, acetylcholine has been shown to modulate theta rhythm oscillations in the hippocampal formation [Fellous and Sejnowski, 2000, Konopacki et al., 2006, Monmaur et al., 1997, Tiesinga et al., 2001]. Theta rhythms have been identified in neural recordings during learning and memory trials [Buzsáki, 2002, Hasselmo, 2005, Nyhus and Curran, 2010, Raghavachari et al., 2001, Tesche and Karhu, 2000] and are thought to enhance mnemonic performance [Griffin et al., 2004]. In addition, computational models of memory have shown that a precise regulation of theta-band oscillations phases might be crucial for performance in memory tasks [Hasselmo et al., 2002]. Moreover, cholinergic neurons are capable of displaying theta-rhythmic firing patterns during the information encoding and decoding phases of memory trials [Hasselmo, 2006]. Taken together, these observation provide valid evidence supporting the hypothesis that acetylcholine could contribute to improving memory and learning.

2.2.2 Cholinergic-Dependent Memory Consolidation

The cholinergic system might also play an important role in mediating memory consolidation. Memory consolidation is the process by which short-term memory traces are converted into longer-lasting memories. According to the standard model, the memory traces to be consolidated are initially encoded and stored in the medial temporal lobe and in the hippocampus [McClelland et al., 1995, Roediger et al., 2007, Squire, 1987, Squire, 1992]. From here, memories are transferred into the neocortex [Buzsáki, 1989, Hasselmo et al., 1996, Qin et al., 1997, Shen and McNaughton,

1994] over long periods of time, in the order of months or even years. This is dubbed the two-stage model of memory storage.

There is compelling evidence indicating that this form of consolidation occurs during sleep [Maingret et al., 2016, Moroni et al., 2007, Power, 2004, Reasor and Poe, 2008, Siegel, 2001, Stickgold, 2005, Walker et al., 2005], although the mechanisms behind hippocampal-cortex consolidation are far from being fully understood. One theory [Hasselmo, 1999] suggests that acetylcholine could mediate memory consolidation during sleep. Indeed, ACh release levels have been shown to vary significantly during waking and sleep (Figure 2.5). Experimental studies measuring acetylcholine in the hippocampus of rats and cats via microdialysis exhibit high amounts of ACh release during wakefulness and free movement [Kametani and Kawamura, 1990, Marrosu et al., 1995]. In contrast, in the same animals, the levels of ACh release during slow-wave sleep significantly decrease to less than one third of the value during waking.

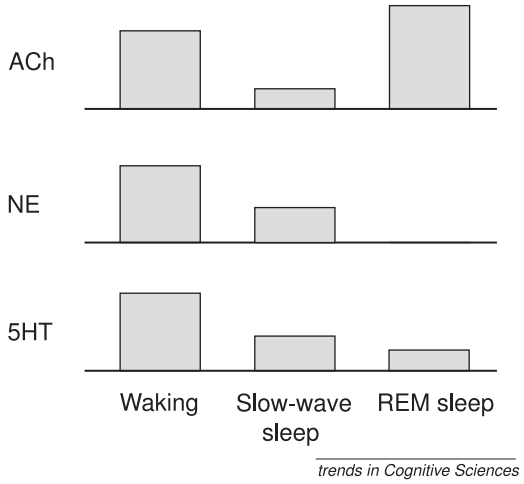

Figure 2.5: Acetylcholine release levels vary significantly between waking and sleep. Hippocampal recordings of rats and cats exhibit high amounts of ACh release during wakefulness and free movement [Kametani and Kawamura, 1990, Marrosu et al., 1995]. In contrast, in the same animals, the levels of ACh release during slow-wave sleep significantly decrease to less than one third of the value during waking. (Adapted from [Hasselmo, 2006] with permission from the publisher.)

The elevated levels of acetylcholine release displayed during waking could provide the neural substrate for the generation of theta oscillations [Marrosu et al., 1995, Monmaur et al., 1997] commonly associated with active behaviours [Buzsáki, 2002, Hasselmo, 2005, Kahana et al., 2001]. In addition, ACh has been shown to suppress the neuronal pathways connecting CA3 to CA1 [Dutar and Nicoll, 1988, Hasselmo and Schnell, 1994, Hounsgaard, 1978, Sheridan and Sutor, 1990, Valentino and Dingledine, 1981] and CA1 to the subiculum [Hasselmo, 1999], effectively inhibiting the propagation of information outside of the hippocampus since the subiculum is the primary gateway into the the entorhinal cortex. Conversely, ACh does not affect the connections between the entorhinal cortex and CA3 [Hasselmo et al., 1995b], nor the connections between the entorhinal cortex and CA1 [Hasselmo and Schnell, 1994], which are the main incoming pathways into the hippocampus. Taken together these observations suggest that, during waking, high acetylcholine release could allow the encoding of new information and the retrieval of old memories in the hippocampus, whilst selectively inhibiting memory consolidation by blocking the pathways connecting the hippocampus to the cortex [Hasselmo, 1999]. Figure 2.6A illustrates the effects of ACh on information routing during wake.

Following this logic, the lower levels of acetylcholine release recorded during slow-wave sleep could mediate an increase in excitation as the cholinergic suppression is lifted. This could entail a reactivation of the outgoing hippocampal pathways (CA3 → CA1 → subiculum → entorhinal cortex),

allowing memories to be consolidated into long-term cortical storage. From a neurological standpoint, this enhanced excitation could be the mechanisms by which sharp-wave ripples [Buzsáki, 1986, Buzsáki, 1989, Buzsáki, 2015] are generated during sleep [Hasselmo, 1999]. In addition, evidence gathered from behavioural experiments on humans [Gais and Born, 2004], suggests that low ACh release during slow-wave sleep might be crucial for memory consolidation. Figure 2.6B illustrates the routing of information from the hippocampus into the neocortex during sleep, as ACh levels drop.

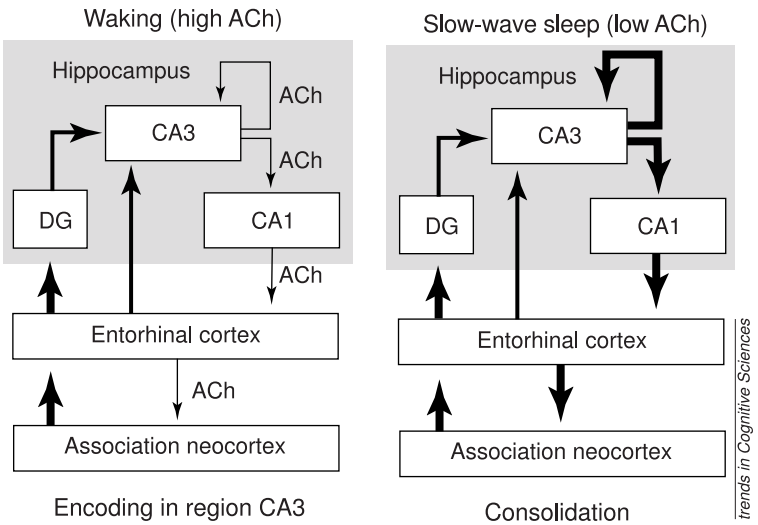

(A) Hich ACh during waking. **(B)** Low ACh during sleep.

Figure 2.6: Acetylcholine mediates memory consolidation during sleep. (A) During waking, memory is encoded and remains in the CA3 area of the hippocampus. The high levels of acetylcholine block the consolidation pathways into the entorhinal cortex and neocortex. (B) During slow-wave sleep, the acetylcholine level lowers, allowing for the memory trace to be replayed in CA3 and transferred into the association neocortex for long-term storage. Thin arrows represent connections which are inhibited by acetylcholine. (Adapted from [Hasselmo, 1999] with permission from the publisher.)

2.2.3 Cholinergic Persistent Firing

Neurons in the entorhinal cortex receive several cholinergic projections. These have been shown to enhance the persistent firing activity of such neurons [Klink et al., 1997]. In this study, in the presence of the cholinergic agonist carbachol (Cch), long-lasting persistent firing was elicited in a cortical neuron given a strong transient stimulus. A similar neuron in standard control condition (in the absence of Cch), on the other hand, will respond to the stimulus and then return to its quiescent state. This behaviour is illustrated in Figure 2.7. The elicited persistent activity is thought to be due to acetylcholine activating an intrinsic calcium-dependent non-specific cationic (CAN) current in the target neuron [Fransén et al., 2002].

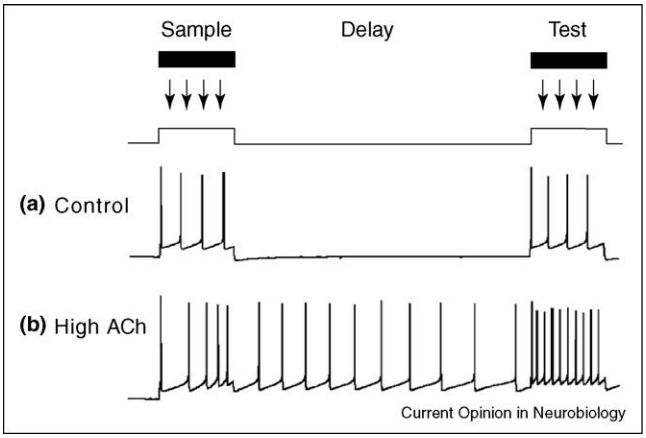

Figure 2.7: Persistent firing is elicited in a cell perfused with the cholinergic agonist carbachol, given a strong transient stimulus. In contrast, the control neuron fires only when stimulated. The concentration of acetylcholine regulates the onset of the persistent firing. (Adapted from [Hasselmo, 2006] with permission from the publisher.)

2.3 Calcium-Activated Non-Specific Cation Channels

Calcium-activated non-specific (CAN) ion channels are characterised by their calcium sensitivity and their non-specificity. The former implies that the channel opening probability is proportional to the intracellular calcium concentration $[Ca]^{2+}$. The latter requires the channel to be permeable to various different ions including Na^+, K^+, Cs^+, Li^+, Ba^{2+} and Ca^{2+}. Is is important to note that the channel permeates only cations. For a more complete review of CAN channels see [Partridge et al., 1994] and [Partridge and Swandulla, 1988].

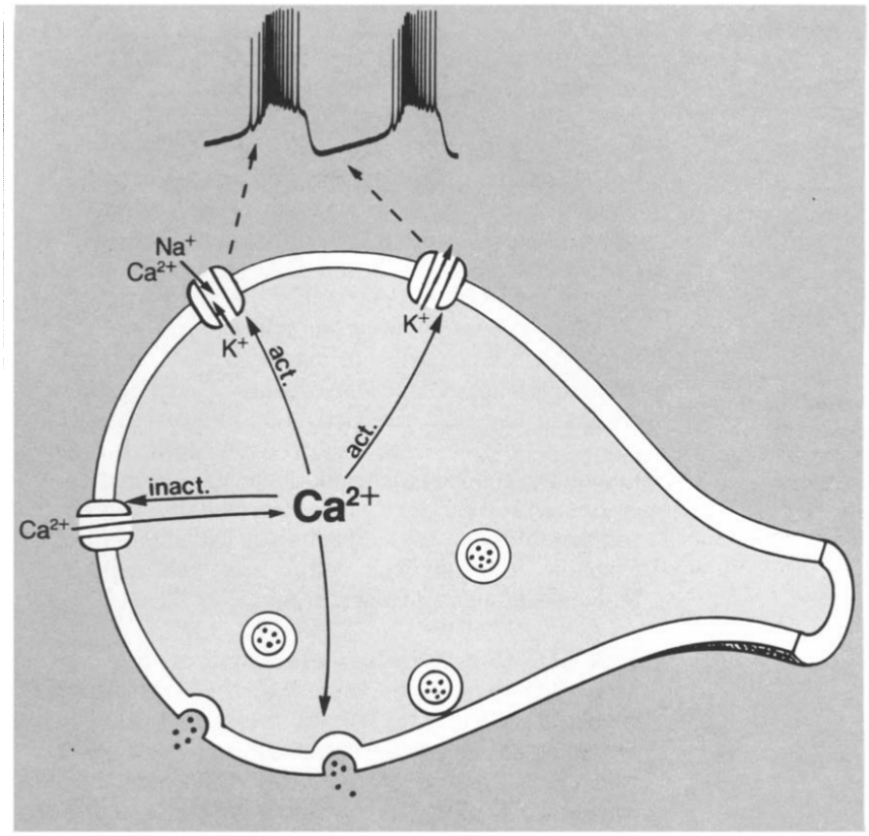

Figure 2.8: Schematic of a CAN channel in a *Helix* bursting neuron as described in [Partridge and Swandulla, 1988]. The first spike causes calcium ions to enter the membrane. This influx activates the CAN channels which open and permeate ions thus generating inward currents. These currents sustain a spike burst which terminates when the efflux of potassium ions causes a strong hyperpolarisation of the membrane potential. (Adapted from [Partridge and Swandulla, 1988] with permission from the publisher.)

2.3.1 CAN Channels Maintain Long-Lasting Depolarisations

CAN ion channels have been identified in various cells in the nervous system such as retinal ganglion cells, bursting neurons, neuroblastomata, pacemaker neurons and many more [Partridge et al., 1994]. In most of these cells the CAN channels play an important role in the maintenance of long-lasting depolarisations bound to cellular Ca^{2+} activity (Figure 2.8). This behaviour is due to its voltage-independence, the slow activation-deactivation kinetics of the channel characterised by a double exponential distribution, and a long mean opening time of the channel, in the order of $10^2\,ms$ [Partridge and Swandulla, 1988]. It is therefore clear how such channels could provide a potential mechanisms for sustained neuronal persistent activity.

2.3.2 Intracellular Calcium Dynamics

The intracellular calcium activity comprises four processes: influx, diffusion, buffering and efflux [Yamada et al., 1989]. The calcium ion influx is regulated by a voltage-dependent calcium current I_{Ca} providing the only link between the membrane potential and the intracellular calcium, as follows:

$$\frac{\mathrm{d}[\mathrm{Ca}]_{\mathrm{i}}^{2+}}{\mathrm{d}t} \propto I_{Ca} \tag{2.1}$$

The inbound calcium ions then diffuse through the cytoplasm and bind to various receptors and protein buffers. The remaining unbound ions are then extruded by dedicated calcium pumps. Two of such transport systems have been described: a sodium-dependent pump which derives the energy required for calcium extrusion from the inward flux of Na^+ ions, and a sodium-independent mechanisms relying on ATP as its energy source [Yamada et al., 1989]. The pump mechanism attempts to maintain a reference equilibrium value $[\mathrm{Ca}]_\infty^{2+}$ for the calcium concentration, by extruding calcium ions at a voltage-dependent rate $\tau_{pump}(V_m)$, and is usually modelled as follows:

$$\frac{\mathrm{d}[\mathrm{Ca}]_\mathrm{i}^{2+}}{\mathrm{d}t} \propto \frac{[\mathrm{Ca}]_\infty^{2+} - [\mathrm{Ca}]_\mathrm{i}^{2+}}{\tau_{pump}(V_m)} \tag{2.2}$$

2.3.3 The CAN Current

The dynamics of calcium influx/efflux through the cell membrane effectively modulate the opening and closing dynamics of the CAN ion channels, thus regulating the evolution of a calcium-dependent non-selective CAN current I_{CAN}:

$$I_{CAN} \propto [\mathrm{Ca}]_\mathrm{i}^{2+} \tag{2.3}$$

Various ions permeate the membrane since the CAN channel is non-specific. Thus the generated CAN current will depend on the reversal potential of such ions. These are often approximated by a unique E_{CAN} reversal potential.

2.4 Persistent Firing Underlying Mnemonic Activity

Persistent firing – also referred to as reverberation – is defined as neural activity which outlasts the stimulation which originally triggered it. Since memory can be thought of as the ability to retain information which attracted our attention and is no longer directly available, persistent firing activity has long been thought to be the neuronal mechanism underlying mnemonic activity. In particular in the context of working memory, which requires not only storage capabilities but also involves an important attentional component. Neural reverberation has in fact been observed in several cortical areas of both human subjects and primates performing working memory tasks [Fuster and Alexander, 1971, Major and Tank, 2004]. The maintenance of sustained activity however is not limited to memory networks but has also been recorded in oculmotor and head-direction systems [Compte, 2006]. This leads to the hypothesis that persistent firing might be:

> "A general computational strategy developed by the nervous system for all those situations where information relevant for the organism but no longer available to the senses needs to be kept over short periods of time for immediate access and evaluation". [Compte, 2006]

The characteristics of persistent firing have been widely investigated [Compte, 2006, Major and Tank, 2004] identifying two main mechanism supporting persistent firing: synaptic interactions, and intrinsic cellular properties. Synaptic persistent firing relies on strong reciprocal excitatory connections within neural assemblies and between brain structures, allowing the propagation and the maintenance of an initial triggering stimulus via excitatory postsynaptic potentials. Conversely, cellular-based persistent firing depends on intrinsic cellular currents which enable long-lasting and self-sustaining membrane depolarisations following the release of action potentials. Although somewhat opposing, there is growing evidence that these two distinct mechanisms might in fact cooperate in generating persistent activity [Major and Tank, 2004].

2.4.1 Synaptic Persistent Activity in Reentrant, Recurrent Networks

Synaptic persistent activity is thought to rely upon strong feedback excitation in the local circuit which absorbs and relays the stimulus across the network thus maintaining elevated firing. Furthermore, from a dynamical point of view, the neurons inside such a memory population must display asynchronous firing patterns. Indeed, if the neurons were to discharge simultaneously at any given time they would then all hyperpolarise and fall into their respective refractory periods. This would effectively cause them to ignore the incoming postsynaptic currents resulting from these action potentials. Non-synchronous discharges are therefore crucial to the maintenance of the activity within the population [Compte, 2006].

Reentrant networks are characterised by a distinct topology which involves both cyclic and feedback connections. This provides the network with temporal dynamics in that the state of the network at time t depends on its state at $t-1$. In simple terms, reentrant networks can be thought of as ensembles of strongly interconnected neurons. These recurrent connections can be thought of as the result of Hebbian learning [Amit, 1995, Hebb, 1949]. This is easily understood if we consider the scenario in which a reentrant population is used to encode a memory item. The neurons within the memory population will cooperate due to their strong internal coupling.

There is a large volume of published studies describing the role of recurrent networks in sustaining reverberation [Amit and Brunel, 1997, Brunel and Wang, 2001, Wang, 1999, Wang, 2001]. The central tenet of this school of thought is that, if sufficiently stimulated, a set of densely and strongly connected neurons can provide the necessary excitation capable of maintaining persistent activity even after the original stimulus has disappeared [Compte, 2006]. Within the hippocampus, the abundantly recurrent CA3 field is a prime candidate supporting the hypothesis of synaptic persistent firing [Hasselmo et al., 1995a, Marr, 1971, McNaughton and Morris, 1987, Treves and Rolls, 1994, Wiebe et al., 1997, Willshaw and Buckingham, 1990]. However, there is growing evidence towards the importance of the much less recurrent CA1 field [Amaral, 1993, Deuchars and Thomson, 1996, Miles and Wong, 1986] for short-term memory [Kesner et al., 2005]. In addition, network models of synaptic persistent activity have been shown to suffer from some limitations.

Arguing Stability

The detailed mechanisms underlying the maintenance of reverberation in a recurrent network are yet to be fully understood. In particular, these types of networks present a number of intrinsic issues which undermine their stability during the persistent activity phase. More specifically, the main caveat with recurrent network models is that of stabilising the reverberation. In a network displaying strong local excitation, what prevents the elevated firing rate to push the entire network into overdrive? Neuronal recordings of persistent activity in neurons in the prefrontal cortex have revealed that these neurons exhibit controlled firing rates in the gamma range [Funahashi et al., 1989, Fuster and Alexander, 1971, Wang, 1999, Young et al., 1997]. This indicates that precise neural mechanisms for modulating the persistent firing frequency of neural assemblies must exist within the brain. Studies have suggested that negative feedback mechanisms could provide the necessary inhibition to maintain the reverberation within a stable range. However, the inhibition must not be excessively strong to avoid it from prevailing over the excitation.

Sensitivity to Noise

Another important issue with reentrant networks is that of their sensitivity to background noise [O'Reilly, 2006]. More specifically, reverberation in a population of strongly connected neurons can be easily triggered by background neural activity. Neurons, in fact, are never fully quiescent but are instead spontaneously active with very low firing rates of $\sim 1\,Hz$ when at rest. An easy solution

to this problem could be lowering the recurrent connection weights although this might not provide the network with enough local excitation. Once again we see that the robustness of this approach relies on a fine-tuned equilibrium between excitation and inhibition.

Terminating the Persistent Activity

Finally, reverberating phenomena in the brain are turned on and off within hundred of milliseconds [Major and Tank, 2004]. The mechanisms by which the excitatory self-sustaining activity is shut down are still largely unknown. Existing models have used several methods including a strong excitatory signal broadcast to all the memory populations in the network [Amit and Brunel, 1997]. This excitatory signal then recruits copious inhibition [Compte et al., 2000] which acts upon the entire network. A more simplistic approach is that of generating a hyperpolarising pulse which, applied to the reverberating neurons, resets the persistent activity [Wang, 1999]. However, this fails to address the provenance and the neurophysiological basis of this inhibitory input.

2.4.2 CAN-Mediated Persistent Activity and its Role in Memory

A valid alternative to the network-based mechanisms for the maintenance of persistent activity could rely upon the intrinsic characteristics of individual neurons. In particular, the slow kinetics of CAN receptors could enable a single neuron to elicit several spikes following an initial stimulus-triggered discharge sequence. Several cells with such characteristics have been identified [Partridge et al., 1994], all with a common denominator: equipped with a calcium-activated non-specific cationic (CAN) current [Partridge and Swandulla, 1988, Tai et al., 2011], which is thought to be mediated by canonical transient receptor potential (TRPC) channels [Reboreda et al., 2011, Zhang et al., 2011], these neurons are capable of maintaining elevated self-sustained persistent firing in the theta range for long periods ($> 30\,s$) [Egorov et al., 2002, Jochems and Yoshida, 2013, Knauer et al., 2013].

A Working Model

Various models of CAN-driven persistent activity exist. In most of these, the individual neurons are modelled as to simulate numerous strong afferent cholinergic projections so to enhance the CAN current. In [Fransén et al., 2002] the authors model two types of excitatory neurons: entorhinal layer II pyramidal cells and stellate cells, both possessing intrinsic CAN current dynamics. The Hodgkin-Huxley model equations resemble those of hippocampal pyramidal cells [Traub and Miles, 1991]. The modelled currents include a high-threshold calcium current I_{CaL} [Traub et al., 1994], a calcium-dependent potassium current $I_{K_{AHP}}$ [Traub and Miles, 1991], a fast calcium- and voltage-dependent potassium current K_C [Traub and Miles, 1991], a persistent-type sodium current I_{NaP} [Magistretti et al., 1999], a non-inactivating muscarinic potassium current I_{KM} [Bhalla et al., 1993] and the CAN current I_{CAN} [Traub and Miles, 1991].

Stimulating the single neurons with a strong transient current pulse elicits fast spiking activity during the stimulation period. This activity is then maintained for a long period of time after the stimulus current drops. This persistent firing behaviour is in accord with that observed in neural recordings from the entorhinal cortex of rats during a continuous delayed match-to-sample task [Young et al., 1997].

Moreover, the neuron seems to be capable of resisting "distractions" in the form of hyperpolarising current pulses, at the end of which the persistent activity restarts. Several such negative pulses have to be delivered to the neuron to terminate the persistent activity. It is however unclear from where such a negative current might come from. Existing hypotheses include strong feedback inhibition

recruited on-demand by the neuron [Wang, 2001]. These mechanisms however often seem ad-hoc solutions to specific modelling problems, which are largely due to our little knowledge of this field.

2.4.3 Persistent Firing in the Hippocampus

The hippocampus has long been thought to play a fundamental role for long term memory [Squire, 1992]. Furthermore, recent studies have complemented this view by identifying the in the hippocampus a key structure for the maintenance of short term memory [Hannula et al., 2006, Hartley et al., 2007]. The common view is that strong recurrent connections in the CA3 area of the hippocampus can support memory-related persistent firing [Hasselmo et al., 1995a, Marr, 1971, McNaughton and Morris, 1987, Treves and Rolls, 1994, Wiebe et al., 1997, Willshaw and Buckingham, 1990]. However, there is growing evidence towards the importance of the CA1 area for short-term memory [Kesner et al., 2005] which contrasts with the view that this area cannot support persistent firing due to it not containing as many strong recurrent excitatory feedback loops as CA3 [Amaral, 1993, Deuchars and Thomson, 1996, Miles and Wong, 1986]. In addition, the effects of the CAN current can be found in various hippocampal pyramidal cells [Caeser et al., 1993], including neurons in CA3 [Jochems and Yoshida, 2013] and CA1 [Knauer et al., 2013].

CAN-Mediated Persistent Activity in CA1 Pyramidal Neurons

The findings described in [Jochems and Yoshida, 2013, Knauer et al., 2013] provide an valuable starting point for modelling CAN-mediated persistent firing in the hippocampus. Jochems, Knauer, and colleagues have in fact identified cells in CA3 [Jochems and Yoshida, 2013] and CA1 [Knauer et al., 2013] capable of eliciting and maintaining persistent activity, similarly to the model presented in [Fransén et al., 2002]. In both studies [Jochems and Yoshida, 2013, Knauer et al., 2013], carbachol-perfused hippocampal pyramidal neurons stimulated with a transient current pulse are shown to display either self-terminating or long-lasting persistent activity.

The persistent activity is due to the effect of the CAN current. This hypothesis was tested by blocking this current using flufenamic acid, resulting in a total blockade of persistent firing in most cells [Jochems and Yoshida, 2013, Knauer et al., 2013]. As in [Fransén et al., 2002] the persistent activity is maintained for several seconds after the stimulus current is disabled, and can be terminated only by injecting a strong, long-lasting negative current.

2.4.4 CAN-Mediated Bursting Activity

In [Aoyagi et al., 2002] the authors present a model of a CAN-equipped neuron capable of firing bursts of two or more spikes when stimulated, dubbed chattering neuron. The bursting behaviour relies on a CAN-like current providing depolarising after potentials (DAPs) which, when carefully balanced with after hyperpolarising potentials (AHPs), allow single neurons to fire bursts of two or more spikes. These neurons are intrinsically rhythmical and the number of spikes within each burst depends on the intensity of the CAN conductance. However, they do not display long-lasting intrinsic persistent firing since all firing activity, bursting or otherwise, requires constant extrinsic stimulation. Chattering neurons can also contribute to the synchronisation of larger ensembles of neurons [Aoyagi et al., 2003], and the switch between asynchronous and synchronous firing is CAN-dependent.

Another model of bursting activity [Rubin et al., 2009] relies on the interaction between an inward CAN current and outward Na^+/K^+ currents for rhythmogenesis in small networks of central pattern generators. Here, bursts are defined as rapid successions of action potentials, during which the membrane potential of the neurons always remains far above its resting potential. The burst

initiation requires afterspike dynamic provided by the CAN current, whereas the burst termination requires Ca^{2+} depletion mechanisms. Once again, the model neurons do not display long-lasting intrinsic persistent firing since all firing activity, bursting or otherwise, requires constant extrinsic stimulation.

In conclusion, all of these studies demonstrate that CAN-mediated depolarising after potentials can be combined with intrinsic after hyperpolarising potentials to generate rhythmic firing. Nevertheless, the models described in [Aoyagi et al., 2002, Rubin et al., 2009] fail exploit the persistent-firing capabilities of pyramidal-CAN neurons which we hypothesise plays an important role in rhythmogenesis, could enhance the robustness of the synchronised activity, and could provide a vast range of oscillation frequencies. In this thesis we explore this research direction. We use mathematical modelling of biologically-inspired persistent-firing hippocampal neurons to test our hypotheses.

2.5 General Anaesthesia

General anaesthesia is a reversible drug-induced coma which is commonly administered to patients undergoing surgery due to its desirable properties, which are: loss of consciousness, analgesia, immobility, and amnesia, all obtained whilst preserving physiological stability [Brown et al., 2010]. Indeed, after the induction of general anaesthesia, patients enter a state of sedation during which they are not aware of the surgery, they do not perceive nor react to the noxious stimuli deriving from it, and they do not remember undergoing it. Although having become a standard operating procedure during surgery – in the United States alone, approximately 60000 patients undergo general anaesthesia every day [Brown et al., 2010] – the chemical and neuronal mechanisms by which these effects are obtained are yet to be fully unravelled. In addition, a vast and growing body of literature (see [Brown et al., 2010, Franks, 2008, Mueller et al., 2011] for in-depth reviews) has recently begun studying the loss of consciousness caused by anaesthesia as a way to indirectly investigate and improve our understanding of consciousness [Alkire et al., 2008]. In the present thesis we focus our attention on the amnesic effect of general anaesthesia, with the aid of computational models, as a means of investigating from a different perspective the mechanisms underlying memory consolidation during wake.

2.5.1 GABA Receptors

GABA receptors are ubiquitous in the brain and central nervous system [Belelli et al., 2009]. Indeed, approximately one third of the synapses in the central nervous system are thought to be GABAergic [Möhler, 2001, Sigel and Steinmann, 2012]. There are two known classes of GABA receptors, namely $GABA_A$ [Henschel et al., 2008, Johnston, 1996] and $GABA_B$ [Chen et al., 2005, Hill and Bowery, 1981]. $GABA_A$ receptors are ligand-gated ionotropic receptors which control the gating of Cl^- into the cell membrane. $GABA_B$ receptors are metabotropic receptors which are coupled to potassium channels via G-proteins gating K^+ out of the cell membrane. In this thesis we will focus solely on $GABA_A$ receptors since these are generally regarded as the primary target of the anaesthetic agents commonly used during surgery under general anaesthesia, and in particular of propofol [Rudolph and Antkowiak, 2004, Zhou et al., 2012] (Figure 2.9). Moreover, propofol is the main anaesthetic agent we focus on due to its widespread surgical use, and the availability of published studies.

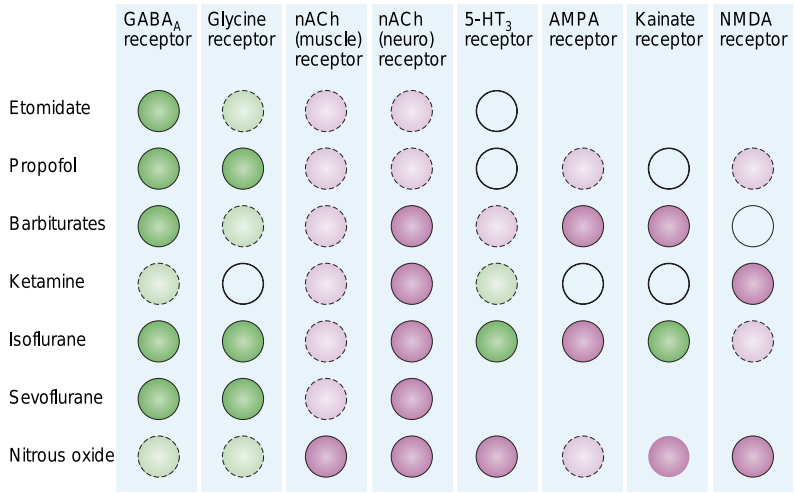

Figure 2.9: GABA$_A$ amongst other ligand-gated receptors are the most common targets for anaesthetic agents. A dark green or dark pink circle indicates significant potentiation or inhibition respectively. A light green or light pink circle indicates little potentiation or inhibition respectively. (Adapted from [Rudolph and Antkowiak, 2004] with permission from the publisher.)

GABA$_A$ receptors can be present both within synaptic clefts, as well as on extrasynaptic locations along the dendrites [Farrant and Nusser, 2005, Luján et al., 2005, Macdonald and Olsen, 1994] (see Figure 2.10 for a schematic). These two different types of GABA$_A$ receptor – synaptic and extrasynaptic – mediate two distinct forms of inhibition. Synaptic receptor activation, following the release of GABA molecules in the synaptic cleft by the presynaptic neuron, causes a short-lasting increase in postsynaptic inhibitory conductance commonly referred to as phasic inhibition. The concentration of available neurotransmitter then decreases over time, as it is diffused away from the postsynaptic cell membrane causing a deactivation of the receptors and the subsequent termination of the synaptic activity.

The presence of GABA in the extracellular space, causes the activation of extrasynaptic GABA$_A$ receptors in locations, such as the dendrites, soma and axon, which are typically distant from the synaptic space where neurotransmitter release occurs. Extrasynaptic GABA$_A$ receptor activation mediates tonic inhibitory currents which last longer than their phasic counterpart, and do not follow the same activation-inactivation patterns [Farrant and Nusser, 2005]. Moreover, GABA$_A$ receptors mediating tonic currents have been shown to be more resistant to desensitisation [Glykys and Mody, 2007].

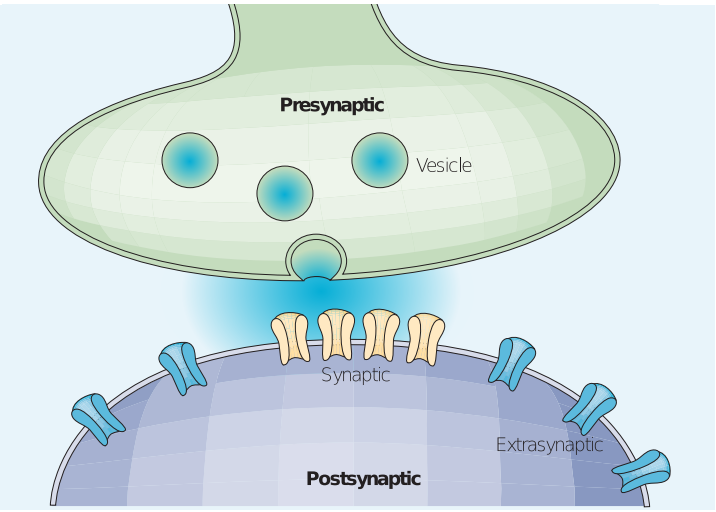

Figure 2.10: GABA receptors can be present both within synaptic clefts, as well as on extrasynaptic locations along the dendrites. (Adapted from [Farrant and Nusser, 2005] with permission from the publisher.)

It is believed that the physiological differences between phasic and tonic inhibition account for their functionally different roles [Farrant and Nusser, 2005]. The asynchronous, slow-desensitising, nature of tonic inhibition causes it to mainly have the effect of increasing membrane resistance and weakening signal integration effectiveness, rendering the postsynaptic neuron less excitable [Semyanov et al., 2003]. Conversely, timing-dependent phasic inhibition plays a variety of more complex roles including synchronising postsynaptic neuron activity in gamma frequencies [Cobb et al., 1995, Jonas et al., 2004], and governing dendritic regenerative electrical activity [Miles et al., 1996, Spruston et al., 1995].

2.5.2 Molecular Effects of the Anaesthetic Agent Propofol

Propofol, 2,6-di-isopropyl-phenol, [Vanlersberghe and Camu, 2008] is an anaesthetic intravenous agent commonly used in surgical operations for the induction and maintenance of general anaesthesia. Propofol-induced sedation is achieved by globally potentiating GABAergic inhibitory activity [Adodra and Hales, 1995, Bai et al., 1999, Bai et al., 2001, Kitamura et al., 2004, McDougall et al., 2008, Song et al., 2011], as the drug binds on $GABA_A$ receptors, both synaptic and extrasynaptic, enhancing their activation [Garcia et al., 2010, Nelson et al., 2002, Rudolph and Antkowiak, 2004, Zhou et al., 2012]. Four main molecular mechanisms are thought to underlie propofol-induced general anaesthesia:

1. An enhancement of the amplitude of $GABA_A$-mediated tonic currents by activating extrasynaptic $GABA_A$ receptors [Bai et al., 2001, McDougall et al., 2008, Song et al., 2011]
2. A potentiation of GABA-mediated synaptic currents by increasing the conductance of synaptic $GABA_A$ receptors [Adodra and Hales, 1995, McDougall et al., 2008]
3. An increase in the baseline of $GABA_A$-mediated synaptic currents by slowing the desensitisation of $GABA_A$ receptors [Bai et al., 1999, Bai et al., 2001, McDougall et al., 2008]
4. An extension in the duration of $GABA_A$-mediated synaptic currents by increasing the closing time of synaptic $GABA_A$ receptors [Bai et al., 2001, Kitamura et al., 2004, McDougall et al., 2008]

Figure 2.11 illustrates the difference in elicited inhibitory postsynaptic potentials in the absence and in the presence of varying concentrations of propofol. Higher dosages of the anaesthetic agent increase the IPSP amplitude and decay time.

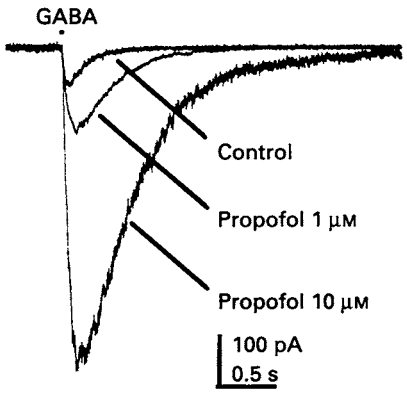

Figure 2.11: Propofol potentiates GABA-mediated synaptic currents by increasing the conductance and the closing time of synaptic $GABA_A$ receptors. (Adapted from [Adodra and Hales, 1995] with permission from the publisher.)

2.5.3 Macroscopical and Behavioural Effects of Anaesthesia

The administration of general anaesthesia is characterised by three distinct phases – induction, maintenance, and emergence – which are marked by the emergence of different behaviours [Brown et al., 2010]. These behaviours are clearly identifiable in electroencephalographical (EEG) recordings of anaesthetised patients [Boly et al., 2012, Cimenser et al., 2011, Purdon et al., 2013]. The induction of anaesthesia is the phase following the initial delivery of the anaesthetic agent. Initially, at low dosages, the EEG signal recorded from the patient shifts from a hight power in the slow alpha waves ($10\,Hz$) commonly associated with wakefulness and closed eyes (Figure 2.12A), to higher power in faster beta oscillations ($13-25\,Hz$) during a state commonly known as paradoxical excitation [Bevan et al., 1997, Brown et al., 2010, Clark and Rosner, 1973, Rampil, 1998] (Figure 2.12B). This phenomenon is dubbed "paradoxical" since it is caused by the administration of drugs which are supposed to suppress excitation rather than fostering it. Paradoxical excitation manifests itself in the form of involuntary purposeless or defensive movements, the expression of incoherent speech, and sometimes euphoria or dysphoria [Bevan et al., 1997, Clark and Rosner, 1973, Gibbs et al., 1936, Kiersey et al., 1951, McCarthy et al., 2008, Rampil, 1998]. As the dosage increases, loss of consciousness is induced, along with loss of skeletal-muscle tone, and a desensitisation to nociceptive stimuli.

Once loss of consciousness ensues, anaesthetic sedation is maintained by constantly administering a combination of drugs including sedatives and anaesthetics. During the maintenance phase, the EEG signals display four different behaviours corresponding to as many sub-phases [Brown et al., 2010]. Phase 1 is the stage of lightest sedation, identified by a decrease in beta power ($13-30\,Hz$) and an increase in alpha ($8-12\,Hz$) and delta ($0-4\,Hz$) power [Feshchenko et al., 2004]. Phase 2 is also known as the antheriorisation phase during which the peak of alpha and delta power shift from posterior to frontal brain regions [Feshchenko et al., 2004, Purdon et al., 2013, Tinker et al., 1977]. During phase 3, the EEG recording shows patterns of alternating flat and alpha and beta activity known as burst suppression [Clark and Rosner, 1973]. Phase 4 is the stage of deepest sedation during which the EEG signal is mainly isoelectric. Surgery is commonly performed during phases 2 and 3, with few exceptions [Brown et al., 2010].

Emergence usually begins as the administered drug dosage is gradually reduced to zero. During this phase the patient slowly regains respiratory control, skeletal-muscle tone, reaction to nociceptive stimuli and ultimately consciousness [Brown et al., 2010]. As this happens, the EEG signals progressively transition from phase 2 or 3 to the patterns commonly associated with the awake state

(Figure 2.12A).

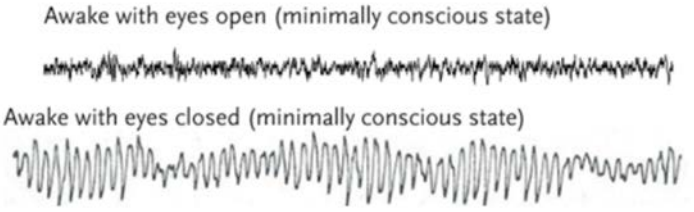

(A) EEG patterns during wakefulness.

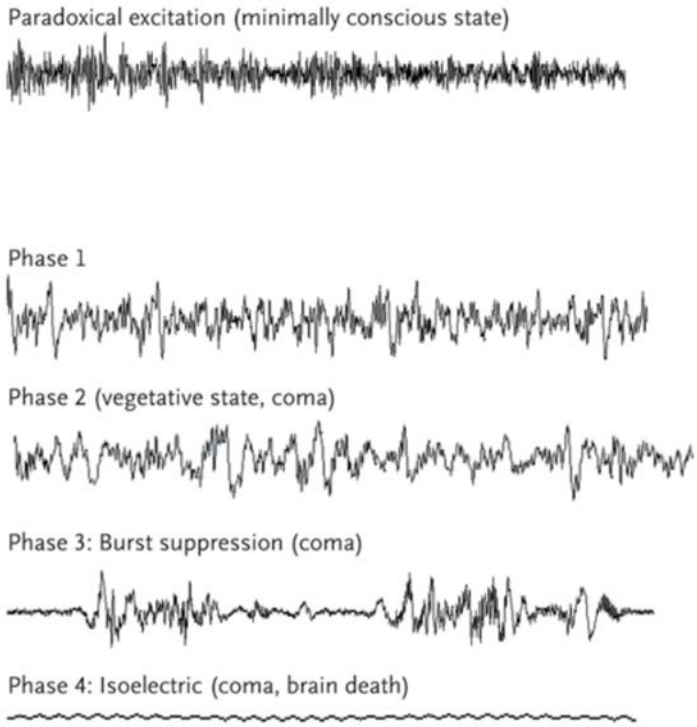

(B) EEG patterns during anaesthesia.

Figure 2.12: Electroencephalographic patterns during wakefulness and anaesthesia. (A) During waking, the EEG displays clearly distinct patterns when the patient's eyes are open and closed. the EEG signal of an awake patient with eyes closed prominently shows alpha ($10\,Hz$) oscillations. (B) During general anaesthesia, the EEG displays five differently identifiable patterns: paradoxical excitation, phase 1 and phase 2, burst suppression, and isoelectric. (Reproduced with permission from [Brown et al., 2010], Copyright Massachusetts Medical Society).

2.5.4 Modelling the Synaptic Actions of Propofol

Recently, mathematical modelling has proven to be a powerful tool in helping describe anaesthetic action and elicited neural behaviours resulting in the emergence of a number of theoretical studies on anaesthesia [Ching et al., 2010, Ching and Brown, 2014, Foster et al., 2011, Hill and Tononi, 2004, McCarthy et al., 2008, Sheeba et al., 2008, Sleigh et al., 2008, Steyn-Ross et al., 2004, Steyn-Ross et al., 2011, Steyn-Ross et al., 2012, Storer and Reeke, 2012]. These models provide valuable

insights and formulate compelling hypotheses aimed at elucidating phenomena which to this date remain largely mysterious.

Paradoxical Excitation

In [McCarthy et al., 2008] the authors present a computational model which studies the emergence of paradoxical excitation at low dosages of anaesthetics by investigating the cellular mechanisms underlying the changes in the EEG signal recorded from anaesthetised patients during paradoxical excitation events – namely an increase in beta power [Gugino et al., 2001]. Their results indicate that an interaction between the GABAergic synaptic current and an intrinsic M-current produces a propofol-dependent switch in inhibitory network activity synchronisation, which enhances excitation in postsynaptic pyramidal neurons [McCarthy et al., 2008] leading to enhanced excitation.

Highly Coherent Alpha Waves

A possible mechanism for the rhythmogenesis of the highly coherent alpha waves recorded throughout anaesthetic sedation [Cimenser et al., 2011, Feshchenko et al., 2004, Purdon et al., 2013] could lie in propofol-enhanced synaptic inhibition [Ching et al., 2010] Binding on synaptic $GABA_A$ receptors, propofol extends the synaptic time constant allowing for slower oscillations than in the absence of anaesthetic agent. The mechanism is similar to that described in the numerous PING studies (see [Kopell et al., 2010] for a review) in which the inhibitory synaptic time constant drives the oscillatory network frequency. The alpha oscillations are also reinforced by the intrinsic membrane current dynamics and reciprocal connectivity of thalamocortical neurons [Ching et al., 2010].

Anteriorisation

Anteriorisation is a phenomenon occurring under general anaesthesia during which the peak of alpha and delta power shift from posterior to frontal brain regions [Feshchenko et al., 2004, Purdon et al., 2013, Tinker et al., 1977]. A recent modelling study [Vijayan et al., 2013] hypothesises that, although propofol enhances globally GABAergic inhibition both in occipital and frontal areas, it also has a selective effect on the thalamocortical neurons which are thought to drive occipital alpha rhythms [Vijayan and Kopell, 2012]. The authors suggest that, since the propofol-mediated weakening of the hyperpolarisation-activated h-current [Ying et al., 2006, Funahashi et al., 2001] was shown to affect these neurons [Vijayan and Kopell, 2012] more than the frontal thalamocortical cells [Ching et al., 2010, Vijayan et al., 2013], this could explain the attenuation of occipital alpha rhythms in favour of frontal alpha.

2.5.5 Modelling Propofol Effects on Tonic Inhibition

All of the afore-mentioned models tend to simplify the effects of propofol on GABAergic inhibition, by reducing it solely to longer inhibitory synaptic opening times, and sometimes increased synaptic conductance. However, propofol binds on both synaptic and extrasynaptic receptors [Bai et al., 2001, McDougall et al., 2008, Song et al., 2011], and this latter effect seems to be ignored by most existing mathematical models. Results from a recent computational study [Hutt and Buhry, 2014] reveal that propofol-enhanced tonic inhibition could play an important role in disrupting cortical synchronisation. These findings support the theory according to which loss of consciousness during general anaesthesia results from an interruption of functional connectivity between brain areas [Mashour, 2005, Tononi, 2004].

2.5.6 Combining Propofol-Enhanced Synaptic and Tonic GABAergic Inhibition

These observations allow us to formulate one compelling research question: what happens to neural synchronisation when affected by both synaptic and extrasynaptic propofol-enhanced inhibition? In this thesis we present a detailed mathematical model including all four of the afore-mentioned effects of propofol on $GABA_A$ receptors. Computational modelling allows us to investigate the emergence of macroscopic behaviours, by simulating neural activity at the microscopic level. This enables us to draw interesting insights of the emergence of paradoxical excitation, intraoperative awareness, and memory consolidation under general anaesthesia.

Summary

In this chapter we presented a survey of our current understanding of various neuroscientific topics, and of the research we conducted in support of this thesis. We described how the neuroanatomy and connectivity of the hippocampus have been shown to account for the roles this structure plays in supporting mnemonic activity. Moreover, the cholinergic system is thought to be implicated in memory consolidation by gating information in and out of the hippocampus. However, the neuronal mechanisms underlying this mechanisms are far from being fully understood. Here, we presented experimental evidence suggesting that networks of persistent-firing hippocampal neurons could be the ideal candidate substrate for memory representation during consolidation, due to their intrinsic properties and firing behaviours. We also introduced recent findings on general anaesthesia and its disrupting effects on synchronous neural behaviours.

CHAPTER

3

THE NEURON MODEL

Contents

Overview

In this chapter we describe the mathematical neuron models we devised and used to simulate neural activity. We begin by describing the hippocampal persistent-firing pyramidal and the hippocampal inhibitory neuron models, their intracellular dynamics, and their parameters. The parameters for the persistent-firing neuron model were derived from experimental in-vitro data. Subsequently, we detail the network configuration and the synaptic interactions we implemented for the simulations. Finally, we describe the computational tools we used when measuring network synchronisation, when identifying oscillations frequency and power, and when analysing the data.

3.1 Persistent-Firing Hippocampal Pyramidal Neurons

A single compartment conductance-based model was used to simulate the persistent-firing hippocampal pyramidal neurons. The current balance equation of the model, representing the evolution of the cell membrane potential over time, is a modified version of the Hodgkin-Huxley formalism [Hodgkin and Huxley, 1952]. Since part of the work presented here involved accurately modelling the electrophysiology of a specific type of hippocampal neuron, we relied upon the Hodgkin-Huxley model to provide us with the highest degree of realism and a precise control over the influence of the individual transmembranal ionic currents on the cell membrane potential. The neuron model is based on the one described in [Jochems and Yoshida, 2015].

3.1.1 Model Equations

The model equation for pyramidal neurons comprises a fast sodium (I_{Na}), potassium (I_K), a leak (I_l) as in [Traub and Miles, 1991], as well as a potassium M-current (I_M) [Yamada et al., 1989] for spike frequency adaptation, a low-threshold calcium current (I_{Ca}) [Reuveni et al., 1993] regulating transmembranal calcium influx, and a CAN current (I_{CAN}) [Destexhe et al., 1994]. Presynaptic spikes received by the neuron generate two synaptic currents I_{synE} and I_{synI} for excitatory and inhibitory synapses respectively. These are summed to produce a total $I_{syn} = I_e + I_i$.

The pyramidal cell model equation takes the form:

$$C_m \cdot \frac{dV_m}{\mathrm{d}t} = -I_l - I_K - I_{Na} - I_M - I_{Ca} - I_{CAN} - I_{syn} + I_{stim} \tag{3.1}$$

Hodgkin-Huxley Ionic Currents

The fast sodium. potassium, and leak current equations are based on the Hodgkin-Huxley model by Traub and Miles [Traub and Miles, 1991], and are defined as:

$$I_l = \overline{g}_l \cdot (V_m - E_l) \tag{3.2}$$
$$I_K = \overline{g}_K \cdot n^4 \cdot (V_m - E_K) \tag{3.3}$$
$$I_{Na} = \overline{g}_{Na} \cdot m^3 \cdot h \cdot (V_m - E_{Na}) \tag{3.4}$$

where V_m is the neuron membrane potential, $\overline{g}_x$ is the maximum channel conductance for each current, E_x is the ion channel reversal potential, for $x \in \{ l, K, Na \}$, and h, n, m are the gating variables of the currents which obey the following rule:

$$\frac{\mathrm{d}x}{\mathrm{d}t} = \alpha_x \cdot (1 - x) - (\beta_x \cdot x) \tag{3.5}$$

for $x \in \{ h, n, m \}$. The α_x and β_x functions are defined below. For the leak, fast sodium and

potassium currents:

$$\alpha_m = \frac{0.32 \cdot (13 - V_m + V_T)}{\exp\left(\frac{13 - V_m + V_T}{4}\right) - 1} \qquad \beta_m = \frac{0.28 \cdot (V_m - V_T - 40)}{\exp\left(\frac{V_m - V_T - 40}{5}\right) - 1} \tag{3.6}$$

$$\alpha_h = 0.128 \cdot \exp\left(\frac{17 - V_m + V_T}{18}\right) \qquad \beta_h = \frac{4}{\exp\left(\frac{40 - V_m + V_T}{5}\right) + 1} \tag{3.7}$$

$$\alpha_n = \frac{0.032 \cdot (15 - V_m + V_T)}{\exp\left(\frac{15 - V_m + V_T}{5}\right) - 1} \qquad \beta_n = 0.5 \cdot \exp\left(\frac{10 - V_m + V_T}{40}\right) \tag{3.8}$$

where V_T is a constant used to shift the resting potential of the neuron from the original Hodgkin-Huxley value of $0\,mV$ [Hodgkin and Huxley, 1952] to a more realistic value. In all our simulations $V_T = 55\,mV$.

Stimulating the neuron with a strong transient current pulse of $I = 400\,pA$ for a $\Delta t_{stim} = 25\,ms$ causes it discharge and record a spike, as shown in Figure 3.1A. The red line below each voltage trace presented in the figures represents the stimulation current. The spike width is approximately $3\,ms$, and the refractory period is approximately $5\,ms$. The contribution of the sodium (I_{Na}) and potassium (I_K) currents to the generation of the action potential, and their corresponding gating variables (m, n, h) are shown in Figure 3.1B and Figure 3.1C respectively.

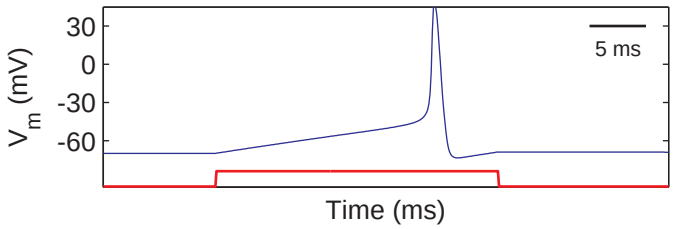

(A) Stimulating the neuron with a strong transient current pulse of $I = 400\,pA$ for a $\Delta t_{stim} = 25\,ms$ causes the neuron to depolarise until a threshold, at which point the neuron discharges and a spike is recorded.

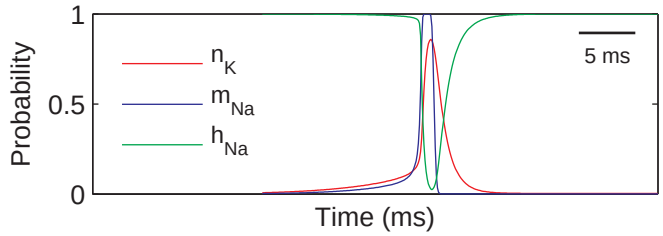

(B) The channel opening and closing dynamics of the Hodgkin-Huxley currents during an action potential.

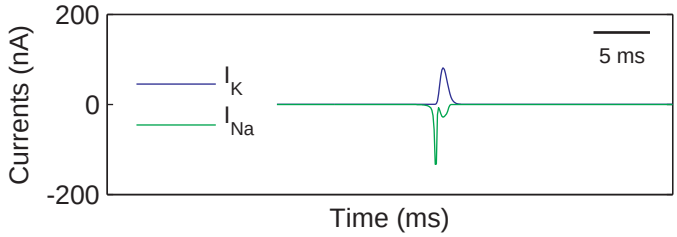

(C) The potassium and sodium Hodgkin-Huxley currents during an action potential.

Figure 3.1: Simulating a single Hodgkin-Huxley neuron until it discharges. The dynamics of the recorded spike are governed by the opening and closing of potassium and sodium channels producing transmembranal currents.

Non-Inactivating Potassic M-Current

The M-current is a slow non-inactivating potassium current which takes its name from the ionic channel it is modulated by. The M channel has the peculiarity of being open at resting potential and of further opening during depolarisation. Therefore, its overall effect is to somewhat raise the activation threshold of the neuron thus modulating its firing rate when subject to a continuous stimulus. This behaviour is known as phasic firing.

The M-current implementation is based on [Yamada et al., 1989] and takes the form:

$$I_M = g_M \cdot p \cdot (V_m - E_K) \tag{3.9}$$

where the gating variable p follows the rule defined in Equation 3.5, and its α and β functions are:

$$\alpha_p = \frac{1}{\tau_M} \cdot \left(3.3 \cdot \frac{\exp\left(\frac{V_m+35}{20}\right) + \exp\left(-\frac{V_m+35}{20}\right)}{\exp\left(\frac{-35-V_m}{10}\right)} + 1 \right) \tag{3.10}$$

$$\tag{3.11}$$

$$\beta_p = \frac{1}{\tau_M} \cdot \left[3.3 \cdot \exp\left(\frac{V_m+35}{20}\right) + \exp\left(-\frac{V_m+35}{20}\right) \cdot \left(1 - \frac{1}{\exp\left(\frac{-35-V_m}{10}\right)+1}\right)\right] \tag{3.12}$$

Injected with a longer stimulation ($I = 200\,pA$ for a $\Delta t_{stim} = 2000\,ms$), the neuron discharges at a firing rate of $f \simeq 43\,Hz$ (Figure 3.2) until the stimulus current drops, in the absence of M, calcium and CAN currents.

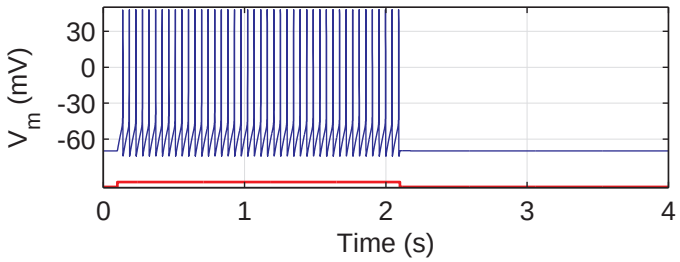

Figure 3.2: Stimulating the neuron with a strong transient current pulse of $I = 200\,pA$ for a $\Delta t_{stim} = 2000\,ms$ causes it to discharge at a firing rate of $f \simeq 43\,Hz$ until the stimulus current drops. The frequency of the firing activity is dependent on the intensity of the stimulation.

In the presence of the M-current, the firing rate of the neuron is now $f \simeq 20\,Hz$ (Figure 3.3A), thus 47% slower than without the M-Current (Figure 3.2). The opening of the modelled M channels increases as the neuron spikes until reaching a maximum opening. This causes the M-current to increase following a similar ramping up profile, as shown in Figure 3.3B. As this current increases so does the activation threshold of the neuron, rendering it less excitable thus less prone to discharging. The resulting effect is a gradual increase of inter-spike intervals corresponding to a slowing down of the firing rate. Eventually, the M current reaches its maximum value and the firing rate of the neuron stabilises at a slower value compared to that of a same neuron without M-current.

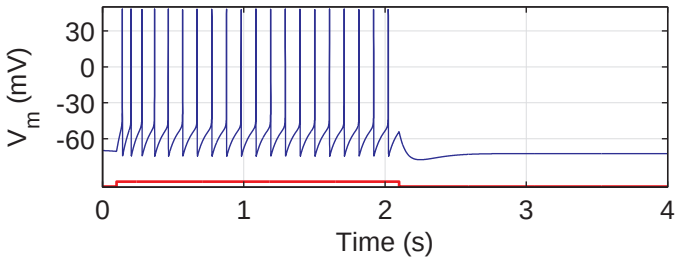

(A) Stimulating the neuron with a strong transient current pulse of $I = 200\,pA$ for a $\Delta t_{stim} = 2000\,ms$ causes it to discharge at a firing rate of $f \simeq 20\,Hz$ until the stimulus current drops. This is 47% slower than the firing rate of a similar neuron without the M-Current component.

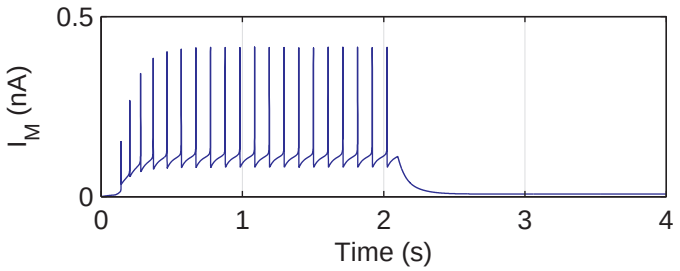

(B) The M-current component increases in intensity at every spike thus rendering the neuron less prone to discharging.

Figure 3.3: The M-current provides the neuron with spike-frequency adaptation. The M-current raises the neuron activation threshold, hence slowing down its firing rate to $f \simeq 20\,Hz$. This firing activity ends when the current stimulus drops. The neuron was stimulated with a transient current of $I = 200\,pA$ for a $\Delta t_{stim} = 2000\,ms$.

Low-Threshold Calcium Current

Adding a low-threshold calcium current component to the model does not modify the firing rate of the neuron which remains stable at $f \simeq 20\,Hz$ (Figure 3.4A). Indeed, the main role of the calcium current is to model the influx of $[\mathrm{Ca}]^{2+}$ ions in the cell membrane. Figure 3.4B shows the evolution of the calcium current over time.

The calcium current was modelled like in [Jochems and Yoshida, 2015]:

$$I_{Ca} = \overline{g}_{Ca} \cdot q^2 \cdot r \cdot (V_m - E_{Ca}) \tag{3.13}$$

where the gating variables q and r follow the rule defined in Equation 3.5, and their α and β functions are:

$$\alpha_q = 0.055 \cdot \frac{-27 - V_m}{\exp\left(\frac{-27-V_m}{3.8}\right) - 1} \qquad \beta_q = 0.94 \cdot \exp\left(\frac{-75 - V_m}{17}\right) \tag{3.14}$$

$$\tag{3.15}$$

$$\alpha_r = 0.000457 \cdot \exp\left(\frac{-13 - V_m}{50}\right) \qquad \beta_r = 0.0065 \cdot \left[\exp\left(\frac{-15 - V_m}{28}\right) + 1\right] \tag{3.16}$$

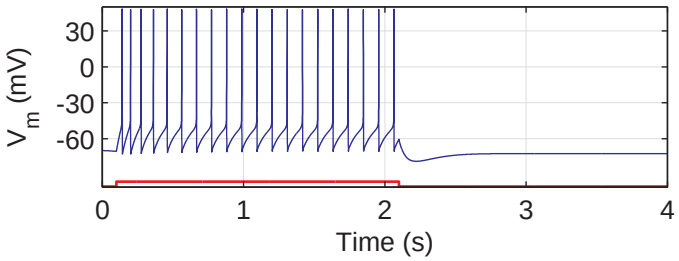

(A) The stimulated neuron discharges at a firing rate of $f \simeq 55\,Hz$ until the stimulus current drops.

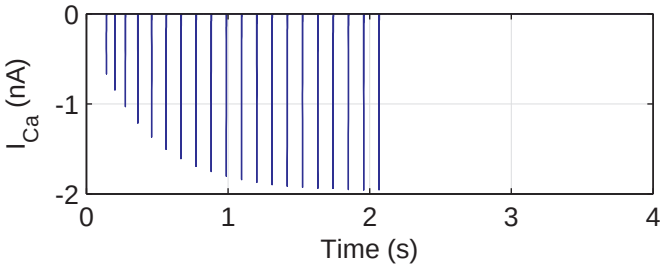

(B) The calcium current governs the inward flux of $[\mathrm{Ca}]^{2+}$ ions in the cell membrane.

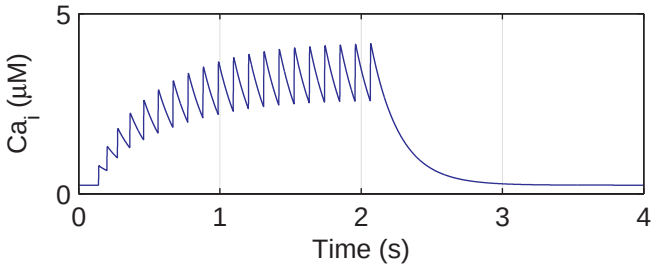

(C) The intracellular calcium concentration increases after each discharge, and decays over time during the after-spike period.

Figure 3.4: The calcium current governs the inward flux of $[\mathrm{Ca}]^{2+}$ ions in the cell membrane. Each spike allows the influx of calcium. The calcium concentration decays over time. The neuron was stimulated with a transient current of $I = 200\,pA$ for a $\Delta t_{stim} = 2000\,ms$.

Intracellular Calcium Dynamics

The transmembranal calcium flux is governed by the calcium current, which causes calcium influx, and a ionic pump, which aims at extruding calcium ions. The dynamics of the diffusion and buffering have been modelled extensively in the literature (see [Yamada et al., 1989]). However, these components are often simplified out of the calcium activity model rendering their effects negligible for the purpose of modelling the CAN current. Indeed, our model does not include diffusion and buffering.

The calcium dynamics are modelled by the following differential equation [Destexhe et al., 1993]:

$$\frac{\mathrm{d}[\mathrm{Ca}]_{\mathrm{i}}^{2+}}{\mathrm{d}t} = \gamma(I_{Ca}) + \frac{[\mathrm{Ca}]_{\infty}^{2+} - [\mathrm{Ca}]_{\mathrm{i}}^{2+}}{\tau_{CAN}} \tag{3.17}$$

where $[\mathrm{Ca}]_{\mathrm{i}}^{2+}$ is the intracellular calcium concentration, $\gamma(I_{Ca})$ is a function of I_{Ca} which represents the opening of the calcium channel, $[\mathrm{Ca}]_{\infty}^{2+}$ is a constant representing the calcium concentration

when the channel is open for a time interval $\Delta t \to \infty$, and τ_{CAN} is a time constant representing the rate of calcium removal from the cell. The calcium influx is modelled as:

$$\gamma(I_{Ca}) = \begin{cases} \frac{-k_u \cdot I_{Ca}}{area} \cdot \frac{1}{2 \cdot F \cdot depth} & : x \geq 0 \\ 0 & : x < 0 \end{cases} \tag{3.18}$$

where k_u is a unit conversion constant, *area* is the surface of the cell membrane, F is Faraday's constant and *depth* is the depth at which the calcium is stored in the cell.

Every time the neuron emits an action potential, the intracellular calcium concentration $[\mathrm{Ca}]_{\mathrm{i}}^{2+}$ increases by a fixed amount $\Delta[\mathrm{Ca}]_{\mathrm{i}}^{2+}$ of approximately $0.5\,\mu M$ (Figure 3.4C). During the after-spike period the calcium concentration decays over time.

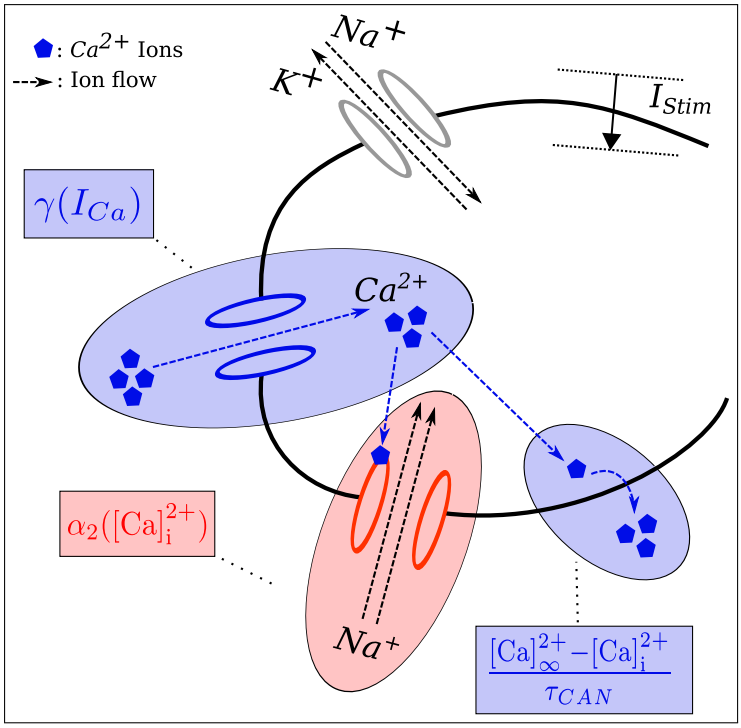

Figure 3.5: Schematic of the calcium dynamics (influx and efflux) and the activated CAN current. Ca^{2+} ions (blue) enter the cell membrane, and bind on CAN receptors (red) causing them to open and permeate Na^+ ions.

Calcium-Activated Non-Specific Current

Part of the intracellular Ca^{2+} ions are in turn responsible for gating calcium-activated non-specific cation (CAN) channels [Partridge et al., 1994]. CAN channels are permeable to K^+ and Na^+ ions [Schultz, 1990] whose flux generates a CAN current I_{CAN}. The CAN current was modelled as in [Destexhe et al., 1994]:

$$I_{CAN} = g_{CAN} \cdot s^2 \cdot (V_m - E_{CAN}) \tag{3.19}$$

where the gating variable s follows the rule defined in Equation 3.5, and its α and β functions are:

$$\begin{aligned} \alpha_s &= \alpha_2([\mathrm{Ca}]_\mathrm{i}^{2+}) \cdot T_{adj} \\ \beta_s &= \beta_{CAN} \cdot T_{adj} \\ \alpha_2([\mathrm{Ca_i}]^{2+}) &= \beta_{CAN} \cdot \left(\frac{[\mathrm{Ca}]_\mathrm{i}^{2+}}{[\mathrm{Ca}]_\mathrm{c}^{2+}} \right)^2 \\ T_{adj} &= 3.0^{\frac{T-295.15}{10}} \end{aligned} \tag{3.20}$$

Here, $\alpha_2([\mathrm{Ca}]_\mathrm{i}^{2+})$ is a function of the intracellular calcium concentration $[\mathrm{Ca}]_\mathrm{i}^{2+}$, β_{CAN} is a constant used to adjust the maximum closing rate of the channel, T_{adj} is a function of the temperature used to adjust the channel opening temperature-dependence, and T is the temperature at which the simulation is run, in Kelvins.

3.1.2 Modelling CAN-Mediated Persistent Firing

When stimulated with a transient current of $I = 200\,pA$ for a $\Delta t_{stim} = 2000\,ms$, the CAN-equipped pyramidal neuron discharges at a frequency of $f \simeq 47\,Hz$ during the stimulation period (3.6A). Once the injected current is removed, the neuron maintains a persistent firing activity at a frequency of $f \simeq 6\,Hz$ (Figure 3.6A). This persistent firing is maintained solely by the CAN current (Figure 3.6B) and its frequency is modulated by the CAN conductance (g_{CAN}).

The action potentials discharged during the initial stimulation allow for enough Ca^{2+} ions to enter the cell membrane so that once the stimulus is removed the CAN current continues to slowly depolarise the neuron until its firing threshold (Figure 3.6C). The neuron then emits an action potential causing further influx of Ca^{2+} ions, effectively rendering this CAN-mediated persistent firing a self-sustaining mechanism. Figure 3.7 illustrates the current-frequency (I-F) curve of a model hippocampal persistent-firing neuron.

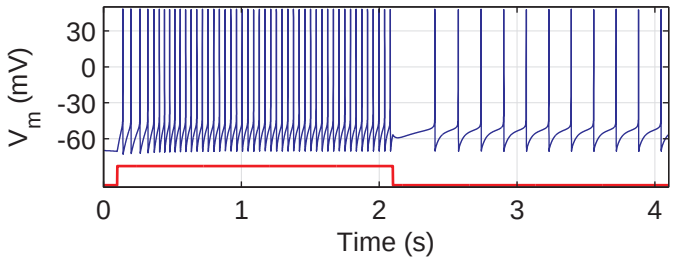

(A) The stimulated neuron discharges at a firing rate of $f \simeq 47\,Hz$ during the stimulation period. Once the input current pulse drop, the neuron maintains its activity at a frequency of $f \simeq 6\,Hz$.

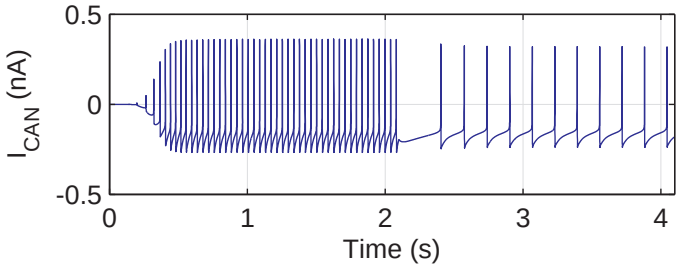

(B) The CAN current enables the neuron to maintain a firing activity at a rate of $f \simeq 6\,Hz$ after the stimulus current pulse drops.

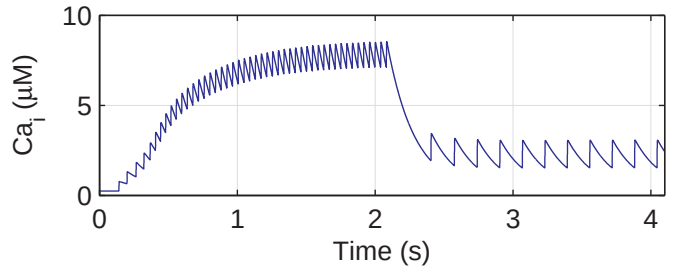

(C) The intracellular calcium concentration increases after each discharge, and decays over time during the after-spike period.

Figure 3.6: The CAN current enables the neuron to maintain a persistent firing activity at a rate of $f \simeq 6\,Hz$ after the stimulus current pulse drops. Each spike allows the influx of calcium in the membrane, which activates the CAN current allowing for subsequent spikes to be discharged. Therefore, this is a self-sustaining mechanism, provided the intracellular calcium concentration remains above a threshold. The neuron was stimulated with a transient current of $I = 200\,pA$ for a $\Delta t_{stim} = 2000\,ms$.

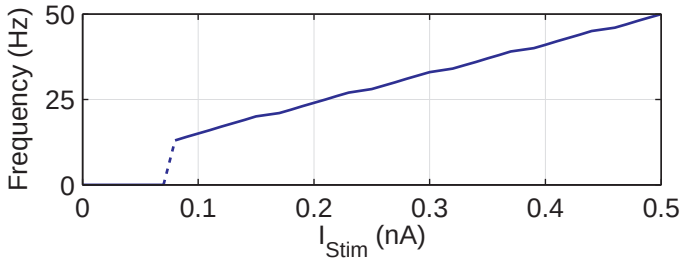

Figure 3.7: Current-voltage curve of the hippocampal pyramidal neuron. The neuron remains quiescent ($f = 0\,Hz$) when stimulated by low-intensity currents ($I_{Stim} \leq 70\,pA$). Increasing the current to $I_{Stim} = 80\,pA$ causes the neuron to suddenly begin firing at a frequency of $f = 13\,Hz$. Further increases in stimulation current cause subsequent increases in firing rate. The neuron was stimulated with a current ranging from $0\,pA$ to $500\,pA$ in steps of $10\,pA$. The firing rate was computed as the average number of spikes during a $5\,s$ stimulation.

3.1.3 Model Parameters

Table 3.1 summarises the parameter values used for the pyramidal CAN-equipped persistent firing neuron model, unless otherwise specified in this manuscript. A horizontal bar above the current conductance indicates that this value is a constant which never changed throughout the simulations (for example $\overline{g}_L$). Conversely, g_M and g_{CAN} values did change depending on the simulation and are therefore represented without the horizontal bar.

Parameter	Value	Parameter	Value
$\overline{g}_l$	$0.01\,mS\,cm^{-2}$	β_{CAN}	$0.00002\,ms$
E_L	$-70\,mV$	$[\mathrm{Ca}]_{\infty}^{2+}$	$2.4 \cdot 10^{-4}\,mol\,m^{-3}$
$\overline{g}_K$	$5\,mS\,cm^{-2}$	τ_{CAN}	$1000\,ms$
E_K	$-100\,mV$	$[\mathrm{Ca}]_{\mathrm{c}}^{2+}$	$0.75 \cdot 10^{-3}\,mol\,m^{-3}$
$\overline{g}_{Na}$	$50\,mS\,cm^{-2}$	$Temp$	$(36 + 273.15)\,K$
E_{Na}	$50\,mV$	k_u	10^4
g_M	$0.03\,mS\,cm^2$	$depth$	$1\,\mu m$
τ_M	$1000\,ms$	$area$	$29000\,\mu m^2$
$\overline{g}_{Ca}$	$0.1\,mS\,cm^2$	C_m	$1\,\mu F\,cm^{-2}$
E_{Ca}	$120\,mV$	V_T	$-55\,mV$
g_{CAN}	$25 \cdot 10^{-3}\,mS\,cm^2$	F	$96489\,C\,mol^{-1}$
E_{CAN}	$-20\,mV$		

Table 3.1: Pyramidal and CAN neuron parameters.

3.2 Hippocampal Inhibitory Neurons

Fast-spiking inhibitory cells comprise only the fast sodium (I_{Na}), potassium (I_K), and leak (I_l) currents in a single current-balance equation, as in [Kopell et al., 2010]. Hippocampal interneurons were shown in vitro to not display persistent firing in response to a single brief stimulation [Sheffield et al., 2011], and therefore do not require calcium and CAN currents. Fast spiking regimes are obtained by appropriately modifying the parameters of the model equation.

3.2.1 Model Equations

The model equations are adapted from [Kopell et al., 2010]:

$$C_m \cdot \frac{\mathrm{d}V_m}{\mathrm{d}t} = -I_l - I_K - I_{Na} - I_{syn} \tag{3.21}$$

where:

$$I_l = \overline{g}_l \cdot (V_m - E_l) \tag{3.22}$$
$$I_K = \overline{g}_K \cdot n^4 \cdot (V_m - E_K) \tag{3.23}$$
$$I_{Na} = \overline{g}_{Na} \cdot m^3 \cdot h \cdot (V_m - E_{Na}) \tag{3.24}$$

The activation variables m, h, n obey the following rule:

$$\frac{\mathrm{d}x}{\mathrm{d}t} = \frac{x_\infty - x}{\tau_x} \qquad x_\infty = \frac{\alpha_x}{\alpha_x + \beta_x} \qquad \tau_x = \frac{0.2}{\alpha_x + \beta_x} \tag{3.25}$$

for $x \in \{ m, h, n \}$. The α and β functions for each activation variable are defined as:

$$\begin{aligned} \alpha_m &= \frac{0.1 \cdot (V_m + 35)}{1 - \exp\left(-\frac{(V_m+35)}{10}\right)} & \beta_m &= 4 \cdot \exp\left(-\frac{(V_m + 60)}{18}\right) \\ \alpha_h &= 0.07 \cdot \exp\left(-\frac{(V_m + 58)}{20}\right) & \beta_h &= \frac{1}{\exp(-0.1 \cdot (V_m + 28)) + 1} \\ \alpha_n &= \frac{0.01 \cdot (V_m + 34)}{1 - \exp(-0.1 \cdot (V_m + 34))} & \beta_n &= 0.125 \cdot \exp\left(-\frac{(V_m + 44)}{80}\right) \end{aligned} \tag{3.26}$$

Stimulated with a $100\,pA$ current pulse lasting for more than $2\,s$, an isolated inhibitory neuron discharges at a frequency of $f \simeq 43\,Hz$ (Fig. 3.8). Once the stimulation ceases the neuron becomes quiescent. Figure 3.9 illustrates the current-frequency (I-F) curve of a model hippocampal inhibitory neuron.

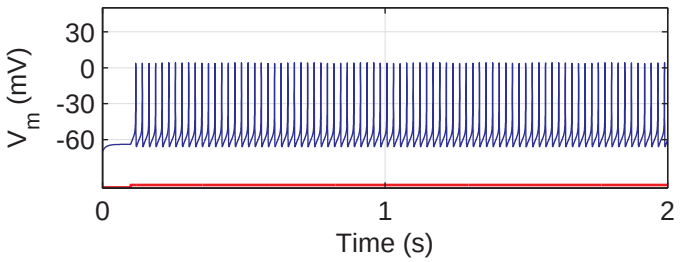

Figure 3.8: Fast-spiking hippocampal inhibitory neurons discharge at a firing rate of $f \simeq 43\,Hz$ during the stimulation period. The firing activity ceases once the stimulus drops. The neuron was stimulated with a current $I_{stim} = 100\,pA$.

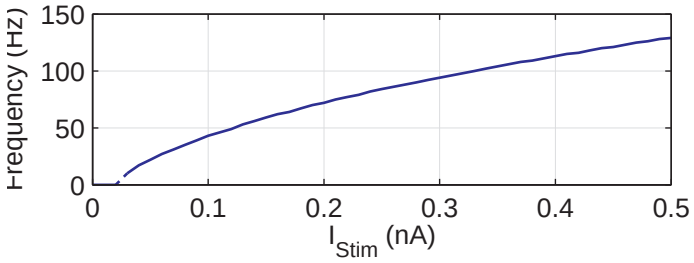

Figure 3.9: Current-voltage curve of the hippocampal inhibitory neuron. The neuron remains quiescent ($f = 0\,Hz$) when stimulated by low-intensity currents ($I_{Stim} \leq 70\,pA$). Increasing the current to $I_{Stim} = 80\,pA$ causes the neuron to suddenly begin firing at a frequency of $f = 13\,Hz$. Further increases in stimulation current cause subsequent increases in firing rate. The neuron was stimulated with a current ranging from $0\,pA$ to $500\,pA$ in steps of $10\,pA$. The firing rate was computed as the average number of spikes during a $5\,s$ stimulation.

3.2.2 Model Parameters

Table 3.2 summarises the parameter values used for the hippocampal inhibitory neuron model, unless otherwise specified in this manuscript.

Parameter	Value	Parameter	Value
$\overline{g}_l$	$0.1\,mS\,cm^{-2}$	$\overline{g}_{Na}$	$35\,mS\,cm^{-2}$
E_l	$-65\,mV$	E_{Na}	$55\,mV$
$\overline{g}_K$	$9\,mS\,cm^{-2}$	$area$	$14000\,\mu m^2$
E_K	$-90\,mV$	C_m	$1\,\mu F\,cm^{-2}$

Table 3.2: Inhibitory neuron parameters.

3.3 Synaptic Connectivity

The synaptic interactions between the neurons are modelled using appropriate excitatory (I_e) and inhibitory (I_i) synaptic currents. These are governed by mono-exponential differential equations.

3.3.1 Synaptic Current Equations

The synaptic currents were modelled with the following equations:

$$I_{syn} = \sum_{x \in \{\, e,i \,\}} I_x \tag{3.27}$$

$$I_x = g_x \cdot (V_m - E_x) \tag{3.28}$$

for $x \in \{\, e, i \,\}$ and $y \in \{\, e, i \,\}$, where E_x is the synaptic resting potential and g_x is the conductance which obeys the following rule, given its time decay constant τ_x:

$$\frac{\mathrm{d}g_x}{\mathrm{d}t} = -\frac{g_x}{\tau_x} \tag{3.29}$$

Two types of synapses were used across all our models: excitatory (e) and inhibitory (i).

Whenever a postsynaptic neuron receives a presynaptic spike its conductance g_x is increased as follows:

$$g_x \leftarrow g_x + w_{yx} \tag{3.30}$$

where w_{xy} is the connection weight between the presynaptic neuron (identified by y) and the postsynaptic neuron (identified by x). For simplicity we relied on single exponential synapses with an instantaneous channel opening rate. Synaptic weights are normalised according to the network size, to ensure that the average synaptic conductance per neuron remains constant.

3.3.2 Connectivity Matrix

The overall network topology can be expressed in terms of the network *connectivity matrix* C_{ji}. This is a square matrix of size $n \times n$ which stores the connection weight between the neurons, where n is the total number of neurons in the network:

$$C_{ji} = \begin{bmatrix} w_{1,1} & \cdots & w_{2,i} & \cdots & w_{2,n} \\ \vdots & \ddots & \vdots & \iddots & \vdots \\ w_{j,1} & \cdots & w_{j,i} & \cdots & w_{j,n} \\ \vdots & \iddots & \vdots & \ddots & \vdots \\ w_{n,1} & \cdots & w_{n,i} & \cdots & w_{n,n} \end{bmatrix}$$

The rows identify the postsynaptic neurons and the columns identify the presynaptic neurons. More precisely, neuron i projects onto neuron j if the entry $w_{ji} \neq 0$.

Unless otherwise specified, the neurons are randomly connected, with a connection probability $p = 0.4$. For a 100-cell network, this yields on average 40 connections per neuron which is commonly regarded as the critical minimum number of synaptic contacts needed to for the emergence of synchronous activity in model networks [Wang and Buzsáki, 1996], independently of network size. In addition, an all-to-all connectivity ($p = 1$) would most likely guarantee the presence of synchronous oscillations, although this would be biologically unrealistic. For these reason we chose a connection probability which is compatible with our network size and considerably smaller than $p = 1$.

3.3.3 Model Parameters

The parameters for the model synaptic currents are summarised in Table 3.3.

Parameter	Value	Parameter	Value
E_e	$0\,mV$	E_i	$-80\,mV$
τ_e	$5\,ms$	τ_i	$10\,ms$

Table 3.3: Synaptic current parameters.

3.4 Network Synchronisation

The network synchronisation is computed using the coherence measure defined in [Wang and Buzsáki, 1996]. The measure computes the pair-wise co-occurrence of neuron action potentials $\kappa_{i,j}(\tau)$ given a time windows of size τ. For any pair of neurons X and Y, given their spike trains

represented as a series of ones and zeroes depending on whether the neuron spiked or did not in the time window respectively:

$$X_i(l),\, Y_j(l) \in \{0, 1\} \tag{3.31}$$

$$l = 1, 2, ..., L \qquad L = \frac{t_{sim}}{\tau} \qquad \tau = 10\,ms \tag{3.32}$$

where t_{sim} is the duration time of the simulation, and L is the number of time windows of size τ. Increasing the size of τ augments the probability of spike co-occurrence and allowing for larger synchronisation values which might be unrealistic. For all our computations we used $\tau = 10\,ms$, which we deemed small enough to capture the dynamics of the network without compromising the reliability of the computed coherence values. The pair-wise coherence measure is quantified as:

$$\kappa_{i,j}(\tau) = \frac{\sum_{l=1}^{L} X_i(l) \cdot Y_j(l)}{\sqrt{\sum_{l=1}^{L} X_i(l) \cdot \sum_{l=1}^{L} Y_j(l)}} \tag{3.33}$$

The network synchronisation measure is then computed as the average $\kappa(\tau)$ for a randomly sampled subset of neuron pairs in the network.

$$\kappa(\tau) = \frac{\sum_{i,j \in P} \kappa_{i,j}(\tau)}{N} \tag{3.34}$$

where $P = \{\,(0, 1), (3, 4), ...\,\}$ is a subset of randomly sampled neuron pairs of size N. Unless otherwise specified, the network synchronisation is averaged over a subset containing 10% of the total neuron pairs in the network, without repetitions. $\kappa(\tau)$ is comprised between 0 and 1, representing an asynchronous population firing and fully synchronised firing respectively.

3.5 Defining Frequencies

In this thesis we often describe two distinct frequency measures – network/population frequency and oscillation frequency. The former captures the average firing rate across all the neurons in the population, and is computed as:

$$f = \frac{n_{spikes}}{t_{sim} \cdot N} \tag{3.35}$$

where n_{spikes} is the total number of spikes elicited by all the neurons, t_{sim} is the duration time of the simulation in seconds, and N is the number of neurons in the population. The latter describes the frequency at which the neurons exhibit synchronous activity, if any.

3.6 Identifying Oscillations

The oscillatory frequency and power spectrum of the activity displayed by a neural populations is computed by applying a one-sided Welch transform [Welch, 1967] to the time series of the average membrane potential of the population. This average signal aims at approximating a local field potential recorded with an electrode inserted at the centre of the neuronal population. We chose this measure over the average excitatory synaptic conductance of the network (see [Wang and Buzsáki, 1996] for an example), as averaging over mono-exponential synaptic activity would yield sharp peaks in the averaged signal which would in turn cause problems to the Welch transform. This would not be the case when averaging over the membrane potential. The main assumption behind

our measure is that the membrane potential is representative of synaptic activity since postsynaptic receptors react to presynaptic action potentials. Although several other methods for computing the LFP from spiking activity exist (see [Mazzoni et al., 2015] for a review), we chose this measure for its simplicity since we did not need to model the precise spatial location of an implanted electrode.

3.7 Simulations and Data Analysis

The simulations were run using the BRIAN spiking neural network simulator [Goodman and Brette, 2009] using version 1.4.1. The differential equations were integrated using the implicit Euler method with a time step $dt = 0.1\,ms$. The data analyses and statistical comparisons for both recordings and simulations were performed using Matlab (MathWorks). Average values are represented as mean $\pm$ standard error of the mean. Statistical significance was a p-value of $\alpha < 0.05$. When comparing the *in vitro* data to the simulated neuron p-values were Bonferroni-corrected for multiple comparisons.

Summary

In this chapter we described the mathematical neuron models we devised and used to simulate neural activity. We began by describing the hippocampal persistent-firing pyramidal and the hippocampal inhibitory neuron models, their intracellular dynamics, and their parameters. The parameters for the persistent-firing neuron model were derived from experimental in-vitro data. Subsequently, we detailed the network configuration and the synaptic interactions we implemented for the simulations. Finally, we described the computational tools we used when measuring network synchronisation, when identifying oscillations frequency and power, and when analysing the data.

CHAPTER

4

MODELLING HIPPOCAMPAL THETA OSCILLATIONS

Contents

Overview

In this chapter we present a biologically-inspired model of self-sustained theta-frequency hippocampal oscillations which relies on intrinsic cellular properties commonly found in hippocampal pyramidal neurons [Knauer et al., 2013, Jochems and Yoshida, 2013]. Our work aims at providing one possible explanation for the generation of theta oscillations in the isolated hippocampus. We hypothesise that local networks of intrinsically persistent firing neurons could provide the neural substrate for hippocampal theta rhythm generators. The work described here is one of the first modelling studies showing that theta oscillations can be maintained in CA1, relying solely on intrinsic cellular properties, and without the need for external inputs. We fitted our model parameters to experimental recordings from CA1 persistent firing cells and the key features of the behaviour of our modelled cells are in accordance with the biological data. Although the septum has been demonstrated to be necessary for the generation of hippocampal theta oscillation [Vinogradova, 1995, Tóth et al., 1997, Kocsis et al., 1999, Fischer et al., 1999, Stewart and Fox, 1990], the hippocampus is also thought to rely on its intrinsic properties to maintain this synchronous activity [Goutagny et al., 2009, Jackson et al., 2011, White et al., 2000, Traub et al., 1989] which is crucial to perform working memory tasks. Our results demonstrate that synchronous rhythmic activity can be maintained in a network of CAN-equipped persistent firing pyramidal neurons, in the absence of external stimulation. The model and the results presented in this chapter were published in [Giovannini et al., 2015b, Giovannini et al., 2016, Giovannini et al., 2017].

4.1 Persistent Firing CA1 Hippocampal Neurons

Intracellular patch-clamp studies of rat brain slices show that persistent firing can be induced in pyramidal hippocampal neurons both in CA3 [Jochems and Yoshida, 2013] and in CA1 [Knauer et al., 2013]. Stimulated with a brief transient current pulse, these neurons continue discharging action potentials after the stimulus ceases. This persistent activity is mediated by cholinergic CAN receptors and can last for long delay periods, in the order of several tens of seconds. Moreover, persistent firing is maintained solely by intrinsic cellular mechanisms, and does not require synaptic activity. Our model neuron and its parameters were derived from experimental in-vitro recordings of persistent firing hippocampal neurons carried out by Beate Knauer [Giovannini et al., 2015b, Giovannini et al., 2016, Giovannini et al., 2017].

4.1.1 In-Vitro Recordings Dataset

The biological dataset contained intracellular patch-clamp recordings from a total of 72 CA1 hippocampal pyramidal neurons. The goal of the experiments was to induce persistent firing and study its behaviour, its dynamics, and its physiological properties. Since persistent firing is a cholinergic-dependent mechanism [Knauer et al., 2013], we perfused the cells with solutions containing varying concentrations of the cholinergic antagonist carbachol (Cch) to investigate its effects on persistent activity. The experimental procedures and stimulation paradigms are described extensively in [Giovannini et al., 2017] and [Knauer, 2015].

Four separate sets of cells were stimulated with a $2\,s$, $100\,pA$ square pulse in the presence of $1, 5, 10$, or $20\,\mu M$ Cch ($n = 4, 17, 40, 11$; respectively). In the presence of either $1, 5, 10$, or $20\,\mu M$ Cch CA1 pyramidal neurons showed a persistent firing frequency of $9.3 \pm 2.9\,Hz, 14.7 \pm 1.2\,Hz, 16.6 \pm 0.8\,Hz$, and $15.4 \pm 1.2\,Hz$, respectively (Figure 4.1A and Figure 4.1B). The Cch concentration had a significant effect on the persistent firing frequency in vitro (one-way ANOVA, $F(3, 68) = 3.02, p = 0.036$). Results indicate that in general, higher Cch concentrations yielded a higher persistent firing frequency in vitro. In addition, previous work from Knauer and colleagues [Knauer et al., 2013]

showed that the persistent firing frequency was shown to be independent of the length of the applied stimulation.

The average persistent firing frequency across all cells in vitro was $15.6 \pm 0.6\,Hz$, $(n = 72)$. In line with the average firing frequency, a fast Fourier transform using Welch's modified periodogram [Welch, 1967] confirmed that the highest power for supra-threshold oscillations was around $15\,Hz$ (Figure 4.2A and Figure 4.2A). Figure 4.3A shows a sample voltage trace recorded from a CA1 pyramidal neuron in the presence of 5 μM Cch displaying persistent firing at a frequency of approximately $6\,Hz$. The persistent firing activity can last for long delay periods ($> 30\,s$) [Knauer et al., 2013].

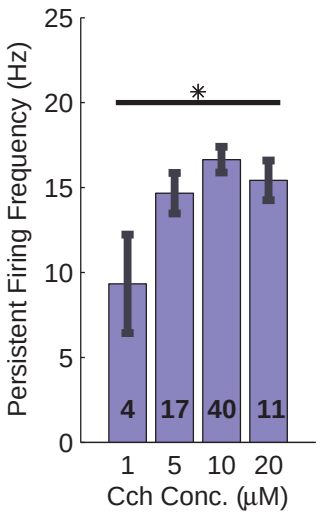

(A) The carbachol concentration (μM) modulates the persistent firing frequency recorded *in vitro*.

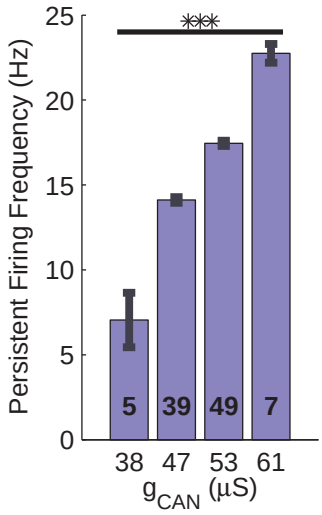

(B) Similary, the CAN conductance (g_{CAN}) modulates the persistent firing frequency of the simulated neurons.

Figure 4.1: The activation of CAN receptors modulates the persistent firing frequency of hippocampal neurons, both *in vitro* and in the model. Line and asterisks over bars indicate statistical significance. Numbers inside the bars represent the cell count. Parameters for the CAN pyramidal neurons shown in the histogram are: $g_{\mathrm{CAN}} = \mathcal{N}(50, 5)\,\mu S\,cm^{-2}$, $g_{\mathrm{M}} = 90\,\mu S\,cm^{-2}$.

4.1.2 Simulating Hippocampal Neurons

Our model neuron allows us to simulate CAN-mediated persistent firing at various different frequencies by adapting the intensity of the CAN current conductance g_{CAN}. In all our simulations the injected current pulse amplitude was $I_{stim} = 200\,pA$. Values of $0\,\mu S\,cm^{-2} \leq g_{CAN} < 36\,\mu S\,cm^{-2}$ did not allow the neuron to display any persistent firing. Persistent firing emerged for values $36\,\mu S\,cm^{-2} \leq g_{CAN} \leq 120\,\mu S\,cm^{-2}$ at firing rates ranging $5\,Hz \leq freq_{pf} \leq 56.26\,Hz$ (Figure 4.4), and lasted indefinitely as long as the intracellular calcium concentration was maintained above a threshold value. Injecting a negative current pulse of the same amplitude as the stimulation current ($-200\,pA$, $\Delta t = 2000\,ms$) interrupted the persistent firing activity (Figure 4.5), indicating that feedback inhibition could provide a robust mechanism to control this persistent activity in a network scenario.

We then ran 20 separate simulations of 100 unconnected model cells assigning varying values of g_{CAN} to each neuron, to fit the model parameters to the experimental dataset. Gaussian-distributed

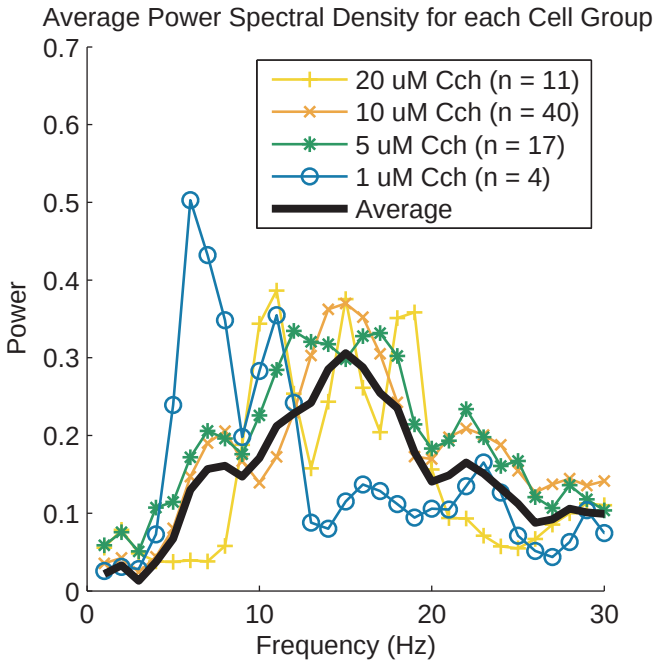

(A) Power spectral density of each group of cells by carbachol concentration (1, 5, 10, and 20 μM for blue circles, red asterisks, orange exes and yellow pluses, respectively), and the average across all groups (thick black line) which shows a peak at $15\,Hz$.

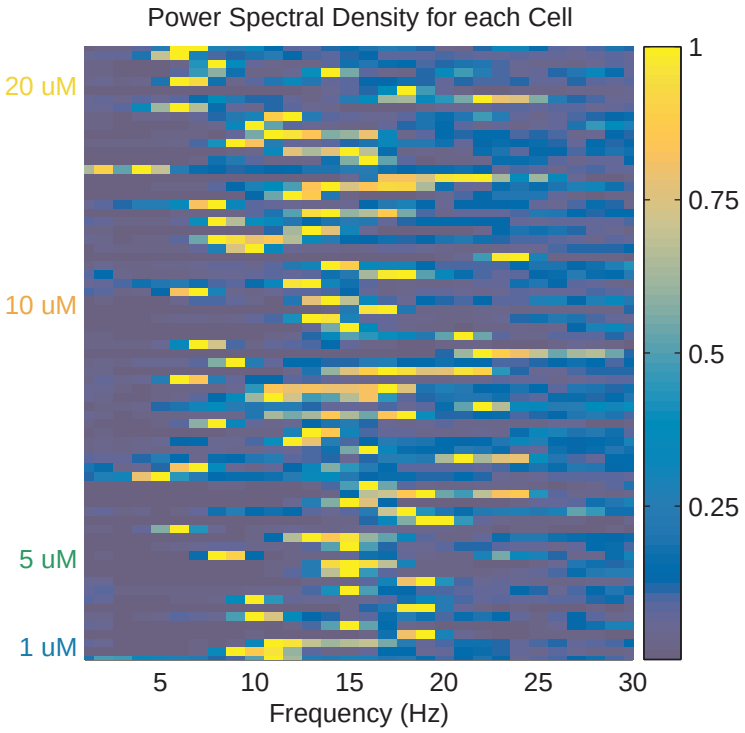

(B) Similary, the power spectral density for each recorded cell shows peaks which are distributed around $15\,Hz$.

Figure 4.2: Power spectral density of the cells recorded *in-vitro*. (A) The average power spectral density across all cells shows a peak at $15\,Hz$. (B) Taken individually, the peak power spectral density of the cells are distributed around $15\,Hz$.

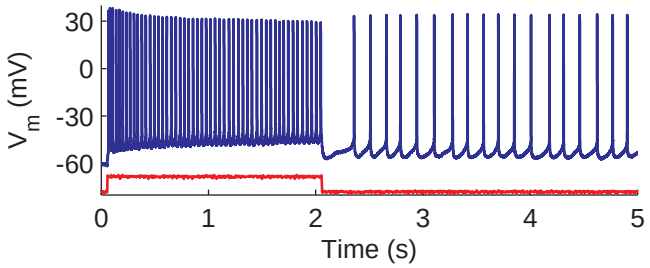

(A) Sample *in-vitro* recording of the membrane potential (V_m) of one CA1 pyramidal neuron showing approximately 6 Hz persistent firing after a 2 s stimulation.

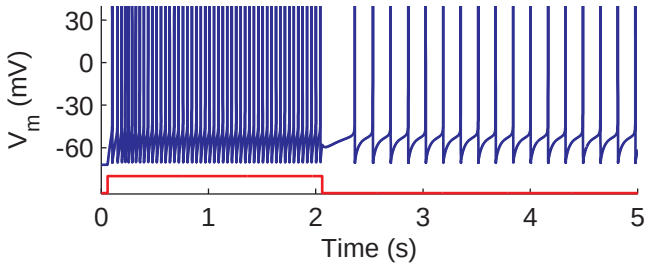

(B) Sample voltage trace for one simulated neuron showing approximately 6 Hz persistent firing after a 2 s stimulation.

Figure 4.3: The model neuron captures the spiking behaviour of the recorded hippocampal cells. In the voltage trace plots the bottom line represents the applied square pulse stimulation current. Persistent firing is elicited after a brief (2 s) stimulation.

heterogeneity was introduced in the CAN conductance ($g_{CAN} = (\mathcal{N}(50, 5)\mu S cm^{-2}$ where $\mathcal{N}(\mu, \sigma)$ indicates a Normal distribution centred on the mean μ with variance σ). The average persistent firing frequency across all cells lay between $15.2 \pm 0.3\,Hz$ and $16.0 \pm 0.3\,Hz$, in accordance with the electrophysiological recordings.

The resulting g_{CAN} values were grouped into four equidistant intervals centred on average g_{CAN} values of $38\,\mu S\,cm^{-2}, 47\,\mu S\,cm^{-2}, 53\,\mu Sc\,m^{-2}$, and $61\,\mu\,Scm^{-2}$, which were each comprised of $5, 39, 49$, and 7 cells, respectively. These groups yielded persistent firing rates of $7.1 \pm 1.6\,Hz, 14.1 \pm 0.2\,Hz, 17.5 \pm 0.2\,Hz, 22.8 \pm 0.6\,Hz$, respectively. We found in all 20 simulations, that an increase in g_{CAN} significantly affected the persistent firing frequency of the pyramidal cells (one-way ANOVA, $F(3, 96) = 176.1$, Bonferroni-corrected $p < 0.001$). Figure 4.1B shows a histogram summarising how different values of g_{CAN} produce different firing rates. These results indicate that higher g_{CAN} values yielded a higher persistent firing frequency. Indeed, modifying g_{CAN} allowed the model neuron to display a rich array of persistent firing rates.

In addition, the average persistent firing frequency across all cells in vitro did not significantly differ from any of the average persistent firing frequencies of the unconnected 100 model cells in 20 separate simulations (2-sample T-test with unequal variances, $0.480 \leq p \leq 0.992$). Figure 4.3B shows a sample voltage trace from a model neuron exhibiting persistent firing at a frequency of approximately 6 Hz with $g_{CAN} = \mathcal{N}(38, 5)\,\mu S\,cm^{-2}$, illustrating how the model captures the main features of the membrane potential dynamics of the recorded cells (displayed in Figure 4.3A). In conclusion, our single neuron model possesses and correctly emulates the characteristics of in vitro intrinsic persistent firing – its frequency range and its positive correlation with CAN current activation (i.e. Cch concentration or g_{CAN}).

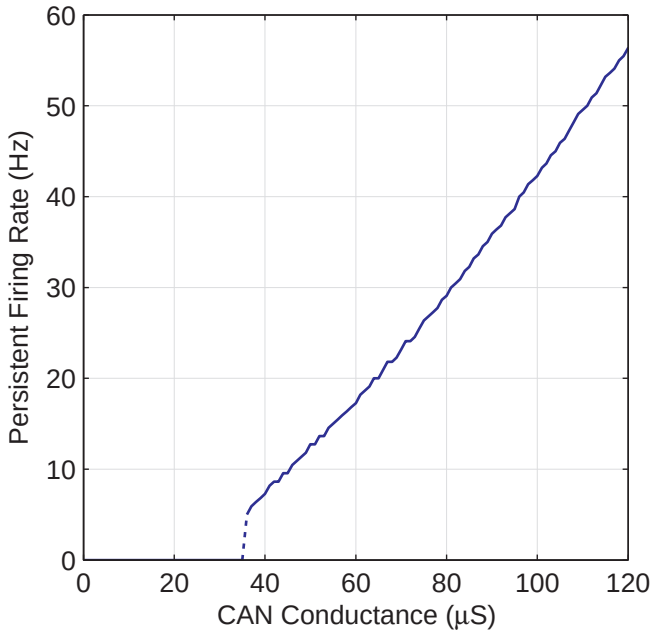

Figure 4.4: The persistent firing frequency increases proportionally to the CAN conductance. The neuron remains quiescent ($freq_{pf} = 0\,Hz$) for $0\,\mu S\,cm^{-2} \leq g_{CAN} < 36\,\mu S\,cm^{-2}$. Persistent firing then abruptly emerges with firing rates ranging $5\,Hz \leq freq_{pf} \leq 56.26\,Hz$ for $36\,\mu S\,cm^{-2} \leq g_{CAN} \leq 120\,\mu S\,cm^{-2}$ The neuron was stimulated with a current of $I_{stim} = 200\,pA$. The firing rate was computed as the average number of spikes recorded $1\,s$ after a $2\,s$ stimulation.

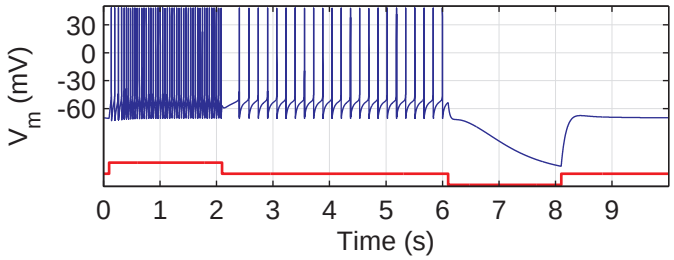

Figure 4.5: The stimulated neuron discharges at a firing rate of $f \simeq 47\,Hz$ during the stimulation period. Once the input current pulse drop, the neuron maintains its activity at a frequency of $f \simeq 6\,Hz$. Injecting a negative current pulse of the same amplitude as the stimulation current ($-200\,pA$, $\Delta t = 2000\,ms$) interrupts the persistent firing activity.

4.2 The Pyramidal-CAN Network

4.2.1 CAN-Equipped Pyramidal Neuron Network Topology

Having obtained a biologically-inspired model of CA1 persistent firing pyramidal neurons (PCAN), we turned our attention to the dynamics of a population comprising 100 of such interconnected neurons. The neurons were randomly connected, with a connection probability of $p = 0.4$ yielding on average 40 connections per neuron, as described in Chapter 3. All the neurons in the network received a $200\,pA$ square current pulse stimulation lasting $250\,ms$. We chose the shortest possible stimulation time which would elicit persistent firing in an isolated neuron, to mimic the brief cue presentation in a delayed match-to-sample working memory task.

4.2.2 Analysing the Persistent Firing Activity of a Hippocampal Pyramidal Population

Intuitively, since our isolated hippocampal neurons are capable of displaying persistent firing, then a network of such interconnected neurons should display similar behaviours. Indeed, our results demonstrate that this statement holds true. Figure 4.6 shows the comparison between the dynamic behaviour of our network of persistent firing neurons and a network of excitatory pyramidal neurons which are not equipped with CAN receptors. We observe how the persistent firing rate of the network was modulated by the strength of the PCAN-to-PCAN synaptic connections (w_{cc}). However, the emergence of the persistent firing behaviour itself did not require synaptic connections ($f = 14\,Hs$ for $w_{cc} = 0\,nS$), due to the intrinsic nature of the persistent firing previously identified *in vitro* [Knauer et al., 2013]. The persistent firing frequency was computed as the average firing rate across the entire population $1\,s$ after the stimulus offset.

The PCAN network displayed a continuous range of persistent firing frequencies, in accordance with [Jochems and Yoshida, 2015], comprised between $14\,Hz$ and $200\,Hz$, with $0\,nS \leq w_{cc} \leq 1.23nS$ and $g_{CAN} = \mathcal{N}(50, 5)\,\mu S\,cm^{-2}$, $g_M = 90\,\mu S\,cm^{-2}$, $0 \leq w_{cc} \leq 1.5\,nS$ (Figure 4.5F top line). Conversely, in the absence of CAN current ($g_{CAN} = 0\,nS$), a similar population of pyramidal neurons (Figure 4.5F bottom line) does not display the same abundance of network dynamics. For synaptic strengths comprised in the range $0\,nS \leq w_{cc} \leq 1.08\,nS$ the population remains quiescent after the stimulus offset (Figure 4.5D). Increasing the synaptic connections ($1.08\,nS \leq w_{cc} \leq 1.32\,nS$) caused an acceleration in the population frequency ($0.08\,Hz \leq f \leq 3.56\,Hz$). This was due to the increased excitation allowing the network activity to persist for a few milliseconds after the stimulus ceased. The activity then quickly faded away as the synaptic activity failed to upkeep it (Figure 4.5E). Further strengthening the synapses ($w_{cc} \geq 1.32\,nS$) enabled the abrupt emergence of fast asynchronous network activity at frequencies greater than $120\,Hz$ (Figure 4.5C).

Neurophysiological recordings of neuronal populations implicated in the short-term maintenance of stimuli during working memory tasks often show elevated firing with frequencies in the gamma range [Funahashi et al., 1989, Fuster and Alexander, 1971, Young et al., 1997]. Experimental studies of hippocampal populations during working memory tasks also show similar activation patterns [McEchron and Disterhoft, 1997, McEchron and Disterhoft, 1999, McEchron et al., 2001], with frequencies spanning $8\,Hz$ to $150\,Hz$ depending on cell type and location. Modelling studies suggest similar activation patterns [Brunel and Wang, 2001, Wang, 1999]. Therefore, the population rates displayed by the CAN network, ranging between $14\,Hz$ and $200\,Hz$, are in accord with both experimental recordings and modelling studies.

4.2.3 Emergence of Self-Sustained Synchronous Activity

A detailed analysis of the raster plots generated by the CAN network showed the emergence of three distinct firing regimes:

- A slow and asynchronous firing regime with persistent firing rates of $14\,Hz \leq f \leq 21\,Hz$, for $0\,nS \leq w_{cc} \leq 0.45\,nS$. Figure 4.5A shows a sample raster plot of this regime with a population rate of $f = 19.45\,Hz$ for $w_{cc} = 0.36\,nS$.
- A synchronous bursting regime in which the network generates oscillatory rhythmic firing, for $0.48\,nS \leq w_{cc} \leq 1.17\,nS$. Figure 4.5B shows a sample raster plot of synchronous oscillations at $f_{osc} = 5\,Hz$ for $w_{cc} = 0.72\,nS$.
- A fast and asynchronous firing regime with firing rates of $f \geq 117\,Hz$, for $w_{cc} \geq 1.2\,nS$. Figure 4.5C shows a sample raster plot of the fast asynchronous firing regime with a population firing rate of $f = 117.3\,Hz$ for $w_{cc} = 1.2\,nS$.

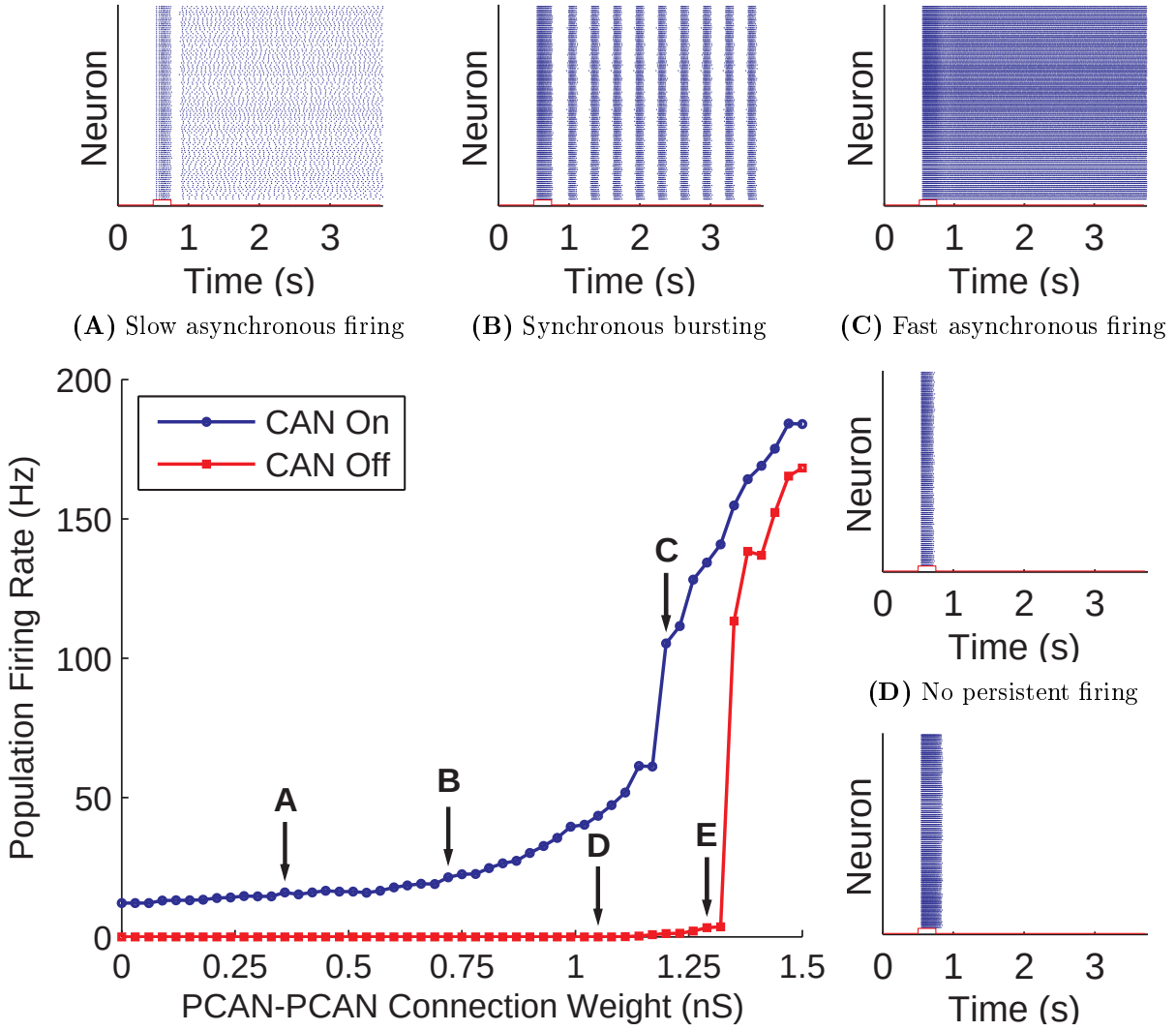

(A) Slow asynchronous firing

(B) Synchronous bursting

(C) Fast asynchronous firing

(D) No persistent firing

(E) No persistent firing

(F) Population firing frequencies of CAN-enabled (top blue line) and CAN-disabled (bottom red line) network as the pyramidal-pyramidal connection weights are strengthened.

Figure 4.6: The CAN current activation allows a 100-cell network to display persistent firing in biologically plausible frequency bands. (A) CAN-enabled Network – Sample raster plot of the slow regime ($0\,nS \leq w_{cc} \leq 0.45\,nS$), with a population firing rate of $f = 19.45\,Hz$ for $w_{cc} = 0.36\,nS$. (B) CAN-enabled Network – Sample raster plot of the synchronous bursting firing regime ($0.48\,nS \leq w_{cc} \leq 1.17\,nS$), showing $f_{osc} = 5\,Hz$ oscillations for $w_{cc} = 0.72\,nS$. (C) CAN-enabled Network – Sample raster plot of the fast firing regime ($w_{cc} \geq 1.2\,nS$), with a population firing rate $f = 117.3\,Hz$ for $w_{cc} = 1.2\,nS$. (D) CAN-disabled Network – Sample raster plot showing the lack of persistent firing in the absence of CAN current ($0\,nS \leq w_{cc} \leq 1.08\,nS$). (E) CAN-disabled Network – Sample raster plot showing firing activity persisting for a few milliseconds after the stimulation is removed ($1.11\,nS \leq w_{cc} \leq 1.32\,nS$), with a population firing rate $0.08\,Hz \leq f \leq 3.56\,Hz$. (F) The population firing frequencies of the CAN pyramidal network span $14\,Hz \leq f \leq 120\,Hz$, with $0\,nS \leq w_{cc} \leq 1.23\,nS$. The CAN network (top line) displays three different firing regimes: a slow regime with firing rates $14\,Hz \leq f \leq 21\,Hz$ (A), a synchronous bursting regime (B), and a fast spiking regime with firing rates $f \geq 117\,Hz$ (C). Conversely, a pyramidal network without CAN current (bottom line) does not display such a rich array of firing regimes (D and E). Parameters are: $g_{\mathrm{CAN}} = \mathcal{N}(50, 5)\,\mu S\,cm^{-2}$, $g_{\mathrm{M}} = 90\,\mu S\,cm^{-2}$, $0 \leq w_{cc} \leq 1.5\,nS$.

The transition between asynchronous slow regime and synchronous bursting depended on the interaction between increased local synaptic excitation and the spike-frequency adaptation provided by the M current. A careful balance between these two currents allowed synchronous oscillations at frequencies within the theta-band [Colgin, 2013] to emerge. Figure 4.7A shows a sample raster plot with synchronous activity at $f_{osc} = 5.5\,Hz$ with a synchronisation of $\kappa(\tau) = 0.38$. Figure 4.7C shows the LFP signal corresponding to the raster plot in Figure 4.7A, highlighting the presence of theta oscillations. Increasing synaptic strengths above a certain threshold, merged the bursts into fast gamma population activity (resembling that displayed in Figure 4.5C), as the local excitation prevailed over the adaptation. Weakening or disabling the M current, by acting on its conductance g_M, caused the bursting regime to disappear in favour of an asynchronous firing regime (similar to that displayed in Figure 4.5A), whose frequency increased as PCAN-to-PCAN synapses were strengthened. Conversely, gradually strengthening the M current ($g_M \geq 12\,\mu S\,cm^{-2}$) slowed the oscillatory frequency and produced thinner bursts which eventually degraded into singlet spikes.

The properties of the model do not critically depend on connection probability. We tested various combinations of network size and connection probability parameters. Scaling up the PCAN network size to 900 pyramidal neurons allowed us to reduce the number of postsynaptic contacts per neuron, in order to model the relatively low recurrent connectivity of CA3 (2% recurrent connections [Miles and Wong, 1986]) and CA1 (1% recurrent connections) [Deuchars and Thomson, 1996]. The parameters for these models were ($p = 0.02$, $w_{cc} = 5.4\,nS$, $g_{CAN} = \mathcal{N}(35, 5)\,\mu S\,cm^{-2}$, $g_M = 7\,\mu S\,cm^{-2}$) and ($p = 0.01$, $w_{cc} = 5.4\ nS$, $g_{CAN} = \mathcal{N}(36.5, 5)\,\mu S\,cm^{-2}$, $g_M = 7\,\mu S\,cm^{-2}$) respectively. In both configurations we were able to elicit theta oscillations at a frequency of approximately $5\,Hz$ (results not shown). We chose a smaller network, comprising only 100 cells, to accelerate simulation time.

4.3 The CAN-In Network

4.3.1 Network Topology

We then connected the CAN pyramidal network to a population of inhibitory neurons (In) in an attempt to further synchronise the network activity by leveraging a PING-like [Kopell et al., 2010] mechanism. This CAN-In network comprises 75 CAN pyramidal neurons and 25 inhibitory neurons. The population of fast-spiking interneurons was driven solely by excitatory input from PCAN neurons, and in turn provided them with strong slow-inactivating feedback inhibition. Connecting two neural populations increases the number of parameters used to define synaptic connections by four. These parameters and their names are summarised in Table 4.1. The probability of connections within and between the populations (PCAN-to-PCAN, PCAN-to-In, In-to-In, and In-to-PCAN) were all set to $p = 0.4$.

Connection Name	Parameter	Connection Probability
PCAN-to-PCAN	w_{cc}	0.4
PCAN-to-Inhibitory	w_{ci}	0.4
Inhibitory-to-Inhibitory	w_{ii}	0.4
Inhibitory-to-PCAN	w_{ic}	0.4

Table 4.1: CAN-In network connection parameters and their connection probabilities.

4.3.2 Feedback Inhibition Increases Network Synchronisation

Figure 4.7B presents a sample raster plot of the CAN-In network activity, and Figure 4.7D its corresponding LFP signal. Our results show that such feedback inhibition enhanced the synchrony

of CAN-mediated oscillatory activity (Figure 4.8E). For a wide range of PCAN-to-PCAN connection strengths ($0.7\,nS \leq w_{cc} \leq 0.9\,nS$), stronger feedback inhibition always led to an increase in synchronization of network activity. Strengthening inhibitory to CAN connections in a CAN-In network displaying asynchronous persistent firing (Figure 4 4.8A, $\kappa(\tau)) = 0.32$ with $w_{ic} = 0\,nS$) slowly synchronised the activity in tight narrow bands (Figure 4.8D, $\kappa(\tau)) = 0.66$ with $w_{ic} \geq 0.8\,nS$. However, when the network already displayed synchronous bursts of activity due to strong excitatory connections whilst in the presence of weak inhibition (Figure 4.8B, $\kappa(\tau) = 0.66$ with $w_{ic} = 0\ nS$), increasing the inhibitory feedback initially caused a desynchronisation as the bursts were decoupled (Figure 4.8C, $0.48 \leq \kappa(\tau)) \leq 0.59$ with $0.4\,nS \leq w_{ic} \leq 0.7\,nS$). Eventually the bursts were further split by increasing inhibitory connection strength and became narrow bands of synchronous doublets or singlets which resulted in an increase of overall network synchronization (Figure 4.8D, $0.66 \leq \kappa(\tau)) \leq 0.77$ with $0.8\,nS \leq w_{ic} \leq 2\,nS$).

Similarly as in a PING [Kopell et al., 2010] setting, feedback inhibition provides pyramidal neurons with precise windows of elevated excitability in which they can be synchronously activated. The activity exhibited by our CAN-In network was more tightly synchronised ($\kappa(\tau)) = 0.78$ in Figure 4.7B), compared with that displayed by the network of solely pyramidal CAN neurons ($\kappa(\tau)) = 0.38$ in Figure 4.7A). The fastest-attainable oscillatory frequency in the CAN-In network was $f_{osc} = 11\,Hz$, and depended on the firing rate of the CAN-mediated persistent activity, and therefore on the CAN conductance. Increasing feedback inhibition strength above a certain threshold caused it to annihilate the effect of local PCAN-PCAN excitation, and the network activity reverted to an asynchronous firing regime driven solely by the CAN current, similar to the behaviour displayed in Figure 4.5A.

To verify that the synchronous activity was maintained by CAN-persistent firing, we removed the CAN current from the pyramidal population in the CAN-In network (setting $g_{CAN} = 0\,nS\,cm^{-2}$). Solely the pyramidal neurons were injected with the same strong transient stimulus as in all our simulations. In the absence of CAN current, and with weak local excitation ($w_{cc} \leq 0.90\,nS$), the pyramidal network activity stopped concurrently with the removal of the external stimulation. However, in the presence of strong pyramidal-to-pyramidal excitatory connections ($w_{cc} \geq 1.36\,nS$), the pyramidal population displayed fast ($f \geq 100\,Hz$) persistent firing activity maintained by the recurrent synaptic connections alone. Overall, this all-or-nothing behaviour closely resembled the one illustrated in by the red data points in Figure 4.6. Simulating the effects of feedback inhibition on this activity yielded monostable dynamics in which the persistent activity either swamped the network, as the inhibition failed to control the strength of the excitation, or faded away, as the inhibition prevailed over the excitation. Careful fine-tuning of excitatory and inhibitory connection weights could allow for richer dynamics [Compte, 2006, Wang, 2001], although this remains outside the scope of the current work.

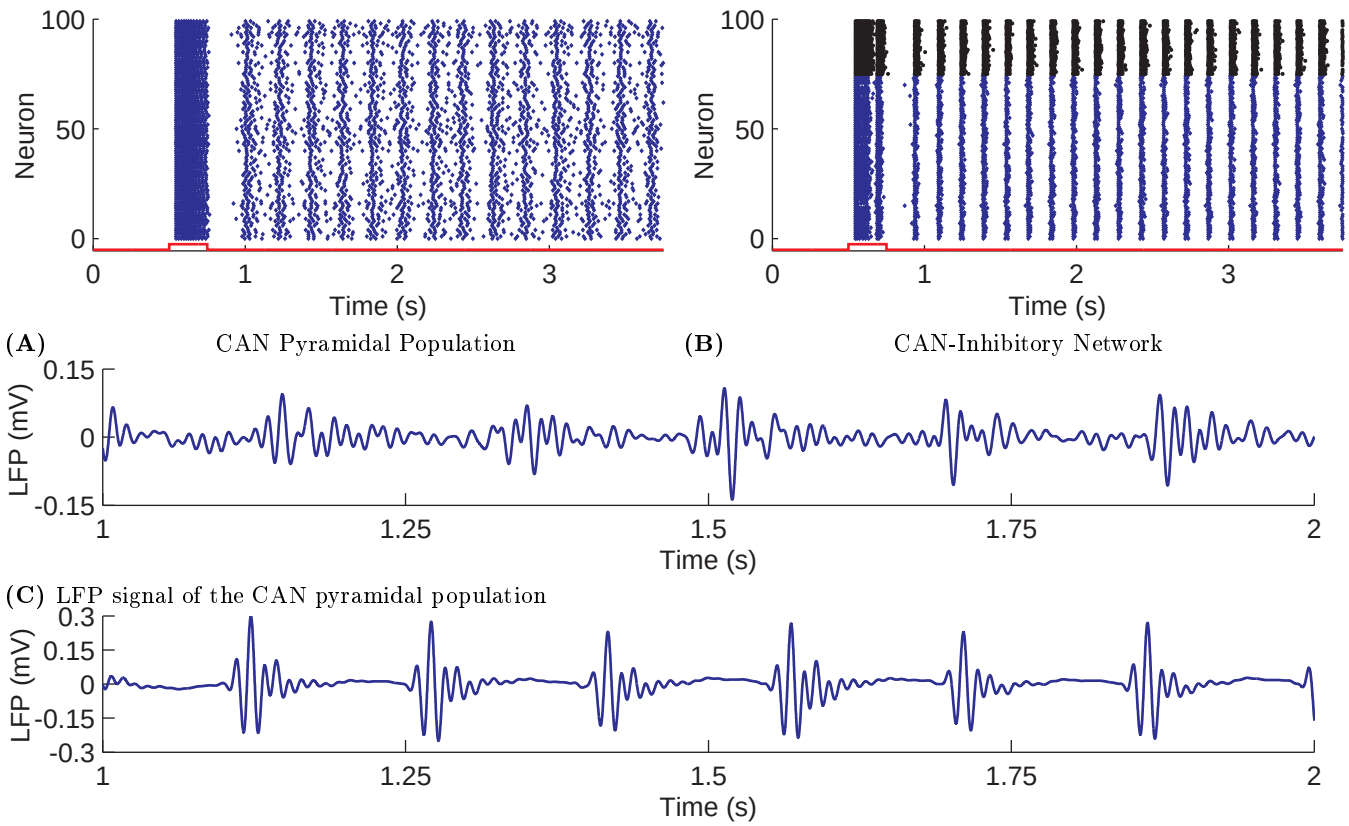

Figure 4.7: Comparison of CAN and CAN-In network dynamics. (A) Raster plot for the 100-cell CAN pyramidal network, showing $5.46\,Hz$ oscillations with a synchronisation of $\kappa(\tau) = 0.38$, $\tau = 10\,ms$. (B) Raster plot for the CAN-Inhibitory network comprising 75 CAN pyramidal cells (cell number $0 - 74$, blue diamonds) and 25 inhibitory cells (cell number $75 - 99$, black dots), showing $6.91\,Hz$ oscillations with a synchronisation of $\kappa(\tau) = 0.78$, $\tau = 10\,ms$. In both plots the red line below the raster represents the applied stimulation current. (C) LFP signal computed from the spiking activity of the CAN pyramidal network shows nested gamma in theta oscillations (one-second extract). (D) LFP signal computed from the spiking activity of the CAN-Inhibitory network shows nested gamma in theta oscillations with higher amplitudes compared to the CAN pyramidal network (one-second extract). Parameters for the CAN-only network are: $g_{\text{CAN}} = \mathcal{N}(50, 5)\,\mu S\,cm^{-2}$, $g_{\text{M}} = 90\,\mu S\,cm^{-2}$, $w_{cc} = 0.48\,nS$. Parameters for the CAN-Inhibitory network are: $g_{\text{CAN}} = \mathcal{N}(50, 5)\,\mu S\,cm^{-2}$, $g_{\text{M}} = 90\,\mu S\,cm^{-2}$, $w_{cc} = 1.44\,nS$, $w_{ci} = 1\,nS$, $w_{ii} = 1.0\,nS$, $w_{ic} = 1.2\,nS$.

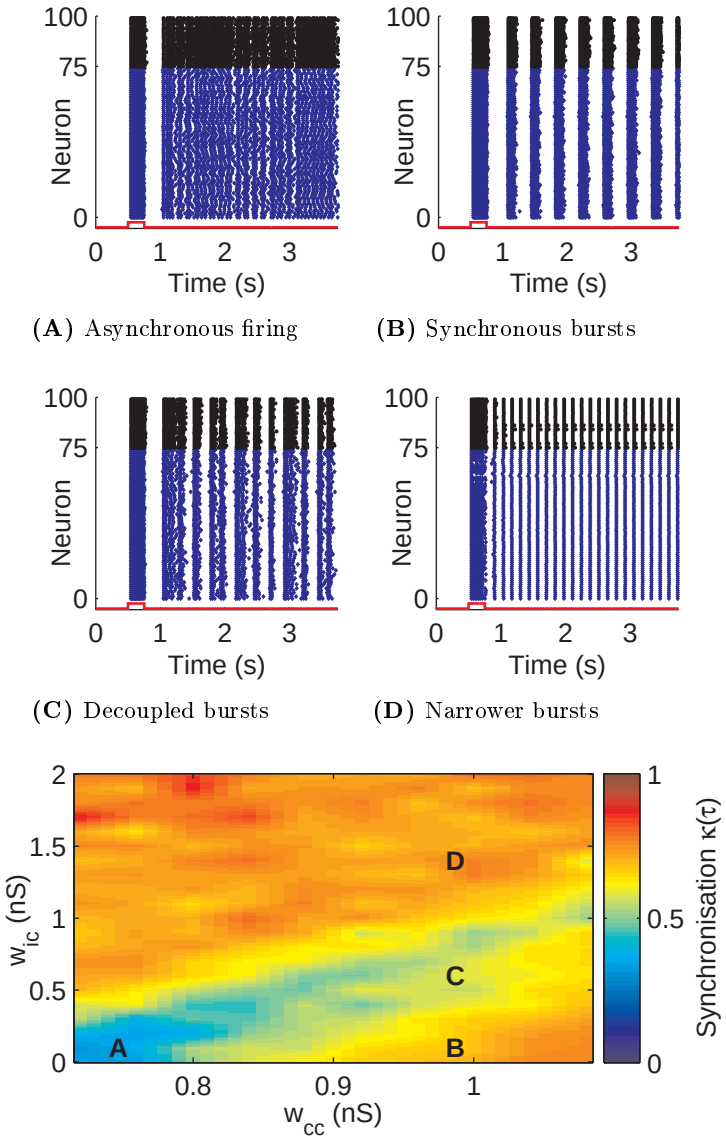

(E) Network synchronisation heatmap as pyramidal-pyramidal and inhibitory-pyramidal connections weights are strengthened.

Figure 4.8: Feedback inhibition synchronises CAN-mediated persistent activity. (A) Sample raster plot of the asynchronous firing regime showing a synchrony measure of $\kappa(\tau) = 0.32$ in the absence of inhibitory feedback ($w_{ic} = 0\,nS$) and weaker local excitation ($w_{cc} < 0.8\,nS$). (B) Sample raster plot of the synchronous bursting firing regime showing a synchrony measure of $\kappa(\tau) = 0.66$ in the absence of inhibitory feedback ($w_{ic} = 0\,nS$) and stronger local excitation ($0.8\,nS \leq w_{ic} \leq 2\,nS$). (C) Increasing inhibition slowly decouples the bursts, causing the overall network synchrony to decrease to $0.48 \leq \kappa(\tau) \leq 0.59$ with $0.4\,nS \leq w_{ic} \leq 0.7\,nS$. (D) Stronger inhibition $0.8\,nS \leq w_{ic} \leq 2\,nS$ eliminates the bursts converting them into narrower bands of synchronous firing, increasing the network synchrony to $0.66 \leq \kappa(\tau) \leq 0.77$. (E) As the inhibitory to CAN connection strength w_{ic} is increased (y axis) the synchronisation of the firing activity ($\kappa(\tau)$) in the CAN population increases from $\kappa(\tau) = 0.32$ (A) to $\kappa(\tau) \geq 0.66$ (D), for several CAN-CAN connection weights $0.72\,nS \leq w_{cc} \leq 1.08\,nS$ (x axis). When starting from a CAN pyramidal synchronous firing regime ($w_{cc} \geq 0.8\,nS$ as shown in (B)) the network synchronisation measure initially decreases as stronger inhibition desynchronises the pyramidal bursts (C). Eventually, the bursts become narrower bands of synchronous firing (C) yielding a higher network synchrony measure. Parameters are: $g_{\text{CAN}} = \mathcal{N}(22.5, 5)\,\mu S\,cm^{-2}$, $g_{\text{M}} = 45\,\mu S\,cm^{-2}$, $w_{cc} = 0.92\,nS$, $w_{ci} = 1\,nS$, $w_{ii} = 0.5\,nS$. $\kappa(\tau)$ is comprised between 0 and 1, representing an asynchronous population firing and fully synchronised firing respectively.

4.4 CAN-Mediated Self-Sustained Theta Oscillations

The CAN current conductance modulated theta oscillations, which accelerated or decelerated proportionally to changes in values of g_{CAN}, within a certain parameter range. Increasing the CAN conductance produced faster oscillations in the PCAN network, with frequencies ranging between $4\,Hz$ and $6\,Hz$ (Figure 4.9A). In addition, the computed theta-band power spectrum of the network activity reflected an increase in power in the theta band, as CAN conductance was increased. The oscillatory frequencies of the PCAN population varied between $4\,Hz \leq f_{osc} \leq 6\,Hz$ for $\mathcal{N}(33,5)\,\mu S\,cm^{-2} \leq g_{CAN} \leq \mathcal{N}(55,5)\,\mu S\,cm^{-2}$, $g_M = 90\,\mu S\,cm^{-2}$, and $w_{cc} = 0.51\,nS$. Figure 4.9A shows a high power range around $5\,Hz$, with the maximum theta power at $f_{osc} = 4.9\,Hz$ for $g_{CAN} = \mathcal{N}(46.5,5)\,\mu S\,cm^{-2}$. Since the average firing rate of each isolated CAN neuron was approximately $15\,Hz$, when connected these produced synchronous bursts at $5\,Hz$ containing on average 3 spikes per neuron (3.05 in Figure 4.9A) thus explaining the peak of power at this frequency.

Feedback inhibition also affected theta oscillation frequencies by accelerating them as inhibitory-to-PCAN pyramidal synapses were strengthened, allowing for richer dynamics compared to a network comprising solely PCAN neurons. Our results indicate that, in the case of the CAN-In network, the strength of the CAN current modulated both theta power and oscillation frequencies (Figure 4.9B). Here, the average oscillation rate of the CAN pyramidal population was $f_{osc} = 7.2 \pm 2.7\,Hz$. The oscillatory frequencies of the isolated PCAN population varied between $4\,Hz \leq f_{osc} \leq 11\,Hz$ for $\mathcal{N}(28,5)\,\mu S\,cm^{-2} \leq g_{CAN} \leq \mathcal{N}(64,5)\,\mu S\,cm^{-2}$, $g_M = 90\,\mu S\,cm^{-2}$, and $w_{cc} = 1.4\,nS$. Furthermore, the power spectrum of the CAN Pyramidal neurons firing activity showed a peak at $f_{osc} = 8.5\,Hz$ for $g_{CAN} = \mathcal{N}(56.9,5)\,\mu S\,cm^{-2}$.

The elicited oscillations were stable in both frequency and amplitude, and lasted for as long as the underlying persistent firing. Previous reports have shown that cholinergic-dependent persistent activity can last for longer than $30\,s$ [Knauer et al., 2013]. The oscillations could be terminated in our model by depolarizing the cells with an external input of the same magnitude as the depolarizing stimulation. In addition, in both PCAN and CAN-In network configurations, increasing and decreasing the CAN conductance during the simulations allowed for a dynamic modulation of the oscillation frequency accelerating and decelerating it respectively.

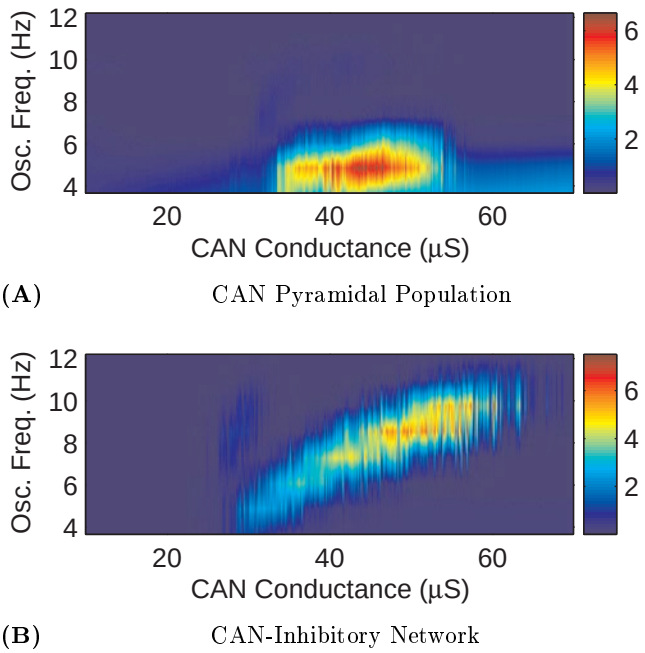

Figure 4.9: Modulating theta oscillations frequency and power. (A) Theta oscillations power is modulated by the CAN conductance in the 100-cell CAN pyramidal network, showing a peak at $f_{osc} = 4.88\,Hz$ for $g_{\text{CAN}} = \mathcal{N}(46.5, 5)\,\mu S\,cm^{-2}$. The theta frequency range displayed by the network is $4\,Hz \leq f_{osc} \leq 7\,Hz$. (B) CAN Conductance modulates theta oscillations frequency and power in the CAN-Inh network. Increasing the CAN conductance accelerates the firing rate of the pyramidal neurons which in turn causes them to receive a surge of feedback inhibition, tightening the synchronisation and accelerating their oscillatory behaviour. The maximum theta power is at $f_{osc} = 8.54\,Hz$ for $g_{CAN} = \mathcal{N}(56.9, 5)\,\mu S\,cm^{-2}$. The theta frequency range displayed by the network is $4\,Hz \leq f_{osc} \leq 11\,Hz$. Parameters for the CAN-only network are: $\mathcal{N}(20, 5)\,\mu S\,cm^{-2} \leq g_{\text{CAN}} \leq \mathcal{N}(70, 5)\,\mu S\,cm^{-2}$, $g_{\text{M}} = 90\,\mu S\,cm^{-2}$, and $w_{cc} = 0.51\,nS$. Parameters for the CAN-Inh network are: $\mathcal{N}(20, 5)\,\mu S\,cm^{-2} \leq g_{\text{CAN}} \leq \mathcal{N}(70, 5)\,\mu S\,cm^{-2}$, $g_{\text{M}} = 90\,\mu S\,cm^{-2}$, $w_{cc} = 1.44\,nS$, $w_{ci} = 0.8\,nS$, $w_{ii} = 1.0\,nS$, and $w_{ic} = 1.4\,nS$.

4.4.1 Gamma-in-Theta Rhythms

The oscillatory frequencies displayed by the CAN population, both with and without inhibition, closely resemble those of nested gamma in theta rhythms as illustrated in Figure 4.7C and Figure 4.7D showing the LFP signal computed from the PCAN and CAN-In network activities respectively. As previously described, the neurons synchronise their activity in theta-frequency bursts of activity ($f_{osc} = 5.46\,Hz$ in Figure 4.7A). In addition, the frequency of the pyramidal population activity accelerated during these bursts, producing intra-burst frequencies which were within the gamma band ($f_{intra} = 38.03 \pm 0.61\,Hz$). Investigating the firing patterns and the LFP signal of the synchronous bursting regime (Figure 4.7C) yielded a synchronisation of $\kappa(\tau)) = 0.38$, which was higher than that displayed by the slow asynchronous firing regime (Figure 4.5A) at $\kappa(\tau)) = 0.24$.

Feedback inhibition (Figure 4.7B) further tightened the synchronisation of intra-burst spikes, increasing the coherence value to $\kappa(\tau)) = 0.78$. As a result, the oscillatory frequency of the PCAN-In network accelerated to $f_{osc} = 6.9\,Hz$. In this configuration, the CAN population fires synchronously with an average robust intra-burst frequency of $f_{intra} = 57.3 \pm 1.4\,Hz$ as highlighted by the LFP signal of the CAN-In network (Figure 4.7D).

4.5 Discussion

In this chapter we presented a biologically-inspired model of self-sustained hippocampal oscillations which relies on intrinsic cellular properties commonly found in hippocampal pyramidal neurons [Jochems and Yoshida, 2013, Knauer et al., 2013]. The work described here is one of the first modelling studies showing that theta oscillations can be maintained in CA1, relying solely on intrinsic cellular properties, and without the need for external inputs. Our model was shown to possess various essential features supporting the maintenance of theta oscillations in the isolated hippocampus.

4.5.1 Reproducing Phenomena Observed In-Vitro

We fitted our model parameters to experimental recordings from CA1 persistent firing cells. The key features of our model cell behaviour are in accordance with the biological data (Figure 4.1 and Figure 4.3). The aspect in which our cell model deviates from the in vitro data is the maximum achievable persistent firing frequency. The model persistent firing frequency linearly increases until the highest g_{CAN} values, whereas the in vitro data did not show further increase in the presence of $20\,\mu M$ Cch (Figure 4.1A and Figure 4.1B). This inconsistency can be explained by the tendency of CA1 pyramidal neurons to engage in depolarization block in the presence of elevated ($\geq 10\mu M$) Cch concentrations [Fraser and MacVicar, 1996, Fraser et al., 2001, Knauer et al., 2013, Knauer, 2015]. An implementation of depolarization block in the model was beyond the scope of our current work. By confining ourselves to in vitro recordings that exhibited persistent firing, we introduced a bias towards less excitable cells in the presence of Cch. This is evident in the fraction of cells showing persistent firing relative to the total sample size as reported in the method section (i.e. 100, 68, 58, and 17% persistent firing cells in $1, 5, 10$, and $20\mu M$ Cch, respectively). Hence, at higher Cch concentrations a higher fraction of cells had to be excluded because they exhibited depolarization block. Between 15 and $25\,Hz$ appears to lie a cell-specific persistent firing frequency limit in CA1 pyramidal neurons, beyond which cells tend to show depolarization block [Knauer, 2015]. Unpublished recordings from our laboratory (n = 19 Long-Evans rats, 14-24 days old, 68% males) in the presence of 0.1 ($n = 6$), 0.25 ($n = 6$), 1 ($n = 5$), and 2.5 ($n = 5$)μM Cch showed average persistent firing frequencies of $1.5, 0.7, 6.9$ and $14.9\,Hz$, respectively. The use of a different intracellular solution in these recordings (KMeSO4 based) may not allow direct comparison with the data presented here [Kaczorowski et al., 2007]. However, these data indicate that the dynamic range of persistent firing frequencies may extend well into lower concentrations of Cch and that the plateau observed here (Figure 4.1A) is a result of the relatively high Cch concentrations chosen.

4.5.2 CAN-Mediated Synchronous Oscillations

Our results demonstrate that synchronous rhythmic activity can be maintained in a network of CAN-equipped persistent firing pyramidal neurons, in the absence of external stimulation. The CAN-mediated rhythm generator leverages the interaction between local excitation provided by synaptic activity, and the hyperpolarisation provided by modulating potassium current (IM). At each firing cycle, the persistent firing activity mediated by the CAN current increases postsynaptic excitation within the network. As a result, the neurons rapidly discharge several subsequent action potentials which strengthen the M current, attempting to slow down their firing rate. Eventually, the M current hyperpolarization prevails over synaptic excitation causing the termination of the burst. The bursts are then restarted by the underlying CAN-mediated persistent firing acting as a pacemaker, precisely regulating the onset of the oscillatory activity.

This mechanism is similar to that described in [Aoyagi et al., 2003], in which a CAN-like current provides depolarising after potentials (DAPs) which, when carefully balanced with after hyperpo-

larising potentials (AHPs), allow single neurons to fire bursts of two or more spikes. In our work and in that of Aoyagi and colleagues, the pyramidal neurons are intrinsically rhythmical, although not intrinsically bursting (see Figure 4.3A and Figure 4.3B for sample voltage traces). This rhythm can be entrained in their postsynaptic targets in the form of rapid bursts. In our model the bursts of activity persist over long time spans and are maintained without the need for external stimulation, in contrast with the bursting neuron model [Aoyagi et al., 2003] which requires constant stimulation. This allows our network of CAN pyramidal neurons to simulate the hippocampal firing regimes commonly recorded throughout the delay phase of delayed memory tasks [Egorov et al., 2002, Fransén et al., 2002], during which the hippocampus displays elevated firing, initiated by a transient stimulus salient enough to be retained long after its cessation. Our results demonstrate that the network elicits an ample range of biologically plausible firing rates which are supported solely by the CAN current, suggesting that the CAN current could contribute to the stability and robustness of rhythmic activity of local populations of hippocampal pyramidal neurons.

Recent studies have identified CAN-mediated persistent firing in CA1 [Knauer et al., 2013], an area which is commonly believed to comprise significantly less recurrent connectivity than other hippocampal regions [Andersen et al., 2007, Deuchars and Thomson, 1996]. These results are in accord with those presented here, because our network model relies upon a relatively sparse connectivity. Moreover, the density of the connections within the network does not significantly affect the population firing regimes, and strong recurrent connections alone do not yield biologically realistic firing frequencies (Figure 4.5F). Network firing rates and oscillation frequencies are maintained solely by the intensity of the CAN current. Taken together, these observations suggest that our model could be used to represent several different hippocampal areas.

4.5.3 Theta Oscillations in the Isolated Hippocampus

A vast body of literature has highlighted the importance of the medial septum in the generation and maintenance of theta-frequency hippocampal oscillations [Vinogradova, 1995, Tóth et al., 1997, Kocsis et al., 1999, Fischer et al., 1999, Stewart and Fox, 1990]. Nevertheless, the results recent experimental studies [Goutagny et al., 2009, Jackson et al., 2011] supported by existing theoretical models [White et al., 2000, Traub et al., 1989] indicate that the hippocampus might possess the necessary circuitry to sustain theta oscillations in the absence of septal drive. Therefore, intrinsic mechanisms within the hippocampus might be required to support theta oscillations triggered by projections from the medial septum.

Here, we present a simple hippocampal network comprising at most two types of cell. The crucial feature of our model is that local networks of CAN-equipped pyramidal neurons, independent of extrinsic septal drive, can contribute to maintaining theta rhythms within the hippocampus. Therefore, we hypothesise that local circuits comprising CAN pyramidal neurons could provide a neural basis for hippocampal theta oscillations.

Theta frequency and power are both modulated by the intensity of the intrinsic CAN current, which allows for a rich range of oscillation frequencies within the theta band (4 - 11 Hz). CAN channels are modulated by muscarinic acetylcholine receptors [Magistretti et al., 2004] which could be the target of cholinergic projections, providing a stimulation triggering and modulating hippocampal theta oscillations. In the absence of septal afferents, the activation of the CAN current in the pyramidal neurons may originate from local populations of cholinergic interneurons [Frotscher et al., 1986, Yi et al., 2015]. The cholinergic activation could also derive from cholinergic interneurons in the medial septum [Simon et al., 2006], which do not display rhythmic theta firing patterns and are thus thought to act solely as frequency modulators for hippocampal theta oscillators [Colgin, 2013].

Existing models [White et al., 2000] of hippocampal theta require the presence of slow-inactivating inhibition mediated by oriens lacunosum-moleculare (O-LM) interneurons, forming a tightly coupled

oscillator with their postsynaptic pyramidal neurons [Cobb et al., 1995]. The O-LM neurons provide the pyramidal neurons with precise windows of enhanced excitability, synchronising their activity at theta-band frequencies. This circuitry seems to play an important role in the maintenance of theta oscillations in the isolated hippocampus [Goutagny et al., 2009], although the provenance of the inhibitory afferents involved in the circuit remains unclear. In our model, a single type of CAN pyramidal cell is necessary and sufficient for the appearance of theta oscillations, due to its inherent rhythmicity and spike-frequency adaptation. Therefore, our work could provide a simpler explanation for this phenomenon. Including feedback inhibition to these pyramidal neurons merely enhances the synchronisation of the CAN population. Moreover, inhibition improves the robustness of fast theta oscillations by precisely modulating the inter-burst interval of the pyramidal population.

4.5.4 Implications for Hippocampal Theta

Although the septum has been demonstrated to be necessary for the generation of hippocampal theta oscillation, the hippocampus is also thought to rely on its intrinsic properties to maintain this synchronous activity which is crucial to perform working memory tasks. Taken together, our results show that maintenance of rhythmic activity within the hippocampus in the absence of extrinsic drive can be achieved by leveraging intrinsic cellular mechanisms, namely CAN-mediated persistent firing.

4.5.5 Cholinergic-Dependent Memory Consolidation

Memory consolidation is the process by which short-term memory traces are converted into longer-lasting memories. According to the two-stage model of consolidation, memories are encoded in the hippocampus during wake [McClelland et al., 1995, Roediger et al., 2007, Squire, 1987, Squire, 1992] and are transferred into cortical long-term storage during sleep [Buzsáki, 1989, Hasselmo et al., 1996, Qin et al., 1997, Shen and McNaughton, 1994]. One theory [Hasselmo, 1999] suggests that acetylcholine could mediate memory consolidation during sleep as the release levels of this neurotransmitter vary significantly compared to during wake. Interestingly, acetylcholine governs the oscillatory frequencies in our model by modulating the underlying CAN current. These observations allow our model to raise the compelling hypothesis that networks of pyramidal-CAN neurons could be involved in cholinergic-dependent memory consolidation. CAN-mediated persistent firing could form a neural substrate allowing memories to remain in the hippocampus for as long as needed, as long as the levels of acetylcholine remain sufficiently high.

4.5.6 The CAN-PING Model

Arguably, the most extensively studied computational model for hippocampal gamma oscillations is the PING network [Kopell et al., 2010]. In this configuration, tightly coupled inhibitory neurons provide pyramidal postsynaptic neurons with precise windows of decreased, and therefore increased, excitability controlling their spiking patterns and producing synchronous oscillations. A vast body of literature (see [Kopell et al., 2010] for a reviews), comprising in vitro and in vivo experiments, supports this hypothesis. However, although the PING rhythmogenetic mechanism might be biologically plausible, the maintenance of the oscillatory activity does depend on a persistent stimulation whose provenance and neurophysiology is unknown. As a possible solution, we suggest integrating a population of pyramidal-CAN neurons in the PING network to provide a memory maintenance mechanism dependent on persistent firing. Preliminary results from our simulations of the activity of such a CAN-PING model (not shown here) suggest that, in a simple configuration in which the PCAN neurons project solely on the pyramidal neurons in the PING network, the CAN-mediated asynchronous persistent firing allows for self-sustained gamma oscillations in the PING network. In

addition, it is conceivable that a CAN-PING network could produce robust self-sustained nested gamma in theta rhythms, by combining the synchronous theta frequency activity of the PCAN network with the PING gamma oscillations.

Conclusion

In this chapter we presented a biologically-inspired model of self-sustained theta-frequency hippocampal oscillations which relies on intrinsic cellular properties commonly found in hippocampal pyramidal neurons [Knauer et al., 2013, Jochems and Yoshida, 2013]. Our work aimed at providing one possible explanation for the generation of theta oscillations in the isolated hippocampus. We hypothesise that local networks of intrinsically persistent firing neurons could provide the neural substrate for hippocampal theta rhythm generators. Our results demonstrate that synchronous rhythmic activity can be maintained in a network of CAN-equipped persistent firing pyramidal neurons, in the absence of external stimulation. Our model predicts that the hippocampus might locally incorporate the necessary cells and circuitry to allow for spontaneous emergence of theta oscillations. Therefore, CAN-mediated persistent firing could be the neural substrate underlying theta oscillations observed during working memory tasks [Buzsáki, 2002, Raghavachari et al., 2001, Tesche and Karhu, 2000]. In addition, since this persistent firing is modulated by cholinergic receptors, we suggest that networks of pyramidal-CAN neurons could be involved in cholinergic-dependent memory consolidation [Hasselmo, 1999].

CHAPTER

5

STUDYING THE EFFECTS OF ANAESTHESIA ON NEURAL OSCILLATIONS

Contents

Overview

In this chapter we present our study of the effects of anaesthesia on hippocampal oscillations. This work investigates the effect of propofol-induced tonic and phasic inhibition on the oscillations elicited in a network of hippocampal Hodgkin-Huxley $GABA$ interneurons. Hippocampal interneurons are thought to possess self-synchronising capabilities [Kopell et al., 2010, White et al., 2000, Wang and Buzsáki, 1996] and thus provide us with a robust baseline from which we begin our analysis. We begin by implementing an existing model network [Wang and Buzsáki, 1996] which we then modify to incorporate the actions of propofol on GABAergic synaptic and extrasynaptic receptors. We then perform an in-depth parameter study and we demonstrate that propofol-mediated tonic inhibition contributes to enhancing synchronous neural activity Finally, we describe the implication and predictions deriving from our study. The model and the results presented in this chapter were published in [Giovannini et al., 2015a], and a follow-up article was recently submitted [Giovannini and Buhry, 2017].

5.1 Inhibitory Neuron Model

The model used for the inhibitory hippocampal neurons used for the current work was the one described in Chapter 3. In addition, we modified Equation 3.25, describing the rule governing the ionic current gating variables, which became:

$$\frac{\mathrm{d}x}{\mathrm{d}t} = \frac{x_\infty - x}{\tau_x} \qquad x_\infty = \frac{\alpha_x}{\alpha_x + \beta_x} \qquad \tau_x = \frac{10}{7 \cdot (\alpha_x + \beta_x)} \tag{5.1}$$

5.1.1 Network Configuration

We reimplemented the model network of hippocampal interneurons described in [Wang and Buzsáki, 1996], after appropriately modifying it for compatibility with the Brian simulator (see Chapter 3 for more details). The network comprised 100 fast-spiking hippocampal inhibitory neurons, which were randomly connected with a certain probability (p). $p = 0$ indicates that the neurons make zero synaptic contacts with other neurons, whereas $p = 1$ represents a fully connected network in which all neurons project on all other neurons (including themselves). The results presented in [Wang and Buzsáki, 1996] identify a critical number of synaptic contacts ($\simeq 40$) per neuron within a network, independently on the number of cells in the network, required for the emergence of synchronous activity. For 100 neurons, this would equate to a critical connection probability of $p = 0.4$. In our network, the connection probability was set to $p = 0.6$ so as to be higher than this critical probability, ensuring the presence of synchronous network activity.

5.1.2 External Current Stimulation

Throughout all our simulations, the network was stimulated with a constant current $I_{stim} = 0.4\,nA$. Heterogeneity was introduced in the form of Gaussian-distributed noise when initialising the resting potential and the synaptic conductance values of the neurons.

5.1.3 Modelling the Effects of Anaesthetics

The effect of the anaesthetic agent propofol [Vanlersberghe and Camu, 2008] is to globally enhance GABA-mediated inhibitory currents in postsynaptic neurons [Adodra and Hales, 1995, Bai et al.,

1999, Bai et al., 2001, Kitamura et al., 2004, McDougall et al., 2008, Song et al., 2011] by binding on $GABA_A$ receptors (see Chapter 2 for an in-depth explanation). Four main molecular mechanisms are thought to underlie propofol-induced general anaesthesia:

1. An enhancement of the amplitude of $GABA_A$-mediated tonic currents by activating extrasynaptic $GABA_A$ receptors [Bai et al., 2001, McDougall et al., 2008, Song et al., 2011]
2. A potentiation of GABA-mediated synaptic currents by increasing the conductance of synaptic $GABA_A$ receptors [Adodra and Hales, 1995, McDougall et al., 2008]
3. An increase in the baseline of $GABA_A$-mediated synaptic currents by slowing the desensitisation of $GABA_A$ receptors [Bai et al., 1999, Bai et al., 2001, McDougall et al., 2008]
4. An extension in the duration of $GABA_A$-mediated synaptic currents by increasing the closing time of synaptic $GABA_A$ receptors [Bai et al., 2001, Kitamura et al., 2004, McDougall et al., 2008]

The novelty of the work presented in this chapter lies in the precise modelling of all of these four effects. Figure 5.1 depicts a schematic showing propofol binding on synaptic and extrasynaptic $GABA_A$ receptors.

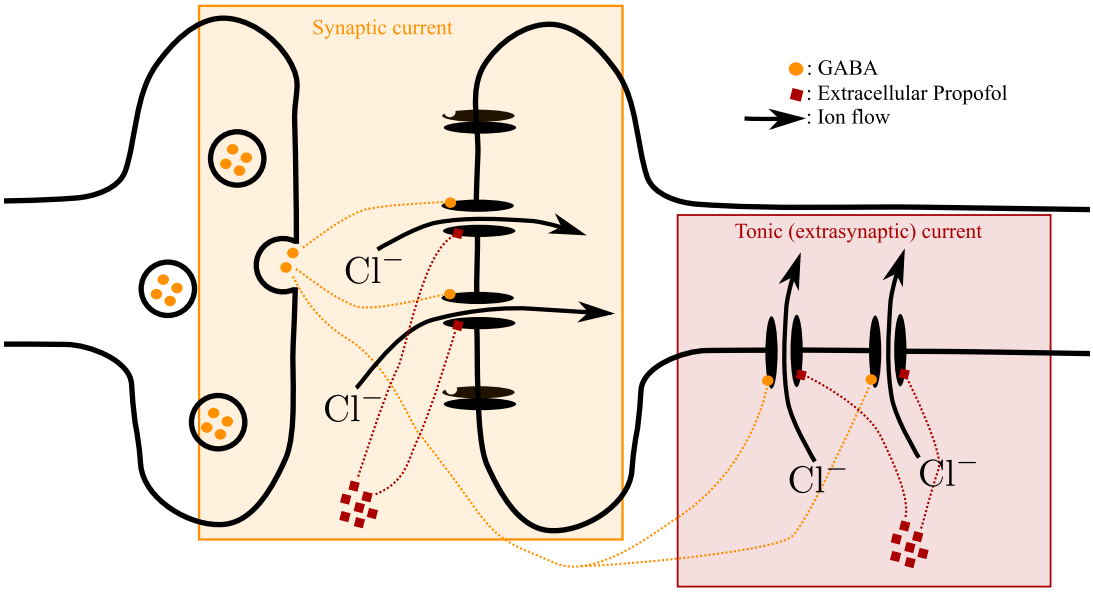

Figure 5.1: Schematic of $GABA$ (orange) binding on synaptic and extrasynaptic receptors causing Cl^- ion influx in the postsynaptic neuron. Extrasynaptic $GABA$ receptors mediate tonic inhibition, and are potentiated by extracellular propofol (red). Propofol also binds on synaptic $GABA$ receptors mediating phasing inhibition.

Extrasynaptic Tonic Inhibition

The action of propofol on extrasynaptic GABAergic receptors was modelled by varying the conductance g_{ton} of a tonic current I_{ton}. This current was added to the model neuron described by Equation 3.21, which became:

$$C_m \cdot \frac{\mathrm{d}V_m}{\mathrm{d}t} = -I_l - I_K - I_{Na} - I_{syn} - I_{ton} + I_{stim} \tag{5.2}$$

The tonic inhibition current takes the form:

$$I_{ton} = g_{ton} \cdot (V_m - E_i) \tag{5.3}$$

as described in [Hutt and Buhry, 2014], where E_i is the same reversal potential used for the synaptic inhibitory current I_i (see Chapter 3 for more details and parameter values) to maintain the equivalence between tonic and shunting inhibition. Increasing propofol dosage reflects in an increase in the tonic conductance g_{ton}, as described in the literature [McDougall et al., 2008, Song et al., 2011]. This produces a non-inactivating tonic inhibitory current which is not governed by activation-deactivation kinetics, as is the case for its synaptic counterpart.

Synaptic Phasic Inhibition

Propofol also binds on synaptic $GABA_A$ receptors enhancing their conductance [Adodra and Hales, 1995] and increasing their closing time [Bai et al., 1999]. We modelled this effect by acting on the inhibitory synaptic weights w_i and decay time τ_i parameters as in [McCarthy et al., 2008]. Increasing propofol dosage reflects in an increase in both of these values.

In addition, we modelled the slowing desensitisation of $GABA_A$ receptors caused by exposure to propofol [Bai et al., 1999, McDougall et al., 2008] by modifying the synaptic current equation, which became:

$$I_{syn} = I_i = g_i \cdot (V_m - E_i) + k_{bas} \tag{5.4}$$

where k_{bas} is a constant we used to modify the baseline of the synaptic current. In the absence of propofol this parameter was set to $k_{bas} = 0\,pA$. Since the synaptic conductance g_i obeys the rule described in Equation 3.29, $k_{bas} = 0\,pA$ indicates that the synaptic current decays to $0\,pA$ as the ionic channel closes. However, increasing the value of k_{bas} ensures that the synaptic current does not dip below the specified baseline. To the best of our knowledge, propofol-induced receptor desensitisation has never been modelled in existing computational studies.

5.2 Gamma Oscillations in a Network of Interneurons

Synaptic GABAergic interactions between sparsely connected interneurons are thought to play an important role in the generation and maintenance of rhythmic neural activity, in particular in the γ-band $(20 - 80)\,Hz$ [Bartos et al., 2007, Cobb et al., 1995, Jonas et al., 2004]. Oscillations arise because inhibitory neurons provide their postsynaptic targets with precise windows of reduced excitability, and consequently of increased excitability once the inhibition fades away. Therefore, these neurons effectively act as a pacemaker, controlling the onset and offset of the network activity.

This oscillatory frequency range is often recorded in functionally-coupled brain regions for cooperation during memory tasks. One such example is cortico-hippocampal synchronisation during long-term memory consolidation [Axmacher et al., 2006].

5.2.1 Different Oscillatory Frequencies in a PING Network

Given a constant stimulation, the network is capable of synchronising its activity, generating oscillations in the gamma frequency range $(25 - 80\,Hz)$ [Wang and Buzsáki, 1996]. The oscillation frequency is modulated by the time constant of the inhibitory synapse (τ_i) [Kopell et al., 2010, Wang and Buzsáki, 1996]. As expected, the longer the inhibitory synapses remains open and active (high τ_i values), the stronger the postsynaptic inhibition, which produces slower oscillations. Conversely, shorter synaptic time constants (low τ_i values) engender faster oscillations.

Figure 5.2A shows the raster plot of a network of interneurons oscillating at $f_{osc} = 41.91\,Hz$ for $\tau_i = 10\,ms$, and a synchronisation of $\kappa(\tau) = 0.4$. Increasing τ_i to $15, 20$ and $25\,ms$ produces oscillations

at frequencies of $f_{osc} = 29.82, 30.46$ and $21.48\,Hz$, with synchronisation values of $\kappa(\tau) = 0.3$, 0.46 and 0.24 respectively (Figures 5.2B, 5.2C, and 5.2D respectively).

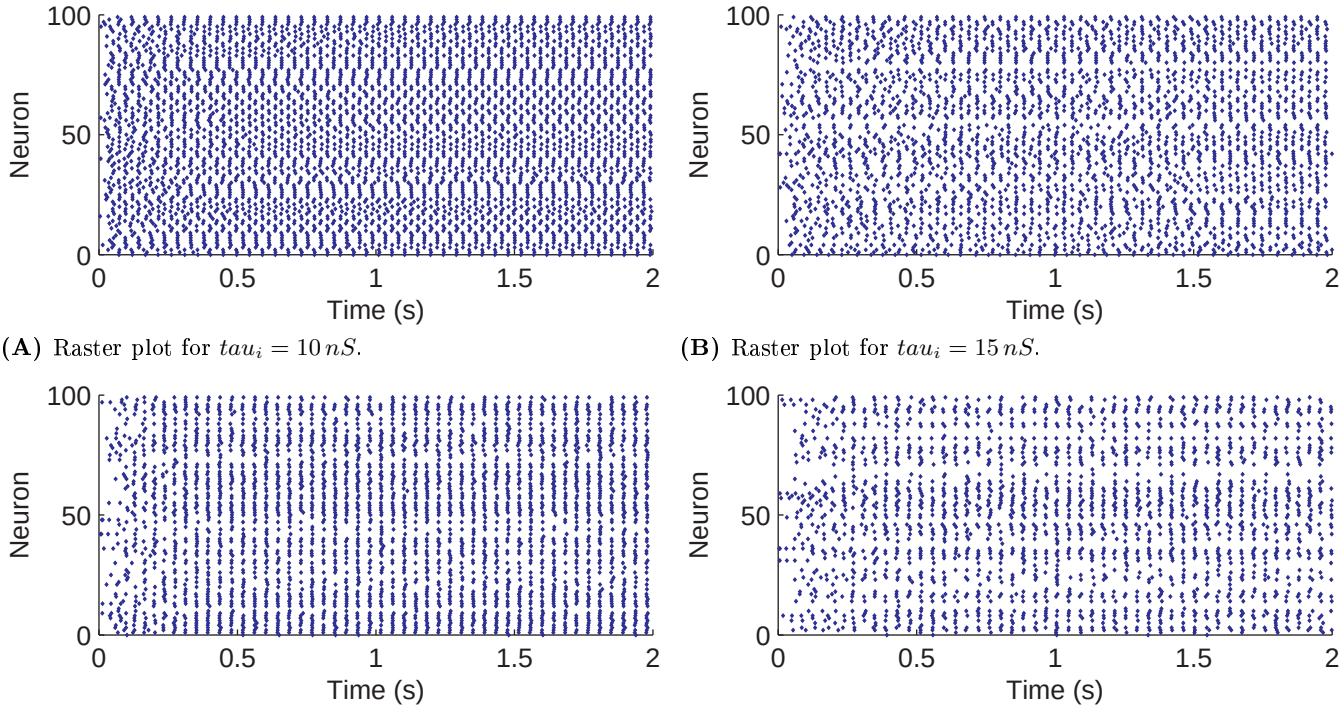

(A) Raster plot for $tau_i = 10\,nS$.

(B) Raster plot for $tau_i = 15\,nS$.

(C) Raster plot for $tau_i = 20\,nS$.

(D) Raster plot for $\tau_i = 25\,nS$.

Figure 5.2: The inhibitory synaptic time constant controls the oscillation frequency in a network of interneurons. Longer synaptic closing times produce slower oscillations. (A) Raster plot for the 100-cell inhibitory network in the absence of propofol ($g_{ton} = 0\,nS$) and an inhibitory synaptic time constant $\tau_i = 10\,ms$, showing $f_{osc} = 41.91\,Hz$ oscillations with a synchronisation of $\kappa(\tau) = 0.4$, $\tau = 10\,ms$. (B) Raster plot for the same network with a longer inhibitory synaptic time constant ($\tau_i = 15\,ms$), showing $f_{osc} = 29.82\,Hz$ oscillations with a synchronisation of $\kappa(\tau) = 0.3$, $\tau = 10\,ms$. (C) Raster plot for the same network with a longer inhibitory synaptic time constant ($\tau_i = 20\,ms$), showing $f_{osc} = 30.46\,Hz$ oscillations with a synchronisation of $\kappa(\tau) = 0.46$, $\tau = 10\,ms$. (D) Raster plot for the same network with a longer inhibitory synaptic time constant ($\tau_i = 25\,ms$), showing $f_{osc} = 21.48\,Hz$ oscillations with a synchronisation of $\kappa(\tau) = 0.24$, $\tau = 10\,ms$. The network was stimulated with a constant current $I_{stim} = 0.4\,nA$.

5.3 Studying Tonic Inhibition

5.3.1 Tonic Inhibition Improves Neural Synchronisation

To measure the synchronisation of the neural activity in the network we used the coherence metric $\kappa(\tau)$ defined in [Wang and Buzsáki, 1996], as described in Chapter 3, using a time window of $\tau = 10\,ms$. In the absence of tonic inhibition $g_{ton} = 0\,nS$, the network synchronised its activity with $\kappa(\tau) = 0.40$ (Figure 5.3A) at a population frequency of $f = 20.72\,Hz$ (Figure 5.3B), and an oscillatory frequency of $f_{osc} = 42.67\,Hz$ (Figure 5.3C). Increasing doses of propofol reduced the overall network activity and slowed down its oscillations, whilst the network synchronisation remained stable at an average value of $\overline{\kappa(\tau)} = 0.42 \pm 0.01$. When the tonic inhibition reached a critical value of $g_{ton} = 14\,nS$ at which the synchronisation increased abruptly reaching $\kappa(\tau) = 0.72$, and the mean firing rate increased to $f \simeq 18\,Hz$. The network synchronisation remained unchanged at an average plateau value of $\overline{\kappa(\tau)} = 0.76 \pm 0.00$ until further strengthening the effects of propofol

$g_{ton} = 21\,nS$ caused the overall network activity to drastically decrease ($\kappa(\tau) = 0.02$, $f = 4.98\,Hz$ and $f_{osc} = 13.04\,Hz$), until it faded away ($\kappa(\tau) = 0$, $f = 0\,Hz$ and $f_{osc} = 0\,Hz$ for $g_{ton} \geq 21.5\,nS$).

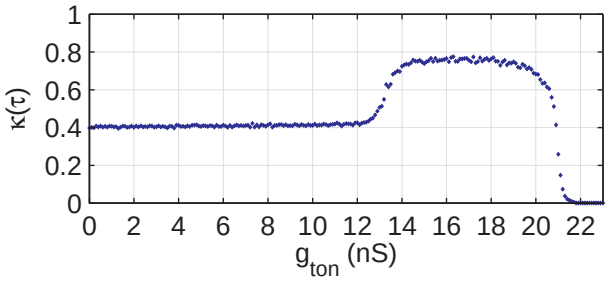

(A) Network synchronisation as tonic inhibition increases.

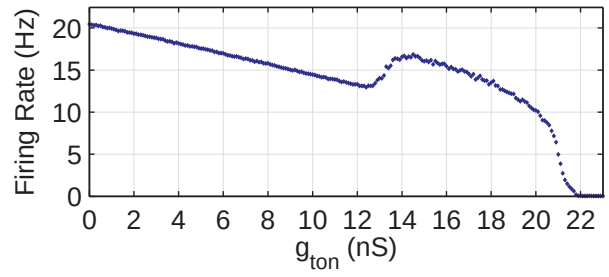

(B) Network firing rate as tonic inhibition increases.

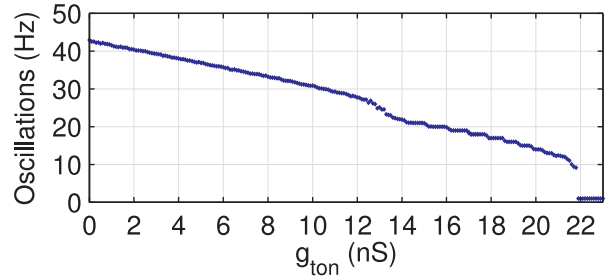

(C) Network oscillation frequency as tonic inhibition increases.

Figure 5.3: Increasing propofol enhances network synchronisation. (A) At low values of propofol ($0\,nS \leq g_{ton} \leq 13\,nS$) the network synchronisation is stable at an average value of $\overline{\kappa(\tau)} = 0.43 \pm 0.01$. Increasing the propofol dosage – by acting on the tonic conductance g_{ton} – causes the overall activity of the network to decrease, until a critical value of $g_{ton} = 14\,nS$ at which both the network synchronisation (A), and the firing rate (B) increase to $\kappa(\tau) = 0.72$, and $f = 16.57\,Hz$ respectively. The oscillation frequency (C) follows a monotonically decelerating trend. When the concentration value reaches a value of $g_{ton} \geq 21.5\,nS$ the activity, synchronous or otherwise, fades out ($\kappa(\tau) = 0$, $f = 0\,Hz$ and $f_{osc} = 0\,Hz$ for $g_{ton} >= 21.5\,nS$).

Figure 5.4 shows the activity of the network for increasing values of g_{ton}, in the form of raster plots. Their corresponding computed LFP signals are shown in Figure 5.5. At $g_{ton} = 0\,nS$ the network displayed gamma frequency oscillations ($f_{osc} = 42.67\,Hz$) with an average population frequency of $f = 20.72\,Hz$ and a synchronisation of $\kappa(\tau) = 0.40$. This indicates that, on average, approximately half of the neurons fire synchronously at any given time, as shown in Figure 5.4A. In addition, each individual neuron fired once every two cycles. Taken together, these two observations indicate that the intrinsic firing rate of each isolated neuron was $f = 42.67\,Hz$, although the presence of synaptic inhibition halved it.

Increasing tonic inhibition above a threshold value of $14\,nS$ produced slower population firing rates,

and slower oscillations. At $g_{ton} = 15\,nS$, the network activity oscillated at $f_{osc} = 20.67\,Hz$ with a population frequency of $f = 17.27\,Hz$ (Figure 5.4B). Similarly, at $g_{ton} = 18\,nS$, the network activity oscillated at $f_{osc} = 17.33\,Hz$ with a population frequency of $f = 14.08\,Hz$. (Figure 5.4C). We observe that, although slower, the oscillatory activity was approximately twice as synchronised ($\overline{\kappa(\tau)} = 0.76 \pm 0.00$ for $14\,nS \leq g_{ton} \leq 19\,nS$) compared to the same network in the absence of tonic inhibition ($g_{ton} = 0\,nS$). As inhibition increased, the neurons in the network became less prone to discharging action potentials and the population frequency slowed down. In addition, stronger inhibition provided the neurons with tighter windows of increased excitability, ensuring that most of the neurons in the network (approximately 80%) would fire concurrently, which explains the enhanced network synchronisation.

Figure 5.4D shows weak, albeit synchronous activity at $f_{osc} = 12.67\,Hz$ with a population frequency of $f = 3.85\,Hz$ for $g_{ton} = 21\,nS$. Further strengthening the tonic inhibition caused the neurons to emit fewer and fewer action potentials, until eventually the network activity faded away ($g_{ton} > 21\,nS$).

The LFP signal computed from the network activity reflected its synchronous behaviour (Figure 5.5). In the absence of propofol ($g_{ton} = 0\,nS$ in Figure 5.5A) the LFP oscillated between $-0.6\,mV$ and $0.7\,mV$ at $f_{osc} = 42.67\,Hz$. Increasing the effects of anaesthetics caused an increase in the amplitude of the LFP signal, which oscillated between $-1\,mV$ and $1.2\,mV$ at $f_{osc} = 20.67\,Hz$ for $g_{ton} = 15\,nS$ (Figure 5.5B), and $-0.95\,mV$ and $1.3\,mV$ at $f_{osc} = 17.33\,Hz$ for $g_{ton} = 18\,nS$ (Figure 5.5C). This increase in amplitude reflected the increase in network synchronisation as the more neurons fire concurrently at any given time the stronger the generated LFP signal will be. Similarly, the LFP amplitude decreased for $g_{ton} = 21\,nS$ (Figure 5.5D) as less neurons fire due to the strong tonic inhibition, producing an LFP signal which oscillated between $-0.32\,mV$ and $0.47\,mV$ at $f_{osc} = 12.67\,Hz$.

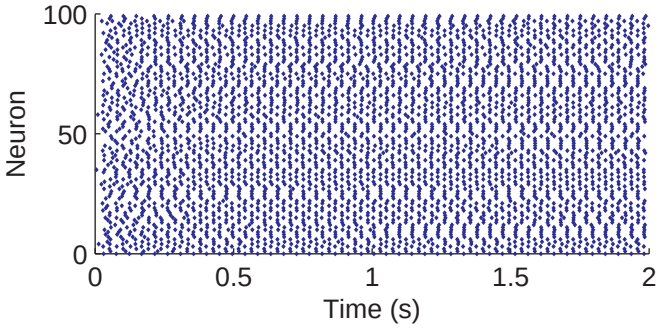

(A) Raster plot for $g_t = 0\,nS$.

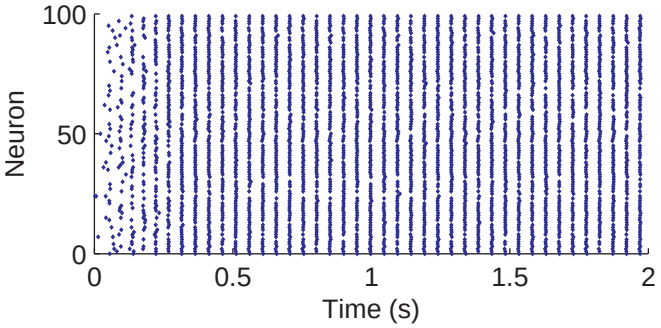

(B) Raster plot for $g_t = 15\,nS$.

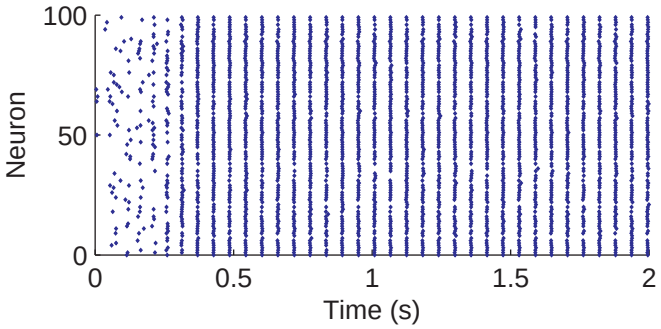

(C) Raster plot for $g_t = 18\,nS$.

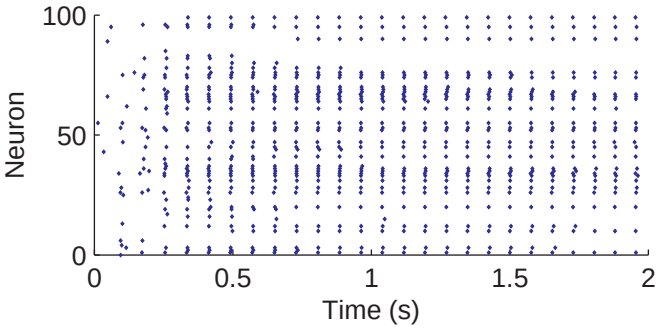

(D) Raster plot for $g_t = 21\,nS$.

Figure 5.4: Increasing propofol dosage enhances network synchronisation. (A) Raster plot for the 100-cell inhibitory network in the absence of propofol ($g_{ton} = 0\,nS$), showing $f_{osc} = 42.67\,Hz$ oscillations with a synchronisation of $\kappa(\tau) = 0.4$, $\tau = 10\,ms$. (B) Raster plot for the same network with a higher dose of propofol ($g_{ton} = 15\,nS$), showing $f_{osc} = 20.67\,Hz$ oscillations with a synchronisation of $\kappa(\tau) = 0.8$, $\tau = 10\,ms$. (C) Raster plot for the same network with a higher dose of propofol ($g_{ton} = 18\,nS$), showing $f_{osc} = 17.33\,Hz$ oscillations with a synchronisation of $\kappa(\tau) = 0.8$, $\tau = 10\,ms$. (D) Raster plot for the same network with a higher dose of propofol ($g_{ton} = 21\,nS$), showing $f_{osc} = 12.67\,Hz$ oscillations with a synchronisation of $\kappa(\tau) = 0.8$, $\tau = 10\,ms$. The network was stimulated with a constant current $I_{stim} = 0.4\,nA$.

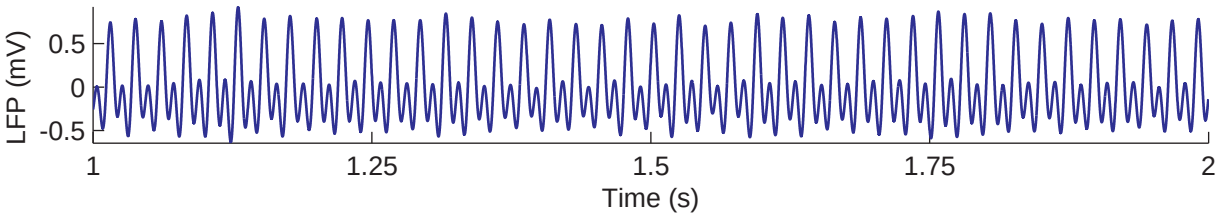

(A) LFP for $g_t = 0\,nS$.

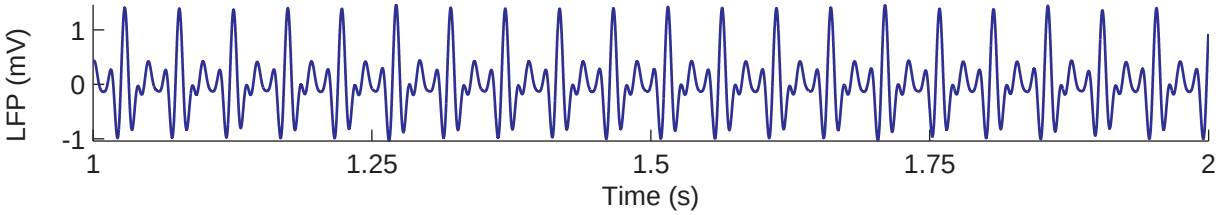

(B) LFP for $g_t = 15\,nS$.

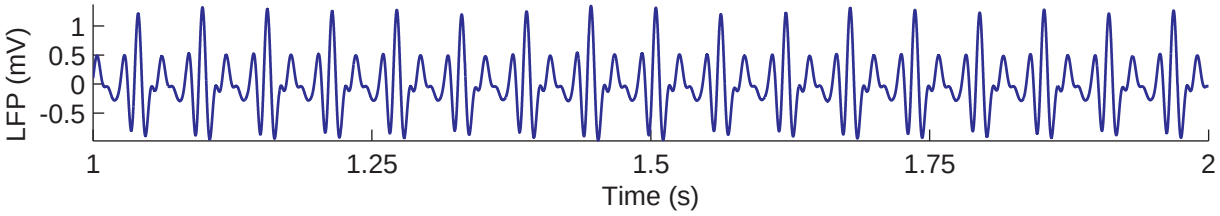

(C) LFP for $g_t = 18\,nS$.

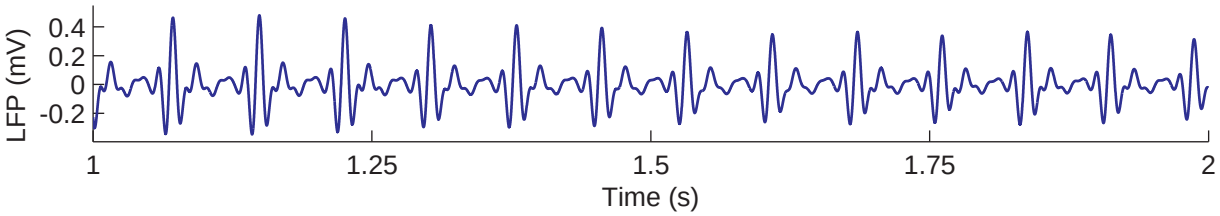

(D) LFP for $g_t = 21\,nS$.

Figure 5.5: The synchronous activity displayed by the interneuron network is reflected in the computed LFP signals. (A) LFP signal computed from the spiking activity of the inhibitory network in the absence of propofol shows $f_{osc} = 42.67\,Hz$ oscillations with a synchronisation of $\kappa(\tau) = 0.4$, $\tau = 10\,ms$ (one-second extract). (B) LFP signal computed from the spiking activity of the inhibitory network with a higher dose of propofol ($g_{ton} = 15\,nS$), showing $f_{osc} = 20.67\,Hz$ oscillations with a synchronisation of $\kappa(\tau) = 0.8$, $\tau = 10\,ms$ (one-second extract). (C) LFP signal computed from the spiking activity of the inhibitory network with a higher dose of propofol ($g_{ton} = 18\,nS$), showing $f_{osc} = 17.33\,Hz$ oscillations with a synchronisation of $\kappa(\tau) = 0.8$, $\tau = 10\,ms$ (one-second extract). (D) LFP signal computed from the spiking activity of the inhibitory network with a higher dose of propofol ($g_{ton} = 21\,nS$), showing $f_{osc} = 12.67\,Hz$ oscillations with a synchronisation of $\kappa(\tau) = 0.8$, $\tau = 10\,ms$ (one-second extract).

5.4 Combining the Effects of Tonic and Phasic Inhibition

We then turned our attention towards analysing the joint effects of both synaptic and extrasynaptic propofol-enhanced inhibition. As previously explained, we modelled the action of propofol on synaptic $GABA_A$ receptors by increasing the inhibitory synaptic conductance, time constant, and current baseline. Our results show that solely the tonic inhibition was responsible for enhancing the network synchronisation in the presence of the anaesthetic agent.

5.4.1 Propofol-Enhanced Inhibitory Synaptic Conductance Does not Hinder Synchronisation

Increasing the inhibitory synaptic conductance did not hinder the synchronising properties of tonic inhibition (Figure 5.7). Figure 5.7A and Figure 5.7B depict the evolution of the average population frequency and synchronisation ($\kappa(\tau)$) respectively (vertical z axis), as both the synaptic weight w_i (y axis) and the tonic conductance g_{ton} (x axis) are increased, for a fixed synaptic time constant $\tau_i = 10\,ms$. Similarly, Figure 5.7C and Figure 5.7D illustrate the evolution of the average population frequency and synchronisation, for a fixed synaptic time constant $\tau_i = 14\,ms$. Finally, Figure 5.7E and Figure 5.7F show the evolution of the average population frequency and synchronisation, for a fixed synaptic time constant $\tau_i = 30\,ms$. The synaptic weights ranged between $1.4\,nS \leq w_i \leq 2.6\,nS$ and the tonic conductance ranged between $0\,nS \leq g_{ton} \leq 20\,nS$.

The overall population frequency decelerated from a maximum of $f = 21.97 \pm 0.06\,Hz$ to a minimum of $f = 7.78 \pm 0.25\,Hz$ as both w_i and g_{ton} grew (Figure 5.7A). However, whilst the firing rate followed a generally decreasing trend as synaptic weights were strengthened, it showed an up-and-down profile as tonic inhibition was enhanced, similar to that described previously in the absence of propofol-enhanced synaptic activity. Indeed, given $g_{ton} = 0\,nS$, the frequency slowed from $f = 21.97 \pm 0.06\,Hz$ for $w_i = 1.4\,nS$ to $f = 16.59 \pm 0.14\,Hz$ for $w_i = 2.6\,nS$. At $g_{ton} = 15\,nS$, the frequency slowed from $f = 16.81 \pm 0.18\,Hz$ for $w_i = 1.4\,nS$ to $f = 13.46 \pm 0.18\,Hz$ for $w_i = 2.6\,nS$. At $g_{ton} = 20\,nS$, the frequency slowed from $f = 10.53 \pm 0.26\,Hz$ for $w_i = 1.4\,nS$ to $f = 7.78 \pm 0.25\,Hz$ for $w_i = 2.6\,nS$. In contrast, we can observe a sharp increase in network frequency as tonic inhibition strengthens, given fixed synaptic weights. At $w_i = 1.4\,nS$, the frequency slowed from $f = 21.97 \pm 0.06\,Hz$ for $g_{ton} = 0\,nS$ to $f = 13.99 \pm 0.06\,Hz$ for $g_{ton} = 12\,nS$, then accelerated to $f = 16.81 \pm 0.18\,Hz$ for $g_{ton} = 15\,nS$, and finally dropped to $f = 10.53 \pm 0.26\,Hz$ for $g_{ton} = 20\,nS$. A similar bump pattern can be seen at all other values of w_i on Figure 5.7A. For example, at $w_i = 2.4\,nS$, the frequency slowed from $f = 17.08 \pm 0.12\,Hz$ for $g_{ton} = 0\,nS$ to $f = 13.08 \pm 0.35\,Hz$ for $g_{ton} = 10\,nS$, then accelerated to $f = 15.62 \pm 0.25\,Hz$ for $g_{ton} = 12\,nS$, and finally dropped to $f = 8.14 \pm 0.46\,Hz$ for $g_{ton} = 20\,nS$.

A similar trend can be observed, having fixed g_{ton}, on the evolution of the network synchronisation with respect to increasing values of w_i (Figure 5.7B). For example, at $g_{ton} = 0\,nS$, the synchronisation was $\kappa(\tau) = 0.34 \pm 0.02$ for $w_i = 1.4\,nS$, and $\kappa(\tau) = 0.36 \pm 0.01$ for $w_i = 2.6\,nS$, with a mean value of $\overline{\kappa(\tau)} = 0.36 \pm 0.00$. At $g_{ton} = 15\,nS$, the synchronisation was $\kappa(\tau) = 0.70 \pm 0.01$ for $w_i = 1.4\,nS$, and $\kappa(\tau) = 0.63 \pm 0.07$ for $w_i = 2.6\,nS$, with a mean value of $\overline{\kappa(\tau)} = 0.67 \pm 0.01$. At $g_{ton} = 20\,nS$, the synchronisation was $\kappa(\tau) = 0.65 \pm 0.01$ for $w_i = 1.4\,nS$, and $\kappa(\tau) = 0.48 \pm 0.04$ for $w_i = 2.6\,nS$, with a mean value of $\overline{\kappa(\tau)} = 0.59 \pm 0.01$. Comparing the stepwise synchronisation values with the average across all w_i values for a fixed g_{ton} indicated that synaptic inhibition accounts for little to no variability in the enhanced synchronous activity displayed by the network. Conversely, Figure 5.7B illustrates how the network synchronisation tightened for increasing values of g_{ton} given fixed synaptic weights, as previously observed (Figure 5.3A). At $w_i = 1.4\,nS$, the synchronisation remained stable at an average value of $\overline{\kappa(\tau)} = 0.37 \pm 0.01$ for $0\,nS \leq g_{ton} \leq 12\,nS$, then increased to an average value of $\overline{\kappa(\tau)} = 0.65 \pm 0.04$ for $g_{ton} > 12\,nS$. This synchronisation bump pattern was preserved across all values of w_i. For example, at $w_i = 2.4\,nS$, the synchronisation stabilised at an average value of $\overline{\kappa(\tau)} = 0.36 \pm 0.01$ for $0\,nS \leq g_{ton} \leq 10\,nS$, then increased to an average value of $\overline{\kappa(\tau)} = 0.57 \pm 0.09$ for $g_{ton} > 10\,nS$.

In addition, we observed that stronger synaptic inhibition had a tendency to shift the tonic inhibition-mediated frequency rebound peak towards lower values of g_{ton}. Our results show that this seemed to be the sole effect of propofol-enhanced GABAergic phasic inhibition. For $1.4\,nS \leq w_i \leq 2\,nS$ the peak was centred around $g_{ton} = 15\,nS$, with a maximum frequency value of $16.81 \pm 0.18\,Hz$ (Figure 5.6A), and a corresponding coherence value of $\kappa(\tau) = 0.71 \pm 0.01$ (Figure 5.6B) at $w_i = 1.4\,nS$. Stronger synaptic weights ($w_i > 2\,nS$) moved the centre of the peak around $g_{ton} = 12\,nS$, with a

maximum frequency value of $16.21 \pm 0.27\,Hz$ (Figure 5.6A), and a corresponding coherence value of $\kappa(\tau) = 0.63 \pm 0.02$ (Figure 5.6B) at $w_i = 2.1\,nS$. Likewise, the peak of the tonic inhibition-mediated synchronisation rebound was also affected by stronger synaptic activity. For $1.4\,nS \leq w_i \leq 2.4\,nS$ it remained centred around $g_{ton} = 15\,nS$, with a maximum coherence value of $\kappa(\tau) = 0.72 \pm 0.01$ (Figure 5.6B), and a corresponding frequency value of $16.66 \pm 0.21\,Hz$ (Figure 5.6A) at $w_i = 1.5\,nS$. Stronger synaptic weights ($w_i > 2.4\,nS$) moved the centre of the peak around $g_{ton} = 12\,nS$, with a maximum coherence value of $\kappa(\tau) = 0.63 \pm 0.01$ (Figure 5.6B), and a corresponding frequency value of $15.43 \pm 0.17\,Hz$ (Figure 5.6A) at $w_i = 2.6\,nS$. This behaviour is to be expected since the presence of stronger inhibition invariably caused a reduction in overall network activity thus producing slower firing rates.

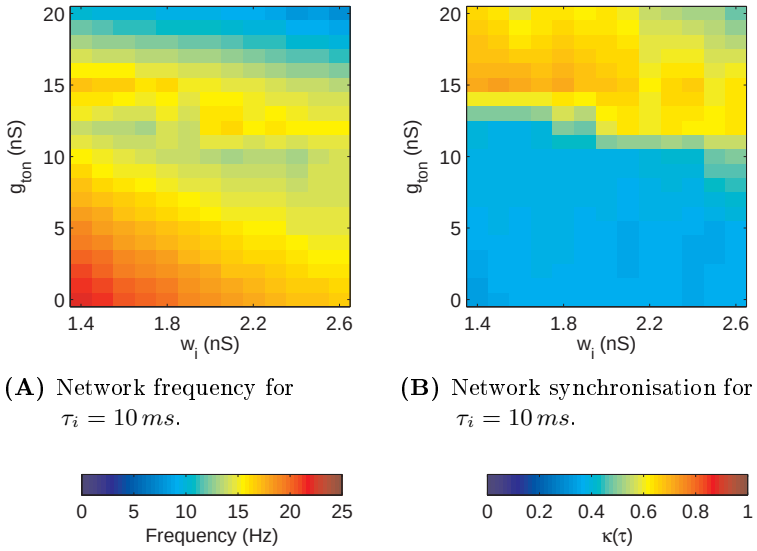

(A) Network frequency for $\tau_i = 10\,ms$.

(B) Network synchronisation for $\tau_i = 10\,ms$.

Figure 5.6: Propofol-enhanced tonic inhibition allows for tighter network synchronisation, regardless of the presence of stronger inhibitory synapses. (A) Increasing tonic inhibition (y axis) causes an abrupt acceleration at $g_{ton} = 15\,nS$. The sole effect of synaptic inhibition (x axis) is to shift the peak of the acceleration towards lower g_{ton} values. (B) Similarly, tonic inhibition causes an abrupt enhanced synchronisation, whose peak is shifted towards lower g_{ton} values as w_i increases. The network was stimulated with a constant current $I_{stim} = 0.4\,nA$.

5.4.2 Prolonged Synapse Closing Times Allow for Synchronisation with Weaker Tonic Inhibition

Propofol also enhances synaptic inhibitory currents by extending the closing time of the synapse [Bai et al., 2001, Kitamura et al., 2004, McDougall et al., 2008], allowing for longer lasting currents. We modelled this effect by prolonging the synaptic time constant τ_i. Figure 5.7A, Figure 5.7C and Figure 5.7E depict the relationship between the network frequency and the synaptic and tonic inhibition as τ_i is increased, from $10\,ms$ to $14\,ms$ to $30\,ms$ respectively. Intuitively, longer synaptic time constants should reduce the firing frequency of the network, as is reflected in our results. At $\tau_i = 10\,ms$ the maximum firing rate was $f = 21.97 \pm 1.24\,Hz$ for $w_i = 1.4\,nS$ and $g_{ton} = 0\,nS$ (Figure 5.7A). A longer time constant $\tau_i = 14\,ms$ decelerated the maximum firing rate to $f = 17.42 \pm 0.14\,Hz$ for $w_i = 1.4\,nS$ and $g_{ton} = 0\,nS$ (Figure 5.7C). Further extending τ_i to $14\,ms$ reduced the maximum firing rate to $f = 9.28 \pm 0.24\,Hz$ for $w_i = 1.4\,nS$ and $g_{ton} = 0\,nS$ (Figure 5.7E). In general, the network frequency was slower at all values of w_i and g_{ton} as τ_i was increased.

Longer synaptic time constants also affected the network synchronisation and its propofol-dependent bump-like evolution. Figure 5.7B, Figure 5.7D and Figure 5.7F depict the relationship between the

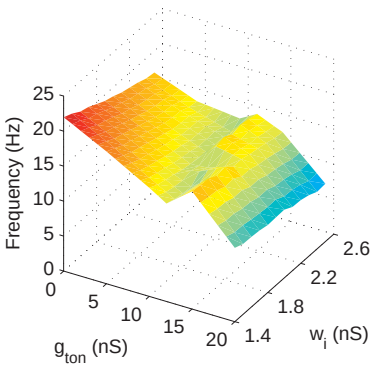

(A) Network frequency for $\tau_i = 10\,ms$.

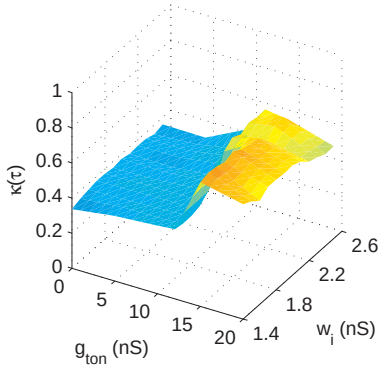

(B) Network synchronisation for $\tau_i = 10\,ms$.

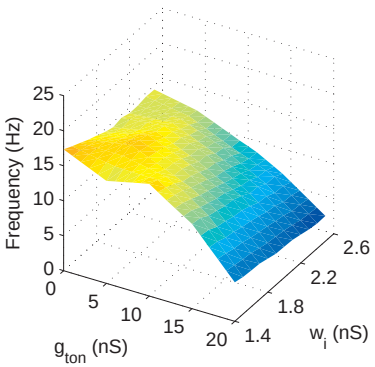

(C) Network frequency for $\tau_i = 14\,ms$.

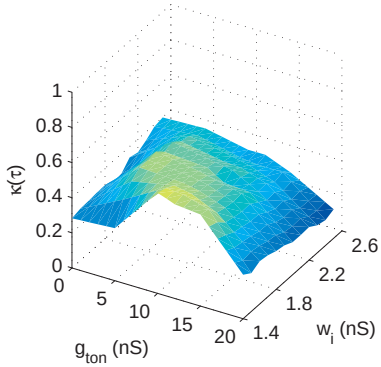

(D) Network synchronisation for $\tau_i = 14\,ms$.

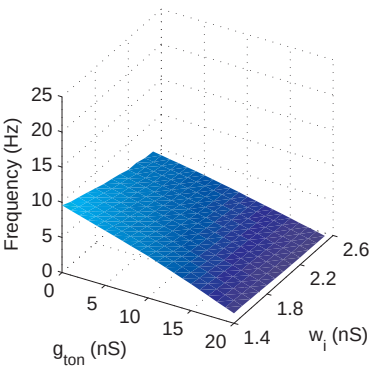

(E) Network frequency for $\tau_i = 30\,ms$.

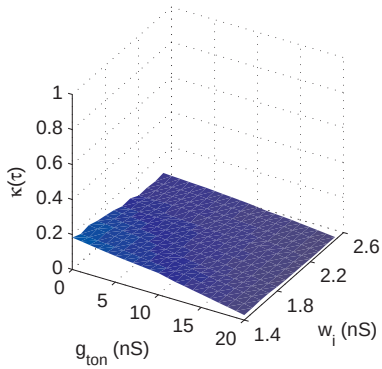

(F) Network synchronisation for $\tau_i = 30\,ms$.

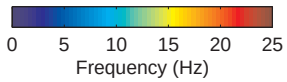

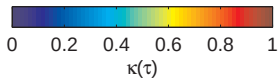

Figure 5.7: Propofol-enhanced tonic inhibition allows for tighter network synchronisation, regardless of the presence of stronger inhibitory synapses. In all the plots, the x axis represents the tonic conductance (g_{ton}) and the y axis represents the inhibitory synaptic weight (w_i). (A) Given $\tau_i = 10\,ms$, the network frequency decelerates as tonic inhibition strengthens until a critical value at which it accelerates. (B) This acceleration is due to an abrupt increase in network synchronisation at $g_{ton} \geq 15\,nS$ for all values of w_i. (C) A longer synaptic time constant ($\tau_i = 14\,ms$) shifts the network frequency bump towards lower values of g_{ton}. (D) Similarly, the network synchronisation bump shifts towards lower values of g_{ton}. (E) Extending the synaptic time constant ($\tau_i = 30\,ms$) causes the bump-like pattern of the network frequency to disappear in favour of a linearly decelerating trend. (F) Similarly, the bump-like pattern of the network synchronisation disappears in favour of a linearly decelerating trend. The network was stimulated with a constant current $I_{stim} = 0.4\,nA$.

network synchronisation and the synaptic and tonic inhibition as τ_i is increased, from $10\,ms$ to $14\,ms$ to $30\,ms$ respectively. Interestingly, we observe that extending the duration of the inhibitory synaptic current enhanced the network synchronisation at lower g_{ton} values, as longer time constants shifted the peak of the synchronisation bump towards the lower end of the x axis. At $\tau_i = 14\,ms$ (Figure 5.7D), given $w_i = 1.4nS$ the synchronisation stabilised at an average value of $\overline{\kappa(\tau)} = 0.29 \pm 0.01$ for $0\,nS \leq g_{ton} \leq 5\,nS$, then increased to an average value of $\overline{\kappa(\tau)} = 0.59 \pm 0.02$ for $5 < g_{ton} \leq 15\,nS$, and proceeded to drop to an average value of $\overline{\kappa(\tau)} = 0.31 \pm 0.01$ for $g_{ton} > 15\,nS$. Once again, this synchronisation bump pattern was preserved across all values of w_i. For example, a similar evolution can be observed at $w_i = 2.2\,nS$ where the synchronisation stabilised at an average value of $\overline{\kappa(\tau)} = 0.34 \pm 0.06$ for $0\,nS \leq g_{ton} \leq 5\,nS$, then increased to an average value of $\overline{\kappa(\tau)} = 0.41 \pm 0.02$ for $5 < g_{ton} \leq 15\,nS$, and proceeded to drop to an average value of $\overline{\kappa(\tau)} = 0.18 \pm 0.02$ for $g_{ton} > 15\,nS$.

Further extending the synapse closing time caused further network frequency deceleration, as the number of spikes elicited were drastically reduced by the presence of stronger inhibition. Eventually, the network reverted to a slow, asynchronous firing regime. Figure 5.7E and Figure 5.7F illustrate the network frequency and synchronisation, respectively, for $\tau_i = 30\,ms$. The maximum frequency was reduced to $f = 9.28 \pm 0.24\,Hz$ for $w_i = 1.4\,nS$ and $g_{ton} = 0\,nS$. Whereas the maximum network synchronisation was reduced to $\kappa(\tau) = 0.18 \pm 0.01$. Both frequency and synchronisation followed decreasing trends as w_i and g_{ton} were increased, and the bump pattern was absent.

5.4.3 Tonic Inhibition-Mediated Synchronisation Is Unaffected by Potentiated Inhibitory Synaptic Baseline Currents

In vitro experimental studies [Jin et al., 2009, McDougall et al., 2008] have reported that exposure to propofol causes a concentration-dependent increase in GABAergic baseline currents in postsynaptic neurons. We modelled this effect by adding a constant $0\,pA \leq k_{bas} \leq 100\,pA$ to the inhibitory synaptic current I_i, where $k_{bas} = 0\,pA$ indicates the absence of propofol. To our knowledge, ours is the first computational study to include propofol-induced receptor desensitisation in its model. Our results indicate that a propofol-mediate shift in inhibitory synaptic baseline current does not interfere with the enhanced synchronisation provided by tonic inhibition. Figure 5.8 illustrates the relationship between the network frequency (vertical z axis) and the combined effects of tonic and synaptic inhibition – namely, increasing tonic conductance (x axis), shifting the inhibitory synaptic current baseline (y axis), enhancing synaptic current amplitudes (horizontally distributed surface plots), and prolonging synaptic current duration (vertically distributed surface plots). In particular, the top row of surface plots in Figure 5.8 depict the network frequency for $\tau_i = 10\,ms$ and increasing values of w_i i.e. $1.6\,nS$ (Figure 5.8A), $1.9\,nS$ (Figure 5.8B), and $1.9\,nS$ (Figure 5.8C) respectively. The middle row of surface plots in Figure 5.8 depict the network frequency for $\tau_i = 14\,ms$ and increasing values of w_i i.e. $1.6\,nS$ (Figure 5.8D), $1.9\,nS$ (Figure 5.8E), and $2.2\,nS$ (Figure 5.8F) respectively. The bottom row of surface plots in Figure 5.8 depict the network frequency for $\tau_i = 30\,ms$ and increasing values of w_i i.e. $1.6\,nS$ (Figure 5.8G), $1.9\,nS$ (Figure 5.8H), and $2.2\,nS$ (Figure 5.8I) respectively.

Similarly, Figure 5.9 illustrates the relationship between the network synchronisation (vertical z axis) and the combined effects of tonic and synaptic inhibition – namely, increasing tonic conductance (x axis), shifting the inhibitory synaptic current baseline (y axis), enhancing synaptic current amplitudes (horizontally distributed surface plots), and prolonging synaptic current duration (vertically distributed surface plots). In particular, the top row of surface plots in Figure 5.9 depict the network frequency for $\tau_i = 10\,ms$ and increasing values of w_i i.e. $1.6\,nS$ (Figure 5.9A), $1.9\,nS$ (Figure 5.9B), and $1.9\,nS$ (Figure 5.9C) respectively. The middle row of surface plots in Figure 5.9 depict the network frequency for $\tau_i = 14\,ms$ and increasing values of w_i i.e. $1.6\,nS$ (Figure 5.9D), $1.9\,nS$ (Figure 5.9E), and $2.2\,nS$ (Figure 5.9F) respectively. The bottom row of surface plots

in Figure 5.9 depict the network frequency for $\tau_i = 30\,ms$ and increasing values of w_i i.e. $1.6\,nS$ (Figure 5.9G), $1.9\,nS$ (Figure 5.9H), and $2.2\,nS$ (Figure 5.9I) respectively.

The presence of a non-zero inhibitory baseline current had a general tendency to produce lower network firing rates. Indeed for $g_{ton} = 0\,nS$, $w_i = 1.6\,nS$, and $\tau_i = 10\,ms$, the network frequency was $20.83 \pm 0.07\,Hz$ at $k_{bas}0 = pA$, and decelerated to $16.76 \pm 0.07\,Hz$ at $k_{bas} = 100\,pA$. Moreover, for $g_{ton} = 20\,nS$, $w_i = 1.6\,nS$, and $\tau_i = 10\,ms$, the network frequency was $10.10 \pm 0.18\,Hz$ at $k_{bas}0 = pA$, and decelerated to $0.04 \pm 0.00\,Hz$ at $k_{bas} = 100\,pA$. However, the sharp acceleration of the network frequency caused by tonic inhibition remained unaffected, aside from increasing k_{bas} values causing the peak of the acceleration bump to shift towards lower g_{ton} values. For example, in Figure 5.8A for $w_i = 1.6\,nS$, $\tau_i = 10\,ms$, and $k_{bas} = 0\,pA$ the peak of the acceleration was at $g_{ton} = 15\,nS$ with a frequency of $16.28 \pm 0.23\,Hz$. Increasing k_{bas} to $40\,pA$ shifted the peak to $g_{ton} = 12\,nS$ with a frequency of $15.73 \pm 0.25\,Hz$. Further increasing k_{bas} to $90\,pA$ shifted the peak to $g_{ton} = 10\,nS$ with a frequency of $15.26 \pm 0.17\,Hz$. This effect is comparable to that caused by stronger synaptic weights w_i, in that both increasing k_{bas} and w_i effectively correspond to an enhancement of global network inhibition.

As expected, longer synaptic time constants shifted the acceleration peak towards lower tonic inhibition strengths, regardless of the increasing synaptic baseline current. This shift can be observed when comparing the surface plots in Figure 5.8 vertically. Taking the first column of Figure 5.8 as an example, $w_i = 1.6\,nS$, $\tau_i = 10\,ms$, and $k_{bas} = 40\,pA$ the peak of the acceleration was at $g_{ton} = 15\,nS$ (Figure 5.8A). Extending the synaptic time constant to $\tau_i = 14\,ms$ shifts the peak to $g_{ton} = 5\,nS$ for $k_{bas} = 40\,pA$ (Figure 5.8D). A longer time constant $\tau_i = 30\,ms$ shifts the peak to $g_{ton} = 0\,nS$ for $k_{bas} = 40\,pA$ (Figure 5.8G). Finally, stronger inhibitory synaptic weights globally decelerated the network activity (Figure 5.8A, Figure 5.8B, and Figure 5.8C), whilst preserving the bump-like pattern in the population frequency. These behaviours are consistent with our previously reported findings within this Chapter.

In addition, the network tonic-inhibition mediated synchronisation seemed to remain unaffected as k_{bas} increased (Figure 5.9). The network continued to display enhanced synchronisation in the presence of critical degrees of tonic inhibition. Intensifying shifts in inhibitory baseline currents solely slightly shifted the synchronisation peak towards lower tonic conductance values. For example, in Figure 5.9A the synchronisation peak for $k_{bas} = 0\,pA$ was at $g_{ton} = 0\,nS$ with a synchronisation of $\kappa(\tau) = 0.70 \pm 0.01$ for $w_i = 1.6\,nS$, and $\tau_i = 10\,ms$. Increasing k_{bas} to $60\,pA$ shifted the peak to $g_{ton} = 12\,nS$ with a synchronisation of $\kappa(\tau) = 0.72 \pm 0.01$.

Longer synaptic time constants shifted the synchronisation peak towards lower tonic inhibition strengths, regardless of the increasing synaptic baseline current. This shift can be observed when comparing the surface plots in Figure 5.9 vertically. Finally, stronger inhibitory synaptic weights globally decreased the maximum attainable network synchronisation (Figure 5.9A, Figure 5.9B, and Figure 5.9C), whilst preserving the enhanced synchronisation phenomenon observed in the presence of tonic inhibition.

5.4.4 Tonic Inhibition Allows for the Emergence of Elevated Network Synchronisation

Having isolated the two model parameters which were responsible for significantly affecting the synchronisation exhibited by the network activity – namely, the tonic conductance g_{ton} and the synaptic time constant τ_i – we simulated an experiment in which we varied both of these parameters concurrently. The purpose of this simulation was to study the effect of the absorption of increasing doses of anaesthetic agent over time on network activity. We increased g_{ton} from $0\,nS$ to $20\,nS$ in steps of $2\,nS$, and τ_i from $10\,ms$ to $20\,ms$ in steps of $1\,ms$, in $2\,s$ intervals. Figure 5.10 depicts the raster plot of the network activity for the first $14\,s$ of simulation time, and Figure 5.10 the last $6\,s$

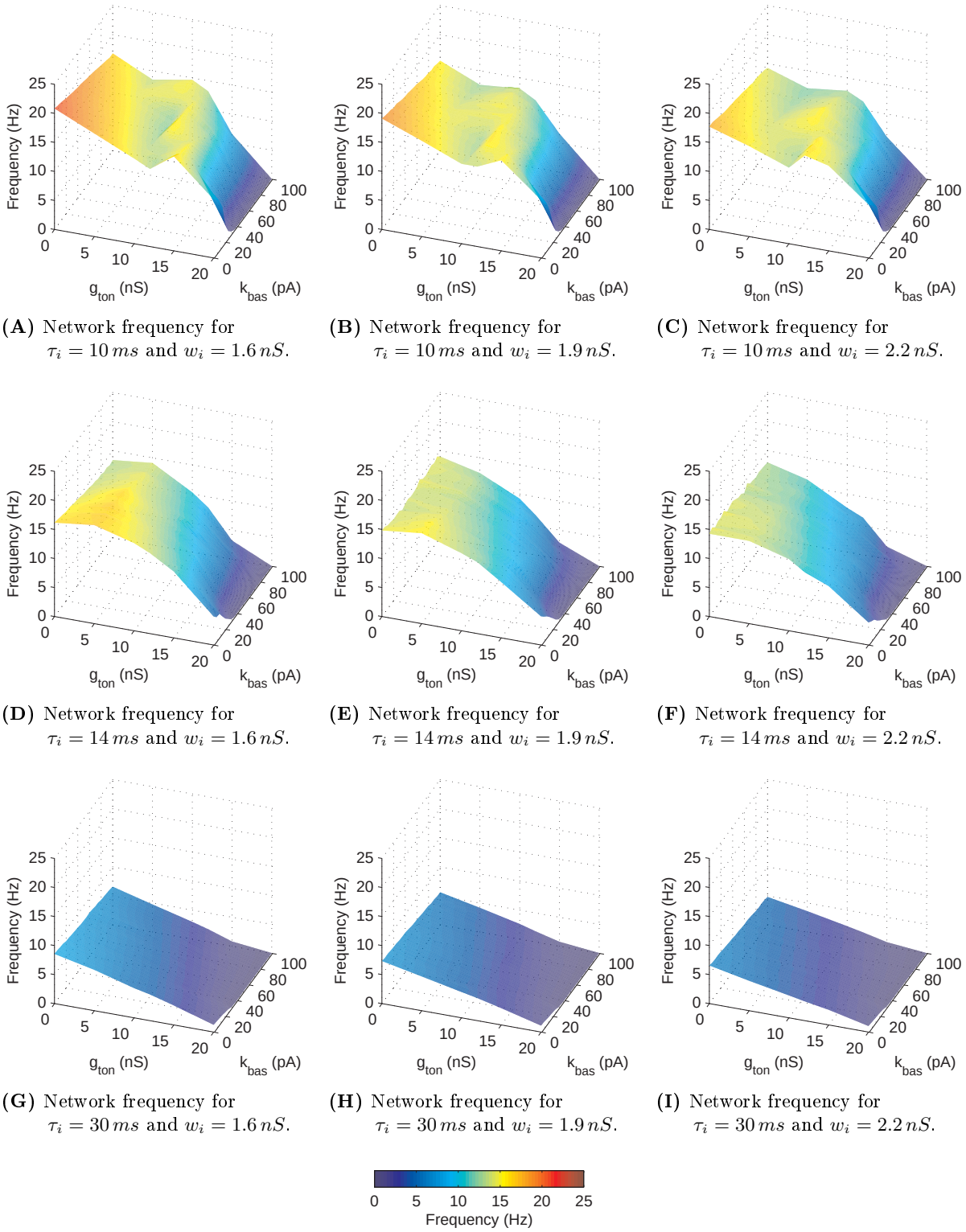

(A) Network frequency for $\tau_i = 10\,ms$ and $w_i = 1.6\,nS$.

(B) Network frequency for $\tau_i = 10\,ms$ and $w_i = 1.9\,nS$.

(C) Network frequency for $\tau_i = 10\,ms$ and $w_i = 2.2\,nS$.

(D) Network frequency for $\tau_i = 14\,ms$ and $w_i = 1.6\,nS$.

(E) Network frequency for $\tau_i = 14\,ms$ and $w_i = 1.9\,nS$.

(F) Network frequency for $\tau_i = 14\,ms$ and $w_i = 2.2\,nS$.

(G) Network frequency for $\tau_i = 30\,ms$ and $w_i = 1.6\,nS$.

(H) Network frequency for $\tau_i = 30\,ms$ and $w_i = 1.9\,nS$.

(I) Network frequency for $\tau_i = 30\,ms$ and $w_i = 2.2\,nS$.

Figure 5.8: Propofol-enhanced tonic inhibition decelerates the population firing rate, regardless of the presence of a stronger inhibitory baseline current. (A) Given $\tau_i = 10\,ms$ and $w_i = 1.6\,nS$, the bump-like pattern caused by the tonic inhibition-mediated (x axis) deceleration followed by an acceleration of the network frequency is unaffected by the presence of a non-zero synaptic baseline current (y axis). These only slightly shift the peak of the acceleration towards lower g_{ton} values. The acceleration bump is unaffected by stronger synaptic weights – $w_i = 1.9\,nS$ in (B), and $w_i = 1.6\,nS$ in (C). (D) Given $\tau_i = 14\,ms$ and $w_i = 1.6\,nS$, the peak of the acceleration shifts towards lower g_{ton} values. This behaviour is unaffected by stronger synaptic weights – $w_i = 1.9\,nS$ in (E), and $w_i = 1.6\,nS$ in (F). (G) Given $\tau_i = 30\,ms$ and $w_i = 1.6\,nS$, the network acceleration follows a decreasing trend as g_{ton} and k_{bas} are increased. This behaviour is unaffected by stronger synaptic weights – $w_i = 1.9\,nS$ in (H), and $w_i = 1.6\,nS$ in (I). The network was stimulated with a constant current $I_{stim} = 0.4\,nA$.

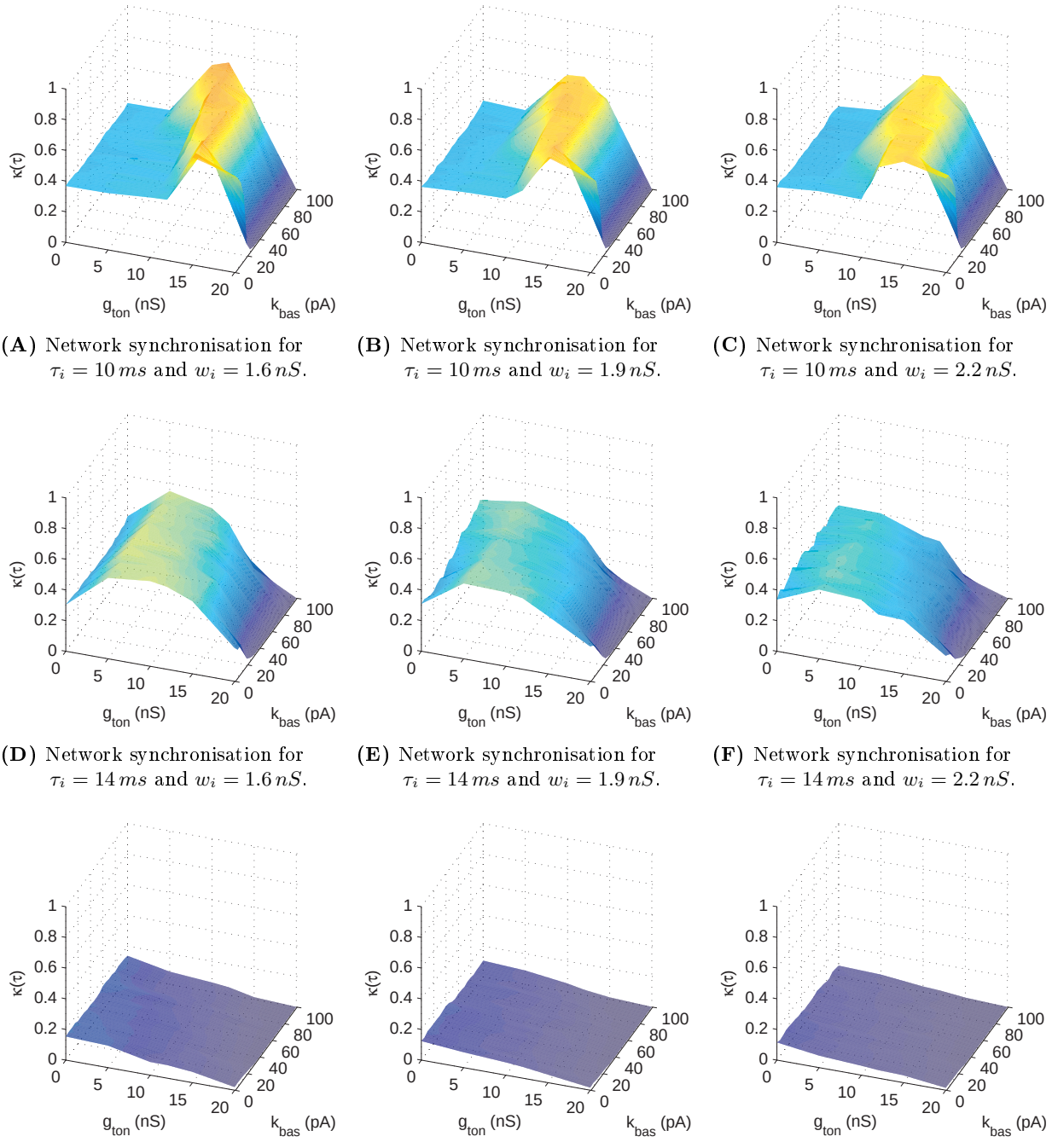

(A) Network synchronisation for $\tau_i = 10\,ms$ and $w_i = 1.6\,nS$.

(B) Network synchronisation for $\tau_i = 10\,ms$ and $w_i = 1.9\,nS$.

(C) Network synchronisation for $\tau_i = 10\,ms$ and $w_i = 2.2\,nS$.

(D) Network synchronisation for $\tau_i = 14\,ms$ and $w_i = 1.6\,nS$.

(E) Network synchronisation for $\tau_i = 14\,ms$ and $w_i = 1.9\,nS$.

(F) Network synchronisation for $\tau_i = 14\,ms$ and $w_i = 2.2\,nS$.

(G) Network synchronisation for $\tau_i = 30\,ms$ and $w_i = 1.6\,nS$.

(H) Network synchronisation for $\tau_i = 30\,ms$ and $w_i = 1.9\,nS$.

(I) Network synchronisation for $\tau_i = 30\,ms$ and $w_i = 2.2\,nS$.

Figure 5.9: Propofol-enhanced tonic inhibition allows for tighter network synchronisation, regardless of the presence of a stronger inhibitory baseline current. (A) Given $\tau_i = 10\,ms$ and $w_i = 1.6\,nS$, the bump-like pattern caused by the tonic inhibition-mediated (x axis) enhanced synchronisation is unaffected by the presence of a non-zero synaptic baseline current (y axis). These only slightly shift the peak of the synchronisation towards lower g_{ton} values. The synchronisation bump is unaffected by stronger synaptic weights – $w_i = 1.9\,nS$ in (B), and $w_i = 1.6\,nS$ in (C). (D) Given $\tau_i = 14\,ms$ and $w_i = 1.6\,nS$, the peak of the synchronisation shifts towards lower g_{ton} values. This behaviour is unaffected by stronger synaptic weights – $w_i = 1.9\,nS$ in (E), and $w_i = 1.6\,nS$ in (F). (G) Given $\tau_i = 30\,ms$ and $w_i = 1.6\,nS$, the network synchronisation follows a decreasing trend as g_{ton} and k_{bas} are increased. This behaviour is unaffected by stronger synaptic weights – $w_i = 1.9\,nS$ in (H), and $w_i = 1.6\,nS$ in (I). The network was stimulated with a constant current $I_{stim} = 0.4\,nA$.

of simulation time. Each raster plot is divided into $6\,s$ intervals with an overlap of $2\,s$ between them i.e. Figure 5.10A shows the network spikes between $0\,s$ and $6\,s$, Figure 5.10B shows the network spikes between $4\,s$ and $10\,s$, Figure 5.10C shows the network spikes between $8\,s$ and $14\,s$, Figure 5.10D shows the network spikes between $12\,s$ and $18\,s$, and Figure 5.10E shows the network spikes between $16\,s$ and $22\,s$.

We observe how the network activity was fast ($\overline{f} = 18.79 \pm 0.03\,Hz$) but loosely synchronised ($\overline{\kappa(\tau)} = 0.41 \pm 0.01$) between $0\,s \leq t \leq 6\,s$ (Figure 5.10A), where $0\,nS \leq g_{ton} \leq 4\,nS$ and $10\,ms \leq \tau_i \leq 12\,ms$. During this period of time, the population frequency (Figure 5.11B) decelerated from $\overline{f} = 20.77 \pm 0.01\,Hz$ to $\overline{f} = 17.14 \pm 0.12\,Hz$, whilst the network synchronisation remained centred around $\kappa(\tau) = 0.41 \pm 0.01$ (Figure 5.11A). As the neurons began absorbing stronger doses of propofol ($6\,nS \leq g_{ton} \leq 8\,nS$ and $13\,ms \leq \tau_i \leq 14\,ms$) tighter synchronous activity emerged increasing up to a maximum value of $\kappa(\tau) = 0.63 \pm 0.00$ for $g_{ton} = 8\,nS$ and $\tau_i = 14\,ms$. Concurrently, the network frequency accelerated to a maximum of $\overline{f} = 19.13 \pm 0.17\,Hz$ ($g_{ton} = 6\,nS$ and $\tau_i = 13\,ms$) and subsequently began decelerating. The enhanced synchronisation is reflected in the raster plots in Figure 5.10B showing its emergence at $t \simeq 6.5\,s$ and in Figure 5.10C illustrating how the synchronisation persisted.

$g_{ton} = 12\,nS$ and $\tau_i = 16\,ms$ at $t = 12\,s$ (Figure 5.10D) marked the end of the synchronisation rebound with $\kappa(\tau)$ decreasing from 0.63 ± 0.00 to 0.42 ± 0.00 and population frequency decelerating to $\overline{f} = 18.04 \pm 0.04\,Hz$. Finally, further increases in propofol dosage (Figure 5.10E) caused a gradual weakening of global network activity ($g_{ton}geq14\,nS$, $\tau_i \geq 17\,ms$, and $t \geq 14\,s$), whose frequency eventually decayed to $\overline{f} = 2.74 \pm 0.02\,Hz$ with a synchronisation of $\kappa(\tau) = 0.08 \pm 0.00$ at $t = 22\,s$.

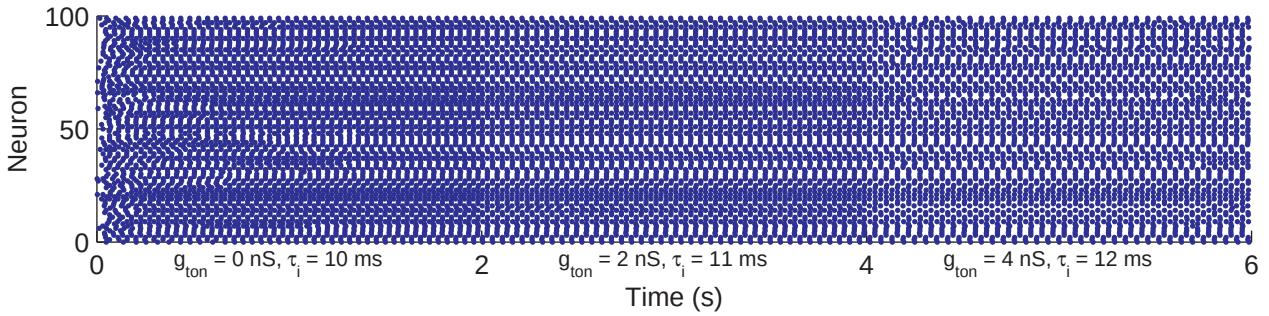

(A) Raster plot for $0\,s \leq t \leq 6\,s$

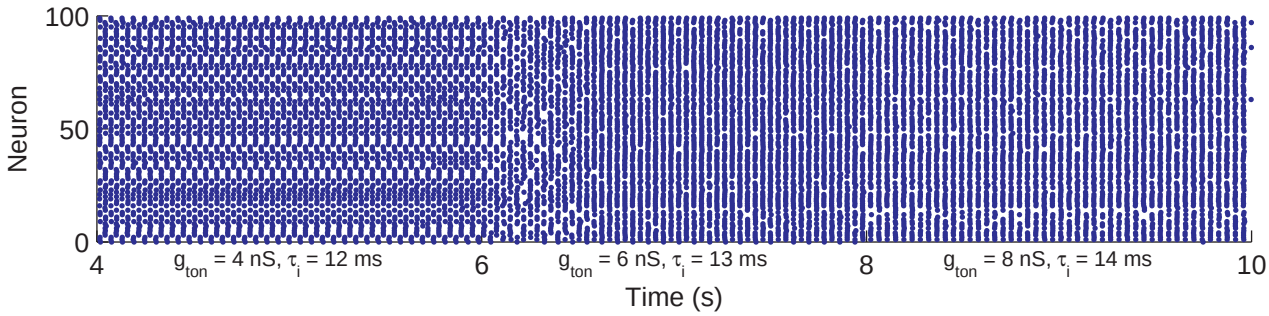

(B) Raster plot for $4\,s \leq t \leq 10\,s$

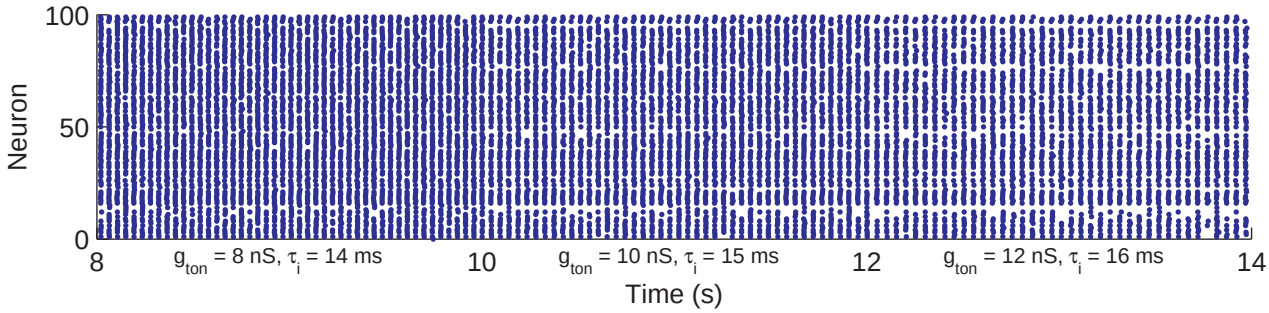

(C) Raster plot for $8\,s \leq t \leq 14\,s$

Figure 5.10: Enhanced network synchronisation emerges as tonic inhibition is strengthened and synaptic time constants are prolonged. g_{ton} and τ_i are increased every $2\,s$ in steps of $2\,nS$ and $1\,ms$ respectively. (A) Initially the network activity is fast ($\overline{f} = 18.79 \pm 0.03\,Hz$) but loosely synchronised ($\overline{\kappa(\tau)} = 0.41 \pm 0.01$) between $0\,s \leq t \leq 6\,s$, where $0\,nS \leq g_{ton} \leq 4\,nS$ and $10\,ms \leq \tau_i \leq 12\,ms$. (B) Enhanced synchronisation emerges at $t \simeq 6.5\,ms$, and the network activity accelerates to a maximum of $\overline{f} = 19.13 \pm 0.17\,Hz$ for $g_{ton} = 6\,nS$ and $\tau_i = 13\,ms$. (C) The maximum synchronisation ($\overline{\kappa(\tau)} = 0.63 \pm 0.00$) occurs for $g_{ton} = 8\,nS$ and $\tau_i = 14\,ms$ at $8\,s \leq t \leq 10\,s$. The network was stimulated with a constant current $I_{stim} = 0.4\,nA$.

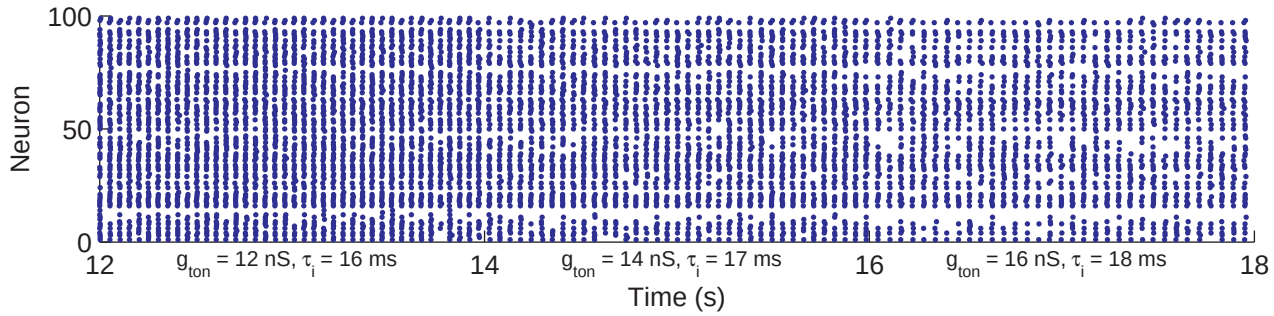

(D) Raster plot for $12\,s \leq t \leq 18\,s$

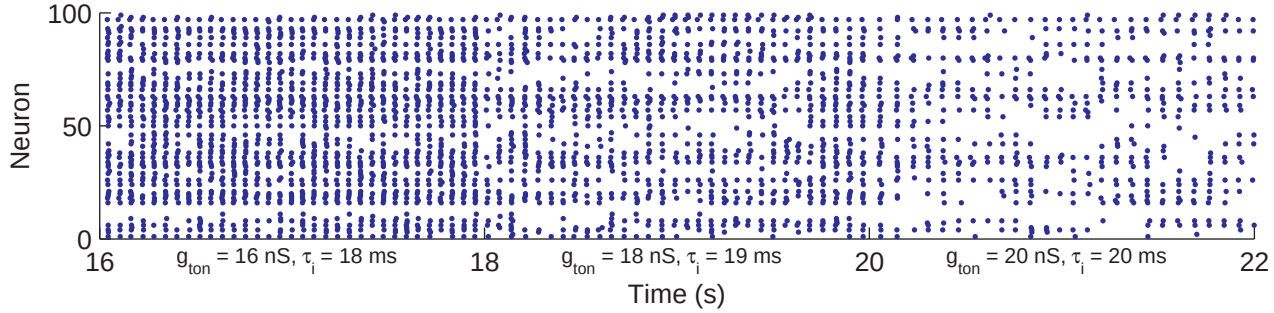

(E) Raster plot for $16\,s \leq t \leq 22\,s$

Figure 5.10: (cont.) **Enhanced network synchronisation emerges as tonic inhibition is strengthened and synaptic time constants are prolonged.** g_{ton} and τ_i are increased every $2\,s$ in steps of $2\,nS$ and $1\,ms$ respectively. (D) $g_{ton} = 12\,nS$ and $\tau_i = 16\,ms$ at $t = 12\,s$ mark the end of the synchronisation rebound with $\kappa(\tau)$ decreasing 0.42 ± 0.00 and population frequency decelerating to $\overline{f} = 18.04 \pm 0.04\,Hz$. (E) Further increases in propofol dosage cause a gradual weakening of global network activity ($g_{ton} geq 14\,nS$, $\tau_i \geq 17\,ms$, and $t \geq 14\,s$), whose frequency eventually decays to $\overline{f} = 2.74 \pm 0.02\,Hz$ with a synchronisation of $\kappa(\tau) = 0.08 \pm 0.00$ at $t = 22\,s$. The network was stimulated with a constant current $I_{stim} = 0.4\,nA$.

5.5 Discussion

GABAergic inhibition is thought to play an important role in the generation of oscillatory rhythmic activity in neural populations [Bartos et al., 2002, Bartos et al., 2007, Buzsáki and Wang, 2012, Cobb et al., 1995, Colgin, 2016]. In addition, GABA receptors have been shown to be the primary target of anaesthetic agents [Mueller et al., 2011, Rudolph and Antkowiak, 2004] and in particular of propofol [Vanlersberghe and Camu, 2008]. Indeed, propofol has been shown to target both synaptic and extrasynaptic GABA receptors with the effect of amplifying and extending the duration of inhibitory postsynaptic currents [Adodra and Hales, 1995, Bai et al., 2001, Kitamura et al., 2004, McDougall et al., 2008], enhancing extrasynaptic tonic inhibition [Bai et al., 2001, McDougall et al., 2008, Song et al., 2011], and slowing the receptor desensitisation [Bai et al., 1999, Bai et al., 2001, Jin et al., 2009, McDougall et al., 2008]. In this chapter we presented an in-depth study of the action of anaesthesia on neural oscillations by modelling all of the afore-mentioned effects on a network of hippocampal interneurons.

5.5.1 Tonic Inhibition Produces Tighter Synchronous Activity

Our results show how propofol-mediated tonic inhibition contributes to enhancing network synchronisation in a network of hippocampal interneurons. Whilst propofol does also act on the phasic inhibition mediated by synaptic $GABA_A$ receptors, neither the increase in the amplitude and duration of the synaptic response, nor the desensitisation due to propofol binding on these receptors

seemed to account for an increase in network synchronisation. The sole significant effect of phasic inhibition was to lower the threshold of tonic conductance necessary for the emergence of enhanced network synchronisation, by prolonging the duration of inhibitory postsynaptic currents. Taken together, these observations allow us to conclude that the enhanced network synchronisation we observed was mostly dependent on tonic inhibition mediated by extrasynaptic GABA receptors.

5.5.2 Enhanced Synchronisation for Neuronal Communication under General Anaesthesia

The role of neural oscillations has been extensively described in the literature, giving rise to a number of stimulating theories. Neural oscillations may represent the stable, unperturbed state of the brain [Buzsáki and Draguhn, 2004] during sleep, and can also be used as indicators of certain sleep stages [Llinas and Ribary, 1993]. In addition, experimental studies have linked synchronous activity with perception [Engel et al., 2001] stimulus encoding and representation [Gray et al., 1989], information integration and memory [Colgin and Moser, 2010, Engel et al., 2001, Kahana et al., 2001, Lisman, 2010, Lisman and Jensen, 2013, Varela et al., 2001] The common denominator of all of these theories is the hypothesis of neuronal communication through coherence [Fries, 2005], according to which synchronous activity enables communication and cooperation between neural ensembles. Indeed, functionally-linked brain regions have been shown to synchronise their operational frequency when collaborating. These include, and are not limited to, parietal and occipital regions during visual attention tasks [Fries et al., 2001]; hippocampus and (pre) frontal cortex during memory tasks [Fell et al., 2001] and consolidation during sleep [Maingret et al., 2016]; motor cortex and spinal motor neurons during movement tasks [Conway et al., 1995].

Intraoperative Awareness

The enhanced synchronisation described here could provide a possible mechanism supporting the occurrence of intraoperative awareness, intended as the explicit recollection of perceived stimuli during sedation. Patients who report having experienced intraoperative awareness often describe their ability to hear voices and sounds, to perceive visual stimuli such as the surgical lighting, to feel touch, and sometimes discomfort or pain [Ghoneim et al., 2009, Moerman et al., 1993, Ranta et al., 1998, Sandin et al., 2000, Schwender et al., 1998], accompanied by a feeling of helplessness and the inability to communicate. Although rarely occurring – 0.1% to 0.3% of patients according to experimental studies [Ghoneim et al., 2009, Jones, 1994, Ranta et al., 1998] which, if we consider that in the US alone approximately 60000 patients undergo general anaesthesia every day [Brown et al., 2010], equates to 60 to 180 patients per day –, intraoperative awareness is a traumatic experience which engenders fear and mistrust towards surgery and general anaesthesia, and can even sometimes lead to post-traumatic stress disorder [Osterman and Van Der Kolk, 1998, Osterman et al., 2001, Schwender et al., 1998]. The commons causes of intraoperative awareness are thought to be: insufficient drug dosages, increased anaesthetic requirements, damaged of defective drug delivery systems [Ghoneim et al., 2009, Mashour, 2010]. These findings indicate that the occurrence of intraoperative awareness is heavily dependent on the concentration of the anaesthetic agent administered to, and absorbed by, the patient.

General anaesthetics inhibit the conscious perception of pain but fail to fully cut off the pain transmission pathways from the sympathetic to the central nervous system. This is reflected in the haematological and metabolical responses commonly recorded under general anaesthesia, showing prototypical indicators of the surgical stress response – namely, increased heart rate and blood flow, and changes in skin conductance [Longnecker David E et al., 2008, Storm, 2008] – as well as in the statistical analyses of postoperative patient reports indicating that up to 30% of intraoperatively

aware patients recall experiencing pain [Sebel et al., 2004]. Taken together, these observations indicate that the sympathetic and central nervous of system anaesthetised patients are capable of processing noxious stimuli. This allows us to postulate that propofol-enhanced network synchronisation could provide the favourable conditions needed for the perception of pain under general anaesthesia. Precise timing between the surgical incision and the anaesthesia-dependent improved synchronous activity could facilitate the transmission of pain stimuli to the central nervous system in anaesthetised patients.

Implicit Memory Formation

There is a large volume of published studies describing the formation of implicit memories under general anaesthesia [Andrade and Deeprose, 2007, Bonett et al., 2014, Cork et al., 1996, Ghoneim and Block, 1997, Jones, 1994, Kihlstrom et al., 1990]. According to these, anaesthetised patients perceive and remember auditory stimuli, and are capable of recalling them in postoperative interviews, without being able to consciously identify when and how these stimuli were encoded. A recent study described how propofol enables a dose-dependent increase in synchronous activity within the human medio-temporal lobe under general anaesthesia [Fell et al., 2005]. These results, coupled with the theory that neural synchronisation between the entorhinal cortex and the hippocampus correlates with memory formation in humans [Fell et al., 2001], provide a possible neural substrate underlying mnemonic processes during anaesthesia. Our model supports this view by making the compelling prediction that anaesthetic agents could facilitate the communication between brain structures which should supposedly be not allowed to do so under general anaesthesia. Therefore, memory formation under general anaesthesia could be facilitated by a propofol-dependent enhancement in rhinal-hippocampal coherence.

Paradoxical Excitation

Paradoxical excitation is a state of increased arousal which commonly occurs shortly during the initial phases of the induction of anaesthesia [Brown et al., 2010]. Although the mechanisms behind have been extensively investigated [Bevan et al., 1997, Clark and Rosner, 1973, Gibbs et al., 1936, Kiersey et al., 1951, McCarthy et al., 2008, Rampil, 1998], these are far from being fully unravelled. This phenomenon is dubbed "paradoxical" since it is caused by the administration of drugs which are supposed to suppress excitation rather than fostering it. Paradoxical excitation manifests itself in the form of involuntary purposeless or defensive movements, the expression of incoherent speech, and sometimes euphoria or dysphoria [Bevan et al., 1997, Clark and Rosner, 1973, Gibbs et al., 1936, Kiersey et al., 1951, McCarthy et al., 2008, Rampil, 1998].

One possible explanation behind the emergence of paradoxical excitation under general anaesthesia is based on the circuit hypothesis [Schiff and Posner, 2007, Schiff, 2008]. This theorises that a dosage-dependent disinhibition of striatothalamic pathways may allow the reactivation of stimuli which were temporarily stored within the thalamus prior to the induction of sedation. Since thalamocortical circuits have been shown to be involved in arousal regulation [Schiff, 2008] it is conceivable that a temporary stimulation of the thalamus could awaken anaesthetised subjects. Indeed, this was demonstrated to be the case in various experimental studies [Alkire et al., 2007, Schiff et al., 2007]. However, the mechanisms mediating this disinhibition under general anaesthesia remain unclear.

A theoretical model [McCarthy et al., 2008] attempted to provide another explanation for the occurrence of paradoxical excitation. Here, the authors investigated the cellular mechanisms underlying the changes in the EEG signal recorded from anaesthetised patients during paradoxical excitation events – namely an increase in beta power [Gugino et al., 2001]. Their results indicate that an interaction between the GABAergic synaptic current and an intrinsic M-current produces

a propofol-dependent switch in inhibitory network activity synchronisation, which enhances excitation in postsynaptic pyramidal neurons [McCarthy et al., 2008] leading to enhanced excitation. However, the model fails to account for the effects of propofol-mediated tonic inhibition. We suggest including these as an avenue for future work.

5.5.3 Limitations and Controversies

The Availability of Neural Recordings

The most limiting factor in neuroscientific research on general anaesthesia is the availability of multi-scale recordings of neural activity acquired during surgery on human patients. Firstly, recording electrodes are commonly not installed during surgery for a number of reasons including their complexity and the time required for set-up. Secondly, the recordings systems used in operating rooms must be non-invasive, unless the patient requires the implantation of invasive electrodes which require their own surgical procedure and can cause irreparable damage to the brain and infections [Dubeau and McLachlan, 2000]. Scalp electroencephalography (EEG) [Niedermeyer and Lopes da Silva, 2005] is arguably the mostly used non-invasive system, whose main drawback is a relatively poor spatial resolution, allowing the detection of postsynaptic signals of brain regions which are in close proximity to the skull. Conversely, signals originating from deeper brain regions will inevitably be distorted, confounded with, or even lost within those generated by sources which are stronger solely due to their proximity to the electrodes. Moreover, reliably localising and reconstructing the source of the recorded EEG signal is a classical example of an ill-posed inverse problem [Niedermeyer and Lopes da Silva, 2005], to which no unique robust and reliable solution has been found to date although promising efforts are being made in this direction (for a review see [Michel et al., 2004]).

Clinically, human intracranial recordings are commonly obtained from patients suffering from epilepsy which were implanted with the purpose of monitoring their epileptic activity and detecting its focus. Not only are these patients rare, but the location of the electrodes is dependent on the supposed location of the epileptogenic brain structure. This renders intracranial recordings of human hippocampal activity scarcely available, which has obvious crippling consequences on research on memory formation and consolidation. We are currently addressing this limitation by initiating a collaboration project between our research team, the anaesthesiology and the epileptology departments of the local university hospital (CHRU Nancy) and a research team specialising in signal processing. The aim of the project is to conduct behavioural experiments, consisting of various memory tasks, on intracranially-implanted human subjects under varying depths of general anaesthesia. Analysing these data will allow us to shed some light on the several open questions in this field.

Intra-Study and Intra-Patient Variability

The vast body of literature concerning implicit memory formation under general anaesthesia indicates that the underlying mechanisms are yet to be fully understood. One reason is the non-conclusiveness of most studies due to a significant intra-patient variability. Indeed, the effects of anaesthetic agents depend on factors which are specific to the patient such as their age, their weight, their gender, and the presence of pre-existing medical conditions [Longnecker David E et al., 2008]. Accounting for most of these would require a vast number of different patients and trials, which are often either unavailable. In addition, due to the rarity of the occurrence of intraoperative awareness, gathering the required amount of experimental data would become an interminable endeavour.

Monitoring and Testing for Implicit Memory

The formation of implicit memory under general anaesthesia has been extensively studied [Andrade and Deeprose, 2007, Bonett et al., 2014, Cork et al., 1996, Ghoneim and Block, 1997, Jones, 1994, Kihlstrom et al., 1990]. However, the topic remains controversial. Although these studies report that anaesthetised patients are able to store implicit memories, it is not clear if this happens during unconsciousness or during short periods of intraoperative awareness [Bailey and Jones, 1997, Bejjani et al., 2009, Deeprose et al., 2004, Kerssens et al., 2005, Lubke et al., 1999, Willems et al., 2005]. Answering this question requires integrating anaesthesia monitors in the experimental protocols to help in gauging the depth of the anaesthetic sleep. However, since these monitors are commercially-available products, they tend to use private, close-source, undocumented algorithms which can effectively compromise their trustworthiness in a clinical setting.

Another challenge which must be addressed is the reliability of the behavioural tasks and the control groups used to assess implicit memory. This is an intrinsically complex task since implicit memory, by definition, is information that is stored without knowing why or when it was stored. Therefore, it is conceivable that implicit memories could be mistaken as false memories, interpretation, or imagination. Recently, behavioural studies have identified in gamma oscillation, a possible marker which could be used to discern between true and false memories [Sederberg et al., 2007, van Vugt et al., 2010]. These documented results describe an increase in gamma power in the medial temporal lobe and the hippocampus during recollection of memorised words, and a lower power when the same subject claims to recall a previously unseen word. Unfortunately, these signals were recorded using invasive intracranial EEG, which limits the usability of this technique on healthy patients.

Extending the Model

We modelled a network of inhibitory neurons since these have been shown to possess self-synchronising capabilities [Kopell et al., 2010, White et al., 2000, Wang and Buzsáki, 1996]. Therefore, this model provided us with a robust baseline of synchronous activity which then enabled us to investigate the disrupting effects of anaesthetics on these oscillations. It is conceivable that extending the model to include interconnected pyramidal neurons, for example using a PING-like topology [Kopell et al., 2010], should amplify the phenomena we described in this chapter. In addition, inasmuch as EEG records solely the signals generated by excitatory neurons [Niedermeyer and Lopes da Silva, 2005], including them in our model will endow it with improved biological realism.

Conclusion

The results described in this chapter indicate that propofol-mediated tonic inhibition contributes to enhancing synchronous neural activity. Our model makes the compelling prediction that, at certain dosages, anaesthetic agents could facilitate the communication between brain structures which should supposedly be not allowed to do so under general anaesthesia. This could account for several phenomena observed during general anaesthesia including intraoperative awareness events and memory formation, and could even provide a possible explanation for the occurrence of paradoxical excitation. The work presented here aims at shedding some light on the effects of anaesthetics on the brain, a topic that to date remains mostly a mystery.

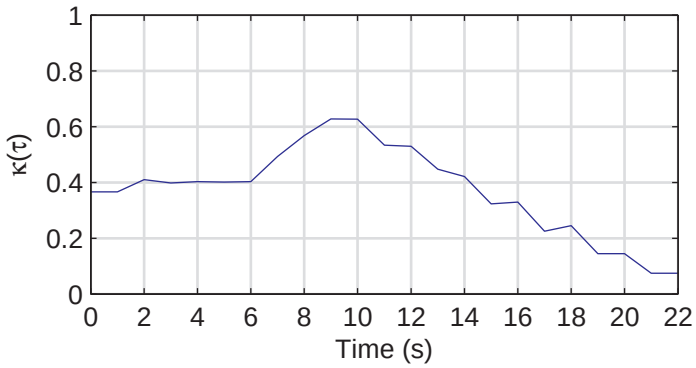

(A) Evolution of the network synchronisation over time as g_{ton} and τ_i increase.

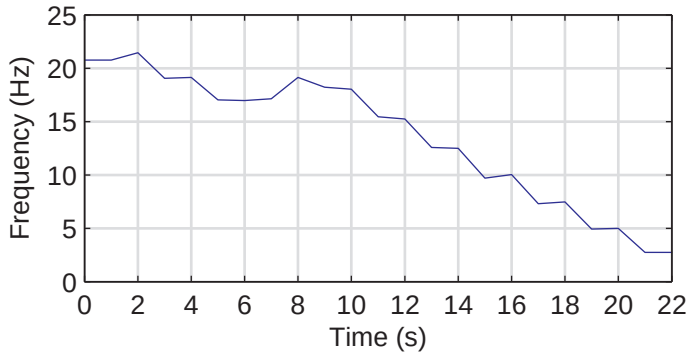

(B) Evolution of the network frequency over time as g_{ton} and τ_i increase.

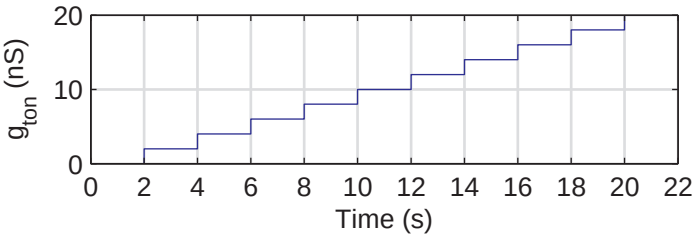

(C) Evolution of g_{ton} over time.

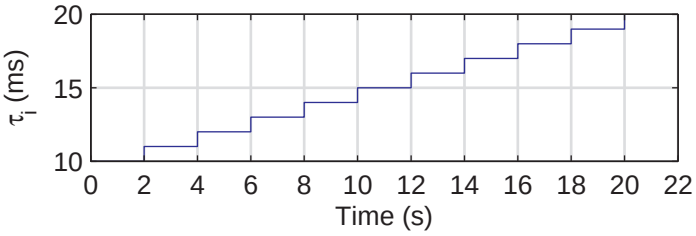

(D) Evolution of g_{ton} over time.

Figure 5.11: Enhanced network synchronisation emerges as tonic inhibition is strengthened and synaptic time constants are prolonged. (A) The network synchronisation follows a bump-like pattern, increasing from a baseline of $\overline{\kappa(\tau)} = 0.41 \pm 0.01$ between $0\,s \leq t \leq 6\,s$ to a maximum of $\overline{\kappa(\tau)} = 0.63 \pm 0.00$ for $g_{ton} = 8\,nS$ and $\tau_i = 14\,ms$ at $8\,s \leq t \leq 10\,s$. Further anaesthetic dosages gradually lower the network synchronisation. (B) The network frequency follows a bump-like pattern, decelerating between $0\,s \leq t \leq 6\,s$ and then accelerating to a maximum of $\overline{f} = 19.13 \pm 0.17\,Hz$ for $g_{ton} = 6\,nS$ and $\tau_i = 13\,ms$ at $6\,s \leq t \leq 8\,s$. Further anaesthetic dosages gradually decelerate the network frequency. (C) g_{ton} is increased from an initial value of $0\,nS$ in steps of $2\,nS$ every $2\,s$. (B) τ_i is increased from an initial value of $10\,ms$ in steps of $1\,ms$ every $2\,s$.

CHAPTER

6

CONCLUSIONS AND PERSPECTIVES

Contents

Overview

This chapter summarises the work presented in this manuscript and highlights our contributions. In this thesis we investigated two macroscopical phenomena from a neuroscientifical standpoint: memory and anaesthesia. In particular, we used biologically-inspired mathematical modelling and simulations of neural activity to shed some light on the emergence of hippocampal mnemonic activity during wake, and the amnesia and paradoxical memory consolidation occurring under propofol-induced general anaesthesia. Our results indicate that hippocampal synchronous rhythmic activity can be maintained locally within networks of CAN-equipped persistent firing pyramidal neurons, in the absence of external stimulation. These findings reinforce the view that the hippocampus might locally incorporate the necessary cells and circuitry to allow for spontaneous emergence, and maintenance, of memory-related theta oscillations. In addition, our modelling study on propofol anaesthesia suggests that, at certain dosages, anaesthetic agents could facilitate the communication between brain structures which should supposedly be not allowed to do so under general anaesthesia. This could account for several phenomena observed during general anaesthesia including intraoperative awareness events and memory formation, and could even provide a possible explanation for the occurrence of paradoxical excitation. Finally, we describe potential avenues for future work.

6.1 Mathematical Modelling of Self-Sustained Hippocampal Oscillations

6.1.1 Contributions

In this thesis we asked ourselves one fundamental question: what are the neural mechanisms underlying memory? Being an immensely broad question, we narrowed our focus to the role and the emergence of memory-related neural activity recorded in the hippocampus during wake, and the amnesia and paradoxical memory consolidation occurring under propofol-induced general anaesthesia. In this section we summarise our findings and contributions regarding the former.

The hippocampus has been shown to be implicated in working memory and memory consolidation [Andersen et al., 2007, Corkin, 1984, Corkin, 2002, Kandel et al., 2000b, Scoville and Milner, 1957]. Furthermore, recent studies have identified a specific type of persistent-firing hippocampal pyramidal neuron [Knauer et al., 2013, Knauer, 2015, Jochems and Yoshida, 2013] which we hypothesise could play an important role in generating and maintaining memory-related hippocampal oscillations, due to its electrophysiological properties and elicited spiking behaviours. Here, we introduced a novel mathematical model capturing the features of these biological neurons [Giovannini et al., 2015b]. In accord with experimental studies [Knauer et al., 2013, Knauer, 2015, Jochems and Yoshida, 2013], the persistent firing frequency depends solely on the intensity of the CAN current, which is mediated by cholinergic receptors. In addition, the firing frequencies elicited by the model neuron are representative of those observed in-vitro.

Moreover, we studied the dynamics of a network of persistent-firing hippocampal neurons, and illustrated how the CAN current allows the network to self-synchronise its activity in the theta band. Furthermore, we showed that connecting the pyramidal-CAN network to a population of inhibitory interneurons allows for more robust and tighter synchronisation. Our findings indicate that, in both network configurations, the frequency of the oscillatory activity is modulated by the intensity of the CAN current. This indicates that the intrinsic properties of persistent-firing hippocampal neurons could provide the neural substrate for rhythmogenesis [Giovannini et al., 2016]. Our model network of persistent firing pyramidal-CAN neurons is a biologically plausible mechanism for the maintenance of synchronous theta oscillations in the hippocampus, which aims at extending the traditional models of septum-driven hippocampal rhythmic activity. The work described here is one of the first modelling studies showing that theta oscillations can be maintained in CA1, relying solely on intrinsic cellular properties, and without the need for external inputs. The full model, its analysis, and its findings were published in a research article [Giovannini et al., 2017].

6.1.2 Future Work

Reducing the Neuron Model

Our current neuron model of persistent-firing pyramidal hippocampal neurons is nine-dimensional since it comprises nine variables – V_m, h, m, n, p, q, r, s, $[\mathrm{Ca}]_\mathrm{i}^{2+}$ – representing the evolution of the membrane potential over time, the gating variable for the inactivation and activation of the sodium current, the activation of the potassium current, the activation of the M-current, the activation and inactivation of the calcium current, the activation of the CAN current, and the calcium concentration dynamics, respectively. This makes analysing the spiking dynamics and the contribution of each variable a cumbersome task, due to the high dimensionality of the resulting phase space.

A first step could involve reducing the number of variables to three or less, to simplify the model complexity. Studying the dynamics of such a reduced model, could allow us to examine the parameters regulating the emergence of persistent activity. Since the rhythmic activity requires the

interaction between depolarising after potentials (DAPs) and afterhyperpolarizations (AHPs), we would need to devise a three-variable models with these characteristics. One idea could be extending the adaptive exponential integrate and fire (adEx) model [Brette and Gerstner, 2005], which includes AHP dynamics provided by a spike-frequency adaptation mechanism, by integrating the calcium dynamics governing an externally injected CAN current. This would yield a total of three variables.

Integrating Cholinergic Projections from the Septum

CAN-mediated persistent firing is a cholinergic mechanism which we hypothesise could support the maintenance of theta-frequency oscillations in the hippocampus. However, a vast body of literature has highlighted the importance of the medial septum in the generation and maintenance of these oscillations [Vinogradova, 1995, Tóth et al., 1997, Kocsis et al., 1999, Fischer et al., 1999, Stewart and Fox, 1990]. Therefore, we could integrate cholinergic projections from the septum in the model for increased biological realism. These would modulate the intensity of the CAN current effectively providing the clocking to the CAN-In network, synchronising its activity in the theta band.

Simulating Delta Oscillations and Memory Consolidation

The oscillatory frequencies displayed by our model network depend on, and are limited by, the intrinsic persistent firing rate of the individual hippocampal neurons. Experimentally, these neurons were shown to activate at frequencies ranging between $9.3 \pm 2.9\,Hz$ and $15.4 \pm 1.2\,Hz$, in the presence of $1\,\mu M$ and $20\,\mu M$ of carbachol respectively [Giovannini et al., 2017]. In the model network configuration described within this manuscript we chose parameters which would produce firings rates rapid enough to sustain theta oscillations. It follows that choosing slower intrinsic firing rates would generate slower oscillations, for example in the delta frequency band $(0.5 - 4\,Hz)$.

Delta oscillations are commonly observed in recordings of neural activity during slow-wave sleep [Amzica and Steriade, 1998, Kalia, 2010, Sleigh et al., 2011]. Slow-wave sleep is thought to play an important role in memory consolidation [Buzsáki, 2006, Hobson and Pace-Schott, 2002, Maingret et al., 2016, Power, 2004, Roediger et al., 2007, Squire, 1987, Walker, 2009]. Therefore, given that CAN-equipped neurons have been identified in cortical locations [Egorov et al., 2002, Fransén et al., 2006, Hasselmo, 2006] as well as in the hippocampus, our model network could be used to simulate the neural activity behind long-term memory formation.

Our CAN-In network could be incorporated in a broader model of sleep-dependent memory consolidation. According to the two-stage model of consolidation, memories are encoded in the hippocampus during wake [McClelland et al., 1995, Roediger et al., 2007, Squire, 1987, Squire, 1992] and are transferred into cortical long-term storage during sleep [Buzsáki, 1989, Hasselmo et al., 1996, Qin et al., 1997, Shen and McNaughton, 1994]. One theory [Hasselmo, 1999] suggests that acetylcholine could mediate memory consolidation during sleep as the release levels of this neurotransmitter vary significantly compared to during wake. Since acetylcholine governs the oscillatory frequencies in our model, we could envisage using it to simulate the delta oscillations commonly recorded during memory consolidation. This research direction is partly being undertaken by Amélie Aussel, a Ph.D. student who recently joined our research team, in collaboration with the ESPaCE[1] (Study of Physiological Signals for Cognition and Epilepsy) team at the CRAN (Centre for Research in Automation) in Nancy, France.

[1] http://www.cran.univ-lorraine.fr/anglais/themes_rech/sbs/espace/index.php

In-Vivo Working Memory Experiments on Knockout Mice

In order to verify the hypotheses our model makes – namely that cholinergic persistent firing neurons could form the neural substrate for the neural oscillations observed in recordings during memory tasks – we suggest performing in-vivo experiments on animals. CAN receptors are thought to belong to the family of canonical transient receptor potential channels (TRPCs) [Reboreda et al., 2011, Vazquez et al., 2004, Zhang et al., 2011]. We would need to devise an experimental protocol with a purposely bred strain of mice, in which the genes expressing TRPC receptors [Hardie and Minke, 1993] have been knocked out, performing the same working memory and spatial memory tasks as a group of genetically-normal control animals. Comparing the performance between the two groups could yield interesting insights on the participation of CAN channels in generating mnemonic neural activity. However, this approach has one crucial limitation lying in the ubiquitousness of TRPC channels in the central nervous system [Freichel et al., 2005] implying that knocking them out could have globally disrupting effects on neuronal activity. In addition, genetics and experimental neuroscience are not within our domains of expertise, neither within the our research team nor within the laboratory. Nevertheless, the vast amount of research on the role of muscarinic acetylcholine receptor using knockout mice (for a review see [Wess, 2004]) indicate that this could be a valid research direction. Setting up such a project could foster the creation of multidisciplinary collaborations between researchers.

Simulating Spatial Working Memory Task with Robots

Complementary to the afore-mentioned experimental studies, and bearing in mind that we completed this thesis in an informatics laboratory, we could envisage testing our hypotheses by experimenting on robotic platforms. Indeed, various robotic platforms are used by other research teams across the laboratory. Compact robotics vehicles, such as the Khepera[2], provide robust out-of-the-box solutions which can be used to test bio-mimetic sensing [Martinez et al., 2006, Moraud and Martinez, 2010], navigation [Franz and Mallot, 2000], exploration [Arleo and Gerstner, 2000], resiliency [Cully et al., 2015], and swarm behaviour [Brambilla et al., 2013] algorithms. We suggest devising a spatial memory experiment in which robots perform tasks similar to those commonly used in behavioural in-vivo experiments, such as navigating a Y-maze in search of a reward associated with a visual stimulus. We could then rely on our model to provide the robot with a biologically-inspired working memory maintenance mechanism.

6.2 Propofol-Induced Network Synchronisation under General Anaesthesia

6.2.1 Contributions

Following the assumption that understanding how anaesthetics inhibit memory consolidation could enable us to shed some light on memory consolidation processes, we also investigated the amnesic effect of anaesthesia and the resulting disruption of hippocampal rhythms. This allowed us to approach the afore-mentioned fundamental question from another angle. In addition, mathematical modelling of neural activity proves to be an extremely powerful and useful tool in research in anaesthesiology, due to the scarcity of available datasets and the invasiveness of the recording techniques used.

In this thesis, we introduced a mathematical model of propofol-induced sedation aimed at simulating the action of general anaesthesia on hippocampal oscillations. The novelty resides in the precise

[2] http://www.k-team.com/khepera-iv

modelling of the four main effects of propofol on GABAergic inhibition – namely the amplification and prolongation of inhibitory postsynaptic currents [Adodra and Hales, 1995, Bai et al., 2001, Kitamura et al., 2004, McDougall et al., 2008], the enhancement of extrasynaptic tonic inhibition [Bai et al., 2001, Giovannini et al., 2015a, McDougall et al., 2008, Song et al., 2011], and the reduction of receptor desensitisation [Bai et al., 1999, Bai et al., 2001, Jin et al., 2009, McDougall et al., 2008]. This is an in-depth study which allows us to draw compelling hypotheses.

Our results indicate that propofol-mediated tonic inhibition could produce an enhancement in synchronous network activity under general anaesthesia. This effect seemed to be mostly independent of receptor desensitisation. In addition, the amplified and prolonged phasic inhibition resulting from propofol uptake by synaptic $GABA_A$ receptors seemed solely to shift the threshold dosage of propofol required for augmented synchronisation towards lower values. We hypothesise that this dosage-dependent enhancement in network synchronisation could account for several phenomena observed during general anaesthesia including intraoperative awareness events [Ghoneim et al., 2009, Moerman et al., 1993, Ranta et al., 1998, Sandin et al., 2000, Schwender et al., 1998] and memory formation [Andrade and Deeprose, 2007, Bonett et al., 2014, Cork et al., 1996, Ghoneim and Block, 1997, Jones, 1994, Kihlstrom et al., 1990]. Moreover, the observed inhibitory actions of propofol could even provide a possible explanation for the occurrence of paradoxical excitation [Bevan et al., 1997, Clark and Rosner, 1973, Gibbs et al., 1936, Kiersey et al., 1951, McCarthy et al., 2008, Rampil, 1998]. We are currently drafting a research article [Giovannini and Buhry, 2017] describing the model and its findings.

6.2.2 Future Work

Studying the Effects of Anaesthesia on the CAN-In Network

The anaesthetic agents most commonly used during surgery have been shown to target the cholinergic system [Mueller et al., 2011] causing drug-dependent and region-dependent effects. In general, the levels of acetylcholine release decrease under general anaesthesia induced with the administration of most anaesthetic agents, with the exception of ketamine and N_2O [Rudolph and Antkowiak, 2004]. This raises challenging questions and compelling hypotheses on the memory formation mechanisms in anaesthetised patients. For example, if the lowered acetylcholine levels recorded during slow-wave sleep are comparable with those recorded under general anaesthesia then these might cause the activation of hippocampal-cortical consolidation pathways [Hasselmo, 1999] during sedation. This in turn, could provide a possible explanation behind the implicit encoding in memory of stimuli perceived during surgeries, as reported by patients [Andrade and Deeprose, 2007, Bonett et al., 2014, Cork et al., 1996, Ghoneim and Block, 1997, Jones, 1994, Kihlstrom et al., 1990].

We could envisage simulating the effects of propofol anaesthesia on our CAN-In model for hippocampal theta oscillations. According to the results described within this manuscript, this anaesthetic agent should enhance the synchronisation of the network activity displayed by the CAN-In network in frequency bands which are regarded as critical for memory consolidation. In addition, we could investigate the existence of a critical level of acetylcholine supporting the emergence of synchronous activity and the neuromodulation provided by general anaesthesia.

Stereo-EEG Recordings of Anaesthetised Human Patients

Recordings of hippocampal neural activity in humans are scarcely available due to the rarity of experimental subjects and the invasiveness of the recording procedures, some of which require implanting deep intracranial electrodes. This has obvious crippling consequences on research on memory formation and consolidation. We are currently addressing this limitation by initiating a

collaboration project between our research team, the anaesthesiology and the epileptology departments of the local university hospital (CHRU Nancy), and a research team in another laboratory specialising in signal processing. The aim of the project is to conduct behavioural experiments, consisting of various memory tasks, on intracranially-implanted human subjects under varying depths of general anaesthesia, and during sleep. Analysing these data will allow us to shed some light on the several open questions in this field.

6.3 Technical Contributions

6.3.1 Neuron Model Templates and Ionic Current Implementations Library

We developed a Brian[3]-compatible library containing various ionic currents to be assembled together to create template neurons. The purpose of these is to accelerate simulation set-up time and reduce code duplication across simulation scripts since often several simulations use the same neuron models. The library was developed in Python[4] and uses YAML[5] configuration files.

Template neurons are defined by the ionic currents that flow through their membrane. Currently implemented templates include:

- Hodgkin-Huxley pyramidal neuron (leak, sodium and potassium) as in [Traub and Miles, 1991]
- Hodgkin-Huxley pyramidal neuron with CAN receptors (leak, sodium, potassium, M-current, low-threshold calcium, calcium-activated non-selective cationic) as in [Giovannini et al., 2017]
- Hodgkin-Huxley fast-spiking inhibitory hippocampal neuron (leak, sodium, potassium) as in [Wang and Buzsáki, 1996]
- Hodgkin-Huxley fast-spiking inhibitory hippocampal neuron (leak, sodium, potassium) as in [Kopell et al., 2010]

Implemented ionic current libraries include:

- Hodgkin-Huxley ionic currents (I_{Leak}, I_K, I_{Na}) implementation described in [Traub and Miles, 1991]
- M-Current (I_M) implementation described in [Yamada et al., 1989]
- Calcium current (I_L) implementation described in [Reuveni et al., 1993]
- Calcium pump mechanisms ($\frac{\mathrm{d}Ca}{\mathrm{d}t}$) implementation described in [Reuveni et al., 1993]
- Calcium-activated non-selective current (I_{CAN}) implementation described in [Destexhe et al., 1994]
- Wang and Buszáki inhibitory Hodgkin-Huxley (I_{Leak}, I_K, I_{Na}) implementation described in [Wang and Buzsáki, 1996]

This library is freely available on GitHub[6] and is easily extensible by third-party users due to its hierarchical design. The template neurons and their currents are defined as YAML[7] files, which are conveniently parsed by the library, acting as an interface to the BRIAN simulator API's.

Brian Simulation Parameter Library

We developed a library which acts as a wrapper for Brian simulations, allowing the user to define simulation parameters in external YAML files, which are then parsed and forwarded to the

[3] http://www.briansimulator.org
[4] http://www.python.org
[5] http://www.yaml.org
[6] https://github.com/JoErNanO/brianmodel
[7] http://www.yaml.org/

BRIAN simulator. In addition, simulation parameters can be overridden via the command-line when invoking the python script containing the simulation. The library was developed in Python.

Setting up a simulation involves defining several commonly reusable parameters including:

- The maximum simulation time
- The stimulation current intensity and its duration
- The network connections (if any) and the connection weights
- The presence or absence of certain ionic currents
- Whether or not to save the resulting data and where

This library is freely available on GitHub[8] and is easily extensible by third-party users due to its hierarchical design.

Parallelised Data Logger

In order to accelerate simulation time, we developed a data logger capable of swiftly saving the data resulting from our simulations. This tool relies on the Python multiprocessing[9] package to create a pool of worker processes which save one dataset at a time in parallel. Once a worker is done with its task it can take up another task automatically, until there are no more datasets to save. The data logger is freely available on GitHub[10] and is easily extensible by third-party users due to its hierarchical design.

General Conclusions

In conclusion, in this thesis we asked ourselves one fundamental question: what are the neural mechanisms underlying memory? Memory endows us with the ability to encode, store, and recall information we perceived, which renders it an innate and familiar behaviour. Nevertheless, the interior workings of the brain which provide us with such faculties are far from being fully unravelled. Various questions remain unanswered to date, including how does electrochemical neural activity contribute to the emergence of our mnemonic faculties? These are all immensely broad, and magnificently intriguing questions, which must be broken down into manageable pieces if one wishes to aim at answering them. For the purpose of this thesis, we narrowed our focus to the memory-related neural activity recorded in the hippocampus during waking. In addition, we studied the disruptive actions of general anaesthesia on hippocampal mnemonic activity, as a way to shed some light on memory consolidation by investigating the amnesic effect of anaesthesia. This was an intense, yet fulfilling, endeavour which allowed us to explore the marvel that is the brain, and to contribute to unravelling the wonder that is cognition.

[8] https://github.com/JoErNan0/briansims
[9] https://docs.python.org/2/library/multiprocessing.html
[10] See note n. 8

REFERENCES

[Abbott, 2008] Abbott, L. F. (2008). Theoretical neuroscience rising. *Neuron*, 60(3):489–95.

[Adodra and Hales, 1995] Adodra, S. and Hales, T. G. (1995). Potentiation, activation and blockade of GABAA receptors of clonal murine hypothalamic GT1-7 neurones by propofol. *British Journal of Pharmacology*, 115(6):953–960.

[Adrian and Matthews, 1934] Adrian, E. D. and Matthews, B. H. C. (1934). The interpretation of potential waves in the cortex. *The Journal of Physiology*, 81(4):440–471.

[Alkire et al., 2008] Alkire, M. T., Hudetz, A. G., and Tononi, G. (2008). Consciusness and Anesthesia. *Science*, 7(322):876–880.

[Alkire et al., 2007] Alkire, M. T., McReynolds, J. R., Hahn, E. L., and Trivedi, A. N. (2007). Thalamic Microinjection of Nicotine Reverses Sevoflurane-induced Loss of Righting Reflex in the Rat. *Anesthesiology*, 107(2):264–272.

[Alonso and Llinás, 1989] Alonso, A. and Llinás, R. R. (1989). Subthreshold Na+-dependent theta-like rhythmicity in stellate cells of entorhinal cortex layer II. *Nature*, 342(6246):175–177.

[Amaral, 1993] Amaral, D. G. (1993). Emerging principles of intrinsic hippocampal organization. *Current opinion in neurobiology*, 3:225–229.

[Amit, 1995] Amit, D. J. (1995). The Hebbian paradigm reintegrated: Local reverberations as internal representations. *Behavioural brain science*, 18:617–626.

[Amit and Brunel, 1997] Amit, D. J. and Brunel, N. (1997). Model of global spontaneous activity and local structured activity during delay periods in the cerebral cortex. *Cerebral cortex (New York, N.Y. : 1991)*, 7(3):237–52.

[Amzica and Steriade, 1998] Amzica, F. and Steriade, M. (1998). Electrophysiological correlates of sleep delta waves. *Electroencephalography and Clinical Neurophysiology*, 107(2):69–83.

[Andersen et al., 2007] Andersen, P., Morris, R., Amaral, D. G., Bliss, T., and O'Keefe, J. (2007). *The Hippocampus Book*. Oxford University Press.

[Andrade and Deeprose, 2007] Andrade, J. and Deeprose, C. (2007). Unconscious memory formation during anaesthesia. *Best Practice & Research Clinical Anaesthesiology*, 21(3):385–401.

[Aoyagi et al., 2002] Aoyagi, T., Kang, Y., Terada, N., Kaneko, T., and Fukai, T. (2002). The role of Ca2+-dependent cationic current in generating gamma frequency rhythmic bursts: Modeling study. *Neuroscience*, 115(4):1127–1138.

[Aoyagi et al., 2003] Aoyagi, T., Takekawa, T., and Fukai, T. (2003). Gamma rhythmic bursts: coherence control in networks of cortical pyramidal neurons. *Neural computation*, 15(5):1035–61.

[Arleo and Gerstner, 2000] Arleo, A. and Gerstner, W. (2000). Modeling Rodent Head-direction Cells and Place Cells for Spatial Learning in Bio-mimetic Robotics. *From Animals to Animats*, 6:236–245.

[Asano et al., 2005] Asano, E., Juhász, C., Shah, A., Muzik, O., Chugani, D. C., Shah, J., Sood, S., and Chugani, H. T. (2005). Origin and propagation of epileptic spasms delineated on electrocorticography. *Epilepsia*, 46(7):1086–1097.

[Atri et al., 2004] Atri, A., Sherman, S., Norman, K. A., Kirchhoff, B. A., Nicolas, M. M., Greicius, M. D., Cramer, S. C., Breiter, H. C., Hasselmo, M. E., and Stern, C. E. (2004). Blockade of Central Cholinergic Receptors Impairs New Learning and Increases Proactive Interference in a Word Paired-Associate Memory Task. *Behavioral Neuroscience*, 118(1):223–236.

[Axmacher et al., 2006] Axmacher, N., Mormann, F., Fernández, G., Elger, C. E., and Fell, J. (2006). Memory formation by neuronal synchronization. *Brain research reviews*, 52(1):170–82.

[Baddeley, 2000] Baddeley, A. (2000). The episodic buffer: a new component of working memory? *Trends in cognitive sciences*, 4(11):417–423.

[Baddeley, 2002] Baddeley, A. (2002). *Episodic Memory*. Oxford University Press.

[Baddeley et al., 1975] Baddeley, A., Buchanan, M., and Thomson, N. (1975). Word Length and the Structure of Short-Term Memory. *Journal of Verbal Learning and Verbal Behaviour*, 14(6):575.

[Baddeley and Hitch, 1974] Baddeley, A. and Hitch, G. J. (1974). Working Memory. *In The Psychology of Learning and Motivation*, 8:47–89.

[Bai et al., 1999] Bai, D., Pennefather, P. S., MacDonald, J. F., and Orser, B. A. (1999). The general anesthetic propofol slows deactivation and desensitization of GABA(A) receptors. *The Journal of neuroscience : the official journal of the Society for Neuroscience*, 19(24):10635–10646.

[Bai et al., 2001] Bai, D., Zhu, G., Pennefather, P., Jackson, M. F., MacDonald, J. F., and Orser, B. A. (2001). Distinct functional and pharmacological properties of tonic and quantal inhibitory postsynaptic currents mediated by g -aminobutyric acid(A) receptors in hippocampal neurons. *Molecular Pharmacology*, 59(4):814–824.

[Bailey and Jones, 1997] Bailey, A. R. and Jones, J. G. (1997). Patients' memories of events during general anaesthesia. *Anaesthesia*, 52(5):460–476.

[Bailey et al., 2004] Bailey, D. L., Townsend, D. W., and Valk, P. E. (2004). *Positron Emission Tomography: Basic Sciences*. Springer.

[Banks et al., 1998] Banks, M. I., Li, T.-B., and Pearce, R. A. (1998). The Synaptic Basis of GABAA,slow. *The journal of neuroscience*, 18(4):1305–1317.

[Bartos et al., 2002] Bartos, M., Vida, I., Frotscher, M., Meyer, A., Monyer, H., Geiger, J. R. P., and Jonas, P. (2002). Fast synaptic inhibition promotes synchronized gamma oscillations in hippocampal interneuron networks. *Proceedings of the National Academy of Sciences of the United States of America*, 99(20):13222–13227.

[Bartos et al., 2007] Bartos, M., Vida, I., and Jonas, P. (2007). Synaptic mechanisms of synchronized gamma oscillations in inhibitory interneuron networks. *Nature reviews. Neuroscience*, 8(January):45–56.

[Bejjani et al., 2009] Bejjani, G., Lequeux, P.-Y., Schmartz, D., Engelman, E., and Barvais, L. (2009). No Evidence of Memory Processing During Propofol-Remifentanil Target-Controlled Infusion Anesthesia With Bispectral Index Monitoring in Cardiac Surgery. *Journal of Cardiothoracic and Vascular Anesthesia*, 23(2):175–181.

[Belelli et al., 2009] Belelli, D., Harrison, N. L., Maguire, J., Macdonald, R. L., Walker, M. C., and Cope, D. W. (2009). Extrasynaptic GABAA receptors: form, pharmacology, and function. *The Journal of Neuroscience : the official journal of the Society for Neuroscience*, 29(41):12757–63.

[Berman et al., 2009] Berman, M. G., Jonides, J., and Lewis, R. L. (2009). In search of decay in verbal short-term memory. *Journal of experimental psychology. Learning, memory, and cognition*, 35(2):317–33.

[Bevan et al., 1997] Bevan, J. C., Veall, G. R., Macnab, a. J., Ries, C. R., and Marsland, C. (1997). Midazolam premedication delays recovery after propofol without modifying involuntary movements. *Anesthesia and analgesia*, 85(1):50–4.

[Bhalla et al., 1993] Bhalla, U. S., Bower, J. M., Leng, G., Hashimoto, H., Tsuji, C., Sabatier, N., Ludwig, M., Bhalla, S., and Bower, J. M. (1993). Exploring parameter space in detailed single neuron models : simulations of the mitral and granule cells of the olfactory bulb Exploring Parameter Space in Detailed Single Neuron Models : Simulations of the Mitral and Granule Cells of the Olfactory Bulb. *Journal of neurophysiology*, 69:1948–1965.

[Bliss and Lomo, 1973] Bliss, T. and Lomo, T. (1973). Long-lasting potentiation of synaptic transmission in the dentate area of the anaesthetized rabbit following stimulation of the perforant path. *The Journal of Physiology*, 232:331–356.

[Boly et al., 2012] Boly, M., Moran, R., Murphy, M., Boveroux, P., Bruno, M.-A., Noirhomme, Q., Ledoux, D., Bonhomme, V., Brichant, J.-F., Tononi, G., Laureys, S., and Friston, K. (2012). Connectivity Changes Underlying Spectral EEG Changes during Propofol-Induced Loss of Consciousness. *Journal of Neuroscience*, 32(20):7082–7090.

[Bonett et al., 2014] Bonett, E., Pham, X., Smith, K. R., Howard, K., Sheppard, S., and Davidson, A. (2014). Implicit memory formation using the word stem completion task during anesthesia in children. *Paediatric Anaesthesia*, 24(3):290–296.

[Boulton et al., 1990] Boulton, A. A., Baker, G. B., and Vanderwolf, C. H. (1990). *Neurophysiological techniques: applications to neural systems*. Humana Press, Clifton, New Jersey.

[Brambilla et al., 2013] Brambilla, M., Ferrante, E., Birattari, M., and Dorigo, M. (2013). Swarm robotics: A review from the swarm engineering perspective. *Swarm Intelligence*, 7(1):1–41.

[Bramham and Messaoudi, 2005] Bramham, C. R. and Messaoudi, E. (2005). BDNF function in adult synaptic plasticity: The synaptic consolidation hypothesis. *Progress in Neurobiology*, 76(2):99–125.

[Brette and Gerstner, 2005] Brette, R. and Gerstner, W. (2005). Neuronal Activity. *Journal of Neurophysiology*, 94:3637–3642.

[Brown et al., 2010] Brown, E. N., Lydic, R., and Schiff, N. D. (2010). General anesthesia, sleep, and coma. *The New England journal of medicine*, 363(27):2638–50.

[Brunel and Wang, 2001] Brunel, N. and Wang, X.-J. (2001). Effects of Neuromodulation in a Cortical Network Model of Object Working Memory Dominated by Recurrent Inhibition. *Journal of Computational Neuroscience*, 11:63–85.

[Buzsáki, 1986] Buzsáki, G. (1986). Hippocampal sharp waves: Their origin and significance. *Brain Research*, 398(2):242–252.

[Buzsáki, 1989] Buzsáki, G. (1989). Two-stage model of memory trace formation: a role for 'noisy' brain states. *Neuroscience*, 31(3):551–570.

[Buzsáki, 2002] Buzsáki, G. (2002). Theta Oscillations in the Hippocampus. *Neuron*, 33(f):325–340.

[Buzsáki, 2004] Buzsáki, G. (2004). Large-scale recording of neuronal ensembles. *Nature Neuroscience*, 7(5):446–451.

[Buzsáki, 2006] Buzsáki, G. (2006). *Rhythms of the brain*. Oxford University Press.

[Buzsáki, 2015] Buzsáki, G. (2015). Hippocampal sharp wave-ripple: A cognitive biomarker for episodic memory and planning. *Hippocampus*, 25(10):1073–1188.

[Buzsáki and Draguhn, 2004] Buzsáki, G. and Draguhn, A. (2004). Neuronal oscillations in cortical networks. *Science (New York, N.Y.)*, 304(5679):1926–9.

[Buzsáki and Moser, 2013] Buzsáki, G. and Moser, E. I. (2013). Memory, navigation and theta rhythm in the hippocampal-entorhinal system. *Nature neuroscience*, 16(2):130–8.

[Buzsáki and Wang, 2012] Buzsáki, G. and Wang, X.-J. (2012). Mechanisms of Gamma Oscillations. *Annual Review of Neuroscience*, 35(1):203–225.

[Caeser et al., 1993] Caeser, M., Brown, D. A., Gahwiler, B. H., and Knopfel, T. (1993). Characterization of a Calcium-dependent Current Generating a Slow Afterdepolarization of CA3 Pyramidal Cells in Rat Hippocampal Slice Cultures. *European Journal of Neuroscience*, 5:560–569.

[Chen et al., 2005] Chen, K., Li, H. Z., Ye, N., Zhang, J., and Wang, J. J. (2005). Role of GABAB receptors in GABA and baclofen-induced inhibition of adult rat cerebellar interpositus nucleus neurons in vitro. *Brain Research Bulletin*, 67(4):310–318.

[Cheung, 2008] Cheung, J. (2008). Neurons, nerve tissues, & the nervous system. Website. [electronic image] http://biomedicalengineering.yolasite.com/neurons.php Accessed 22/08/2012.

[Ching and Brown, 2014] Ching, S. and Brown, E. N. (2014). Modeling the dynamical effects of anesthesia on brain circuits. *Current opinion in neurobiology*, 25(January):116–22.

[Ching et al., 2010] Ching, S., Cimenser, A., Purdon, P. L., Brown, E. N., and Kopell, N. J. (2010). Thalamocortical model for a propofol-induced alpha-rhythm associated with loss of consciousness. *Proceedings of the National Academy of Sciences*, 107(52):22665–22670.

[Churchland et al., 1990] Churchland, P. S., Koch, C., and Sejnowski, T. J. (1990). What is computational neuroscience? In Schwartz, E. L., editor, *Computational neuroscience*, page 12. MIT Press.

[Cimenser et al., 2011] Cimenser, A., Purdon, P. L., Pierce, E. T., Walsh, J. L., Salazar-Gomez, A. F., Harrell, P. G., Tavares-Stoeckel, C., Habeeb, K., and Brown, E. N. (2011). Tracking brain states under general anesthesia by using global coherence analysis. *Proceedings of the National Academy of Sciences of the United States of America*, 108(21):8832–7.

[Clark and Rosner, 1973] Clark, D. L. and Rosner, B. S. (1973). Neurophysiologic effects of general anesthetics. I. The electroencephalogram and sensory evoked responses in man. *Anesthesiology*, 38(6):564–82.

[Cobb et al., 1995] Cobb, S. R., Buhl, E. H., Halasy, K., Paulsen, O., and Somogyi, P. (1995). Synchronization of neuronal activity in hippocampus by individual GABAergic interneurons. *Nature*, 378(6552):75–8.

[Cody, 2011] Cody, T. (2011). Sleep and the gaba receptor. Website. [electronic image] http://changingmindsaboutdownsyndrome.blogspot.co.uk/2011/04/sleep-and-gaba-receptor.html Accessed 27/08/2012.

[Colgin, 2013] Colgin, L. L. (2013). Mechanisms and functions of theta rhythms. *Annual review of neuroscience*, 36:295–312.

[Colgin, 2016] Colgin, L. L. (2016). Rhythms of the hippocampal network. *Nature Reviews Neuroscience*.

[Colgin et al., 2009] Colgin, L. L., Denninger, T., Fyhn, M., Hafting, T., Bonnevie, T., Jensen, O., Moser, M.-B., and Moser, E. I. (2009). Frequency of gamma oscillations routes flow of information in the hippocampus. *Nature*, 462(7271):353–7.

[Colgin and Moser, 2010] Colgin, L. L. and Moser, E. I. (2010). Gamma oscillations in the hippocampus. *Physiology*, 25(5):319–29.

[College, 2013] College, O. (2013). The limbic lobe. Website. [electronic image] http://upload.wikimedia.org/wikipedia/commons/7/7a/1511_The_Limbic_Lobe.jpg Accessed 19/10/2014.

[Commons, 2016] Commons, W. (2016). File:action potential.svg — wikimedia commons,. Website. [electronic image] https://commons.wikimedia.org/w/index.php?title=File:Action_potential.svg&oldid=194679385 Accessed 07/06/2017].

[Compte, 2006] Compte, A. (2006). Computational and in vitro studies of persistent activity: edging towards cellular and synaptic mechanisms of working memory. *Neuroscience*, 139(1):135–51.

[Compte et al., 2000] Compte, A., Brunel, N., Goldman-Rakic, P. S., and Wang, X.-j. (2000). Dynamics Underlying Spatial Working Memory in a Cortical Network Model. *Cerebral Cortex*, 10:910–923.

[Conway et al., 1995] Conway, B. A., Halliday, D. M., Farmer, S. F., Shahani, U., Maas, P., Weir, A. I., and Rosenberg, J. R. (1995). Synchronization between motor cortex and spinal motoneuronal pool during the performance of a maintained motor task in man. *Journal of Physiology*, 489(3):917–924.

[Cork et al., 1996] Cork, R. C., Heaton, J. F., Campbell, C. E., and Kihlstrom, J. F. (1996). Is there implicit memory after propofol sedation? *British journal of anaesthesia*, 76(4):492–8.

[Corkin, 1984] Corkin, S. (1984). Lasting Consequences of Bilateral Medial Temporal Lobectomy: Clinical Course and Experimental Findings in H.M.

[Corkin, 2002] Corkin, S. (2002). What's new with the amnesic patient H.M.? *Nature Reviews Neuroscience*, 3(2):153–160.

[Cossu et al., 2005] Cossu, M., Cardinale, F., Castana, L., Citterio, A., Francione, S., Tassi, L., Benabid, A. L., and Lo Russo, G. (2005). Stereoelectroencephalography in the Presurgical Evaluation of Focal Epilepsy: A Retrospective Analysis of 215 Procedures. *Neurosurgery*, 57(4):706–718.

[Cowan, 2008] Cowan, N. (2008). What are the differences between long-term, short-term, and working memory? *Progress in Brain Research*, 169:323–338.

[Csicsvari et al., 2003] Csicsvari, J., Jamieson, B., Wise, K. D., and Buzsáki, G. (2003). Mechanisms of gamma oscillations in the hippocampus of the behaving rat. *Neuron*, 37(2):311–322.

[Cully et al., 2015] Cully, A., Clune, J., Tarapore, D., and Mouret, J.-B. (2015). Robots that can adapt like animals. *Nature*, 521(7553):503–507.

[Dayan and Abbott, 2001] Dayan, P. and Abbott, L. F. (2001). Neural Encoding I: Firing Rates and Spike Statistics. In *Theoretical neuroscience: Computational and mathematical modeling of neural systems*, chapter 1: Neural, pages 1–42. MIT Press, Cambridge, MA.

[Deeprose et al., 2004] Deeprose, C., Andrade, J., Varma, S., and Edwards, N. (2004). Unconscious learning during surgery with propofol anaesthesia. *British Journal of Anaesthesia*, 92(2):171–177.

[Destexhe et al., 1993] Destexhe, A., Babloyantz, A., and Sejnowski, T. J. (1993). Ionic mechanisms for intrinsic slow oscillations in thalamic relay neurons. *Biophysical journal*, 65(4):1538–52.

[Destexhe et al., 1994] Destexhe, A., Contreras, D., Sejnowski, T. J., and Steriade, M. (1994). A model of spindle rhythmicity in the isolated thalamic reticular nucleus. *Journal of neurophysiology*, 72(2):803–18.

[Deuchars and Thomson, 1996] Deuchars, J. and Thomson, A. M. (1996). CA1 pyramid-pyramid connections in rat hippocampus in vitro: Dual intracellular recordings with biocytin filling. *Neuroscience*, 74(4):1009–1018.

[DeVries, 1994] DeVries, P. L. (1994). *A first course in computational physics*. Wiley & Sons, 1 edition.

[Dubeau and McLachlan, 2000] Dubeau, F. and McLachlan, R. S. (2000). Invasive electrographic recording techniques in temporal lobe epilepsy. *The Canadian journal of neurological sciences. Le journal canadien des sciences neurologiques*, 27 Suppl 1(May 2017):S29–S34; discussion S50–S22.

[Dudai, 2002] Dudai, Y. (2002). Molecular bases of long-term memories: A question of persistence. *Current Opinion in Neurobiology*, 12(2):211–216.

[Dudai, 2004] Dudai, Y. (2004). The Neurobiology of Consolidations, Or, How Stable is the Engram? *Annual Review of Psychology*, 55(1):51–86.

[Dutar and Nicoll, 1988] Dutar, P. and Nicoll, R. a. (1988). Classification of muscarinic responses in hippocampus in terms of receptor subtypes and second-messenger systems: electrophysiological studies in vitro. *The Journal of neuroscience : the official journal of the Society for Neuroscience*, 8(11):4214–4224.

[Egorov et al., 2002] Egorov, A. V., Hamam, B. N., Fransén, E., Hasselmo, M. E., and Alonso, A. (2002). Graded persistent activity in entorhinal cortex neurons. *Nature*, 420:173–178.

[Eichenbaum and Cohen, 2004] Eichenbaum, H. and Cohen, N. J. (2004). *Oxford University Press: From Conditioning to Conscious Recollection*. Oxford University Press.

[Ekstrom et al., 2005] Ekstrom, A. D., Caplan, J. B., Ho, E., Shattuck, K., Fried, I., and Kahana, M. J. (2005). Human hippocampal theta activity during virtual navigation. *Hippocampus*, 15(7):881–889.

[Engel et al., 2001] Engel, A. K., Fries, P., and Singer, W. (2001). Dynamic predictions: Oscillations and synchrony in top–down processing. *Nature Reviews Neuroscience*, 2(10):704–716.

[Engel et al., 2005] Engel, A. K., Moll, C. K. E., Fried, I., and Ojemann, G. A. (2005). Invasive recordings from the human brain: clinical insights and beyond. *Nature Reviews Neuroscience*, 6(1):35–47.

[Euler, 1768] Euler, L. (1768). *Institutionum calculi integralis*. Impensis Academiae Imperialis Scientiarum.

[Farrant and Nusser, 2005] Farrant, M. and Nusser, Z. (2005). Variations on an inhibitory theme: phasic and tonic activation of GABA(A) receptors. *Nature reviews. Neuroscience*, 6(3):215–29.

[Fell et al., 2001] Fell, J., Klaver, P., Lehnertz, K., Grunwald, T., Schaller, C., Elger, C. E., and Fernández, G. (2001). Human memory formation is accompanied by rhinal-hippocampal coupling and decoupling. *Nature neuroscience*, 4(12):1259–64.

[Fell et al., 2005] Fell, J., Widman, G., Rehberg, B., Elger, C. E., and Fernández, G. (2005). Human mediotemporal EEG characteristics during propofol anesthesia. *Biological cybernetics*, 92(2):92–100.

[Fellous and Sejnowski, 2000] Fellous, J. M. and Sejnowski, T. J. (2000). Cholinergic induction of oscillations in the hippocampal slice in the slow (0.5-2{Hz}), theta (5-12{Hz}) and gamma bands. *Hippocampus*, 10(November 1999):187–197.

[Fenton et al., 2010] Fenton, A. A., Lytton, W. W., Barry, J. M., Lenck-Santini, P. P., Zinyuk, L. E., Kubik, S., Bures, J., Poucet, B., Muller, R. U., and Olypher, A. V. (2010). Attention-Like Modulation of Hippocampus Place Cell Discharge. *Journal of Neuroscience*, 30(13):4613–4625.

[Feshchenko et al., 2004] Feshchenko, V. A., Veselis, R. A., and Reinsel, R. A. (2004). Propofol-induced alpha rhythm. *Neuropsychobiology*, 50(3):257–266.

[Fischer et al., 1999] Fischer, Y., Gaehwiler, B. H., and Thompson, S. M. (1999). Activation of intrinsic hippocampal theta oscillations by acetylcholine in rat septo-hippocampal cocultures. *The Journal of Physiology*, 519(2):405–413.

[FitzHugh, 1961] FitzHugh, R. (1961). Impulses and Physiological States in Theoretical Models of Nerve Membrane. *Biophysical Journal*, 1(6):445–466.

[Foster et al., 2011] Foster, B. L., Bojak, I., and Liley, D. T. (2011). Understanding the effects of anesthetic agents on the EEG through neural field theory. *Conf Proc IEEE Eng Med Biol Soc*, 2011:4709–4712.

[Franks, 2008] Franks, N. P. (2008). General anaesthesia: from molecular targets to neuronal pathways of sleep and arousal. *Nature reviews. Neuroscience*, 9(5):370–86.

[Fransén et al., 2002] Fransén, E., Alonso, A., and Hasselmo, M. E. (2002). Simulations of the Role of the Muscarinic-Activated Calcium- Sensitive Nonspecific Cation Current I NCM in Entorhinal Neuronal. *The Journal of neuroscience : the official journal of the Society for Neuroscience*, 22(3):1081–1097.

[Fransén et al., 2006] Fransén, E., Tahvildari, B., Egorov, A. V., Hasselmo, M. E., and Alonso, A. (2006). Mechanism of graded persistent cellular activity of entorhinal cortex layer v neurons. *Neuron*, 49(5):735–46.

[Franz and Mallot, 2000] Franz, M. O. and Mallot, H. A. (2000). Biomimetic robot navigation. *Robotics and autonomous Systems*, 30:133–153.

[Fraser et al., 2001] Fraser, D. D., Doll, D., and MacVicar, B. A. (2001). Serine/threonine protein phosphatases and synaptic inhibition regulate the expression of cholinergic-dependent plateau potentials. *Journal of Neurophysiology*, 85(3):1197–1205.

[Fraser and MacVicar, 1996] Fraser, D. D. and MacVicar, B. a. (1996). Cholinergic-dependent plateau potential in hippocampal CA1 pyramidal neurons. *The Journal of Neuroscience*, 16(13):4113–4128.

[Freichel et al., 2005] Freichel, M., Vennekens, R., Olausson, J., Stolz, S., Philipp, S. E., Weißgerber, P., and Flockerzi, V. (2005). Functional role of TRPC proteins in native systems: implications from knockout and knock-down studies. *The Journal of Physiology*, 567(1):59–66.

[Fries, 2005] Fries, P. (2005). A mechanism for cognitive dynamics: neuronal communication through neuronal coherence. *Trends in cognitive sciences*, 9(10):474–80.

[Fries et al., 2001] Fries, P., Reynolds, J. R., Rorie, A. E., and Robert, D. (2001). Modulation of Oscillatory Neuronal Synchronization by Selective Visual Attention. *Science*, 291(5508):1560–1563.

[Frotscher et al., 1986] Frotscher, M., Schlander, M., and Leranth, C. (1986). Cholinergic neurons in the hippocampus. *Cell and Tissue Research*, 246:293–301.

[Funahashi et al., 2001] Funahashi, M., Higuchi, H., Miyawaki, T., Shimada, M., and Matsuo, R. (2001). Propofol suppresses a hyperpolarization-activated inward current in rat hippocampal CA1 neurons. *Neurosci.Lett.*, 311(3):177–180.

[Funahashi et al., 1989] Funahashi, S., Bruce, C. J., and Goldman-Rakic, P. S. (1989). Mnemonic Coding of Visual Space in the Monkey's Dorsolateral Prefrontal Cortex. *Journal of Neurophysiology*, 61:331–349.

[Fuster, 2008] Fuster, J. (2008). *The Prefrontal Cortex*. Academic Press, 4 edition.

[Fuster and Alexander, 1971] Fuster, J. and Alexander, G. E. (1971). Neuron Activity Related to Short-Term Memory. *Science*, 173(3997):652–654.

[Gais and Born, 2004] Gais, S. and Born, J. (2004). Low acetylcholine during slow-wave sleep is critical for declarative memory consolidation. *Proceedings of the National Academy of Sciences of the United States of America*, 101(7):2140–4.

[Garcia et al., 2010] Garcia, P. S., Kolesky, S. E., and Jenkins, A. (2010). General anesthetic actions on GABA(A) receptors. *Current neuropharmacology*, 8(1):2–9.

[Gerstner et al., 2012] Gerstner, W., Sprekeler, H., and Deco, G. (2012). Theory and Simulation in Neuroscience. *Science*, 338(6103):60–65.

[Ghoneim and Block, 1997] Ghoneim, M. M. and Block, R. I. (1997). Learning and Memory during General Anesthesia An Update. *Anesthesiology*, 87:387–410.

[Ghoneim et al., 2009] Ghoneim, M. M., Block, R. I., Haffarnan, M., and Mathews, M. J. (2009). Awareness during anesthesia: Risk factors, causes and sequelae: A review of reported cases in the literature. *Anesthesia and Analgesia*, 108(2):527–535.

[Gibbs et al., 1936] Gibbs, F. A., Gibbs, E. L., and Lennox, W. G. (1936). Effect on the electroencephalogram of certain drugs which influence nervous activity. *Archives of Internal Medicine*, 60(1):154–166.

[Gil et al., 1997] Gil, Z., Connors, B. W., and Amitai, Y. (1997). Differential Regulation of Neocortical Synapses by Neuromodulators and Activity. *Neuron*, 19(3):679–686.

[Gioanni et al., 1999] Gioanni, Y., Rougeout, C., Clarke, P. B. S., Lepousé, C., Thierry, A. M., and Vidal, C. (1999). Nicotinic receptors in the rat prefrontal cortex: increase in glutamate release and facilitation of mediodorsal thalamo-cortical transmission. *European Journal of Neuroscience*, 11:18–30.

[Giocomo and Hasselmo, 2005] Giocomo, L. M. and Hasselmo, M. E. (2005). Nicotinic modulation of glutamatergic synaptic transmission in region CA3 of the hippocampus. *The European journal of neuroscience*, 22(6):1349–56.

[Giovannini and Buhry, 2017] Giovannini, F. and Buhry, L. (2017). Tonic inhibition mediates a synchronisation enhancement during propofol anaesthesia in a network of hippocampal interneurons: a modelling study. *Journal of computational neuroscience (Submitted)*.

[Giovannini et al., 2016] Giovannini, F., Knauer, B., Yoshida, M., and Buhry, L. (2016). Spiking regimes in model networks of hippocampal persistent firing neurons. In *Neuroscience 2016*.

[Giovannini et al., 2017] Giovannini, F., Knauer, B., Yoshida, M., and Buhry, L. (2017). The CAN-In neural network: a mathematical model for theta oscillations and memory maintenance in the hippocampus. *Hippocampus*, 27(4):450–463.

[Giovannini et al., 2015a] Giovannini, F., Schneider, J. J.-B. M., and Buhry, L. (2015a). Investigating the effects of propofol-induced tonic inhibition on rhythmic neural activity in a hippocampal interneuron network. In *Proceedings of the 11th Bernstein Conference*, Heidelberg, Germany.

[Giovannini et al., 2015b] Giovannini, F., Yoshida, M., and Buhry, L. (2015b). Mathematical modelling of ICAN-mediated persistent firing in hippocampal neurons. In *Proceedings of the Twenty Fourth Annual Computational Neuroscience Meeting: CNS*2015*, Prague, Czech Republic.

[Gloveli et al., 2010] Gloveli, T., Kopell, N., and Dugladze, T. (2010). Neuronal Activity Patterns During Hippocampal Network Oscillations In Vitro. In Cutsuridis, V., editor, *Hippocampal Microcircuits A Computational Modeler's Resource Book*, pages 247–276. Springer New York.

[Glykys and Mody, 2007] Glykys, J. and Mody, I. (2007). Activation of GABAA receptors: views from outside the synaptic cleft. *Neuron*, 56(5):763–70.

[Gold, 1999] Gold, I. (1999). Does 40-Hz oscillation play a role in visual consciousness? *Consciousness and cognition*, 8:186–195.

[Gold, 2008] Gold, P. E. (2008). Protein synthesis inhibition and memory: formation vs amnesia. *Neurobiology of Learning and Memory*, 89(3):201–211.

[Goodman and Brette, 2009] Goodman, D. F. M. and Brette, R. (2009). The Brian simulator. *Frontiers in Neuroscience*, 3(SEP):192–197.

[Goutagny et al., 2009] Goutagny, R., Jackson, J., and Williams, S. (2009). Self-generated theta oscillations in the hippocampus. *Nature neuroscience*, 12(12):1491–3.

[Gray et al., 1989] Gray, C. M., König, P., Engel, A. K., and Singer, W. (1989). Oscillatory responses in cat visual cortex exhibit inter-columnar synchronization which reflects global stimulus properties.

[Green et al., 2005] Green, A., Ellis, K. A., Ellis, J., Bartholomeusz, C. F., Ilic, S., Croft, R. J., Phan, K. L., and Nathan, P. J. (2005). Muscarinic and nicotinic receptor modulation of object and spatial n-back working memory in humans. *Pharmacology Biochemistry and Behavior*, 81(3):575–584.

[Griffin et al., 2004] Griffin, A. L., Asaka, Y., Darling, R. D., and Berry, S. D. (2004). Theta-contingent trial presentation accelerates learning rate and enhances hippocampal plasticity during trace eyeblink conditioning. *Behavioral neuroscience*, 118(2):403–11.

[Gugino et al., 2001] Gugino, L. D., Chabot, R. J., Prichep, L. S., John, E. R., Formanek, V., and Aglio, L. S. (2001). Quantitative EEG changes associated with loss and return of consciousness in healthy adult volunteers anaesthetized with propofol or sevoflurane. *British Journal of Anaesthesia*, 87(3):421–428.

[Hämäläinen et al., 1993] Hämäläinen, M. S., Hari, R., Ilmoniemi, R. J., Knuutila, J., and Lounasmaa, O. V. (1993). Magnetoencephalography - theory, instrumentation, and applications to noninvasivee studies of the working human brain.

[Hamill et al., 1981] Hamill, O. P., Marty, A., Neher, E., Sakmann, B., and Sigworth, F. J. (1981). Improved patch-clamp techniques for high-resolution current recording from cells and cell-free membrane patches. *Pflügers Archiv European Journal of Physiology*, 391(2):85–100.

[Hannula and Ranganath, 2008] Hannula, D. E. and Ranganath, C. (2008). Medial Temporal Lobe Activity Predicts Successful Relational Memory Binding. *Journal of Neuroscience*, 28(1):116–124.

[Hannula et al., 2006] Hannula, D. E., Tranel, D., and Cohen, N. J. (2006). The long and the short of it: relational memory impairments in amnesia, even at short lags. *The Journal of neuroscience : the official journal of the Society for Neuroscience*, 26(32):8352–9.

[Hansel et al., 1995] Hansel, D., Mato, G., and Meunier, C. (1995). Synchrony in Excitatory Neural Networks. *Neural Computation*, 7(2):307–337.

[Hardie and Minke, 1993] Hardie, R. C. and Minke, B. (1993). Novel Ca2+ channels underlying transduction in Drosophila photoreceptors: implications for phosphoinositide-mediated Ca2+ mobilization. *Trends in Neurosciences*, 16(9):371–376.

[Hartley et al., 2007] Hartley, T., Bird, C. M., Chan, D., Cipolotti, L., Husain, M., Vargha-Khadem, F., and Burgess, N. (2007). The hippocampus is required for short-term topographical memory in humans. *Hippocampus*, 17(1):34–48.

[Hasselmo, 1999] Hasselmo, M. E. (1999). Neuromodulation: acetylcholine and memory consolidation. *Trends in Cognitive Sciences*, 3(9):351–359.

[Hasselmo, 2005] Hasselmo, M. E. (2005). What is the function of hippocampal theta rhythm? - Linking bahavioral data to phasic properties of field potential and unit recording data. *Hippocampus*, 15(7):936–949.

[Hasselmo, 2006] Hasselmo, M. E. (2006). The role of acetylcholine in learning and memory. *Current opinion in neurobiology*, 16(6):710–5.

[Hasselmo et al., 2002] Hasselmo, M. E., Bodelón, C., and Wyble, B. P. (2002). A proposed function for hippocampal theta rhythm: separate phases of encoding and retrieval enhance reversal of prior learning. *Neural computation*, 14(4):793–817.

[Hasselmo and McGaughy, 2004] Hasselmo, M. E. and McGaughy, J. (2004). High acetylcholine levels set circuit dynamics for attention and encoding and low acetylcholine levels set dynamics for consolidation. *Progress in Brain Research*, 145:207–231.

[Hasselmo and Schnell, 1994] Hasselmo, M. E. and Schnell, E. (1994). Laminar selectivity of the cholinergic suppression of synaptic transmission in rat hippocampal region CA1: computational modeling and brain slice physiology. *The Journal of neuroscience : the official journal of the Society for Neuroscience*, 14(6):3898–3914.

[Hasselmo et al., 1995a] Hasselmo, M. E., Schnell, E., and Barkai, E. (1995a). Dynamics of learning and recall at excitatory recurrent synapses and cholinergic modulation in rat hippocampal region CA3. *The Journal of neuroscience : the official journal of the Society for Neuroscience*, 15(7 Pt 2):5249–5262.

[Hasselmo et al., 1995b] Hasselmo, M. E., Schnell, E., Berke, J., and Barkai, E. (1995b). A model of the hippocampus combining self-organization and associative memory function. *Advances in Neural Information Processing Systems 7*, pages 77–84.

[Hasselmo et al., 1996] Hasselmo, M. E., Wyble, B. P., and Wallenstein, G. V. (1996). Encoding and retrieval of episodic memories: Role of cholinergic and GABAergic modulation in the hippocampus. *Hippocampus*, 6(6):693–708.

[Hebb, 1949] Hebb, D. O. (1949). *The Organization of Behavior*. Wiley & Sons, New York.

[Henschel et al., 2008] Henschel, O., Gipson, K. E., and Bordey, A. (2008). GABAA receptors, anesthetics and anticonvulsants in brain development. *CNS & neurological disorders drug targets*, 7(2):211–224.

[Hill and Bowery, 1981] Hill, D. R. and Bowery, N. G. (1981). 3H-baclofen and 3H-GABA bind to bicuculline-insensitive GABA B sites in rat brain. *Nature*, 290(5802):149–152.

[Hill and Tononi, 2004] Hill, S. and Tononi, G. (2004). Modeling Sleep and Wakefulness in the Thalamocortical System. *Journal of Neurophysiology*, 93(3):1671–1698.

[Hobson and Pace-Schott, 2002] Hobson, J. A. and Pace-Schott, E. F. (2002). The cognitive neuroscience of sleep: neuronal systems, consciousness and learning. *Nature Reviews Neuroscience*, 3(9):679–693.

[Hodgkin and Huxley, 1939] Hodgkin, A. L. and Huxley, A. (1939). Action Potentials Recorded from Inside a Nerve Fibre. *Nature*, 144:710–711.

[Hodgkin and Huxley, 1952] Hodgkin, A. L. and Huxley, A. (1952). A Quantitative Description of Membrane Current and Application to Conduction and Excitation in Nerve. *Journal of Physiology*, 117:500–544.

[Hounsgaard, 1978] Hounsgaard, J. (1978). Presynaptic Inhibitory Action of the of Acetylcholine Hippocampus in Area. *Experimental Neurology*, 62:787–797.

[Howard et al., 2003] Howard, M. W., Rizzuto, D. S., Caplan, J. B., Madsen, J. R., Lisman, J. E., Aschenbrenner-Scheibe, R., Schulze-Bonhage, A., and Kahana, M. J. (2003). Gamma Oscillations Correlate with Working Memory Load in Humans. *Cerebral Cortex*, 13(12):1369–1374.

[Huettel et al., 2009] Huettel, S. A., Song, A. W., and McCarthy, G. (2009). *Functional Magnetic Resonance Imaging*. Sinauer Associates Inc.

[Hughes, 2008] Hughes, J. R. (2008). Gamma, fast, and ultrafast waves of the brain: Their relationships with epilepsy and behavior. *Epilepsy and Behavior*, 13(1):25–31.

[Huster et al., 2012] Huster, R. J., Debener, S., Eichele, T., and Herrmann, C. S. (2012). Methods for Simultaneous EEG-fMRI: An Introductory Review. *Journal of Neuroscience*, 32(18):6053–6060.

[Hutt and Buhry, 2014] Hutt, A. and Buhry, L. (2014). Study of GABAergic extra-synaptic tonic inhibition in single neurons and neural populations by traversing neural scales: application to propofol-induced anaesthesia. *Journal of computational neuroscience*, 37(3):417–37.

[Iberri, 2004] Iberri, D. (2004). File:synapse with nmdar and ampar.png. Website. [electronic image] http://en.wikipedia.org/wiki/File:Synapse_with_NMDAR_and_AMPAR.png Accessed 27/08/2012.

[Izhikevich, 2003] Izhikevich, E. M. (2003). Simple model of spiking neurons. *IEEE transactions on neural networks / a publication of the IEEE Neural Networks Council*, 14(6):1569–72.

[Izhikevich, 2004] Izhikevich, E. M. (2004). Which model to use for cortical spiking neurons? *IEEE transactions on neural networks / a publication of the IEEE Neural Networks Council*, 15(5):1063–70.

[Izhikevich, 2007] Izhikevich, E. M. (2007). *Dynamical Systems in Neuroscience: The Geometry of Excitability and Bursting*. MIT Press.

[Jackson et al., 2011] Jackson, J., Goutagny, R., and Williams, S. (2011). Fast and slow gamma rhythms are intrinsically and independently generated in the subiculum. *The Journal of neuroscience : the official journal of the Society for Neuroscience*, 31(34):12104–12117.

[Jasper and Penfield, 1949] Jasper, H. and Penfield, W. (1949). Electrocorticograms in man: Effect of voluntary movement upon the electrical activity of the precentral gyrus. *Archiv für Psychiatrie und Nervenkrankheiten*, 183(1-2):163–174.

[Jin et al., 2009] Jin, Y. H., Zhang, Z., Mendelowitz, D., and Andresen, M. C. (2009). Presynaptic actions of propofol enhance inhibitory synaptic transmission in isolated solitary tract nucleus neurons. *Brain Research*, 1286:75–83.

[Jochems and Yoshida, 2013] Jochems, A. and Yoshida, M. (2013). Persistent firing supported by an intrinsic cellular mechanism in hippocampal CA3 pyramidal cells. *The European journal of neuroscience*, 38(2):2250–9.

[Jochems and Yoshida, 2015] Jochems, A. and Yoshida, M. (2015). A robust in vivo-like persistent firing supported by a hybrid of intracellular and synaptic mechanisms. *PloS one*, 10(4):e0123799.

[Johnston, 1996] Johnston, G. A. R. (1996). GABAA receptor pharmacology. *Pharmacology and Therapeutics*, 69(3):173–198.

[Jonas et al., 2004] Jonas, P., Bischofberger, J., Fricker, D., and Miles, R. (2004). Interneuron Diversity series: Fast in, fast out - Temporal and spatial signal processing in hippocampal interneurons. *Trends in Neurosciences*, 27(1):30–40.

[Jones, 1994] Jones, J. G. (1994). Perception and memory during general anaesthesia. *British Journal of Anaesthesia*, 73(1):31–37.

[Jonides et al., 2008] Jonides, J., Lewis, R. L., Nee, D. E., Lustig, C. A., and Berman, M. G. (2008). The Mind and Brain of Short-Term Memory. *Annual Review of Psychology*, 59:193–224.

[Kaczorowski et al., 2007] Kaczorowski, C. C., Disterhoft, J., and Spruston, N. (2007). Stability and plasticity of intrinsic membrane properties in hippocampal CA1 pyramidal neurons: effects of internal anions. *The Journal of physiology*, 578(Pt 3):799–818.

[Kahana et al., 2001] Kahana, M. J., Seelig, D., and Madsen, J. R. (2001). Theta returns. *Current Opinion in Neurobiology*, 11(6):739–744.

[Kalia, 2010] Kalia, M. (2010). Neurobiology of sleep. *Clinics in Chest Medicine*, 31(2):309–318.

[Kametani and Kawamura, 1990] Kametani, H. and Kawamura, H. (1990). Alterations in acetylcholine release in the rat hippocampus during sleep-wakefulness detected by intracerebral dialysis. *Life Sciences*, 47(5):421–426.

[Kandel, 2001] Kandel, E. R. (2001). The Molecular Biology of Memory Storage: A Dialogue Between Genes and Synapses. *Bioscience Reports*, 21(5):565–611.

[Kandel et al., 2000a] Kandel, E. R., Schwartz, J. H., and Jessel, T. M. (2000a). Chapter 2: Nerve Cells and Behaviour. In *Principles of Neural Science*, chapter 2, pages 19–35. McGraw-Hill.

[Kandel et al., 2000b] Kandel, E. R., Schwartz, J. H., and Jessel, T. M. (2000b). Chapter 62: Learning and Memory. In *Principles of Neural Science*, chapter 62, pages 1227–1246. McGraw-Hill.

[Kandel et al., 2000c] Kandel, E. R., Schwartz, J. H., and Jessel, T. M. (2000c). Chapter 9: Propagated Signalling: The Action Pontential. In *Principles of Neural Science*, chapter 9, pages 150–170. McGraw-Hill.

[Kandel and Siegelbaum, 2000] Kandel, E. R. and Siegelbaum, S. A. (2000). Chapter 12: Synaptic Integration. In *Principles of Neural Science*, pages 207–228. McGraw-Hill.

[Kerssens et al., 2005] Kerssens, C., Ouchi, T., and Sebel, P. S. (2005). No Evidence of Memory Function during Anesthesia with Propofol or Isoflurane with Close Control of Hypnotic State. *Anesthesiology*, 102(1):57–62.

[Kesner et al., 2005] Kesner, R. P., Hunsaker, M. R., and Gilbert, P. E. (2005). The role of CA1 in the acquisition of an object-trace-odor paired associate task. *Behavioral neuroscience*, 119(3):781–6.

[Kiersey et al., 1951] Kiersey, D. K., Bickford, R. G., and Faulconer, A. (1951). Electroencephalographic patterns produced by thiopental sodium during surgical operations: Description and classification. *British Journal of Anaesthesia*, 23(3):141–152.

[Kihlstrom et al., 1990] Kihlstrom, J. F., Schacter, D. L., Cork, R. C., Hurt, C. a., and Behr, S. E. (1990). Implicit and Explicit Memory Following Surgical Anesthesia. *Psychological Science*, 1(5):303–306.

[Kitamura et al., 2004] Kitamura, A., Sato, R., Marszalec, W., Yeh, J. Z., Ogawa, R., and Narahashi, T. (2004). Halothane and propofol modulation of gamma-aminobutyric acidA receptor single-channel currents. *Anesthesia and analgesia*, 99(2):409–15, table of contents.

[Klimesch et al., 2007] Klimesch, W., Sauseng, P., and Hanslmayr, S. (2007). EEG alpha oscillations: The inhibition-timing hypothesis. *Brain Research Reviews*, 53(1):63–88.

[Klink et al., 1997] Klink, R., Alonso, A., Hinton, E. A., Wheeler, M. G., Gourley, S. L., Anderson, R. W., Strowbridge, B. W., Ray, S., Naumann, R., Burgalossi, A., Tang, Q., Schmidt, H., Schmidt-hieber, C., and Häusser, M. (1997). Muscarinic Modulation of the Oscillatory and Repetitive Firing Properties of Entorhinal Cortex Layer II Neurons Muscarinic Modulation of the Oscillatory and Repetitive Firing Properties of Entorhinal Cortex Layer II Neurons. *Journal of neurophysiology*, 77:1813–1828.

[Knauer, 2015] Knauer, B. (2015). *Persistent firing and depolarization block in rat Ca1 pyramidal neurons*. PhD thesis, Ruhr University Bochum.

[Knauer et al., 2013] Knauer, B., Jochems, A., Valero-Aracama, M. J., and Yoshida, M. (2013). Long-lasting intrinsic persistent firing in rat CA1 pyramidal cells: a possible mechanism for active maintenance of memory. *Hippocampus*, 23(9):820–31.

[Kocsis et al., 1999] Kocsis, B., Bragin, A., and Buzsáki, G. (1999). Interdependence of multiple theta generators in the hippocampus: a partial coherence analysis. *The Journal of neuroscience : the official journal of the Society for Neuroscience*, 19(14):6200–6212.

[Kondylis et al., 2014] Kondylis, E. D., Wozny, T. A., Lipski, W. J., Popescu, A., DeStefino, V. J., Esmaeili, B., Raghu, V. K., Bagic, A., and Richardson, R. M. (2014). Detection of high-frequency oscillations by hybrid depth electrodes in standard clinical intracranial EEG recordings. *Frontiers in Neurology*, 5 AUG(August):1–10.

[Konopacki et al., 2006] Konopacki, J., Eckersdorf, B., Kowalczyk, T., and Gołębiewski, H. (2006). Firing cell repertoire during carbachol-induced theta rhythm in rat hippocampal formation slices. *European Journal of Neuroscience*, 23(7):1811–1818.

[Kopell et al., 2010] Kopell, N. J., Boergers, C., Pervouchine, D., Malerba, P., and Tort, A. (2010). Gamma and theta rhythms in biophysical models of hippocampal circuits. In Cutsuridis, V., Graham, B., Cobb, S., and Vida, I., editors, *Hippocampal Microcircuits A Computational Modeler's Resource Book*, chapter Gamma and, pages 423–457. Springer New York, New York, NY.

[Lalo et al., 2007] Lalo, E., Gilbertson, T., Doyle, L., Di Lazzaro, V., Cioni, B., and Brown, P. (2007). Phasic increases in cortical beta activity are associated with alterations in sensory processing in the human. *Experimental Brain Research*, 177(1):137–145.

[Lapique, 1907] Lapique, L. (1907). Recherches quantitatives sur l'excitation electrique des nerfs traitee comme une polarization. *J Physiol Pathol Gen*.

[Lega et al., 2012] Lega, B. C., Jacobs, J., and Kahana, M. (2012). Human hippocampal theta oscillations and the formation of episodic memories. *Hippocampus*, 22(4):748–761.

[Lenck-Santini et al., 2008] Lenck-Santini, P.-P., Fenton, A. A., and Muller, R. U. (2008). Discharge properties of hippocampal neurons during performance of a jump avoidance task. *Growth (Lakeland)*, 23(1):1–7.

[Lewandowsky et al., 2004] Lewandowsky, S., Duncan, M., and Brown, G. D. a. (2004). Time does not cause forgetting in short-term serial recall. *Psychonomic bulletin & review*, 11(5):771–790.

[Lewandowsky et al., 2009] Lewandowsky, S., Oberauer, K., and Brown, G. D. a. (2009). No temporal decay in verbal short-term memory. *Trends in cognitive sciences*, 13(3):120–6.

[Lisman, 2010] Lisman, J. E. (2010). Working memory: The importance of theta and gamma oscillations. *Current Biology*, 20(11):R490–R492.

[Lisman and Jensen, 2013] Lisman, J. E. and Jensen, O. (2013). The Theta-Gamma Neural Code. *Neuron*, 77(6):1002–1016.

[Llinas and Ribary, 1993] Llinas, R. and Ribary, U. (1993). Coherent 40-Hz oscillation characterizes dream state in humans. *Proceedings of the National Academy of Sciences*, 90(5):2078–2081.

[Llinas, 1988] Llinas, R. R. (1988). Intrinsic Electrophysiological Properties Central Nervous System Function. *Science*, 242(3):1654–1664.

[Llinas et al., 1991] Llinas, R. R., Grace, A. A., and Yarom, Y. (1991). In vitro neurons in mammalian cortical layer 4 exhibit intrinsic oscillatory activity in the 10- to 50-Hz frequency range. *Proceedings of the National Academy of Sciences*, 88(3):897–901.

[Logothetis et al., 2001] Logothetis, N. K., Pauls, J., Augath, M., Trinath, T., and Oeltermann, A. (2001). Neurophysiological investigation of the basis of the fMRI signal. *Nature*, 412(6843):150–157.

[Longnecker David E et al., 2008] Longnecker David E, Brown, D. L., Newman, M. F., and Zapol, W. M. (2008). *Anesthesiology*. McGraw-Hill.

[Lubke et al., 1999] Lubke, G. H., Kerssens, C., Phaf, H., and Sebel, P. S. (1999). Dependence of explicit and implicit memory on hypnotic state in trauma patients. *Anesthesiology*, 90:670–680.

[Luján et al., 2005] Luján, R., Shigemoto, R., and López-Bendito, G. (2005). Glutamate and GABA receptor signalling in the developing brain. *Neuroscience*, 130(3):567–580.

[Macdonald and Olsen, 1994] Macdonald, R. L. and Olsen, R. W. (1994). GABAA receptor channels. *Annu Rev Neurosci*, 17:569–602.

[Magistretti et al., 2004] Magistretti, J., Ma, L., Shalinsky, M. H., Lin, W., Klink, R., and Alonso, A. (2004). Spike Patterning by Ca2+-Dependent Regulation of a Muscarinic Cation Current in Entorhinal Cortex Layer II Neurons. *Journal of Neurophysiology*, 92:1644–1657.

[Magistretti et al., 1999] Magistretti, J., Ragsdale, D. S., and Alonso, A. (1999). High Conductance Sustained Single-Channel Activity Responsible for the Low-Threshold Persistent Na+ Current in Entorhinal Cortex Neurons. *The Journal of neuroscience : the official journal of the Society for Neuroscience*, 19(17):7334–7341.

[Maingret et al., 2016] Maingret, N., Girardeau, G., Todorova, R., Goutierre, M., and Zugaro, M. (2016). Hippocampo-cortical coupling mediates memory consolidation during sleep. *Nature Neuroscience*, 19:959–964.

[Major and Tank, 2004] Major, G. and Tank, D. (2004). Persistent neural activity: prevalence and mechanisms. *Current opinion in neurobiology*, 14(6):675–84.

[Malenka and Bear, 2004] Malenka, R. C. and Bear, M. F. (2004). LTP and LTD: An embarrassment of riches. *Neuron*, 44(1):5–21.

[Marr, 1971] Marr, D. (1971). Simple Memory : a Theory for Archicortex. *Philosophical Transactions of the Royal Society B: Biological Sciences*, 262(841):23–81.

[Marrosu et al., 1995] Marrosu, F., Portas, C., Mascia, M. S., Casu, M. A., Fà, M., Giagheddu, M., Imperato, A., and Gessa, G. L. (1995). Microdialysis measurement of cortical and hippocampal

acetylcholine release during sleep-wake cycle in freely moving cats. *Brain Research*, 671(2):329–332.

[Martin and Chao, 2001] Martin, A. and Chao, L. L. (2001). Semantic memory and the brain: structure and processes. *Current Opinion in Neurobiology*, 11(2):194–201.

[Martinez et al., 2006] Martinez, D., Rochel, O., and Hugues, E. (2006). A biomimetic robot for tracking specific odors in turbulent plumes. *Autonomous Robots*, 20(3):185–195.

[Mashour, 2005] Mashour, G. A. (2005). Cognitive Unbinding in Sleep and Anesthesia. *Science (New York, N.Y.)*, 310(5755):1767–1768.

[Mashour, 2010] Mashour, G. A., editor (2010). *Consciousness, Awareness, and Anesthesia*. Cambridge University Press.

[Mastin, 2010] Mastin, L. (2010). Types of human memory. Website. [electronic image] http://www.human-memory.net/types.html, Accessed 05/06/2017.

[Mazzoni et al., 2015] Mazzoni, A., Lindén, H., Cuntz, H., Lansner, A., Panzeri, S., and Einevoll, G. T. (2015). Computing the Local Field Potential (LFP) from Integrate-and-Fire Network Models. *PLoS Computational Biology*, 11(12):1–38.

[McCarthy et al., 2008] McCarthy, M. M., Brown, E. N., and Kopell, N. J. (2008). Potential network mechanisms mediating electroencephalographic beta rhythm changes during propofol-induced paradoxical excitation. *The Journal of neuroscience : the official journal of the Society for Neuroscience*, 28(50):13488–13504.

[McClelland et al., 1995] McClelland, J. L., McNaughton, B. L., and O'Reilly, R. C. (1995). Why there are complementary learning systems in the hippocampus and neocortex: Insights from the successes and failures of connectionist models of learning and memory. *Psychological Review*, 102(3):419–457.

[McDougall et al., 2008] McDougall, S. J., Bailey, T. W., Mendelowitz, D., and Andresen, M. C. (2008). Propofol enhances both tonic and phasic inhibitory currents in second-order neurons of the solitary tract nucleus (NTS). *Neuropharmacology*, 54(3):552–563.

[McEchron and Disterhoft, 1997] McEchron, M. D. and Disterhoft, J. F. (1997). Sequence of single neuron changes in CA1 hippocampus of rabbits during acquisition of trace eyeblink conditioned responses. *Journal of neurophysiology*, 78(2):1030–44.

[McEchron and Disterhoft, 1999] McEchron, M. D. and Disterhoft, J. F. (1999). Hippocampal encoding of non-spatial trace conditioning. *Hippocampus*, 9(4):385–396.

[McEchron et al., 2001] McEchron, M. D., Weible, A. P., and Disterhoft, J. F. (2001). Aging and learning-specific changes in single-neuron activity in CA1 hippocampus during rabbit trace eyeblink conditioning. *Journal of neurophysiology*, 86(4):1839–57.

[McNaughton and Morris, 1987] McNaughton, B. L. and Morris, R. G. M. (1987). Hippocampal synaptic enhancement and information storage within a distributed memory system. *Trends in Neurosciences*, 10(10):408–415.

[Michel et al., 2004] Michel, C. M., Murray, M. M., Lantz, G., Gonzalez, S., Spinelli, L., and Grave De Peralta, R. (2004). EEG source imaging. *Clinical Neurophysiology*, 115(10):2195–2222.

[Miles et al., 1996] Miles, R., Tóth, K., Gulyás, A. I., Hájos, N., and Freund, T. F. (1996). Differences between somatic and dendritic inhibition in the hippocampus. *Neuron*, 16(4):815–823.

[Miles and Wong, 1986] Miles, R. and Wong, R. K. S. (1986). Excitatory synaptic interactions between ca3 neurones in the guinea-pig hippocampus. *Journal of Physiology*, 373:397–418.

[Miller, 1994] Miller, G. A. (1994). The magical number seven, plus or minus two: some limits on our capacity for processing information. 1956. *Psychological review*, 101(2):343–52.

[Misanin et al., 1968] Misanin, J. R., Miller, R. R., and Lewis, D. J. (1968). Retrograde Amnesia Produced by Electroconvulsive Shock after Reactivation of a Consolidated Memory Trace Author (s): James R . Misanin , Ralph R . Miller and Donald J . Lewis Published by : American Association for the Advancement of Science Stable URL. *Science*, 160(3827):554–555.

[Moerman et al., 1993] Moerman, N., Bonke, B., and Oosting, J. (1993). Awareness and recall during general anesthesia: Facts and feelings. *Anesthesiology*, 79:454–464.

[Möhler, 2001] Möhler, H. (2001). Pharmacology of GABA and Glycine Neurotransmission. In M?hler, H., editor, *Handbook of Experimental Pharmacology*, volume 150 of *Handbook of Experimental Pharmacology*. Springer Berlin Heidelberg, Berlin, Heidelberg.

[Monmaur et al., 1997] Monmaur, P., Collet, a., Puma, C., Frankel-Kohn, L., and Sharif, a. (1997). Relations between acetylcholine release and electrophysiological characteristics of theta rhythm: a microdialysis study in the urethane-anesthetized rat hippocampus. *Brain research bulletin*, 42(2):141–146.

[Montgomery and Buzsáki, 2007] Montgomery, S. M. and Buzsáki, G. (2007). Gamma oscillations dynamically couple hippocampal CA3 and CA1 regions during memory task performance. *Proceedings of the National Academy of Sciences of the United States of America*, 104(36):14495–14500.

[Moraud and Martinez, 2010] Moraud, E. M. and Martinez, D. (2010). Effectiveness and robustness of robot infotaxis for searching in dilute conditions. *Frontiers in Neurorobotics*, 4(MAR):1–8.

[Moroni et al., 2007] Moroni, F., Nobili, L., Curcio, G., De Carli, F., Fratello, F., Marzano, C., De Gennaro, L., Ferrillo, F., Cossu, M., Francione, S., Russo, G. L., Bertini, M., and Ferrara, M. (2007). Sleep in the human hippocampus: A stereo-EEG study. *PLoS ONE*, 2(9).

[Morris and Lecar, 1981] Morris, C. and Lecar, H. (1981). Voltage oscillations in the barnacle giant muscle fiber. *Biophysical Journal*, 35(1):193–213.

[Mueller et al., 2011] Mueller, C. P., Pum, M. E., Amato, D., Schüttler, J., Huston, J. P., and Silva, M. a. D. S. (2011). The in vivo neurochemistry of the brain during general anesthesia. *Journal of neurochemistry*, 119(3):419–46.

[Nader et al., 2000] Nader, K., Schafe, G. E., and Le Doux, J. E. (2000). Fear memories require protein synthesis in the amygdala for reconsolidation after retrieval. *Nature*, 406(6797):722–726.

[Nagumo et al., 1962] Nagumo, J., Arimoto, S., and Yoshizawa, S. (1962). An Active Pulse Transmission Line Simulating Nerve Axon. *Proceedings of the IRE*, 50(10):2061–2070.

[Nairne, 2002] Nairne, J. S. (2002). Remembering Over the Short-Term: The Case Against the Standard Model. *Annual Review of Psychology*, 53(1):53–81.

[Nelson et al., 2002] Nelson, L. E., Guo, T. Z., Lu, J., Saper, C. B., Franks, N. P., and Maze, M. (2002). The sedative component of anesthesia is mediated by GABA(A) receptors in an endogenous sleep pathway. *Nature neuroscience*, 5(10):979–84.

[Niedermeyer, 1997] Niedermeyer, E. (1997). Alpha rhythms as physiological and abnormal phenomena. *International Journal of Psychophysiology*, 26(1-3):31–49.

[Niedermeyer and Lopes da Silva, 2005] Niedermeyer, E. and Lopes da Silva, F. H. (2005). *Electroencephalography: Basic Principles, Clinical Applications, and Related Fields*. Lippincott Williams and Wilkins, 5 edition.

[Nyhus and Curran, 2010] Nyhus, E. and Curran, T. (2010). Functional role of gamma and theta oscillations in episodic memory. *Neuroscience and biobehavioral reviews*, 34(7):1023–35.

[O'Keefe et al., 1998] O'Keefe, J., Burgess, N., Donnett, J. G., Jeffery, K. J., and Maguire, E. A. (1998). Place cells, navigational accuracy, and the human hippocampus. *Philosophical Transactions of the Royal Society B: Biological Sciences*, 353(1373):1333–1340.

[O'Keefe and Dostrovsky, 1971] O'Keefe, J. and Dostrovsky, J. (1971). The hippocampus as a spatial map. Preliminary evidence from unit activity in the freely-moving rat. *Brain Research*, 34(1):171–175.

[O'Keefe and Recce, 1993] O'Keefe, J. and Recce, M. L. (1993). Phase relationship between hippocampal place units and the EEG theta rhythm. *Hippocampus*, 3(3):317–330.

[O'Reilly, 2006] O'Reilly, R. C. (2006). Biologically based computational models of high-level cognition. *Science (New York, N.Y.)*, 314(5796):91–4.

[Osipova et al., 2006] Osipova, D., Takashima, A., Oostenveld, R., Fernández, G., Maris, E., and Jensen, O. (2006). Theta and gamma oscillations predict encoding and retrieval of declarative memory. *The Journal of neuroscience : the official journal of the Society for Neuroscience*, 26(28):7523–31.

[Osterman et al., 2001] Osterman, J. E., Hopper, J., Heran, W. J., Keane, T. M., and Van Der Kolk, B. A. (2001). Awareness under anesthesia and the development of posttraumatic stress disorder. *General hospital psychiatry*, 23:198–204.

[Osterman and Van Der Kolk, 1998] Osterman, J. E. and Van Der Kolk, B. A. (1998). Awareness during anesthesia and posttraumatic stress disorder. *General hospital psychiatry*, 20(5):274–81.

[Owen et al., 1995] Owen, A. M., Sahakian, B. J., Semple, J., Polkey, C. E., and Robbins, T. W. (1995). Visuo-spatial short-term recognition memory and learning after temporal lobe excisions, frontal lobe excisions or amygdalo-hippocampectomy in man. *Neuropsychologia*, 33(1):1–24.

[Palmini, 2006] Palmini, A. (2006). The concept of the epileptogenic zone: A modern look at Penfield and Jasper's views on the role of interictal spikes. *Epileptic Disorders*, 8(SUPPL. 2):10–15.

[Palva and Palva, 2007] Palva, S. and Palva, J. M. (2007). New vistas for α-frequency band oscillations. *Trends in Neurosciences*, 30(4):150–158.

[Partridge et al., 1994] Partridge, L. D., Muller, T. H., and Swandulla, D. (1994). Non-selective channels in the nervous system. *Brain research reviews*, 19:319–325.

[Partridge and Swandulla, 1988] Partridge, L. D. and Swandulla, D. (1988). Calcium-activated non-specific cation channels. *Trends in neurosciences*, 11(2):69–72.

[Pastalkova et al., 2008] Pastalkova, E., Itskov, V., Amarasingham, A., and Buzsáki, G. (2008). Internally Generated Cell Assembly Sequences in the Rat Hippocampus. *Science*, 321(5894):1322–1327.

[Pastoll et al., 2013] Pastoll, H., Solanka, L., van Rossum, M. C. W., and Nolan, M. F. (2013). Feedback Inhibition Enables Theta-Nested Gamma Oscillations and Grid Firing Fields. *Neuron*, 77(1):141–154.

[Penttonen et al., 1998] Penttonen, M., Kamondi, A., Acsády, L., and Buzsáki, G. (1998). Gamma frequency oscillation in the hippocampus of the rat: Intracellular analysis in vivo. *European Journal of Neuroscience*, 10(2):718–728.

[Poirier and Saint-Aubin, 1995] Poirier, M. and Saint-Aubin, J. (1995). Memory for related and unrelated words: further evidence on the influence of semantic factors in immediate serial recall.

The Quarterly journal of experimental psychology. A, Human experimental psychology, 48(2):384–404.

[Power, 2004] Power, A. E. (2004). Slow-wave sleep, acetylcholine, and memory consolidation. *Proceedings of the National Academy of Sciences*, 101(7):1795–1796.

[Purdon et al., 2013] Purdon, P. L., Pierce, E. T., Mukamel, E. a., Prerau, M. J., Walsh, J. L., Wong, K. F. K., Salazar-Gomez, A. F., Harrell, P. G., Sampson, A. L., Cimenser, A., Ching, S., Kopell, N. J., Tavares-Stoeckel, C., Habeeb, K., Merhar, R., and Brown, E. N. (2013). Electroencephalogram signatures of loss and recovery of consciousness from propofol. *Proceedings of the National Academy of Sciences of the United States of America*, 110(12):E1142–51.

[Qin et al., 1997] Qin, Y.-L., Mcnaughton, B. L., Skaggs, W. E., and Barnes, C. A. (1997). Memory reprocessing in corticocortical and hippocampocortical neuronal ensembles. *Philosophical Transactions of the Royal Society B: Biological Sciences*, 352(1360):1525–1533.

[Radcliffe et al., 1999] Radcliffe, K. a., Fisher, J. L., Gray, R., and Dani, J. a. (1999). Nicotinic Modulation of Glutamate and GABA Synaptic Transmission in Hippocampal Neurons. *Annals of the New York Academy of Sciences*, 868(1 MOLECULAR AND):591–610.

[Raghavachari et al., 2001] Raghavachari, S., Kahana, M. J., Rizzuto, D. S., Caplan, J. B., Kirschen, M. P., Bourgeois, B., Madsen, J. R., and Lisman, J. E. (2001). Gating of human theta oscillations by a working memory task. *The Journal of neuroscience : the official journal of the Society for Neuroscience*, 21(9):3175–3183.

[Ramón y Cajal, 1909] Ramón y Cajal, S. (1909). *Histologie du Systeme Nerveux de l'Homme et des Vertébrés*, volume 1. A. Maloine.

[Rampil, 1998] Rampil, I. J. (1998). A primer for EEG signal processing in anesthesia. *The Journal of the American Society of Anesthesiologists*, 89(4):980–1002.

[Ranta et al., 1998] Ranta, S. O.-V., Laurila, R., Saario, J., Ali-Melkkila, T., and Hynynen, M. (1998). Awareness with Recall During General Anesthesia. *Anesthesia & Analgesia*, 86(5):1084–1089.

[Reasor and Poe, 2008] Reasor, J. D. and Poe, G. R. (2008). Learning and Memory During Sleep and Anesthesia. *International anesthesiology clinics*, 46(3).

[Reboreda et al., 2011] Reboreda, A., Jiménez-Dìaz, L., and Navarro-López, J. D. (2011). TRP Channels and Neural Persistent Activity. In Islam, M. S., editor, *Transient Receptor Potential Channels*, volume 704, chapter 32, pages 517–530. Springer Netherlands, 1 edition.

[Reuveni et al., 1993] Reuveni, I., Friedman, A., Amitai, Y., and Gutnick, M. J. (1993). Stepwise repolarization from Ca2+ plateaus in neocortical pyramidal cells: evidence for nonhomogeneous distribution of HVA Ca2+ channels in dendrites. *The Journal of neuroscience : the official journal of the Society for Neuroscience*, 13(11):4609–21.

[Revlin, 2012] Revlin, R. (2012). *Cognition: theory and practice*. Worth Publishers.

[Roediger et al., 2007] Roediger, H. L. I., Dudai, Y., and Fitzpatrick, S. M. (2007). *Science of memory: concepts*. Oxford University Press.

[Rubin et al., 2009] Rubin, J. E., Hayes, J. a., Mendenhall, J. L., and Del Negro, C. a. (2009). Calcium-activated nonspecific cation current and synaptic depression promote network-dependent burst oscillations. *Proceedings of the National Academy of Sciences of the United States of America*, 106(8):2939–2944.

[Rudolph and Antkowiak, 2004] Rudolph, U. and Antkowiak, B. (2004). Molecular and neuronal substrates for general anaesthetics. *Nature reviews. Neuroscience*, 5(9):709–20.

[Rudy et al., 2006] Rudy, J. W., Biedenkapp, J. C., Moineau, J., and Bolding, K. (2006). Anisomycin and the reconsolidation hypothesis. *Learning & Memory*, 13(1):1–3.

[Sakmann and Neher, 1984] Sakmann, B. and Neher, E. (1984). Patch Clamp Techniques for Studying Ionic Channels in Excitable Membranes. *Annual Review of Physiology*, 46(1):455–472.

[Sandin et al., 2000] Sandin, R. H., Enlund, Gunnar, Samuelsson, P., and Lennmarken, C. (2000). Awareness during anaesthesia. A prospective study. *The Lancet*, 355:707–711.

[Sara, 2000] Sara, S. J. (2000). Retrieval and Reconsolidation: Toward a Neurobiology of Remembering. *Learning & Memory*, 7(2):73–84.

[Schiff, 2008] Schiff, N. D. (2008). Central thalamic contributions to arousal regulation and neurological disorders of consciousness. *Annals of the New York Academy of Sciences*, 1129:105–118.

[Schiff et al., 2007] Schiff, N. D., Giacino, J. T., Kalmar, K., Victor, J. D., Baker, K., Gerber, M., Fritz, B., Eisenberg, B., O'Connor, J., Kobylarz, E. J., Farris, S., Machado, A., McCagg, C., Plum, F., Fins, J. J., and Rezai, A. R. (2007). Behavioural improvements with thalamic stimulation after severe traumatic brain injury. *Nature*, 448(7153):600–603.

[Schiff and Posner, 2007] Schiff, N. D. and Posner, J. B. (2007). Another "Awakenings". *Annals of Neurology*, 62(1):5–7.

[Schultz, 1990] Schultz, J. E. (1990). Potassium Channels. Structure, classification, function and therapeutic potential. Hrsg. Nigel S. Cook. Allis Horwood, Chichester, UK. 1990. 412 S., zahlr. Abb., geb., $ 59.95. *Pharmazie in Unserer Zeit*, 19(4):172–172.

[Schwender et al., 1998] Schwender, D., Kunze-Kronawitter, H., Dietrich, P., Klasing, S., Forst, H., and Madler, C. (1998). Conscious awareness during general anaesthesia: patients' perceptions, emotions, cognition and reactions. *British Journal of Anaesthesia*, 80(2):133–139.

[Scoville and Milner, 1957] Scoville, W. B. and Milner, B. (1957). Loss of Recent Memory After Bilateral Hippocampal Lesions. *Journal of Neurology, Neurosurgery & Psychiatry*, 20(1):11–21.

[Sebel et al., 2004] Sebel, P. S., Bowdle, T. A., Ghoneim, M. M., Rampil, I. J., Padilla, R. E., Gan, T. J., and Domino, K. B. (2004). The incidence of awareness during anesthesia: a multicenter United States study. *Anesthesia and analgesia*, 99(3):833–9, table of contents.

[Sederberg et al., 2007] Sederberg, P. B., Schulze-Bonhage, A., Madsen, J. R., Bromfield, E. B., Litt, B., Brandt, A., and Kahana, M. J. (2007). Gamma oscillations distinguish true from false memories. *Psychological science : a journal of the American Psychological Society / APS*, 18:927–932.

[Semyanov et al., 2003] Semyanov, A., Walker, M. C., and Kullmann, D. M. (2003). GABA uptake regulates cortical excitability via cell type-specific tonic inhibition. *Nature Neuroscience*, 6(5):484–490.

[Shanahan, 2011] Shanahan, M. (2011). Topic 2: Neurons. [Imperial College London, Department of Computing, Module 421: Computational Neurodynamics].

[Sharon et al., 2007] Sharon, D., Hämäläinen, M. S., Tootell, R. B. H., Halgren, E., and John, W. (2007). The advantage of combining MEG and EEG: comparison to fMRI in focally-stimulated visual cortex. *Neuroimage*, 36(4):1225–1235.

[Sheeba et al., 2008] Sheeba, J. H., Stefanovska, A., and McClintock, P. V. (2008). Neuronal Synchrony during Anesthesia: A Thalamocortical Model. *Biophysical Journal*, 95(6):2722–2727.

[Sheffield et al., 2011] Sheffield, M. E. J., Best, T. K., Mensh, B. D., Kath, W. L., and Spruston, N. (2011). Slow integration leads to persistent action potential firing in distal axons of coupled interneurons. *Nature neuroscience*, 14(2):200–207.

[Shen and McNaughton, 1994] Shen, B. and McNaughton, B. L. (1994). Simulation of the spontaneous reactivation of experience-specific hippocampal cell assemblies during sleep. *Society for Neuroscience Abstracts*, 20(1996):1206.

[Sheridan and Sutor, 1990] Sheridan, R. D. and Sutor, B. (1990). Presynaptic M1 muscarinic cholinoceptors mediate inhibition\rof excitatory synaptic transmission in the hippocampus in\rvitro. *Neurosci. Lett.*, 108(3):273–278.

[Siegel, 2001] Siegel, J. M. (2001). The REM Sleep – Memory Consolidation Hypothesis. *Science*, 294(November):1058–1063.

[Sigel and Steinmann, 2012] Sigel, E. and Steinmann, M. E. (2012). Structure, function, and modulation of GABAA receptors. *Journal of Biological Chemistry*, 287(48):40224–40231.

[Simon et al., 2006] Simon, A. P., Poindessous-Jazat, F., Dutar, P., Epelbaum, J., and Bassant, M.-H. (2006). Firing Properties of Anatomically Identified Neurons in the Medial Septum of Anesthetized and Unanesthetized Restrained Rats. *The Journal of Neuroscience*, 26(35):9038–9046.

[Sleigh et al., 2008] Sleigh, J. W., Vizuete, J. A., Voss, L., Steyn-Ross, A., Steyn-Ross, M. L., Marcuccilli, C. J., and Hudetz, A. G. (2008). Theory, The Electrocortical Effects of Enflurane: Experiment and. *Anesthesia and analgesia*, 23(1):1–7.

[Sleigh et al., 2011] Sleigh, J. W., Voss, L., and Wilson, M. T. (2011). Sleep and Anesthesia. In Hutt, A., editor, *Sleep and Anesthesia*, pages 257–258. Springer.

[Song et al., 2011] Song, I., Savtchenko, L., and Semyanov, A. (2011). Tonic excitation or inhibition is set by GABA(A) conductance in hippocampal interneurons. *Nature communications*, 2:376.

[Spira and Hai, 2013] Spira, M. E. and Hai, A. (2013). Multi-electrode array technologies for neuroscience and cardiology. *Nature Nanotechnology*, 8(2):83–94.

[Spruston et al., 1995] Spruston, N., Schiller, Y., Stuart, G., and Sakmann, B. (1995). Activity-dependent action potential invasion and calcium influx into hippocampal CA1 dendrites. *Science*, 268(5208):297–300.

[Squire, 1987] Squire, L. R. (1987). *Memory and brain.* Oxford University Press.

[Squire, 1992] Squire, L. R. (1992). Memory and the hippocampus: A synthesis from findings with rats, monkeys, and humans. *Psychological Review*, 99(2):195–231.

[Squire and Alvarez, 1995] Squire, L. R. and Alvarez, P. (1995). Retrograde amnesia and memory consolidation: a neurobiological perspective. *Current Opinion in Neurobiology*, 5(2):169–177.

[Squire et al., 2004] Squire, L. R., Stark, C. E., and Clark, R. E. (2004). The Medial Temporal Lobe. *Annual Review of Neuroscience*, 27(1):279–306.

[Stein, 1967] Stein, R. B. (1967). Some Models of Neuronal Variability. *Biophysical Journal*, 7(1):37–68.

[Stewart and Fox, 1990] Stewart, M. and Fox, S. E. (1990). Do septal neurons pace the hippocampal theta rhythm? *Trends in Neurosciences*, 13(5):163–169.

[Steyn-Ross et al., 2004] Steyn-Ross, M. L., Steyn-Ross, D. A., and Sleigh, J. W. (2004). Modelling general anaesthesia as a first-order phase transition in the cortex. *Progress in Biophysics and Molecular Biology*, 85(2-3):369–385.

[Steyn-Ross et al., 2012] Steyn-Ross, M. L., Steyn-Ross, D. A., and Sleigh, J. W. (2012). Gap junctions modulate seizures in a mean-field model of general anesthesia for the cortex. *Cognitive Neurodynamics*, 6(3):215–225.

[Steyn-Ross et al., 2011] Steyn-Ross, M. L., Steyn-Ross, D. A., Sleigh, J. W., and Wilson, M. T. (2011). A Mechanism for Ultra-Slow Oscillations in the Cortical Default Network. *Bulletin of Mathematical Biology*, 73(2):398–416.

[Stickgold, 2005] Stickgold, R. (2005). Sleep-dependent memory consolidation. *Nature*, 437(7063):1272–8.

[Storer and Reeke, 2012] Storer, K. P. and Reeke, G. N. (2012). γ-Aminobutyric Acid Receptor Type A Receptor Potentiation Reduces Firing of Neuronal Assemblies in a Computational Cortical Model. *Anesthesiology*, 117(4):780–790.

[Storm, 2008] Storm, H. (2008). Changes in skin conductance as a tool to monitor nociceptive stimulation and pain. *Current Opinion in Anaesthesiology*, 21(6):796–804.

[Sweatt, 1999] Sweatt, J. D. (1999). Toward a Molecular Explanation for Long-Term Potentiation. *Learning & Memory*, 6(5):399–416.

[Tai et al., 2011] Tai, C., Hines, D. J., Choi, H. B., and MacVicar, B. A. (2011). Plasma membrane insertion of TRPC5 channels contributes to the cholinergic plateau potential in hippocampal CA1 pyramidal neurons. *Hippocampus*, 21(9):958–967.

[Talairach et al., 1974] Talairach, J., Bancaud, J., and Szikla, G. (1974). Approche nouvelle de la neurochirurgie de l'epilepsie. Méthodologie stéréotaxique et résultats thérapeutiques. *Neurochirurgie*, 20:183–205.

[Tesche and Karhu, 2000] Tesche, C. D. and Karhu, J. (2000). Theta oscillations index human hippocampal activation during a working memory task. *Proceedings of the National Academy of Sciences of the United States of America*, 97(2):919–924.

[Tiesinga et al., 2001] Tiesinga, P. H. E., Fellous, J. M., José, J. V., and Sejnowski, T. J. (2001). Computational model of carbachol-induced delta, theta, and gamma oscillations in the hippocampus. *Hippocampus*, 11(3):251–274.

[Tinker et al., 1977] Tinker, J. H., Sharbrough, F. W., and Michenfelder, J. D. (1977). Anterior shift of the dominant EEG rhythm during anesthesia in the Java monkey: correlation with anesthetic potency. *Anesthesiology*, 46:252–259.

[Tononi, 2004] Tononi, G. (2004). An information integration theory of consciousness. *BMC Neurosci*, 5:42.

[Tóth et al., 1997] Tóth, K., Freund, T. F., and Miles, R. (1997). Disinhibition of rat hippocampal pyramidal cells by GABAergic afferents from the septum. *The Journal of Physiology*, 500 (Pt 2:463–74.

[Traub et al., 1994] Traub, R. D., Jefferyst, J. G. R., Miles, R., Whittington, M. A., and Tóth, K. (1994). A branching dendritic model of a rodent CA3 pyramidal neurone. *Journal of Physiology*, 481(1):79–95.

[Traub and Miles, 1991] Traub, R. D. and Miles, R. (1991). *Neuronal Networks of the Hippocampus*. Cambridge University Press, New York.

[Traub et al., 1989] Traub, R. D., Miles, R., and Wong, R. K. S. (1989). Model of the origin of rhythmic population oscillations in the hippocampal slice. *Science*, 243:1319–1325.

[Treves and Rolls, 1994] Treves, A. and Rolls, E. T. (1994). Computational analysis of the role of the hippocampus in memory. *Hippocampus*, 4(3):374–391.

[Tronson and Taylor, 2007] Tronson, N. C. and Taylor, J. R. (2007). Molecular mechanisms of memory reconsolidation. *Nature Reviews Neuroscience*, 8(4):262–275.

[Tuckwell, 1988] Tuckwell, H. (1988). *Introduction to theoretical neurobiology. Vol. 1, Linear cable theory and dendritic structure and stochastic theories.* Cambridge University Press.

[Tulving, 1985] Tulving, E. (1985). *Elements of Episodic Memory.* Oxford University Press.

[Valentino and Dingledine, 1981] Valentino, R. J. and Dingledine, R. (1981). Presynaptic inhibitory effect of acetylcholine in the hippocampus. *The Journal of neuroscience : the official journal of the Society for Neuroscience*, 1(7):784–792.

[Van Vreeswijk et al., 1994] Van Vreeswijk, C., Abbott, L. F., and Ermentrout, B. (1994). When inhibition not excitation synchronizes neural firing. *Journal of Computational Neuroscience*, 1(4):313–321.

[van Vugt et al., 2010] van Vugt, M. K., Schulze-Bonhage, A., Litt, B., Brandt, A., and Kahana, M. J. (2010). Hippocampal gamma oscillations increase with memory load. *The Journal of neuroscience : the official journal of the Society for Neuroscience*, 30(7):2694–9.

[Vanderwolf, 2000] Vanderwolf, C. H. (2000). Are neocortical gamma waves related to consciousness? *Brain Research*, 855(2):217–224.

[Vanlersberghe and Camu, 2008] Vanlersberghe, C. and Camu, F. (2008). Propofol. In Schüttler, J. and Schwilden, H., editors, *Modern Anesthetics: Handbook of Experimental Pharmacology*, pages 227–252. Springer Verlag.

[Vardi et al., 2016] Vardi, R., Goldental, A., Sardi, S., Sheinin, A., and Kanter, I. (2016). Simultaneous multi-patch-clamp and extracellular-array recordings: Single neuron reflects network activity. *Scientific Reports*, 6(1):36228.

[Varela et al., 2001] Varela, F., Lachaux, J. P., Rodriguez, E., and Martinerie, J. (2001). The brainweb: phase synchronization and large-scale integration. *Nature reviews. Neuroscience*, 2(4):229–39.

[Vazquez et al., 2004] Vazquez, G., Wedel, B. J., Aziz, O., Trebak, M., and Putney, J. W. (2004). The mammalian TRPC cation channels. *Biochimica et Biophysica Acta - Molecular Cell Research*, 1742(1-3):21–36.

[Vijayan et al., 2013] Vijayan, S., Ching, S., Purdon, P. L., Brown, E. N., and Kopell, N. J. (2013). Thalamocortical Mechanisms for the Anteriorization of Alpha Rhythms during Propofol-Induced Unconsciousness. *Journal of Neuroscience*, 33(27):11070–11075.

[Vijayan and Kopell, 2012] Vijayan, S. and Kopell, N. J. (2012). Thalamic model of awake alpha oscillations and implications for stimulus processing. *Proceedings of the National Academy of Sciences*, 109(45):18553–18558.

[Vinogradova, 1995] Vinogradova, O. S. (1995). Expression, control, and probable functional significance of the neuronal theta-rhythm. *Progress in Neurobiology*, 45(6):523–583.

[Walker, 2009] Walker, M. P. (2009). The role of slow wave sleep in memory processing. *Journal of clinical sleep medicine : JCSM : official publication of the American Academy of Sleep Medicine*, 5(2 Suppl):S20–S26.

[Walker et al., 2005] Walker, M. P., Stickgold, R., Alsop, D., Gaab, N., and Schlaug, G. (2005). Sleep-dependent motor memory plasticity in the human brain. *Neuroscience*, 133(4):911–7.

[Wang, 1993] Wang, X.-J. (1993). Ionic basis for intrinsic 40 Hz neuronal oscillations. *NeuroReport*, 5:221–224.

[Wang, 1999] Wang, X.-J. (1999). Synaptic basis of cortical persistent activity: the importance of NMDA receptors to working memory. *The Journal of Neuroscience : the official journal of the Society for Neuroscience*, 19(21):9587–603.

[Wang, 2001] Wang, X.-J. (2001). Synaptic reverberation underlying mnemonic persistent activity. *Trends in neurosciences*, 24(8):455–63.

[Wang, 2010] Wang, X.-J. (2010). Neurophysiological and Computational Principles of Cortical Rhythms in Cognition. *Physiological reviews*, 90(3):1195–1268.

[Wang and Buzsáki, 1996] Wang, X.-J. and Buzsáki, G. (1996). Gamma oscillation by synaptic inhibition in a hippocampal interneuronal network model. *The Journal of Neuroscience : the official journal of the Society for Neuroscience*, 16(20):6402–13.

[Wang and Rinzel, 1993] Wang, X.-J. and Rinzel, J. (1993). Spindle rhythmicity in the reticularis thalami nucleus: Synchronization among mutually inhibitory neurons. *Neuroscience*, 53(4):899–904.

[Welch, 1967] Welch, P. D. (1967). The use of fast fourier transform for the estimation of power spectra: a method based on time averaging over short modified periodograms. *IEEE Transactions on Audio and Electroacoustics*, 15(2):70–73.

[Wess, 2004] Wess, J. (2004). Muscarinic acetylcholine receptor knockout mice: novel phenotypes and clinical implications. *Annual Review of Pharmacology and Toxicology*, 44(1):423–450.

[White et al., 2000] White, J. A., Banks, M. I., Pearce, R. A., and Kopell, N. J. (2000). Networks of interneurons with fast and slow gamma-aminobutyric acid type A (GABAA) kinetics provide substrate for mixed gamma-theta rhythm. *Proceedings of the National Academy of Sciences of the United States of America*, 97(14):8128–33.

[Wiebe et al., 1997] Wiebe, S. P., Stäubli, U. V., and Ambros-Ingerson, J. (1997). Short-term reverberant memory model of hippocampal field CA3. *Hippocampus*, 7(6):656–665.

[Willems et al., 2005] Willems, S. J., Forster, A., and Linden, M. V. D. (2005). Investigation of Implicit Memory during Isoflurane Anesthesia for Elective Surgery Using the Process. *Anesthesiology*, 103:925–933.

[Willshaw and Buckingham, 1990] Willshaw, D. J. and Buckingham, J. T. (1990). An assessment of Marr's theory of the hippocampus as a temporary memory store. *Philosophical transactions of the Royal Society of London. Series B, Biological sciences*, 329(1253):205–15.

[Wilson and Cowan, 1972] Wilson, H. R. and Cowan, J. D. (1972). Excitatory and Inhibitory Interactions in Localized Populations of Model Neurons. *Biophysical Journal*, 12(1):1–24.

[Yamada et al., 1989] Yamada, W. M., Koch, C., and Adams, P. R. (1989). Multiple Channels and Calcium Dynamics. In Koch, C. and Segev, I., editors, *Methods in neuronal modeling*, pages 97–134. MIT Press.

[Yi et al., 2015] Yi, F., Catudio-Garrett, E., Gábriel, R., Wilhelm, M., Erdelyi, F., Szabo, G., Deisseroth, K., and Lawrence, J. (2015). Hippocampal "cholinergic interneurons" visualized with the choline acetyltransferase promoter: Anatomical distribution, intrinsic membrane properties, neurochemical characteristics, and capacity for cholinergic modulation. *Frontiers in Synaptic Neuroscience*, 7(MAR):1–18.

[Ying et al., 2006] Ying, S. W., Abbas, S. Y., Harrison, N. L., and Goldstein, P. A. (2006). Propofol block of Ih contributes to the suppression of neuronal excitability and rhythmic burst firing in thalamocortical neurons. *European Journal of Neuroscience*, 23(2):465–480.

[Young et al., 1997] Young, B. J., Otto, T., Fox, G. D., and Eichenbaum, H. (1997). Memory Representation within the Parahippocampal Region. *The Journal of neuroscience : the official journal of the Society for Neuroscience*, 17(13):5183–5195.

[Zhang et al., 2011] Zhang, Z., Reboreda, A., Alonso, A., Barker, P. A., and Séguéla, P. (2011). TRPC channels underlie cholinergic plateau potentials and persistent activity in entorhinal cortex. *Hippocampus*, 21(4):386–397.

[Zhou et al., 2012] Zhou, C., Liu, J., and Chen, X.-D. (2012). General anesthesia mediated by effects on ion channels. *World journal of critical care medicine*, 1(3):80–93.

[Zola-morgan et al., 1989] Zola-morgan, S., Squire, L. R., Amaral, D. G., Suzukij, W. A., Mesches, M., and Lockwood, A. (1989). Lesions of Perirhinal and Parahippocampal Cortex That Spare the Amygdala and Hippocampal Formation Produce Severe Memory Impairment. *The Journal of neuroscience : the official journal of the Society for Neuroscience*, 9(12):4355–4370.